Novel Mechanisms for Thermal Control in ECMO

MARCUS MÜLLER

A Dissertation Presented to the
University of Strathclyde
in Candidacy for the Degree of
Doctor of Engineering

Department of Biomedical Engineering

May 2016

This thesis is the result of the author's original research. It has been composed by the author and has not been previously submitted for examination which has led to the award of a degree.

Signed:

Date:

Abstract

Background

Extracorporeal membrane oxygenation (ECMO) is a temporary treatment for patients who suffer from impaired heart- and/or lung functions to degrees of inadequate self-sustainability. The use of an artificial ECMO circuit provides support to the patient to enable the healing processes to occur, with the ultimate objective of returning back to normal organ functions. Since the first application in 1972, ECMO has been responsible for decreasing morbidity in many challenged patient groups, particularly in neonatal care. However, despite the technical advancements, morbidity and mortality rates still remain high, largely based on the invasive nature of the therapy and technical imperfections of the system and the tendency to deploy ECMO as a therapy of last resort. ECMO is associated with many complications, but the focus of this thesis is primarily concerned with the aspects of heat loss. A comprehensive literature review on current ECMO technologies revealed a rather stagnant progression in the evolution of heat exchangers, still employing legacy components dating back to the 1957's. Moreover, most heat-exchange technologies today rely heavily on external power supplies which limits their use in energy-poor environments. For this reason, two novel solutions for thermal control were proposed, one focusing solely on traditional heat-exchange aspects for conventional hospital based ECMO therapy and the second a solution for energy poor transport settings.

Materials and Methods

Both heat exchanger concepts that were developed within this project progressed individually, based on their underlying proposed applications.

Heat exchanger concept 1 (for conventional ECMO): First, design requirements were established based on desired goals and shortcomings of current heat exchangers. These requirements set the boundaries and formed ideas that were evaluated, refined, and ultimately expressed in form of a finalised CAD drawing. The drawing and the underlying physical effects were modelled and optimised using a computational simulation software in order to minimise time to deploy. Temperature controllers were also designed within the computational domain and the completed, integrated model was simulated and validated with physical laboratory data. After successful validation, our virtual model was manufactured and tested under near-clinical conditions.

Heat Exchanger concept 2 (for in-transit ECMO): Similar to the previous strategy, design requirements were established based on expressed clinical aims and implemented in prototype technical drawings. These were used for manufacturing of the device and extensively tested under near-clinical conditions.

Results

This project has produced two miniaturised medical prototypes for thermal management for very distinct ECMO circumstances; one for conventional ECMO and one for in-transit ECMO. Both devices were computationally and physically tested and the results indicated good agreement with set requirements. Limitations were found with heat exchanger concept 1 during the experimentation phase but were remedied by re-design and further development. A second experiment confirmed efficacy levels that achieved satisfactory results. Heat exchanger concept 2 demonstrated capabilities of adding heat to the system under various ambient conditions and thereby slowing the rate of heat loss from the patient-ECMO system. Supplementary

test results indicated the potential for even further reducing the rate of heat loss with the usage of additional low-cost equipment. Through this project, we were able to demonstrate a new direction for thermal management within portable and fixed ECMO settings.

This work includes the following:

- Design of a novel heat exchanger model with the use of computational simulation software.
- Development of a novel and compact heat exchanger for conventional ECMO that does not rely on water supply.
- Development of a novel heat exchanger for mobile ECMO applications that is able to significantly reduce heat loss independent of mains or water supply.
- Demonstrate high accuracy in model correlation between virtual and physical results.

Thesis Outline

In chapter 1, we introduce the subject of human physiology in relation to ECMO procedures. A broad overview is presented to the reader to gain a deeper understanding in the complex processes of chemical and physical functions and interdependabilities of organ systems. The relevance of homeostasis is discussed and the consequences are pointed out when physiological variables are disrupted either pharmacologically or therapy-related.

In chapter 2, we elucidated the clinical procedure of ECMO and highlighted patient selection and contraindications. Further introduced are all relevant ECMO components, perfusion concepts, and control aspects; technical developments are summarised.

In chapter 3, we described the need for our novel device with respect to patients and clinicians leading to the main objectives and methodologies of this project.

In chapter 4, we defined requirements for our proposed devices and reviewed existing technologies and methodologies for possible implementation. Design procedures are described and our prototypes are presented.

In chapter 5, we modelled the system to be controlled. First, equations were derived based on the underlying physics and subsequently applied to individual parts. Components were categorised into subsystems and modelled independently before integration.

In chapter 6, we simulated our model developed in chapter 5 and validated all subsystems as well as the complete system with experimental data.

In chapter 7, we addressed and implemented commercial control strategies based on model- and validation results presented in chapter 6.

In chapter 8, we present temperature control validation and performance results of developed prototypes. Limitations of one prototype lead to re-evaluation and re-design before desired aims could be validated in near-clinical test conditions.

In chapter 9, we conclude our project by discussing goals achieved, limitations and contributions. An overall conclusion is presented and directions for future work are outlined.

Contents

List of Tables

List of Figures

Chapter 1

Physiological Background

1.1 Introduction

The human circulatory system can be considered as a hydraulic system consisting of different parts with various functionalities. This system can be categorised into two circuits, the systemic circulation and pulmonary circulation whereas both are driven by one organ, the heart. The left side of the heart supplies blood to the systemic circulation such as brain, organs, and tissue while the right side maintains blood flow to the lungs. Gas transfer of carbon dioxide and oxygen occurs inside the lungs from where oxygenated blood is first distributed through the arterial side of the circulatory system before returning through the venous circulation. The haemodynamic processes and compensatory mechanisms involved are determined to maintain the distribution of blood even with changing intrinsic or extrinsic conditions such as physical stress, hypothermia or haemorrhages (blood loss). Providing tissue and organ perfusion insures (Martini, 2011):

- Oxygen transport

- Carbon dioxide removal
- Delivery of nutrients and hormones
- Transport of hydrogen ions
- Thermoregulation

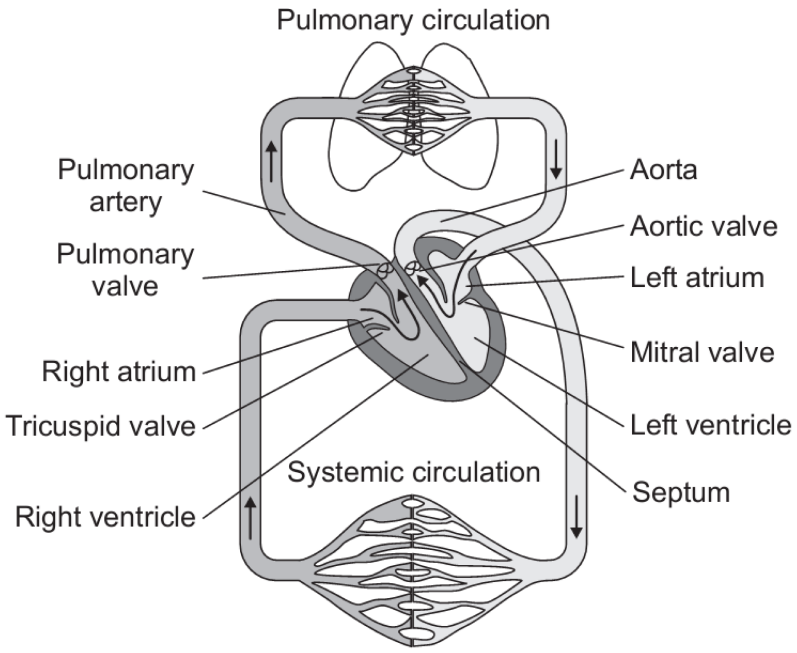

Figure 1.1: Pulmonary and Systemic Circulation (Misgeld, 2006)

1.2 The Human Heart

The human heart is a muscular organ representing the driving force for blood circulation. Left and right side of the heart are separated by a thick wall (septum) with each side being further divided into superior chamber (atrium) and inferior chamber (ventricle). During the cycle of a heartbeat, blood gets ejected by the ventricles during contraction (systole) and collected by the atria during relaxation (diastole). Blood

is leaving the right ventricle through the pulmonary artery (arteria pulmonalis) and heading for the lungs for gas exchange before returning to the left atrium through the pulmonary vein (venae pulmonalis). Upon return, oxygenated blood gets ejected into the systemic circulation through the aorta ascendens and back through the venae cavae to the right atrium. Under normal conditions, the amount of blood ejected into the pulmonary circulation is equal to the amount of blood ejected into the systemic circulation during a cardiac cycle. All chambers are supplied with uni-directional valves to inhibit back flow during diastole. Blood supply to the heart is performed through the coronary circulation.

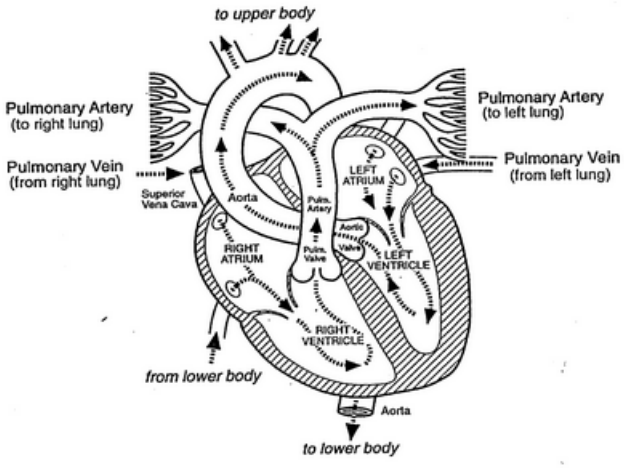

Figure 1.2: Structure of the Human Heart

The vast majority of neonatal cardiac runs are of congenital disorders ($\geq$ 85%) (ELSO, 2011) and depending on severity of the underlying disease require ECMO support for maintaining pulmonary and systemic perfusion while simultaneously allowing the heart to rest for recovery.

1.3 The Systemic Circulation

Blood distribution is provided through the systemic circulation of the human body; a network of many serial and parallel connections. Vessels are categorised according to diameter and function. The biggest vessels are arteries whose purpose is a swift distribution of oxygenated blood to the next group of vessels, the arterioles. Arterioles contain smooth muscle layers in their vessel construction able to dilate and constrict blood flow. Analogy to electrical circuit components resembles a potentiometer in which the resistance can be adjusted to achieve desired current values. This mechanism, caused by autonomic nervous system innervation and numerous circulating hormones, enables the distribution of blood flow, hence perfusion to certain areas. Among all types of vessels in the systemic circulation, it is the collective effect of arterioles which help to regulate the blood pressure. The smallest vessels, capillaries, are part of the microcirculation and connect arterioles and venules. Their narrow diameter allows important exchange of substances such as water, oxygen, carbon dioxide, and nutrients with surrounding tissues.

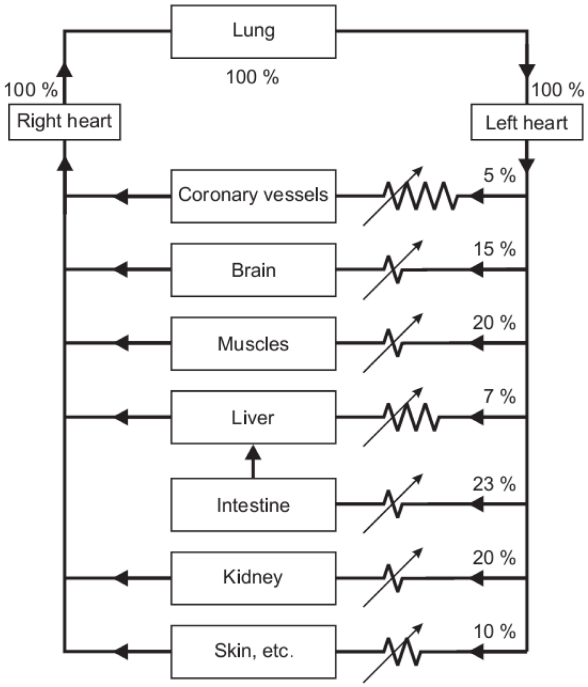

Figure 1.3: Blood distribution during rest and healthy conditions (Misgeld, 2006)

The first section of the venous circulation is comprised of venules which are still considered to be part of the microcirculation, collecting deoxygenated blood from capillary beds. Venules are surrounded by muscular tissue which aid the flow of blood by contraction and expansion. Many venules merge into the bigger veins carrying deoxygenated blood back to the heart.

The overall flow rate in human beings is directly proportional to the individual's size and weight. Higher flow rates of about 5 l/min occur in adults in order provide adequate oxygenation and carbon dioxide removal whereas neonates require about 100 - 120 ml/kg/min which translates to 0 - 500 ml/min (Drummond et al., 2005), (Smith, 2007).

1.4 The Pulmonary Circulation

The other half of the cardiovascular system is the pulmonary circulation through which the entire blood flows first before supplying oxygen to the rest of the body. Oxygen depleted blood leaves the right heart through the pulmonary artery returning to the left heart through the pulmonary vein. Similar in structure to systemic circulation, arteries divide into myriad arterioles and capillaries whereas venules merge into veins. However, the pressure in the pulmonary circulation is comparably much lower than in the systemic circulation due to very low vascular resistance. Oxygen and carbon dioxide exchange between blood circulation and lung occurs at alveolar level. The dense capillary network is almost forming a film of blood surrounding alveoli sacks and allowing diffusion processes to ensue across their very thin membranes (Nose, 1974). The application of VA-ECMO shunts the blood flow away from the lungs to allow recovery of the underlying disease.

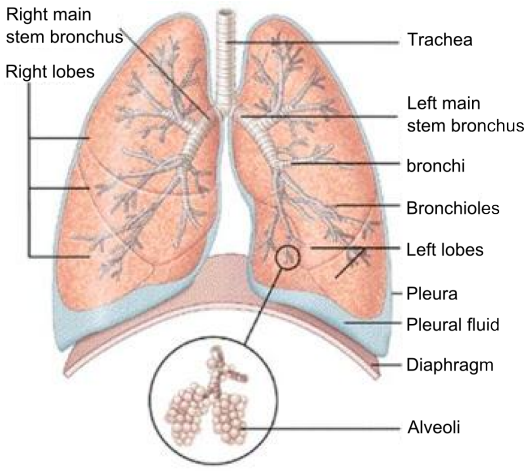

Figure 1.4: Diagram of human lungs (taken from a2zcancers.co.uk)

1.5 Haemodynamics

Haemodynamics can be described as the process of blood flow which is subject to laws of fluid dynamics and hydraulics. The simplified Ohm's law, which is guided by current **I**, resistance **R**, and voltage **V** can also be analogously applied to the physiological haemodynamics of blood flow **F**, resistance to blood flow **R**, and perfusion pressure **P**, respectively (Klabunde, 2011).

$$\mathbf{\Delta U = RI} \tag{1.1}$$

$$\mathbf{\Delta P = P_1 - P_2 = RF} \tag{1.2}$$

The mean arterial pressure **MAP** describes the average blood pressure determined by minima (diastole) and maxima (systole) during a cardiac cycle. A minimum level of **MAP** is required for optimal delivery of oxygen to organs and tissue. In cases where MAP drops below the threshold of critical closing pressure (CCP), vessel wall collapse is imminent which is partly induced by the active tone of arterial smooth muscles. Thus, the importance of maintaining pressure levels above the CCP cannot be overestimated.

One way of determining cardiac output **CO** is by equation (1.3):

$$\mathbf{CO = HR \cdot SV} \tag{1.3}$$

Where **HR**: heart rate [beats per minute] and **SV**: stroke volume [litres per minute]

Uncompromised myocardial functionality results in **CO** being equal to mean arterial flow (MAF), since all of the ejected blood is forwarded into the main artery with no impeding backflow.

The central venous pressure (CVP) is measured in the venae cavae in close approximation of the right atrium. Therefore, (CVP) is often referred as right atrial pressure (RAP) and a measure for efficiency of the right heart to pump blood.

1.6 The Blood

Blood, considered as a major organ, serves several functions in maintaining homeostasis such as heat management, waste removal, nutrition and hormone delivery, and oxygen and carbon dioxide transport. A viscous fluid composed of plasma, red blood cells (erythrocytes), white blood cells (leukocytes), and platelets (thrombocytes), each serving different functions. Blood plasma is again subdivided into several components including serum albumin for controlling the distribution of body fluid, clotting factors necessary for the maintenance of haemostasis, immunoglobulins as part of the immune system to fight bacteria and viruses, and many other proteins and electrolytes. The main function of erythrocytes is to transport oxygen across the entire cardio vascular system to capillary branches where transfer takes place. This occurs with the help of haemoglobin (Hb) in the red blood cell. In addition, different types of leukocytes exist as part of the immune system which fight foreign materials and infectious diseases. Thrombocytes release a multitude of growth factors assisting in the formation of blood clots during haemostatic processes (Chambers, 2015).

Constituents of Human Blood	
Cells	Plasma
Erythrocytes Leukocytes Thrombocytes	Glucose Amino Acid Fatty Acid Carbon Dioxide Urea Lactic acid Serum albumin Blood-clotting factors Immunoglobulins Lipoprotein particles Other proteins Other electrolytes

Figure 1.5: Constituents of Human Blood

1.6.1 Transport of Blood Gases

In normal physiological procedures, deoxygenated blood is pumped through the lungs for gas exchange from the right heart. This process involves both O2 delivery and CO2 removal; both essential for the maintenance or normal physiological function. During ECMO therapy, when lung function is compromised, gas exchange is established via an artificial lung or oxygenator. Operating principles for oxygenation in both environments whether artificial or via the native lungs are very similar. In the normal mammalian lung gas diffusion occurs by pressure differences between two places, the alveoli and capillaries, separated by a membrane. Within the artificial lung, the membrane generally constitutes a microporous hollow fibre separating the blood from the gas phase. Only oxygen and carbon dioxide molecules pass freely across the membrane surface driven by diffusion gradients.

1.6.2 O_2-Transport

In the lungs, the oxygen tension in blood (pO_2) is lower compared to alveolar tension. Ultimately, oxygen molecules diffuse across the alveolar-capillary membrane into the blood of the pulmonary circulation where the majority (99%) react with haemoglobin. Oxygen remnants (1%) which fail to chemically bind to haemoglobin get disolved in the liquid fraction of th blood, the plasma, and distributed through the cardiovascular circulation. Both parts contribute to the overall oxygen concentration in the blood. The concentration of dissolved oxygen depends on the O_2 solubility and the O2 partial pressure in the gas. The amount of oxygen bound to haemoglobin depends on the binding capacity and oxygen saturation. The former is the product of haematocrit and the haemoglobin concentration in the red blood cells whereas the latter is described by a non-linear behaviour. The oxygen saturation curve in Figure 1.6 illustrates the percentage of saturation of haemoglobin (SO_2) depending on O2 partial pressures. At higher O_2 partial pressures, such as in the lungs, oxygen binds more easily to haemoglobin to form oxyhaemoglobin. As oxyhaemoglobin passes through the body of deoxygenated tissues, the O_2 partial pressure will also be decreased, encouraging oxyhaemoglobin to release oxygen (Chambers, 2015).

Higher saturated percentages indicate an increased occupation of available haemoglobin by oxygen whereas the lower spectrum shows the opposite. The ratio and affinity for binding oxygen can be affected by several factors such as temperature, pH-value, pCO_2, and 2.3-Diphosphoglycerate (DPG; control mechanism for releasing oxygen to body tissues).

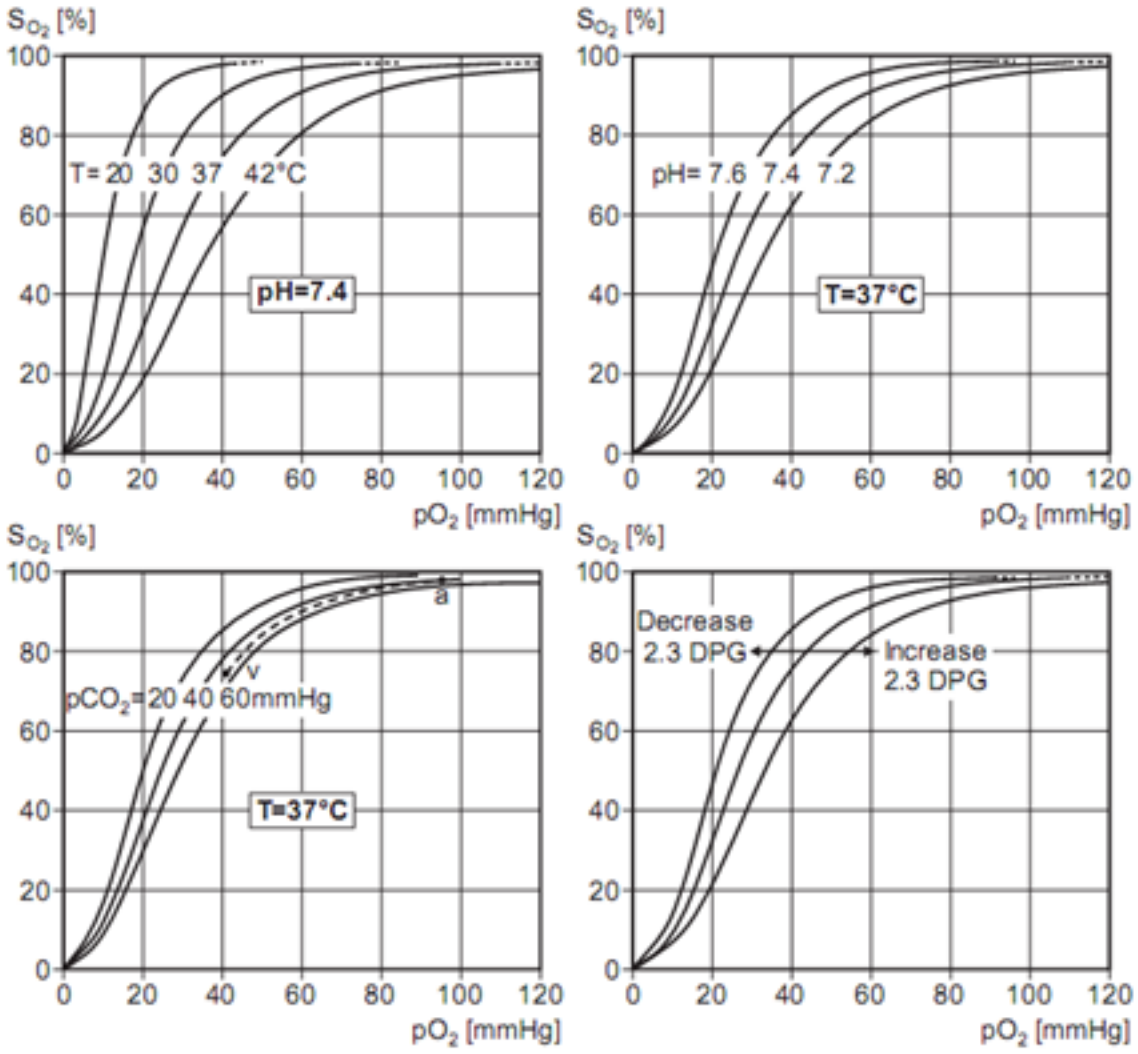

Figure 1.6: Sigmoid shape of the oxyhaemoglobin dissociation curve; alterations are affected by temperature, ph-value, carbon dioxide partial pressure, and 2.3-Diphosphoglycerate (DPG) (Schmidt et al., 2000)

1.6.3 CO_2-Transport

Carbon dioxide a waste product of the general metabolic process has to be eliminated and this is achieved at the pulmonary interface. Carbon dioxide diffuses out of the

cells and into the plasma from where it is transported to the lungs in three ways, namely (Ganong, 2003):

- In physically dissolved form,
- Chemically bound to proteins,
- Buffered as carbonic acid.

Only a small fraction of the physically dissolved CO_2 will remain in plasma and transported to the lungs.

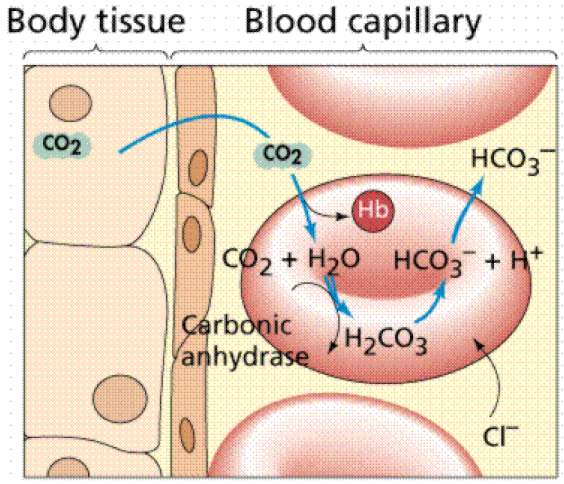

Figure 1.7: Main process for carbon dioxide removal (taken from Life: The Science of Biology)

Approximately 25% of CO_2 binds to haemoglobin to form carbamino haemoglobin ($Hb{\cdot}CO_2$). This process reverses in the lungs driven by CO_2 partial pressure differences comparatively higher in end-capillary blood compared to alveolar sacks.

The majority of CO_2 is buffered and transported in the form of bicarbonate (HCO_3-) which is associated with approximately 70% of systemic carbon dioxide removal. CO_2 reacts with water inside the red blood cell where the enzyme carbonic

anhydrase catalyses the reaction to carbonic acid. The reaction also occurs outside the cell in plasma but at a much slower rate due to the lack of the catalyst. The unstable compound of carbonic acid dissociates very easily into hydrogen and bicarbonate ions. The former reacts with haemoglobin to form an acid-base buffer whereas the latter passes freely through the cell membrane in exchange for chloride ions. The same process occurs within the lungs in the reverse order.

The cumulative amount of carbon dioxide removal described by the above processes is driven by pCO_2 differences between capillary blood and alveolar. The CO_2-dissociation curve illustrates the dependency of carbon dioxide to pCO_2 (Fig. 1.8). All three phases are affected by pCO_2 with additional dependency of carbamino haemoglobin on the saturation of oxyhaemoglobin.

Comparison of both oxygen and carbon dioxide curves in Figure 1.9 illustrate the non-linear behaviour. With increasing partial pressure of oxygen, the content of O2 in blood will eventually reach a point of saturation. However, increasing partial pressure of carbon dioxide will continuously elevate the CO2-content in blood which requires consideration during oxygenator sweep flow adjustments.

1.7 Thermoregulation

Among the millions of chemical reactions occurring in humans every second, some of the energy is produced in form of heat. Body cells require an optimal thermal balance to function properly. In healthy humans, the balance between heat loss and production is controlled by the hypothalamus, situated in the brain. This thermoregulatory control centre receives temperature dependent signals from various receptors which are distributed along peripheral tissues, viscera or internal organs, spinal cord, and the hypothalamus itself (Lloyd, 1986). If deviations from normothermic levels

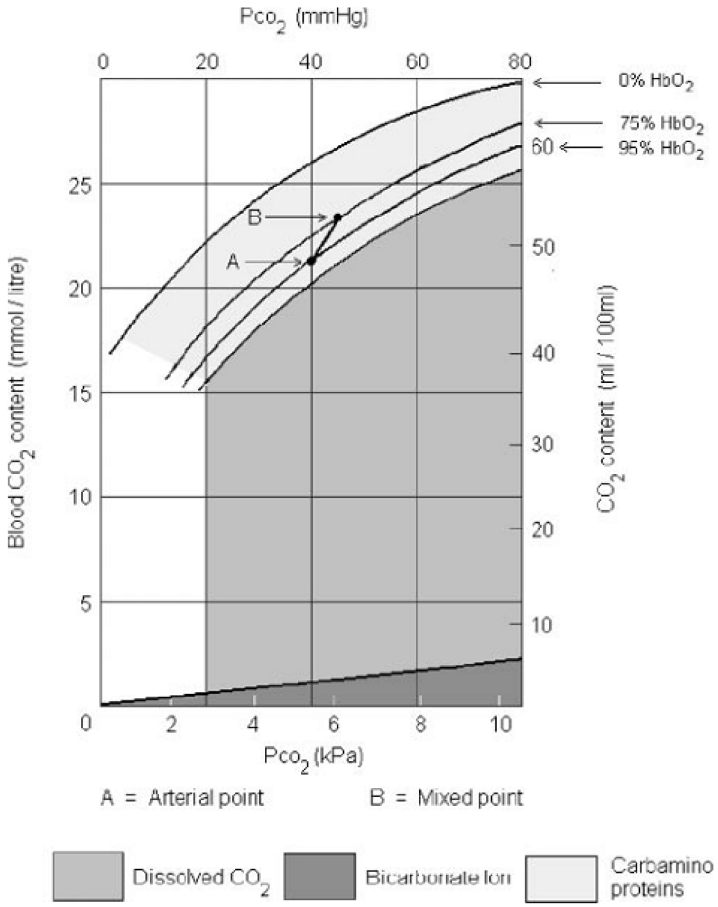

Figure 1.8: Collective amount of CO_2 transported in whole blood (Arthurs and Sudhakar, 2005)

are detected, physical and chemical counter-reactions are initiated to re-establish a balance, called homeostasis.

In adults, behavioural responses such as changing body position, clothing, or movement can positively or negatively influence this thermal balance. Additionally, involuntarily muscle contractions, also named shivering thermogenesis, occur during mild hypothermia and induce heat two to five fold (Hensel, 1981). This intrinsic function and indicator for thermal imbalance, however, is also unavailable to neonates. A different physiological mechanism is available. Infants and young children have larger quantities of brown adipose tissue, also named brown fat which is diffusely

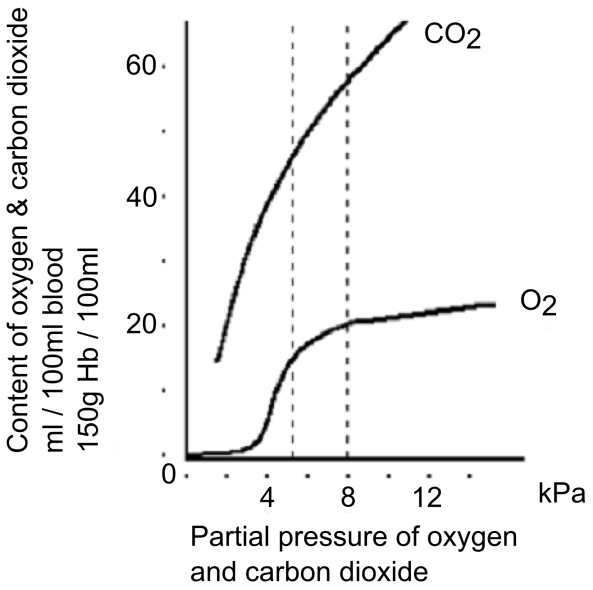

Figure 1.9: Comparison of O_2- and CO_2 content in whole venous blood (Arthurs and Sudhakar, 2005)

distributed across the body. These parts of the body, when their cells are stimulated by the nervous system, do not dissipate the generated energy to the environment but distribute it to the surrounding tissue instead, termed non-shivering thermogenesis. The surrounding tissue ultimately warms up the blood which is redistributed throughout the body. This technique enables heat production with efficiency close to 100% but will also require increased amounts of oxygen and glucose to maintain its functionality (Martini, 2011).

Maintaining normothermia is a major task for neonates. Neonates have a larger body-surface to volume ratio comprising of greater curvature radii of trunk and extremities compared to adults, leading to better air insulation. However, because of the larger body-surface to mass ratio and decreased thickness of skin, neonates are incapable of maintaining normal core temperature at reduced ambient temperatures and are susceptible to heat- and water loss. Limited subcutaneous fat for heat in-

sulation and blood vessels close to the skin surface makes them even more prone to heat loss (Hey and Katz, 1969; Hey, 1972; Sulyok et al., 1973).

Premature infants are even more disadvantaged with less availability of subcutaneous fat and brown fat stores. Additionally, their skin is even thinner than full term neonates with further reduced tone. Therefore, the effects of hypothermia on neonates are even more pronounced compared to adults.

These previous sections have outlined the normal physiological processes and responses from the cardiovascular perspective. ECMO - the focus of the present work - is not a normal physiological process, insofar it depends upon engineered systems and controls, largely independent of normal physiological response patterns. This unusual state will be the focus of following chapters.

Chapter 2

ECMO Technology and Practices

2.1 Evolution of ECMO

2.1.1 ECMO Procedure

Extracorporeal membrane oxygenation (ECMO) is a term describing prolonged cardiopulmonary support for patients suffering from severe but possible reversible cardiac and/or pulmonary insufficiency. Extracorporeal refers to a circuit setup outside the body where the natural lungs are substituted with an artificial membrane oxygenator. The motive of ECMO is to provide a therapy of sufficient duration (1-30 days) to allow the diseased heart and/or lungs to heal. The procedure is performed by draining deoxygenated (venous) blood from the patient's body, extracting carbon dioxide (CO_2) and adding oxygen (O_2) within the oxygenator, before re-infusing the blood back to the patient. Two distinct categories of ECMO have been developed: veno-venous (VV) and veno-arterial (VA), referring to the mode of blood return and capture. If blood is drained and also returned through a vein, the procedure is called VV-ECMO. Otherwise, if the drainage site is a venous vessel and blood is returned

to the patient through an arterial line, the modality is called VA-ECMO (Figure 2.1). The appropriate procedure depends on the underlying nature of the disease. VV-ECMO provides fundamentally pulmonary (lung) support assuming full myocardial functionality whereas VA-ECMO is able to provide both cardiac and pulmonary support, to an extend required by the patient.

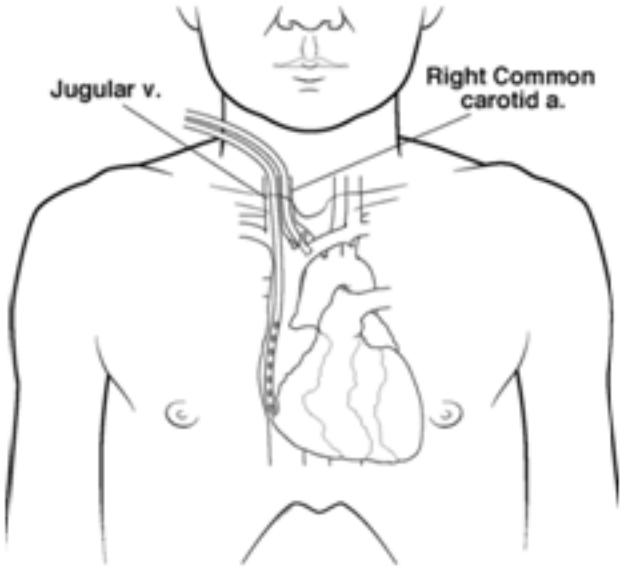

Figure 2.1: VA–ECMO cannulation (Meyer and Jessen, 2000)

Usually, venous drainage is achieved by a catheter placed in the right internal jugular vein. The tip of the venous catheter is sufficiently long to extend to the right atrium of the heart from where blood is drained into the extracorporeal circuit. This deoxygenated blood passes through the first medical device, a bladder, which controls the flow of venous blood into the circuit. In case where the forward pump flow exceeds the rate of venous drainage from the patient, the bladder will collapse, tripping an audible alarm and automatically reducing the pump speeds (Frenckner and Radell, 2008). The next device within the extracorporeal circuit is the pump which drives and maintains the blood flow to the patient. Blood passing the pump

enters the oxygenator, facilitating gas exchange by removing CO_2 and introducing O_2. In modern oxygenators, this process is facilitated generally by either membrane or hollow fibre oxygenators. Heat exchangers are necessary to maintain the blood temperature between physiological limits before re-infusion into patient circulation compensating for heat loss in the system or inducing desired hypothermia. Maintaining normothermic levels is especially relevant in neonatal patients who are prone to heat loss and immature thermoregulatory development. In most cases, placement of the heat exchanger is distal in the artificial circuit (increasingly incorporated into oxygenators) compensating for prior heat losses. Subsequently, normothermic and oxygenated blood is returned to the patient through the right common carotid artery (VA-ECMO), or internal jugular vein or femoral vein (VV-ECMO) (Cornish and Clark, 1995).

Respiratory Support Mode [%]		**Cardiac Support Mode** [%]	
VA	76.0	VA	92.3
VVDL (double lumen catheter)	20.3	VA+V	4.8
VA+V	5.3	VVDL (double lumen catheter)	0.9
Conversion from VV to VA	2.9	Conversion from VV to VA	0.6
VVDL+V	2.6	VV	0.5
VV	1.5	Other	0.9
Other	0.4		

Table 2.1: Cumulative comparison of ECMO modes for respiratory and cardiac support since 1986 (ELSO, 2011)

According to the ELSO database, VA-ECMO seems to be the preferred mode for both respiratory and cardiac procedures (ELSO, 2011). More than two thirds of all

neonatal respiratory operations are performed by VA-ECMO, suggesting additional patient related cardiac diseases which are supported by this particular mode but not with VV-ECMO.

2.1.2 Indications for ECMO

The vast majority of the ECMO patient population are neonates with more than 25100 reported cases for neonatal ECMO support for respiratory and 4658 cases for cardiac failure, submitted to ELSO (Extracorporeal Life Support Organisation) since 1986. [1]

	Total number of cases	**Average number of hours on ECMO**
Neonatal respiratory	25,100	192
Paediatric respiratory	5,099	277
Neonatal cardiac	4,658	161
Adult respiratory	2,693	248
Adult cardiac	1,885	128

Table 2.2: Categorical comparison of ECMO population since 1986 (ELSO, 2011)

Overall neonatal survival rates for respiratory- and cardiac runs in 2011 are reported to be 63 percent and 43 percent, respectively. An excerpt of ELSO's international summary report from 2011 states several categorised conditions that are typically treated with ECMO (ELSO, 2011):

- Sepsis

[1] ELSO, represented by an international consortium of health care specialists and scientists maintains a database of all patients treated with ECMO at participating institutions (Custer and Bartlett, 1992)

- Bridge to transplantation
- Postoperative support
- Heart defects

  Acute myocardial failure/Myocarditis

  Left to right shunt

  Left-sided obstruction

  Hypoplastic left heart

  Right-sided obstruction

  Cyanotic increased/decreased pulmonary blood flow

  Cyanotic increased pulmonary congestion

- Congenital respiratory failure

  Meconium aspiration syndrome (MAS)

  Congenital diaphragmatic hernia (CDH)

  Respiratory distress syndrome (RDS)

  Primary pulmonary hypertension (PPH) / Persistent fetal circulation (PFC)

Many other conditions which are not mentioned above can be successfully treated with ECMO. The timing for initiating ECMO is of utmost importance for preventing hypoperfusion and potential irreversible organ damage. Chaturvedi et al. (2004) reported an increased survival rate by initiating post-cardiac ECMO support inside the operating room rather than postponing to intensive care stay.

2.1.3 Patient Selection

Due to the dangers and severe risks involved in ECMO therapy, this technique has generally been reserved for last resort circumstances where other less invasive interventions have failed. However, based on evolving techniques and procedures, patient safety, and new technologies, the paradigm of a "rescue therapy" has shifted towards a more proactive, therapeutic and even preventative strategy.

Several criteria were established to specifically select patients in whom the benefits of ECMO therapy outweigh the risks and allow physicians to make an informed decision (Rosenberg and Seguin, 1995).

- Gestational age $\geq$ 34 weeks

  Increased morbidity is related to intracranial haemorrhages (bleeding) on younger patient population (Cilley et al., 1986).

- Birthweight $\geq$ 2 kg

  Cannulation requires a certain diameter to provide adequate ECMO flow rates. The law of fluid dynamics dictate that flow is proportional to the radius^4 and cannula sizes below 2.7mm diameter or 8 French gauge (Fr.) is discouraged.

- No significant coagulopathy or uncontrollable bleeding

  Patients suffering from uncontrolled bleeding, coagulopathy, or sepsis are exposed to increased risks of bleeding during conduct of ECMO. Whenever blood is in contact with a foreign surface, physiological defence mechanisms are initiated to form thrombi. More than twenty different plasma proteins, platelets, chemical factors, and fibrin are involved in the process of trapping red and white blood cells to form blood clots. Systemic heparinisation is imperative

in ECMO to inhibit the formation of blood clots but on the contrary can further contribute to the risks for bleeding (Sell et al., 1986).Patients should be tested and if positive corrected before initiation of ECMO.

- No major intracranial haemorrhage

  Blood properties are changed under the influence of heparin. The tendency for haemorrhagic complications is increased on a systemic basis. Special care is required in neonates with jugular and/or carotid ligation which alters cerebral blood flow imposing further risk on intracranial bleeding events (Cilley et al., 1986).

- Mechanical ventilation

  Mechanical ventilation is a procedure in which breathing is artificially assisted or replaced by a medical device supplying high concentrations of oxygen under pressure. Prolonged use of this method can lead to bronchopulmonary dysplasia, a pulmonary injury due to barotrauma or oxygen toxicity (Northway Jr et al., 1967). Neonatal patient selection criterion suggests the limited use of mechanical ventilation to 10-14 days, or to a state in which lung injury is possibly reversible in order to outweigh the benefits to risks associated with ECMO.

- Identified Cardiopulmonary Anomaly

  Complete cardiac-respiratory evaluation is required before initiation of ECMO. Cardiac defects which are left undetected can adversely influence the mode of cannulation (VV versus VA) affecting other organs and compromising the overall benefits of the treatment.

Therefore, patient selection criteria represent only guidelines with subtle centre-specific variations towards the approach of neonatal ECMO therapy. Each individual ECMO institution has developed a strategy for selecting and managing patients according to centre specific strengths and weaknesses, and experiences.

2.1.4 Contraindications/Discontinuation of ECMO Support

The purpose of ECMO is to provide an artificial circulation to relieve and support the compromised organ(s) for prolonged but temporary periods, potentially reversing the underlying disease, a so called bridge to recovery. Therefore, major contraindications are considered to be conditions which exacerbate the patient's condition during the conduct of ECMO which inevitably could lead to increased mortality. Included are irreparable congenital heart defects, evidence of irreversible CNS (central nervous system) damage, untreatable non-pulmonary diseases such as positive HIV status and immunosuppression, fatal irreversible metabolic diseases, malformations, and anatomic abnormalities. Further reasons for exclusion of ECMO are multi-organ system failure in which two additional organs are majorly compromised besides inadequate cardiac or pulmonary functions (Meyer and Jessen, 2000).

2.1.5 ECMO Components

Simply put, the essential parts of the ECMO circuit include a pump, an oxygenator, and a heat exchanger all connected in series via one main tube through which the blood flows. The pump simulates the heart maintaining blood flow within the extracorporeal circulation (ECC) while the oxygenator replaces the native lungs. The heat exchanger, usually placed proximal to the patient, aims to compensate for temperature loss and keeps the blood temperature at normothermic levels or in some

circumstances moderate hypothermia. The tubing segment prior and after the oxygenator is termed venous return line and arterial line, respectively. Oxygen depleted and carbon-dioxide rich blood is drawn through the venous catheter into the venous return line. The blood then passes through the pump, followed by the oxygenator and heat exchanger before re-infusion occurs.

Various auxiliary elements such as connectors, catheters, filters, bubble detection, and bubble traps all contribute to overall patient safety but will not be covered in this thesis. Sensors and devices which are part of the control and monitoring system will be discussed in Section 7.

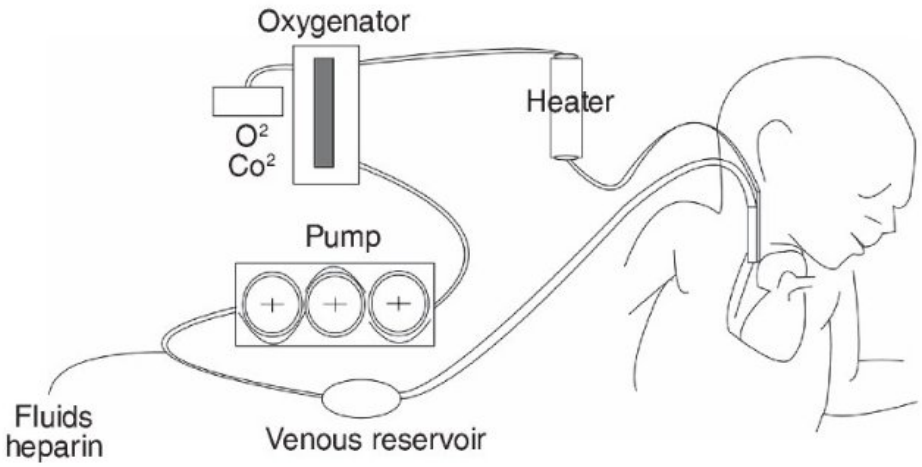

Figure 2.2: ECMO Diagram (Abel et al., 2010)

The arrangement of the ECMO circuit can vary, depending on institution. The arrangement adapted at the Bioengineering Unit of the University of Strathclyde is illustrated in Figure 2.2.

The following section describes the essential ECMO components and historical developments in more detail.

2.1.5.1 Blood Pumps

Blood pumps in ECLS compensate for a compromised heart and allow sufficient time for recovery of the underlying disease until native cardiac function has been restored for adequate self-perfusion. Several blood pumping systems are available, which all should fulfil certain requirements based on the **ideal blood pump**, the human heart.

- The pump must provide enough blood volume for adequate perfusion regardless of outflow line pressure.
- Neither pump surface nor pump motion should induce destruction of cellular and non-cellular blood components, thrombus or foam formation.
- Calibration of the pump should yield reliable and reproducible flow values which must be easily controllable.
- Manual operation in case of emergencies must be incorporated.
- Blood contacting elements of the pump should be disposable.

Roller Pumps The first roller pump developed for clinical use was in 1855 by Porter and Bradley (Cooley, 1987) followed by E. E. Allen in 1887 who introduced a hand operable type design named "surgical pump" (Herdman, July-December 1887) before DeBakey improved and modified Porter and Bradley's design in 1934, with a design that is still extensively employed in ECMO centres (85 per cent) to this day (Lawson, 2011). Drawings of these roller pumps are displayed in Figure 2.3.

In DeBakey's roller pump, a tube is place within the semilunar shape of the housing. Two rollers are fixed at the end of each arm compressing the tubing. As the arm is rotating around its axis in a circular motion, blood is being pushed ahead by the rollers creating positive pressure at the outlet and negative pressure at the

(a) Allen's design of the "Surgical Pump" (1887) (Herdman, July-December 1887)

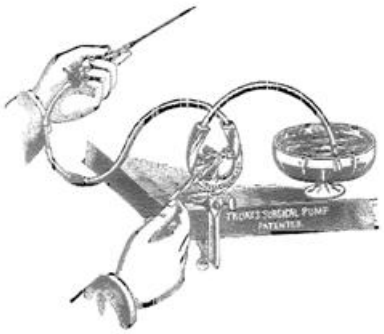

(b) The first double roller pump, improved and manufactured by Truax (1899)

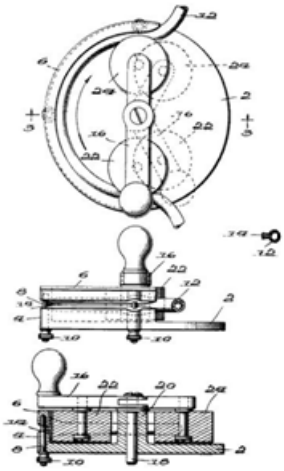

(c) DeBakey Roller Pump (DeBakey, 1934)

Figure 2.3: Evolution of roller pump designs

inlet, thereby establishing constant blood flow. The output of an occlusion roller pump depends on two factors: the revolutions per minute (rpm) of the pump and the volume inside the tube.

Several other innovative types of roller pumps with slight variations to the DeBakey model have been proposed in the past. The number of roller heads determine the pump classification; single, double, and multiple roller pump. Battezzati and Taddei (1954) developed a multiple roller pump system with three rotating rollers which never became clinically available due to haemolysis generation during experimentation. A single roller type system has been utilised in the Mayo-Gibbon heart lung machine and was clinically tested for extracorporeal circulation (Melrose, 1955; Rygg and Kyvsgaard, 1958; Kirklin et al., 1956). DeBakey's double roller pump became clinically adopted on international levels and is still employed in techniques such as ECMO, CPB, and haemodialysis.

However, complications can occur with roller pumps. The influence of tubing occlusion, tubing materials used, and rotary speed can all contribute to detrimental effects such as abrasion of the tubing (Kim and Yoon, 1998), haemolysis (Noon et al., 1985), and tubing rupture possibly leading to haemorrhages (Peek et al., 1999).

(a) Stockert

(b) Jostra HL-20

(c) Sarns 7000

Figure 2.4: Examples of commercially available perfusion systems with occlusion roller pumps

These are generally considered as reliable pump, however, systemic limitations are present. Servoregulation of pressure with regards to flow parameters are basically non-existing and require continuous adjustments by clinical staff. Failure to respond

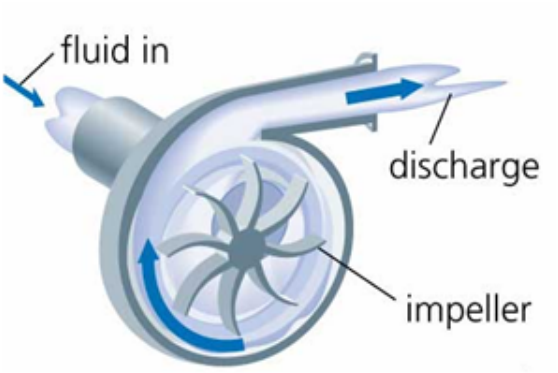

Figure 2.5: Head of a Centrifugal Blood Pump

in a prompt manner may result in excessive negative or positive pressures within the circuit. The former condition may result in air embolism, haemolysis, and/or vessel damage (Hirschl, 2000) whereas the latter could lead to possible catastrophic circuit rupture.

Centrifugal Blood Pump Development of alternative systems motivated by the limitations of the roller system resulted in experimentation with centrifugal blood pumps which became commercially available in 1973 initially produced by Biomedicus Inc. (Eden Prairie, MN) (Lynch et al., 1978). Successful animal experiments in 1975 (Bernstein et al., 1974), and clinical trials in 1978 (Golding et al., 1980) and 1980 (Pennington et al., 1982) for cardiac assistance subsequently lead to a marked increase in centrifugal pump development of various designs.

Modern centrifugal pumps consist of a disposable head unit (Figure 2.5) and pulsatile drive system. Both parts are magnetically coupled during operation ensuring that the pump head is isolated and sealed. A rotating magnetic field induced inside the pump housing drives a magnetically levitated impeller in the pump head, both spinning at the same rate. The impeller is free of any mechanical contact to avoid haemolysis and thromboembolic events encountered in the past (Hoshi et al., 2005).

The motion of the impeller creates a vortex inside the housing resulting in pressure differences between inlet and outlet and thereby initiating blood flow. Figure 2.6 displays some currently available commercial centrifugal pump heads.

(a) Jostra Rotaflow (b) Levitronix (c) Medtronic

Figure 2.6: Commercially available centrifugal pump heads.

In terms of dimensions and weight, the centrifugal pump proves to be more compact compared to the roller pump design. This advantage proves especially helpful during transportation of ECMO patient during treatment. The centrifugal technique offers reduced power consumption and an intrinsic safety feature which in case of kinked tubing on the arterial side leads to pressure build up and the rotor will cease to pump due to decoupling (Leshchinskii et al., 1990).

Despite higher purchasing costs and controversial results suggesting increased haemolysis compared to roller pumps (Hansbro et al., 1999; Rawn et al., 1997), the centrifugal pumps are still favoured in many centres due to their simplicity and reliability (Stammers et al., 2000). 47 per cent of ELSO registered ECMO centres are actively employing centrifugal pumps as their arterial pump (Lawson, 2011).

Axial Flow Pump Development of the axial flow pump started in the 1960's but was first described by Wampler et al. (1988) 28 years later as a ventricular assist

device (VAD), ranging from short-term to long-term support for patients. However, due to their compact architecture, axial flow pumps can be very much considered in neonatal ECMO.

The construction of the axial flow pump is similar to centrifugal and roller pumps; in turn none of them require valves. Blood enters axially through the flow straightener and is subsequently accelerated by an electromagnetically actuated impeller/inducer. The blood exits into the tubing through the diffuser which reduces turbulence. A diagrammatic illustration is depicted in Figure 2.7.

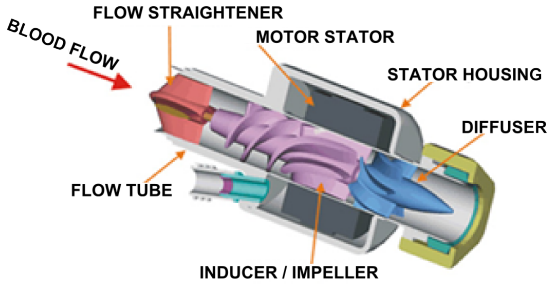

Figure 2.7: Assembly of Axial flow pump (Medgadget, 2003)

The axial flow blood pump offers the smallest design among the non-pulsatile blood pumps. The pump is able to achieve flow rates of up to 5 litres per minute against a pressure gradient of 100 mmHg, with a maximum rotor speed of 25 000 rpm at less than 10 W power consumption (Wieselthaler et al., 2000). Therefore, if high flows and low pressures are the required criteria, axial flow pumps are suitable.

The degree of haemolysis remains a controversial topic with axial flow pumps (Araki et al., 1998; Kawahito and Nosé, 1997). More efficient designs of haemodynamic influencing elements such as straightener, impeller, and diffuser can reduce the exposure time of blood and shear stress, thereby affecting haemolytic events. Also, heat development due to friction of bearings may lead to thrombosis (Reul and Akdis,

2000); especially in areas with low heat convection. Alternatively, blood-immersed parts or magnetic bearings may remedy the situation of thrombus formation and blood destruction.

Pulsatile vs. Non-Pulsatile Blood Pumps Compared to non-pulsatile blood pumps discussed above, pulsatile pumping systems are more complicated in design by aiming to achieve a more physiological haemodynamic pattern. Current state-of-the-art pulsatile blood pumps are employed as long-term support systems; typically associated with bridge-to-transplant therapy.

At first, commercially available roller pump systems did not offer a pulsatility component. Pulsatility was introduced 1959, when Ogata and colleagues modified existing roller pump technology (Ogata et al., 1959). Due to mechanical difficulties, reliable operation still proved to be very limited. However, clinical benefits in terms of haemodynamic improvements were reported by Nonoyama (1960). Further development and improvement of pulsatile pump systems resulted in commercialization of the first pulsatile roller pump systems by the company Stöckert (Stöckert Instrumente GmbH, München, Germany). This system eradicated the problems encountered by Ogata's model and motivated several other roller pump manufacturers to opt for additional pulsatility in blood flow fuelled by the great demand.

Wright (1988) demonstrated that pulsatile roller pumps only produce a 'ripple' and lacks in offering pulsatile blood flow in the strict physiological sense, despite clinical benefits derived from its use. It is hypothesised that the mere ripple pattern of the Stöckert roller pump, which generates only 12.4 per cent in pulsatile power compared to the human heart, are inadequate to deliver enough energy to the tissues for vital exchanges of gas, nutrients, and waste products (Wright et al., 1988).

More energy transfer occurs with alternative pump systems which are discussed below.

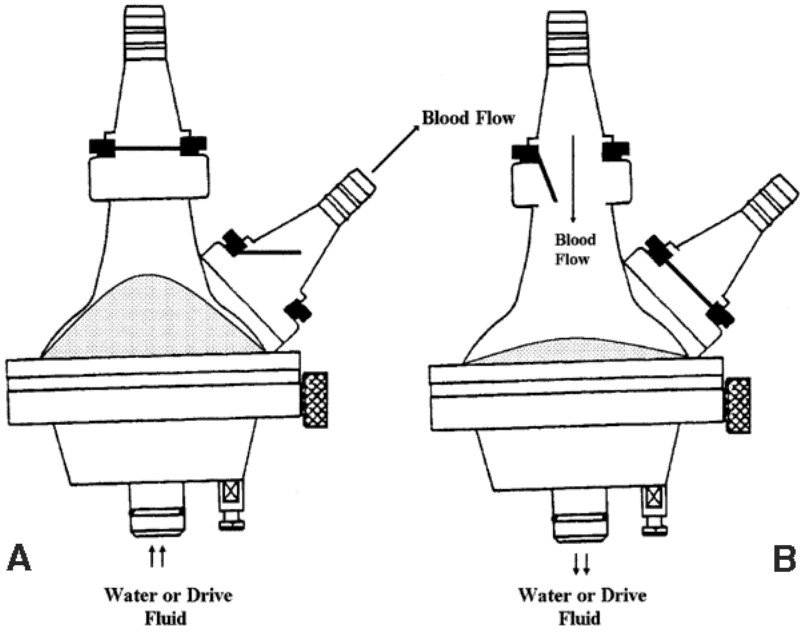

Figure 2.8: Ventricular Pump Mechanism; Compressible sack displaces volume of blood. A) Displacing blood and B) Filling pump (Gourlay and Taylor, 2002)

A pump system with more resemblance in operation to the human heart is the ventricular blood pump (Figure 2.8). The method for generating pulsatile blood flow is similar in assembly to the ventricles, hence the name. Two one-way valves at the inlet and outlet determine the direction of blood and simultaneously prevent backflow. A compressible sack, operated by hydraulic or pneumatic components, drives the blood flow into and out of the ventricle of the pump. The total pump output is determined by stroke volume and frequency.

Successful implementation of the ventricular blood pump during clinical practice is associated with better systemic perfusion compared to patients on non-pulsatile pump systems (Rottenberg et al., 1995). Ventricular pumps are able to achieve at

least as much as 272 per cent of pulsatile power compared to the human heart and are therefore able to transmit more lateral energy into the tissues (Wright, 1988).

Similar in operation to ventricular blood pumps are **compression plate pumps**. Their assembly is constructed in a way to only produce pulsatile blood flow (Figure 2.9). A piece of tubing with two one-way valves is resting on a rigid backplane. An opposing plate compresses the tube, thereby ejecting blood in one direction, defined by the valves. The total blood flow depends on the length of movement of the compression plate (stroke volume) and frequency of compression.

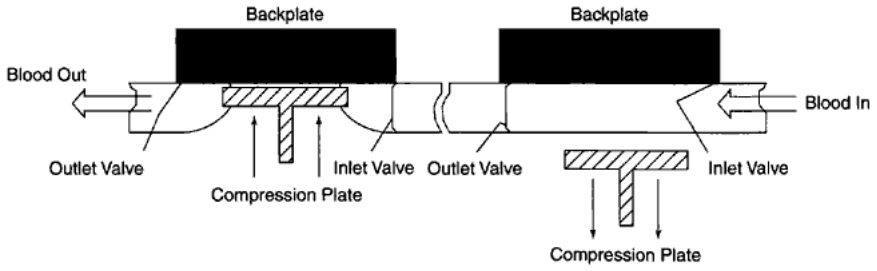

Figure 2.9: Compression Plate Mechanism (Gourlay and Taylor, 2002)

The process of re-filling after blood ejection occurred can be passive or active in nature. In passive filling pumps, a certain amount of pressure is required by inflowing blood at the inlet valve to re-fill the cavity for the next cycle. During active-filling processes, the procedure of refilling is mainly guided by the type of material used. Elastic memory-effect properties allow the tubing to regain to the starting position which during the movement creates a negative pressure at the inlet valve allowing blood to be drawn in.

Despite desirable aspects of the passive filling system such as the prevention of excessively high negative pressures in the circuit or continuous matching inflow and outflow conditions, the preferred mode of pulsatile plate systems seems to be active

filling procedures which have been successfully employed during ECLS (Gourlay, 1997; Sanderson et al., 1973).

Several studies point out the numerous advantages of pulsatile flow compared to non-pulsatile flow on organ perfusion and function of kidney (Kohlstdt and Page, 1940; Hooker, 1910; Many et al., 1967; Nakayama et al., 1963; Mukherjee et al., 1973; Belzer et al., 1968), brain (Sanderson et al., 1972; Taylor et al., 1980; De Paepe et al., Belgium 1979; Briceño and Runge, 1994; Kono et al., 1990), as well as liver and gut (Baća et al., 1979; Saggau et al., 1980; Murray et al., 1981; Pappas et al., 1975; Fiddian-Green, 1990). However, despite their beneficial effects, the general use of pulsatile blood pumps has been hampered by several factors.

Initial designs of pulsatile pump systems were associated with increased thrombolytic events and haemolysis (Di Bella et al., 2000) which have improved with technological advances (Slater et al., 1996). However, further opposing factors for the use of pulsatile perfusion systems are higher cost, bulkier parts, and reduced reliability during operation (Goldstein, 2003; Olsen, 2000).

It is predicted that further research into pulsatile perfusion systems will increasingly display the advantages compared to non-pulsatile pump systems. Coupled with a greater demand would ultimately lead to increased use of designs such as the compression plate and ventricular blood pump.

2.1.5.2 Oxygenation

The oxygenator is the component of the extracorporeal circulation (ECC) that substitutes the function of the patient's natural lungs. However, apart from oxygenation, it performs several other functions such as the elimination of carbon dioxide and the transport of anaesthetics and therapy-related gases in and out of the ECC. Modern

oxygenators also carry integral heat exchangers which perform heating and cooling of the blood with an external heating/cooling system.

Three main types of oxygenators have been developed with several derived forms of each. The main mechanisms are based on film, bubble, and membrane technologies.

Film Oxygenators: The majority of oxygenators used in the early days of ECC were film oxygenators. They all adhere to the same operation method of supplying oxygenation by covering large solid surfaces with a thin layer of blood which is surrounded by an enclosed cavity filled with oxygen.

Surface tension and exposure time between gases and blood as well as haemodynamic flow pattern influence performance characteristics regarding oxygenation and carbon dioxide removal (Dubbelman, 1952; Karlson et al., 1949; Galletti and Brecher, 1962). In film oxygenators, the use of mechanical infusion of oxygen is avoided and thereby reducing the amount of blood trauma. However, due to the greater surface area employed, more priming solution is required (Nose, 1974).

Film oxygenators are further sub-categorised by oxygenation techniques and surface type to screen- and disc oxygenators.

Screen Oxygenators are similar to the design of fins in a heat sink model. In a sealed case, large vertical screens are mounted parallel to each other (Figure 2.10). Venous blood is introduced at the top of the case, allowing to flow down the screens. Oxygen is supplied into the case enveloping the covered screens and permitting gas exchange. A pump is utilised for recirculating blood within the oxygenator for improved oxygenation (Gibbon Jr, 1939, 1954, 1970). Three to 14 screens are used for oxygenation depending on the size of the patient, permitting a flow rate of 500 to 3500 ml per minute. Based on this setup, the turbulent blood flow over the screens

permit oxygenation and carbon dioxide removal of deeper film layers of blood with minimal protein denaturation and air emboli formation. Although blood trauma and post-operative abnormal bleeding occurred in patients using these systems on a regular basis (Moore and Allen, 1958), the degree of trauma was generally less than that of a bubble oxygenators (Nose, 1974).

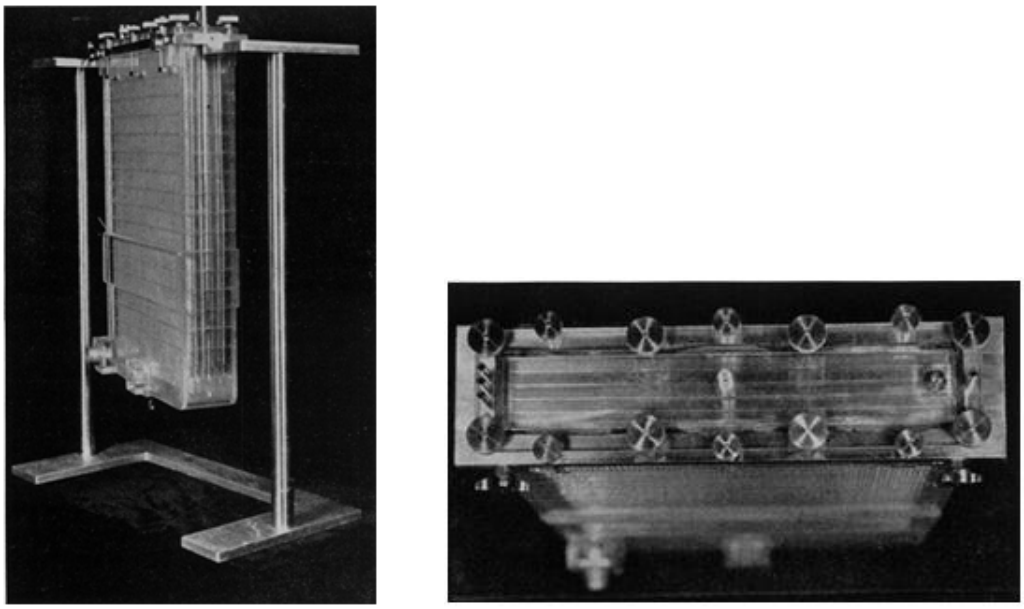

(a) (b)

Figure 2.10: Side and Top view of a screen oxygenator (Miller et al., 1951)

The first oxygenator of this kind was successfully utilised by Gibbon in 1953 which laid the foundation of Kirklin & Jones' research in 1955 for improving this technology which was then employed extensively in surgeries (Kirklin et al., 1955, 1956, 1957).

Disc Oxygenators were developed in order to increase the efficiency of stationary static surface blood filming techniques. This type of oxygenator is similar in operating principle to screen oxygenators by coating surfaces with a film of blood (0.1 to 0.3 mm) which is exposed to a high oxygen environment. Several discs are

centrally aligned on a horizontal axle inside a glass tube capable of spinning up to 120 rpm (Figure 2.11). A gap, maintained by spacers between each disc, allows blood filming when in motion on a surface area of 87.5 square metres (Nose, 1974). Furthermore, a heat exchanger is employed inside the cylinder allowing the regulation of blood temperature during oxygenation.

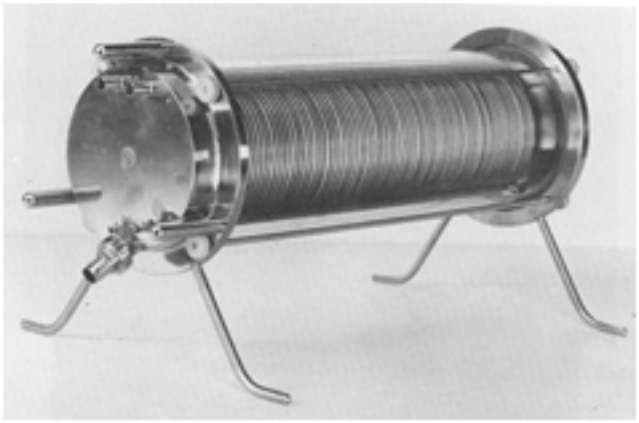

Figure 2.11: Disc Oxygenator with 59 discs of 12.2 cm in diameter spinning at 120 rpm. Materials used for discs: PTFE and silicon. Vents for oxygen- and venous blood inlet were at opposite sides (Cross and Kay, 1957)

The first oxygenator of this kind was built by Bjrk (1948) before being further developed by Cross and Kay (1957). Disc surface modification in 1958 by Kay and colleagues resulted in turbulent blood flow, breaking down boundary layers and improved oxygenation and carbon dioxide elimination. This type of system was in clinical use up until the end of the 1960s (Kay et al., 1958).

Contemprories of Gibbon, Melrose and Aird (1953) developed another kind of disc oxygenator based largely on Björk's design with adequate oxygenation at blood flow rates of up to 3 litres per minute. In his technical setup, 76 plates of Perspex are stacked parallel onto a rotating rod which is positioned 20 degrees to the horizontal (Figure 2.12). Two groups of discs were used which are geometrically different in

nature. One set of annular plates have concentric holes whereas the other comprises of eccentric holes, 2.54 cm off from the true centre. Plates in groups of five are arranged in a way that a cylindrical cavity is formed in a manner of alternating series of platforms and troughs.

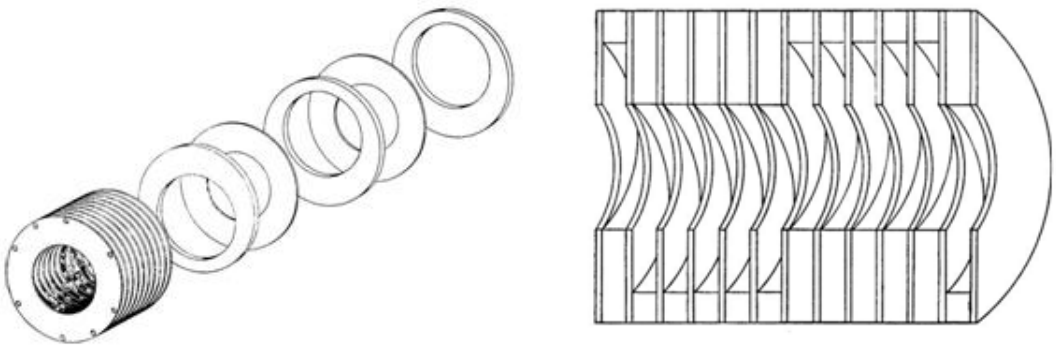

(a) (b)

Figure 2.12: Exploded view (a) and sagittal view (b) of disc oxygenator (Melrose and Aird, 1953)

Passage of blood occurs under the influence of gravity, travelling from one side to the other. As the cylinder rotates, a stream of blood is formed in a cyclic fashion, emptying and re-creating pools of blood. This level of raising and lowering permits a thorough mixing of blood contributing to the exposure of oxygenated gas inside the annular discs.

Maintenance of these disc oxygenators in terms of cleaning and sterilising were reported to be simple and successfully utilised for the first time in 1955 and were used extensively up to the late 1960 (Moore and Allen, 1958).

Bubble Oxygenators: The origins of the bubble oxygenator concept dates back to 1882 (Schröder, 1882). Schröder introduced bubbles into the venous blood for oxygenation for the very first time. Researchers tried to apply this technique in

clinical situations but failed due to excessive foam formation and lack of technological means to eliminate gas before arterial re-infusion. Complications of this kind were resolved by the introduction of silicon defoaming materials in the 1950's.

A bubble oxygenator consists of three consecutive chambers, (1) bubble chamber, (2) de-bubbling chamber, and (3) settling chamber. Gas exchange occurs within the first part, the bubble chamber. Oxygen is injected through a gas sparger consisting of small pores at the bottom of the chamber mixing gas with venous blood. The oxygenated mixture of blood, bubbles, and foam, traverses through to the de-foaming or de-bubbling chamber. It is here where foam and remaining bubbles are removed by a complex of mechanisms including settling, trapping, filtration, or centrifugation. Before re-infusion into the systemic circulation, de-foamed oxygenated blood is buffered in the settling chamber to ensure the removal of all remaining bubbles and simultaneously function as an arterial reservoir.

Due to the direct exposure of blood to gas during this form of oxygenation the trauma particularly in the form of haemolysis caused is among the highest compared to other designs (Nose, 1974).

Variations in form and geometrical constructions led the two most commonly used configurations of bubble oxygenator, linear and concentric bubble oxygenators.

The first prototype of the **linear bubble oxygenator** used in animal studies was developed by Clark et al. (1952) and provided a model for future developments. In his setup, removing excess gas and bubbles in the de-bubbling chamber occurred by surface active substances; a mesh of Teflon, glass beats, and silicon (Figure 2.13).

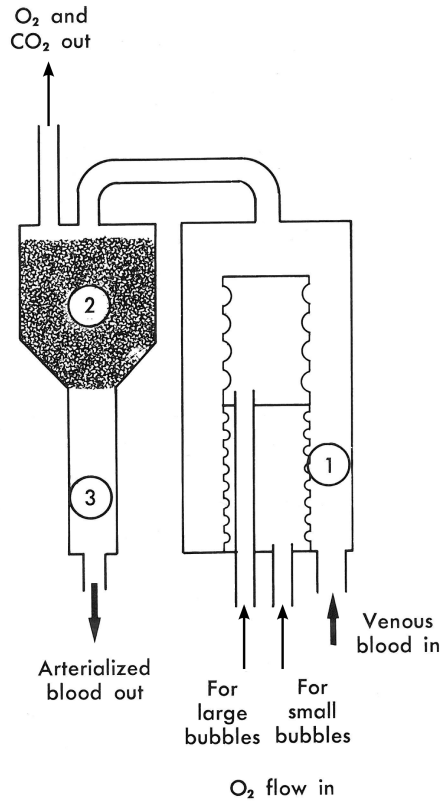

Figure 2.13: First bubble oxygenator; 1) Bubble Chamber, 2) De-bubbling Chamber, and 3) Settling Chamber (Allen, 1958).

An alternative version of the linear bubble oxygenator is the helical reservoir model, developed by DeWall et al. (1956). The working principle is similar to other bubble oxygenators where fine jets of pressurised air form bubbles which during ascent through the column perform gas exchange with venous blood oxygenating and removing CO2 (Figure 2.14). Silicon acts as de-foaming agent, destroying the bubbles inside the de-bubbling chamber before oxygenated blood enters the distinct helical structure of the oxygenator. Any remaining bubbles in this part of the circuit will be trapped at the top of the reservoir coil. The outlet of the arterial reservoir is finally connected to a filter before blood gets re-infused into the patient (DeWall, 2003b).

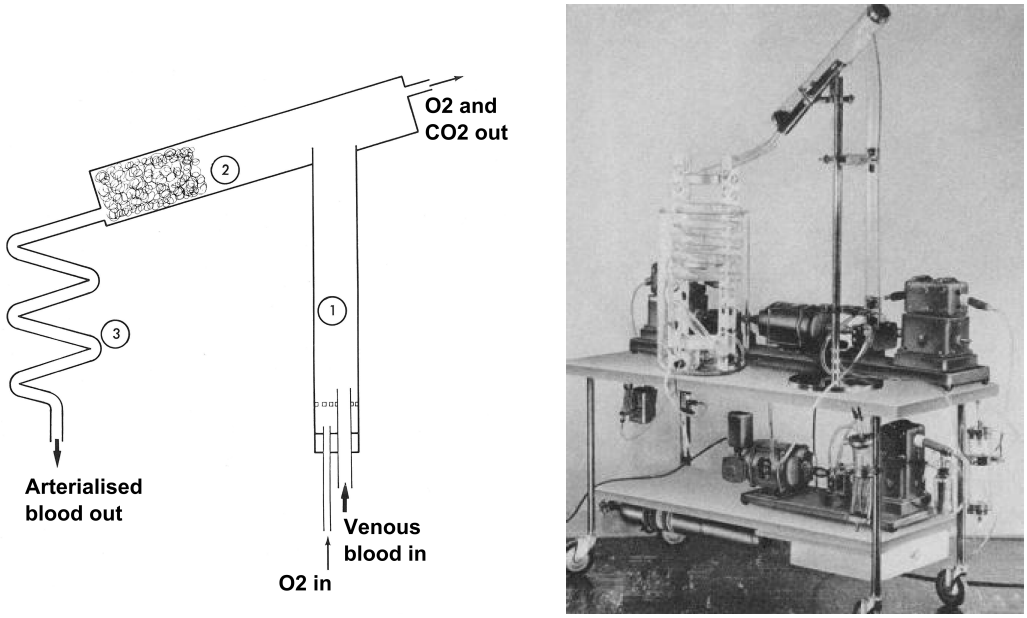

(a) (b)

Figure 2.14: Helical reservoir bubble oxygenator (a) Schematic diagram; 1) Bubble Chamber, 2) De-bubbling Chamber, and 3) Settling Chamber (Allen, 1958). (b) Setup including pumps, oxygen tanks, motors, and filter (DeWall, 2003a).

This system was constructed of disposable materials easily assembled in a modular manner, eliminating the need for cleaning and sterilisation, ultimately leading to the commercially available Lillehei-DeWall-Gott oxygenator (Gott et al., 1957; Gott Vincent et al., 1957; Lillehei et al., 1956), manufactured by Phelan Manufacturing Co. (2029 Washington Ave., Mineapolis, Minn.). The system celebrated a technological breakthrough in artificial organ perfusion leading to increased open heart surgeries in the 1960's and 1970's and is considered as a milestone for future derivatives of this technology (Iwahashi et al., 2004b).

In 1952, Gollan introduced the **concentric bubble oxygenator**, a more compact form of the bubble oxygenators based on the same three-chamber principle (Gollan

et al., 1952), see Figure 2.15. A series of advantages is accompanied due to the compact form compared to alternative bubble oxygenators. Reduction in size resulted in less foreign surfaces, reduced priming volume and heat loss, increased rigidity and convenience for autoclaving and sterilisation. Furthermore, temperature loss is compensated by a glass spiral supplied by a separate water circuit providing heat to the ascending blood in the oxygenation cylinder.

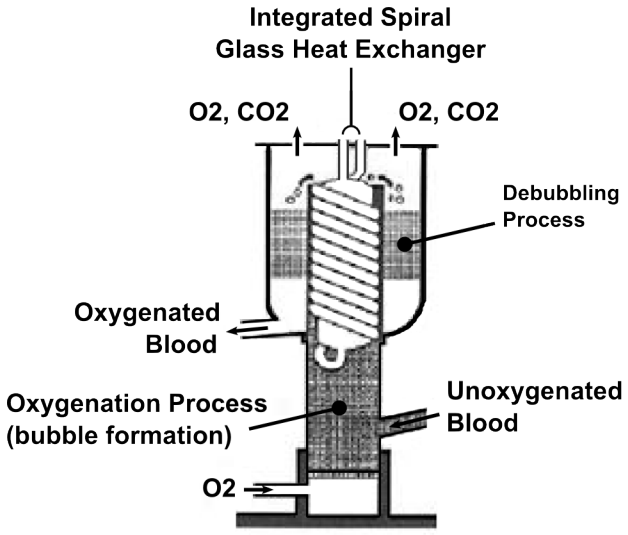

Figure 2.15: Gollan's design of the concentric bubble oxygenator (Gollan et al., 1952)

All bubble oxygenators were based on the fundamental works by Clark, De Wall, Lillehei and Gollan, with many derivatives following the same basic form.

Membrane Oxygenator: Despite successful implementation of DeWall's bubble and Gibbon's screen oxygenator, direct blood-gas exposure still imposes a risk of emboli and protein denaturation thus limiting their use for long-term support (Mirsky,

1941). A technique which avoids a direct blood-gas contact would appear to be more appropriate from the therapeutic perspective, similar to human lungs.

The working principle is established through a physical barrier (membrane) which separates the blood from the gas phase at all times. Gas exchange occurs by the process of diffusion which has several dependencies: (1) gas membrane configuration (Waack et al., 1955; Bell and Grosberg, 1961). The use of membrane oxygenators offer several benefits and eradicate some of the problems encountered with the other types of oxygenators. This indirect contact minimises the risk of air emboli formation and simultaneously makes de-gassing redundant (Iwahashi et al., 2004b). Also, red blood cells, platelets, and leukocytes are less traumatised (Hopf et al., 1962). Owens et al. (1960); Lee Jr et al. (1961) suggest that fat and protein molecules exhibit less denaturation during oxygenation.

Three categories of membrane oxygenators are available; (1) plate type, (2) coil type (3), and capillary type. Differentiation between these types is based on geometry, assembly, and structure.

The first **plate type** of membrane oxygenators, built by Clowes Jr et al. (1956), was based on the original design of Skeggs-Leonards plate dialyser in 1949 (Skeggs Jr, 2000), (Iwahashi et al., 2004b). Clowes' device had 50 flat ethyl cellulose membranes stacked on top of each other, creating a surface of approximately 25 square meters sufficient for adult perfusion which proved successful in a series of cardiac surgeries in 1958 (Clowes and Neville, 1958).

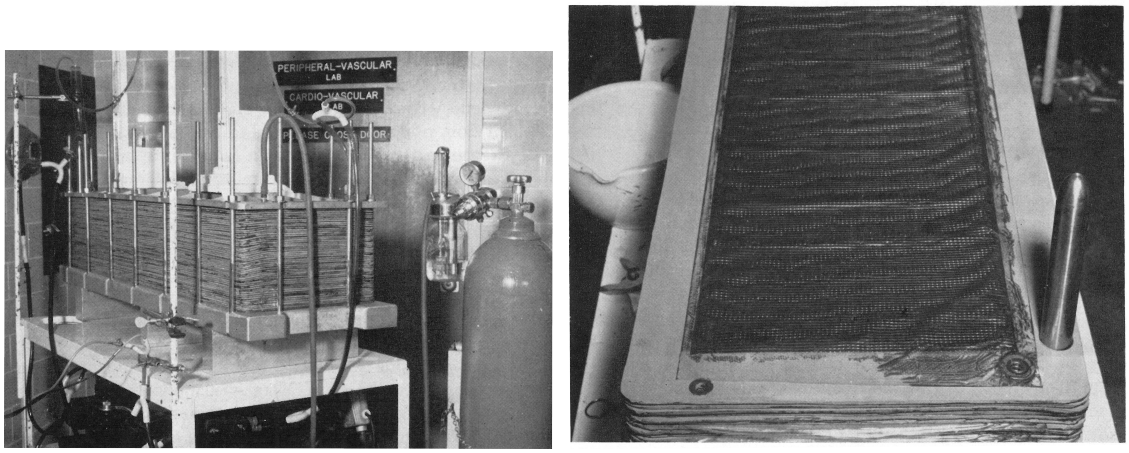

(a) (b)

Figure 2.16: Plate type membrane oxygenator (Allen, 1958). (a) 50 flat membranes in layers amounting to 25m^2 surface area. (b) Oxygenator being disassembled displaying blood-filled membranes.

His design was further developed by Lande and colleagues in 1968 who were able to increase oxygenator efficiency by altering blood flow performance and assembly design (Landé et al., 1968).

In 1965, Bramson et al. developed a plate type oxygenator with integrated heat exchange functionality which found high acceptance in clinical fields despite higher priming volumes (Bramson et al., 1965).

In 1963, Kolobow and Bowman configured a coiled type membrane structure in which a flat silicon membrane tube supported by fibreglass mesh was used for oxygenation (Kolobow and Bowman, 1963). Blood would traverse between the sheets parallel to the centre of the coil while oxygen flow is supplied within the spiral under negative pressure.

For the very first time, a device was capable of perfusing a patient adequately over prolonged periods of time with minimal trauma. Kolobow's device was successfully used in prolonged perfusion on adults (Hill, 1977) and neonates (Bartlett et al., 1976).

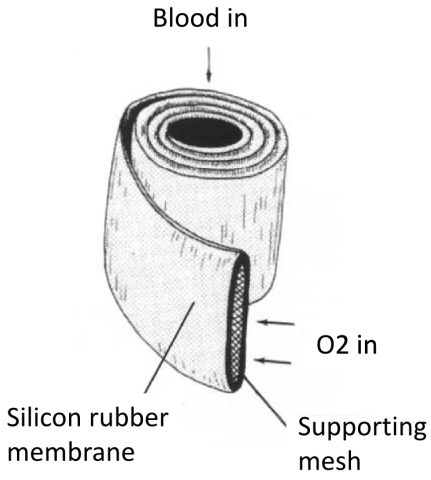

Figure 2.17: Coiled membrane oxygenator based on Kolobow's principle (Iwahashi et al., 2004a).

To this day, Kolobow oxygenators are still commonly used for ECMO (Lawson et al., 2008).

Capillary type oxygenators are based on microporous microtubes arranged in either shell-and-tube or cross-flow configuration (Figure 2.18a). In the former, blood passes within the hollow bundle of microtubes whereas gas flows over the fibres in countercurrent fashion. It was Wilson and colleagues who developed this type of hollow fibre membranes in 1965 (Nose, 1974) based on Bodell's designs (Bodell et al., 1963). However, detrimental effects such as increased pressure requirements due to high blood flow resistance and thrombus formation of the intra-luminal setup lead to the development of the inverse assembly, the extra-luminal mesh-like structure (Drummond et al., 2005), shown in Figure 2.18b. Here, blood passes over the fibres and ventilating gas is circulated through the tubes.

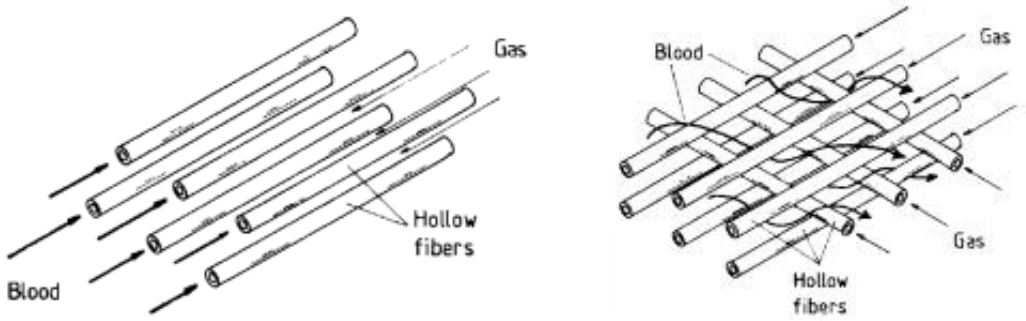

(a) (b)

Figure 2.18: (a) Intra-luminal setup where blood flows through the capillaries surrounded by gas, (b) extra-luminal setup with inverse configuration. (Gaylor and Hickey, 1994)

Early devices proved to be unsuitable for clinical use in the long term setting due to plasma leaking into fibres after 8 to 12 hours of operation, severely reducing oxygenation efficiency (Eash et al., 2004). The time required for ECMO therapy lies beyond the limitation of 12 hours and this key factor needs to be recognised in any oxygenator design.

The new generation of capillary membranes contain additional non-porous hydrophobic layers in which gas exchange occurs only by diffusion circumventing the problem of leakage, thus making the extra-luminal setup the preferred configuration (Eash et al., 2004).

Instead of silicon rubber used for previous models of the capillary type membrane, the development of hollow fibre technology has gained increasingly more importance. The use for respiratory assist devices based on hollow fibre technology has continued to grow from 3 percent in 2002 (Lawson et al., 2004) to 18 per cent in 2008 (Lawson et al., 2008) and 80 per cent in 2011 (Lawson, 2011). The disposable compact form provides low resistance to flow and better surface to volume ratios which helps to reduce the

need for large amounts of priming solution, essential for open heart surgeries and especially in neonatal ECMO (Clowes, 1960; Sirotkina et al., 1970).

2.1.5.3 Heat Exchanger

Relative short periods of decreased body temperature, such as experienced during CPB procedures, are tolerated by the patient without detrimental effects. However, ECMO therapy sometimes can take up to several weeks in order for recovery to occur which ultimately requires maintenance of normothermic levels as neither uncontrolled hyperthermia or hypothermia are beneficial for the patient. The two main reasons for keeping temperature values at normal levels are (1) to avoid interfering factors which can cause undesirable effects such as alterations of acid-base and organ functions, potentially negatively influencing therapy outcomes as discussed in Chapter 1 and (2) to allow a comparison and application of haemodynamic and metabolic criteria to a so-called baseline or physiological state.

Therefore, the heat exchanger is considered to be one of several key components in ECMO besides the pump and oxygenator. The heat exchanger is able to compensate for deviations from normal temperatures whether triggered by physiological conditions or extrinsic factors such as ambient temperature.

Ambient temperatures in clinical settings are assumed to be below normothermic levels and in the majority of cases, blood requires re-warming, compensating for systemic heat losses. The heat exchanger is typically situated after the membrane oxygenator within the extracorporeal circuit for two reasons. (1) A substantial amount of heat is lost to the environment induced by surface area exposure within the circuit. Additionally, the blood is ventilated with cool oxygen and carbon dioxide gas flow further introducing heat loss. Both aspects are exacerbated during low

flow conditions requiring temperature compensation before arterial infusion. (2) Although not primarily designed for, the heat exchangers can prevent the progression of possible air emboli within the circuit.

The first commercially available heat exchanger was jointly developed by engineers at General Motors Corporation and researchers at the Duke University Medical School in 1957 in order to reduce the time for inducing hypothermia required in CPB patients before surgery and allow controlled rewarming afterwards (Emmons and Sacca, 1958).

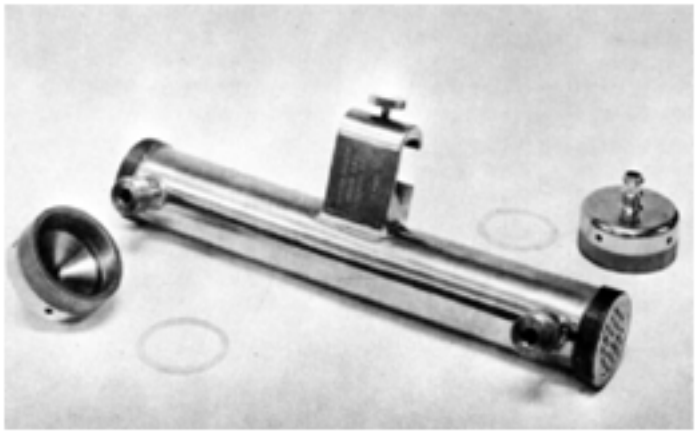

Figure 2.19: First shell-and-tube heat exchanger

The setup of this heat exchanger entailed a cylinder surrounding 32 narrow pipes passing through from top to bottom. Two valves are mounted onto the sides of the cylinder jacket allowing water to enter the interior, circulating around the narrow pipes. The bottom and top end of the heat exchanger allow for blood entry and exit, respectively. As blood runs through slender pipes, thermal energy of the surrounding water is provided for heat exchange by concurrent flow.

Simply put, concurrent flow exists where two mediums, blood and water, enter at the same side of the heat exchanger and traverse parallel (Figure 2.20). Both liquids are separated by a solid thermoconductive wall of stainless steel during passage,

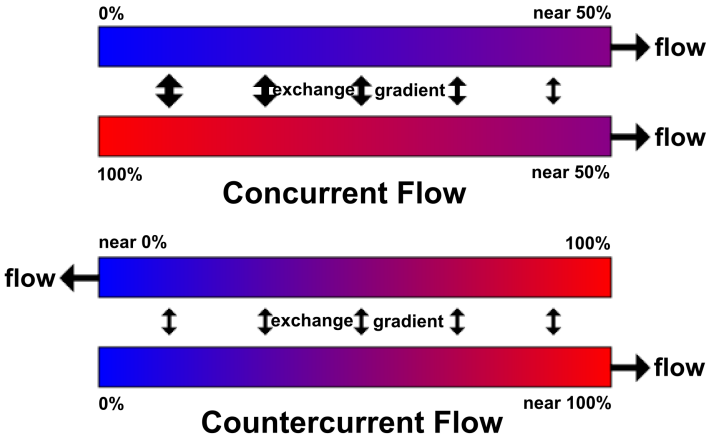

Figure 2.20: Mechanisms of counter-current and concurrent flows in heat exchangers

establishing the exchange of thermal energy through the mechanisms of convection. The primary medium, the blood, is controlled by the secondary medium, the water. Generally, however, greater efficiency and heat transfer rates can be achieved with countercurrent exchange, where both fluids enter and exit at opposite sides of the heat exchanger. Countercurrent heat exchangers are therefore the preferred and most utilised devices.

Temperature regulation is established by mixing ordinary cold and hot tap water at the bottom of the heat exchanger. Temperature can be pre-set by a thermal regulator valve influencing the average water temperature. Two thermistor probes applied to the system detect the temperatures of the water and inform the operator by a visual display, adjustments can then be made responsively to reach desired values.

The conventional design of heat exchangers have undergone only minor changes since commercialisation in 1957. Mainly the core materials of oxygenators have been changed from aluminium to stainless steel after apparent events of aluminium contamination in capillary beds of neonates (Vogler et al., 1988; Braun et al., 1988). However, the fundamental functionality between the models of heat exchangers in 1957 and

2011 have not undergone a paradigm shift. A survey conducted on equipment usage 36 years after commercialisation of the first heat exchanger demonstrated that 79% of ELSO enlisted ECMO centres used Avecor's *ECMOtherm*, 9% Electromedics, 4% Gish, and 6% alternative models (Hultquist et al., 1993). The same models are still being employed in ECMO centres around the globe. An excerpt of heat exchangers currently used in active centres is officially listed with the ELSO (ELSO, 2016).

Avecor's *ECMOtherm* also comprises of a tube-in-shell design similar to the General Motors/Duke University model in 1957. Blood flow is allowed to flow through 7 narrow stainless steel pipes coated with a silicon polymer for biocompatibility. Water, or any other liquid with sufficient heat capacity, flows around the slender pipes in a countercurrent manner influencing blood temperature. Model D1079 from Electromedics diverts water through a fin-type steel core. Blood flow between core and a polycarbonate shell permits visibility to the operator. Temperature measurements are made available through tabs at blood in- and outlet valves. Models HE-3 and HE-4 from Gish both accommodate a helical stainless steel core through which water is directed on the inside and blood on the outside. The temperature of the blood can be monitored at the outlet ports of the HE-4 model.

Even the latest commercially available heat exchangers by Medtronic such as the ECMOtherm II™ incorporates the same principles applied decades earlier. A cylindrical shape in which blood absorbs thermal energy by means of convection supplied by a separate water circuit requiring a heater/cooler systems. Technological advances merely lie in geometry which influences fluid performances of both blood and water phases, material changes to imporove biocompatibility, and design changes for more accessibility.

Figure 2.21: Medtronic ECMOtherm II™ shell and tube heat exchanger

A trend is seen towards a more compact disposable design of heat exchangers which are incorporated into oxygenators reducing blood surface contact and equipment maintenance.

Generally, devices differ by dimensions, geometry, material, and accessibility which all influence performance. These changes are in response to express clinical requirements. However, in most cases, control does not take place at the heat exchanger. It merely constitutes the place where heat transfer occurs with control as an external function being part of the system control mechanism.

Additional equipment is required for controlling the water temperature which ultimately affects the blood. This device termed heater/cooler unit is a water bath that is externally connected to the heat exchanger through a hydraulic circuit of tubes. Water is then pumped through the closed circuit providing thermal energy to the blood at the heat exchanger interface while continuously controlled inside the

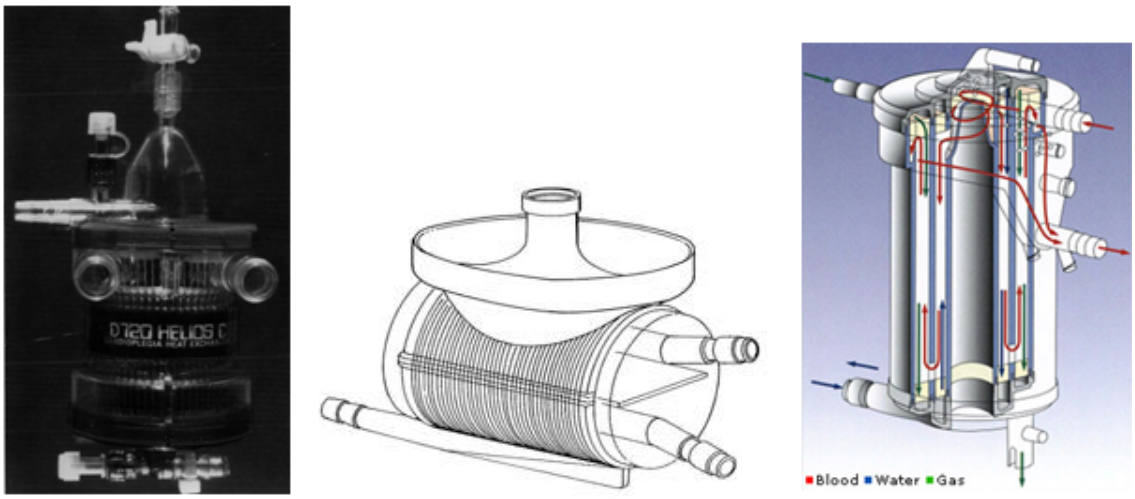

(a) (b) (c)

Figure 2.22: Compact Heat Exchangers build into oxygenators. a) Dideco Helios D720 Heat Exchanger b) Avecor Heat Exchanger c) Medos HILITE® 7000 Hollow Fibre Oxygenator with integrated heat exchanger

heater/cooler unit to compensate for heat loss. Ports for feedback purposes are available which monitor the water temperature, blood temperature or both, depending on the location of sensors and configuration of the system.

The CritiCool™ system (The Surgical Company, 2006) produces a range of products and components that measure the water temperature inside the water bath whereas Medtronic's ECMOtherm-II incorporates a temperature monitoring adapter which is attached to the housing of the heat exchanger, measuring the direct effects of heat transfer (Hirtz, 2006, 2007, 2009) . Other systems such as the ECMO-Heater® from CSZ Medical and Allon™ (MTRE Advanced Technologies) offer sensor connections for skin surface probes as well as esophageal/rectal probes as their feedback parameters.

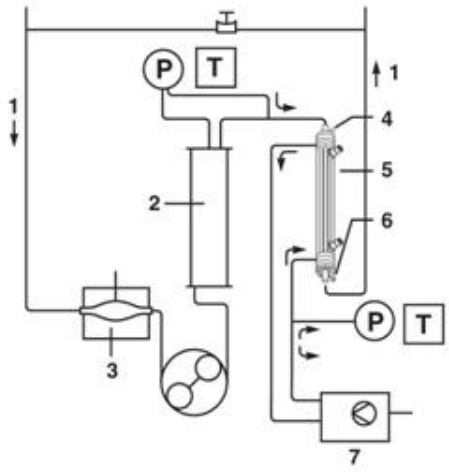

Figure 2.23: Medtronic ECMOtherm-II™ example circuitry: 1. Blood Flow 2. Oxygenator 3. Assist Reservoir 'Bladder' 4. Luer Lock Fitting 5. Heat Exchanger 6. Temperature Monitoring Adapter 7. Heated Water Supply

Figure 2.24: Heater/Cooler system in clinical application

2.1.5.4 Other ECMO Components

Several other devices are required during ECMO procedures besides the three main active components - pump, oxygenator, and heat exchanger - discussed above. These include cannulas/catheters, tubing, and safety/monitoring devices which will be discussed if required.

2.2 Control Aspects in ECMO

2.2.1 Initial Control Approaches

The first heart-lung machine ever to be clinically employed was John Gibbon's apparatus, jointly developed by International Business Machines (IBM) engineers. Unfortunately, the first two patients diagnosed pre-operatively with arterial septal defect (ASD) and right atrial tumour died during the operation (Romaine-Davis, 1991; Shumacker, 1999). However, in May 6, 1953 the first successful patient treated with a heart-lung machine (IBM-Gibbon) was the 18 year-old Cecelia Bovalek who underwent an ASD repair (Gibbon Jr, 1954).

Figure 2.25 shows the components used in the IBM-Gibbon apparatus. Mainly roller pumps were used in this setup, based on DeBakey's original model described above, but with slight modifications. Pumps E and F are both AC driven incorporating variable gears for greater torque at reduced speeds whereas pump K still depends on a DC motor for operation.

Previous DeBakey pumps incorporated a pulsatile component which under high flow and moderate suction induces fluttering in the vein up to a point of possible vein collapse, ultimately interrupting blood flow into the ECC (Miller, 2003). To circumvent this problem, Gibbon and IBM engineers decided to introduce a separate

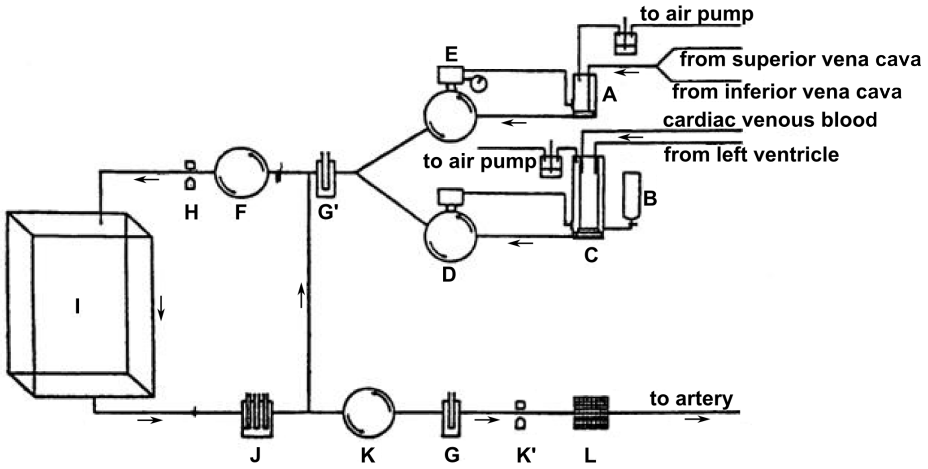

Figure 2.25: Schematic drawing of IBM-Gibbon heat lung machine Model II (Miller et al., 1953)

collecting chamber A, in which venous blood was drawn under constant mild hypobaric pressure. From there the pooled blood is subsequently pumped through to the oxygenator via pump E and F and back to the patient via pump K.

One of the important aspects of any mechanical heart and lung apparatus pointed out by Gibbon Jr (1954) is the maintenance of constant fluid volume at any rate of blood flow, i.e. output of the extra corporeal system must match the input. Failure to supply a constant volume of blood might result in fluid imbalance leading to accumulation of blood in the ECLS circuit possibly voiding the patient's vascular system as well as inducing hypotension. Similarly, reduced unbalanced volumes in the ECLS would result in excessive accumulation of blood in the subject's vascular system. Gibbon's approach was to identify those parts of the system which can vary in blood volume and subsequently implement control procedures to maintain a constant capacity. He recognised three places within the circuit, (1) the venous blood reservoir A, (2) the blood film thickness on the screens of the oxygenator, and (3) the blood

level at the bottom of the oxygenator chamber I, all of which were equipped with control architecture.

The control strategy for measuring the level of blood at the bottom of the venous collecting chamber A is performed by a capacitive sensor. The blood at the bottom of the chamber represents one conductive plate of the capacitor whereas a fixed electrode attached to the case the opposite plate, separated by the plastic housing as the dielectric material. The capacity between blood level and fixed metal electrode is part of a wider electrical circuit forming a tuned 10.7 MHz oscillator. Variations in blood levels directly affect the overall capacity which results in proportionally changing frequencies. Measured deviations from the tuned radio frequency are recognised, amplified, and transferred to push-pull thyratrons, thereby providing power to the venous AC motor E. Decreasing levels of blood automatically decreases the rotational speed of the pump. Similarly, when the level rises, the pump speed increases proportionally. Consequently, venous blood flow is fully controlled by the level of blood inside the collecting chamber. The operator was only required to adjust the knob to desired values with actual flow parameter being displayed at a dial.

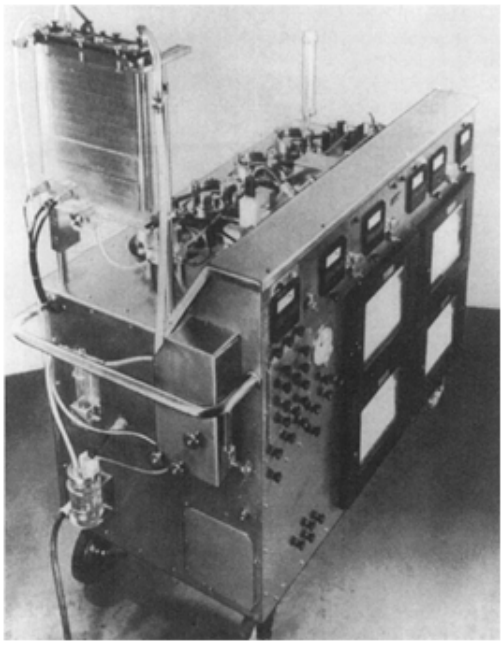

Figure 2.26: IBM-Gibbon Hert-Lung Machine Model II (Romaine-Davis, 1991)

The second place within the ECLS circuit which is subject to blood volume variations is the oxygenator. Specifically affected are blood film thickness on the six stainless steel screens and level of accumulated blood at the bottom of the oxygenator. To control the thickness of the blood film, an additional pump F was incorporated which recirculates accumulated blood from the base of the oxygenator back to the top at constant pump speed greater than the venous pump. This design forces blood, which comes from the venous pump, through the oxygenator before being returned back to the patient. A pressure transducer H incorporated at the outlet of the recirculation pump establishes the maintenance for constant blood flow to the oxygenator. Due to the constant rate of the recirculation pump (which is greater than the sum of pumps E, D, and K), the thickness of the blood film never varies.

To ensure equal amounts of blood to be withdrawn and re-infused from and to the patient, respectively, the arterial pump K also requires control features. In order

not to exceed arterial pressure of 300 mmHg, a separate pressure transducer K' was required for monitoring and safe servo-regulation.

Blood temperature was monitored in venous and arterial lines, G and G'. However, the heat exchanger size requirements turned out to be insufficient for perfusion blood flow rates which lead to temperature gradients above tolerant limits and ultimately resulted in excessive haemolysis (Kurusz, 2012). Therefore, Gibbon decided to discontinue the use of a heat exchanger in subsequent studies.

2.2.2 Further Control Strategies

Automation became relevant in the ECC as soon as CPB and later ECMO procedures were performed successfully. The goal was to increase safety and efficiency aspects of the system starting with the oxygenator volume control. Two parts are included in that process, 1) measurement of the actual blood volume/level inside a reservoir and 2) provide that information to the pump for controlling the speed parameter.

Several techniques and strategies had been proposed for measuring the blood levels in reservoirs. Olmsted et al. (1958) introduced the capacitive sensor model described above in Gibbons' heart-lung apparatus. Crafoord et al. (1958) proposed the idea of a floater inside the reservoir. Alternatively, a photocell was attached to the housing of the oxygenator reservoir receiving rays from a light source at the opposite side (Kantrowitz et al., 1959). Kantrowitz's proposed technique was specifically designed for disc oxygenators where a light beam passes through the case of the chamber onto a cadmium sulphide photocell. The amount of light received depends on the level of blood inside the oxygenator. The photoconductive element behaves like a variable resistor with changing electrical conductivity depending on the amount of

light received. The signal which describes a function of blood volume inside the oxygenator is amplified and forwarded to the arterial pump for potential changes during perfusion. According to Kantrowitz et al. (1959), the damped and extremely stable electrical system allows detection of blood increments of 50 cc in order to precisely manage the volume of blood in the oxygenator.

All three methods mentioned above were used to feedback the arterial pump for speed adjustments according to blood levels. However, the techniques relied heavily on the design of the oxygenator. Irregular reservoir shapes in more advanced models complicated the measurement in terms of accuracy which led to a discontinuation of this approach. Moreover, the floater design exposes blood to additional foreign surfaces possibly contributing to fibrin degradation and thrombi formation. An abstract approach to pump control was chosen by Moss (1961) who considered the patient's weight as a reference value. He assumed blood volume inside the systemic circulation and extracorporeal circuit remains constant at all times except for blood transfusions and haemorrhages in the operative field which both can be weighed by scales. The rationale behind is that a shift in blood volume would reflect a change in body weight and ultimately influence pump speed to restore a state of equilibrium. However, this method does not provide enough information to be able to distinguish pooled blood from circulating blood, nor does it consider fluid shifts caused by oedema.

In 1962, Lewis et al. (1962) developed a simple technique for influencing arterial pump speed. Venous blood would be collected in a flexible plastic bag (also referred to as bladder box) with electrodes on the outside. This collapsible bag would fill with blood and expand during operation thereby closing the two electrodes. As part of a wider electrical circuit, a relay would be activated and subsequently turn on the arterial pump for initiating re-perfusion. This allows the bladder box to deflate

again, thereby losing electrical connectivity and interrupting power to the pump. A waveform-type 'on and off' signal would alternately activate and deactivate a switch which in turn starts and stops the pump. The operator had visual control of the blood level within the reservoir allowing to manually adjust desired average speed settings.

A venous pump, placed in the venous in-flow aspect of the circuit, in the manner deployed by Gibbon, offered another control strategy. One possible method of draining venous blood from the patient has been discussed with the introduction of Gibbon's heart-lung apparatus; by the use of a venous pump in conjunction with a venous reservoir. Alternatively, instead of using this method with its inherent contribution to blood trauma, venous blood can also be drawn into the ECLS circuit by gravity. The accumulation of blood in the bottom of the oxygenator serves as the venous reservoir. The relative vertical level of the patient compared to the artificial circuit requires being elevated to take advantage of gravity induced blood flow.

Kantrowitz and colleagues introduced such a gravity system with a fixed elevation of 75 centimetres of patient to ECMO circuit (Kantrowitz et al., 1959). A motor driven occluding clamp on the venous side effects changes to blood flow rates depending on the patient's venous pressure status. A separate catheter is placed at a superficial vein reaching into the inferior venae cavae through which a sealed mercury manometer was attached. Two electrodes are inserted into the manometer in such a manner that when predefined pressure readings are reached, the motor is subsequently turned on by a simple relay circuit (venous flow controller) which makes adjustments to the clamp position and thereby influencing the amount of blood removed from the venae cavae. A fall in measured venous pressure closes the clamp 1/8 of a turn to reduce extracorporeal blood flow whereas the opposite procedure occurs

during elevated venous pressure readings. The interval for sequential measurement and execution of control procedures amounts to 8 seconds. A similar setup for venous drainage was introduced by Roche et al. (1964), in which an electro-mechanical system was established to automatically alter the height of the venous reservoir relative to the level of the patient thereby influencing blood flow dynamics such as pressure and flow. This type of automatic venous reservoir control allows the pump operator to fully concentrate on bubble-free blood supply to the patient without the otherwise time consuming and inaccurate adjustment of blood flow. Unfortunately, the publication of Roche et al. (1964) contains very limited technical description of the architecture and no comments were made by the authors regarding control mechanisms.

Literature on automation on heart-lung machine components is scarce from the early 1960s to late 1980s when a new era of research on automation begun, mainly aided by computerisation (Barthelemy et al., 1984). First attempts were made involving computers in patient data acquisition and monitoring (Janssenswillem et al., 1984; Janssenwillem et al., 1985; Riley, 1981; Berg and Knudsen, 1988) before Chauveau et al. (1990) introduced what appears to be for the first time a computer-integrated heart-lung machine which automated and controlled the processes of several extracorporeal components as well as monitored patient perfusion data. The computer was used to control the blood level inside the reservoir, make changes to venous tube occlusion, and adjust the arterial pump speed settings. However, the technological principle of measuring the blood level has remained unchanged. Chauveau and colleagues used the same technique developed 25 years earlier by Anderson and his team by which an electrode was used to determine the blood capacity (Murray et al., 1965). However, on this occasion control is achieved by

a software algorithm instead of electronic circuits. Most problematic were non-linear behaviours due to irregular shaped oxygenators. A proposed solution to this problem was the individual calibration and configuration of these to be compatible with a broad range of oxygenator designs. However, this idea seemed unrealistic due to increasing numbers of commercially available oxygenators. Consequently, oxygenator geometries were averaged which resulted in a more general approach to control design compromising between precision and stability. Only a suboptimal proportional-type level control was achieved with compromising accuracy in high flow rates. Integral gain was considered but failed in implementation due to oscillation problems derived from oxygenator deviations. In addition, noisy signals did not allow a derivative term, leaving level regulation with only proportional action when commanding arterial pump rates to adapt to venous blood amounts. Similarly, venous tube occlusion was implemented by the same mechanism -a screw clamp- proposed 31 years earlier by Kantrowitz et al. (1959); except this time a computer would control the closure of the screw clamp by means of a stepper motor. Control signals are supplied to the motor by the level regulator, changing tube diameters and thereby influencing blood flow. Both automatic modules, level regulator, and clamp are coupled into a microcomputer aiming for constant amounts of blood inside the patient.

In 1990, Beppu et al. introduced their automated system in clinical surroundings (Beppu et al., 1995). Their computer sampled data from reservoir blood level sensors, collapsible venous bag sensors, and CVP and aortic pressure (AoP) transducers at intervals of 0.1 seconds. Venous pump and arterial pump speeds are subsequently controlled according to algorithm outputs.

Assisted venous drainage, that relies on a roller pump, requires a compensating bladder box mechanism to prevent the negative effects of excessive vacuum. The collapsible bag operates on the same principle as proposed by Lewis et al. (1962) 28 year earlier. Several photoelectric switches mounted on the outside of the small vinyl bag allowed the detection of vein deflation and collapse thus initiating computer-based counter actions, such as reduced flow rates, to restore blood flow and minimise repetition of collapse.

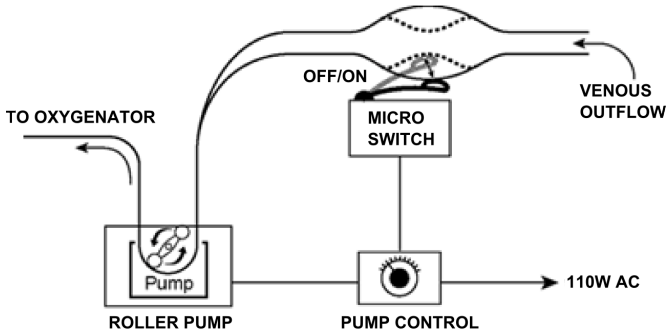

Figure 2.27: Bladder servo-controlled venous pump (Meyer and Jessen, 2000)

A detected fall in reservoir blood volume initiates a reduction of both venous and arterial pump to 80 percent. Further reduction of reservoir level below the minimum leads to pumps being halted until sufficient volume is present again.

Other safety features of Beppu's automated system are filtration of procedure-induced sudden disturbances which interfere with recorded pressure values possibly leading to dangerous flow changes. Additionally, improper sensor outputs can be recognised by algorithms which results in maintaining previous correct flow rates. Warning messages appear to inform the perfusionist of approximate location of faulty equipment and pumps can automatically shut down in case adverse conditions are detected. Beppu and colleagues considered their control system of comparable quality

to the ability of a skilled perfusionist, although no control scheme was mentioned regarding oxygenation.

In 2006, Litzie and her colleagues patented a concept for extracorporeal circulation which gives the impression of being more automated in controlling safety procedures rather than perfusion (Litzi et al., 2004). The difference between a safety system and automated control system is that the former waits for certain triggering even to occur with a subsequent action to compensate the issue. The latter manages the machine within certain boundaries, with the goal of preventing a triggering event altogether.

Further feedback mechanisms in the extracorporeal sector have been developed in recent years. Schwarzhaupt et al. (1998) proposed a model-based control suitable for pulsatile and non-pulsatile perfusion (Misgeld et al., 2005). Other researchers emphasised more on stable control with less attention on speed and complexity (Anbe et al., 1992; Nishida et al., 1995).

2.3 Pathophysiology Associated with ECMO Technologies

In contrast to physiology in which organ and cell functions are viewed under healthy conditions, pathophysiology deals with abnormalities and alterations from the optimal state. The highly invasive nature of the ECMO procedure with its mechanical and pharmacological influences coupled by the underlying pre-existing disease invokes pathophysiological processes which result in alterations of major organ functions.

2.3.1 The Artificial Environment

Haemodilution One of the tasks required before initiation of ECMO is the priming of the extracorporeal circuit to extrude all captured air. This can be done with a colloid solution, isotonic saline, or donor blood. The priming solution is added into the circuit mixing with the neonate's blood, inevitably leading to haemodilution and reducing viscosity in the case of crystalloid and albumin. Additionally, priming the blood with solutions other than donor blood results in reduced haematocrit values and risk of oedema formation. Alternatively, using donor blood may increase the risk of transfusion reactions. Keeping the size of the extracorporeal device to a minimum reduces the priming volume markedly. A circuit volume of 400-500 ml already exceeds the neonate's blood volume twice (Hirschl and Bartlett, 1987).

Haemolysis Turbulence, cavitation, and shear stresses contribute to the breakdown of erythrocytes during ECMO (Leverett et al., 1972). Haemodynamic or immunological response to haemolysis is negligible; however, Hb-content carried by the RBC is redistributed to blood plasma after destruction, where binding to haptoglobin occurs depending on the saturation capacity. Excess haemoglobin is excreted by the kidneys with rare clinical manifestation of erythrocyte deficiency (anaemia).

Artificial Surface contact of the blood leads to multiple complex biochemical reactions involving activation of contact system, intrinsic coagulation pathway which is believed to be a major contributor to coagulation, complement system for stimulating lysis of cell membranes and cell death, deteriorating of platelet function and count (Edmunds Jr et al., 1982). Activation of these contact-induced reactions result

in fibrin formation and thrombocytopenia which - together with other circulating elements such as lipoprotein, platelets, leukocytes, and erythrocyte fragments - can form thrombi (Edmunds Jr and Williams, 1983). Detached and circulating thrombi (emboli) are difficult to detect and once inside the human circulation can lodge in small capillaries and arterioles inhibiting vital blood supply to tissue and organs. Prolonged obstruction to blood flow may result in organ dysfunction, affecting filtration capability of kidneys, induce strokes, and on a greater scale contribute to systemic inflammatory response or post-perfusion syndrome (Horowitz and Lally, 1995). Especially prone to thrombus formation within the artificial circuit are areas of turbulent and stagnant flow mostly appearing at cavitation sights and constrictions (Goldsmith and Turitto, 1986).

The systemic transfusion of **heparin** and use of heparin-coated surfaces help to reduce thrombotic event during ECLS (Splittgerber et al., 1985). This anticoagulant inhibits components of the complement system which are required to form insoluble fibrin during the process of coagulation (Chenoweth et al., 1981). The resultant prolongation of clot formation increases the risk of haemorrhages at surgical sites and open wounds contributing to possible blood reduction. The deficiency of platelet number and function as well as heparin and fibrinolysis can all contribute to bleeding complications during ECLS (Zapol et al., 1979). General ELSO guidelines suggest an initial heparin bolus of 50-100 units per kg body weight at the time of cannulation with subsequent infusions depending on the measured activated clotting time (ACT) levels (ELSO, 2014). A drop in ACT to 300 seconds or below advises dosages of 7.5 - 20 units/kg/hr whereas ACT levels of 180 - 220 seconds recommends heparin infusion rates of 20 - 50 units/kg/hr. Deviations from these guidelines may either

increase the risk of bleeding or contribute to clot formation depending on the amount administered.

Changes in **haemodynamics** are the direct result of using pump systems which exhibit non-ideal performance characteristics with respect to the human heart. The ideal mechanical pump, therefore, should include properties such as negligible haemolysis, pulsatile flow, and adjustable ejection rate inspired by physiological qualities. However, despite technical efforts in recent years, the two most commonly employed mechanical pump systems, the roller- and centrifugal pumps, do not offer pulsatile blood flow and induce haemolysis caused by shear stresses and turbulent flows. Roller pumps reportedly induce more spallation while reducing haemolysis (Göbel et al., 2001) whereas opposite effects are expected from centrifugal pumps (Orenstein et al., 1982). Additionally, resistance and impedance properties of individual components between pump and arterial line catheter have to be taken into account when physiological pressure characteristics are generated as they influence haemodynamic properties.

Pulsatile vs. non-pulsatile perfusion has been a matter of debate for some time (Mori et al., 1988; Brandes et al., 2002; Song et al., 1997; Driessen et al., 1995; Fiedler, 1981) . Under healthy conditions with no interfering factors such as hypothermia, haemodilution, or anaesthesia, reportedly no differences between pulsatile and non-pulsatile perfusion can be found (Bernstein et al., 1974). However, patients requiring ECLS can hardly be considered as healthy subjects and therefore do not qualify categorically. Pulsatile perfusion reportedly increases tissue perfusion on capillary level (Dunn et al., 1974) whereas non-pulsatile perfusion causes an increase

in systemic vasoconstriction caused by secretion of several hormones such as catecholamines, vasopressin, local tissue factor, and renin-angiotensin (Taylor et al., 1979) as well as sinus baroreceptor stimulation (Harrison and Seaton, 1973). Despite systemic vasoconstriction, no adverse effects of oxygen delivery or consumption can be attributed to the use of non-pulsatile perfusion over pulsatile perfusion (Harken, 1975). If sufficient blood flow is maintained (native plus pump) the effects of increased sympathetic tone are minimal (Bartlett, 1994).

2.3.2 Organ and Pathophysiological Response to ECMO Treatment

Oxygen transport capabilities in blood can be compromised during the course of ECMO treatment. According to the oxygen binding curve discussed above, variables such as temperature, pCO_2, and haemoglobin content have an impact on the affinity of binding oxygen. Haemoglobin capacity varies more abruptly at the onset of ECMO and due to haemolysis gradually decreases further during the course of ECMO. The oxygenator's main function is to deliver oxygen to the blood. However, the formation of blood clots in the microporous fibres are commonly experienced during prolonged treatments whereby diffusion processes are obstructed, restricting the main function of the oxygenator, performing gas exchange (Gao et al., 2003).

ECMO requires the use of an artificial pump system for temporarily replacing partial or complete native organ functions. Pressure- and flow deviations have to be within certain limits (as close to physiological values as possible) to allow optimal perfusion of organs. The impact of ECMO procedures are multifaceted with each

organ being affected in a different way through a variety of mechanisms.

The Brain: is able to auto-regulate cerebral perfusion pressure (CPP) and with that maintain cerebral blood flow (CBF) within narrow limits over a wide range of arterial blood pressure (Paulson et al., 1989). This autoregulation is an important function to prevent ischemic episodes and cerebral haemorrhages, caused by hypotension and hypertension, respectively. Studies undertaken between 1989 and 1994 revealed that 30 – 40 percent of all neonatal ECMO patients experienced some form of cerebral abnormality with almost 15 percent suffering from intracranial injuries (Taylor et al., 1989; Lazar et al., 1994). It was found that autoregulatory mechanisms in infants can alter during ECMO increasing the risk for cerebral injury. Prolonged hypoxic events prior to ECMO can result in right to left blood flow alterations indicating compromised cerebral autoregulation. Even during the recovery period the brain is susceptible to cerebral injuries if exposed to hyper- or hypotension.

The Heart: In VA-ECMO, native blood is shunted by the artificial circuit through the venous cannula and arterial line. On partial bypass, 80-99 percent of coronary blood flow is supplied by left ventricular output and therefore requires some degree of constant ventilatory support to allow oxygenation of pulmonary blood (Seeker-Walker et al., 1976; Dudell et al., 1991). During full bypass, coronary blood supply is increasingly provided by re-infused oxygenated blood to establish uncompromised recovery of cardiac diseases. 2.4 – 38 percent of neonates can experience cardiac "stun", a transient state in which the myocardium suffers potentially reversible ischemic ventricular failure lasting for hours to days (Dickson et al., 1990; Braunwald and Kloner, 1982). The aetiology of the "stunned" myocardium

is still controversial and possible causes are hypothesised to be insufficient coronary perfusion with resulting hypoxaemia, hypocalcaemia, ventricular hypertrophy, and reperfusion injury (Fauza et al., 1995). Several attempts to speed up the recovery process pharmacologically have been made with limited success (Martin et al., 1991; Hirschl et al., 1992). Usually, adequate haemodynamic support coupled with sufficient amount of time is recommended for successful recovery.

Kidneys: Approximately 15 percent of neonates receiving respiratory support and 26 percent receiving cardiac support require additional haemofiltration during ECMO support (ELSO, 2011). This might be due to the number of variables upon which renal function is dependent; such as hormones, haemodilution, diuretics, blood flow characteristics, haemolysis, and embolism. ECMO can influence all of those dependencies either directly or indirectly. Haemodilution directly affects free water clearance and positively increases urine volume (Utley et al., 1981). However, reduced renal perfusion pressure during ECLS lowers renal blood flow which over time can lead to impaired organ function (Utely, 1993). Additionally, about 20 percent of the total blood flow (native plus pump) in neonates is diverted to the kidneys exposing them to harmful microemboli which can be detected in urine (Boucher et al., 1974).

Abdominal Organs such as stomach, liver, pancreas, and intestines are also exposed to challenging consequences of ECMO in similar manner to other organs. Altered capillary permeability, microemboli, and imbalanced fluid shifts due to vasoactive substances can cause temporary organ dysfunction mainly induced by blood activation on foreign materials. However, clinical manifestation of severe damage to abdominal organs is limited. Moderate jaundice might develop on the basis of donor

blood transfusion. Increased blood flow rates to stomach, intestines, and adrenal glands can also cause GI complications such as ulcers and haemorrhages.

Chapter 3

Thesis Objectives

3.1 Introduction

Research and development of life support technology represents a highly complex task for engineers, scientists, and designers. This environment presents challenges without single solutions but rather depends upon compromises between conventional and emerging solutions. This has been evident in the slow and gradual development of commercial life support devices and is mirrored in the medical literature. One main component is the heat exchanger which to this day still presents as a relatively old-fashioned bulky technology, as described in the previous chapter. These water-based heating systems pose major challenges to patients and clinicians during conventional ECMO settings as well as during 'in-transit' ECMO. The aim of the present work is to challenge, re-design, and miniaturise conventional heat exchangers within the realm of a life support system to improve patient outcome and in particular to benefit medical staff in handling the device.

3.2 Benefits of Re-Design and Miniaturisation

Miniaturisation is a natural consequence of evolution in technology and offers a myriad of different solutions to common problems associated with conventional solution.

- **Reduction of Foreign Surface Area**

  The degree of blood-related inflammation is directly proportional to the expanse blood-contacting foreign surfaces (Gourlay and Stefanou, 2002). Increased foreign surface areas can also illicit greater potential for thrombo-embolic events within the system. Reducing the surface area of extracorporeal systems offers a solution to this challenge. There are however additional benefits of miniaturisation:

- **Reduction of Priming Volume**

  A miniaturised system would inherently reduce the priming volume of the system and would offer the possibility of using saline instead of donor blood. This allows faster and cheaper deployment of the ECMO system and less frequent inflammatory complications related to foreign blood products (Gourlay et al., 2003; Yamasaki and T. Hayashi, 2006; Hamada et al., 2001).

- **Increased Accessibility**

  The number of beds in ECMO centres are limited partially due to size and complexity of current systems. Reducing the foot-print of bulky components such as the heat exchanger would offer a more flexible deployment option.

- **Improved Handling**

  Manoeuvrability is crucial for the well-being of the patient, especially during

ECMO transport where logistics and risks are pronounced. A miniaturised and compact systems allows for faster response times and offers the possibility of quicker access to treatments that if delayed could effect patient outcome and prolong hospitalisation.

3.3 Project Aims

ECMO therapy involves a number of different technologies, operating in tandem to replace the role of native organs of critically-ill patients. By offering this treatment, compromised organs will be allowed to rest and given time to recover from the underlying critical condition.

From the perspective of thermal control and maintenance, this therapy is highly invasive and in its current form, exposure of blood to non-insulated parts, inevitably leads to temperature loss within the patient. A significant drop in core temperature in turn leads to a number of inherent physiological compensatory mechanisms that can negatively impact the treatment if left untreated. Therefore, one major part of ECMO is temperature management, accomplished through the use of heat exchangers, elevated room temperatures, and Mylar blankets. The most effective and frequently employed option among them is the heat exchanger which has a large footprint, needs external power- and water supply, as well as specialist staff to operate. Periods of shortages of any of these prerequisites combined with the dependency on temperature management pose severe risks to patient mortality.

After extensive literature review and clinical procedure observations, it is clear that in order to improve limitations associated with temperature management that impacts both patient outcome and clinical work environment, the solution lies in the development of a novel miniaturised heat exchanger. This will reduce the footprint

and offer more flexibility and independence on central services.

There is a second challenge associated with deployment of ECMO and that is the technology used to transport patients from centre to centre. These in-transit systems have exactly the same complexities as conventional systems but have less regular power- and water supply solutions. Presently, a proportion of patients who are under in-transit ECMO support have no thermal control because it is not always possible to attach them to a power supply. In addition, conventional ECMO devices are not always appropriate for these patients due to the large footprint and complexity of them. Alternative solutions is to reduce the size of the in-transit ECMO technology, to provide energy and water independent thermal maintenance system. A second strand of this objective is to develop a solution for in-transit thermal control of ECMO patients.

The targeted patient group within the context of this thesis is the neonatal population, as it reflects the majority of ECMO users. However, the application may not be limited to this patient group and future work should focus on potentially impacting paediatric and adult ECMO therapy, too.

The objectives of this work have the potential to be impactful in two important but discrete ways. Firstly, the development of an alternative to a conventional, complex heat exchanger for ECMO, replacing this with an independent, small footprint technology has its primary impact in the user arena. Insofar as, it will require a smaller footprint, easier to use, easier to service, and independent of large water supply tanks, etc. The main impact of this strand of the work is in enabling users to apply ECMO more flexibly with less interaction and requirements to service and supply. The second strand of the project, the development of a power- and water

independent thermal transfer solution for ECMO patients in-transit is impactful in a considerably different way. Primarily, the impact of this technology will be to the patient, insofar as extending thermal stability in patients who are undergoing ECMO transport has a potential to deliver these patients in a more clinically stable condition to the receiving ECMO centre.

The principle objectives of this work are therefore:

- Develop a new waterless ECMO thermal control system for conventional in-hospital ECMO support.
- To develop a power and water independent thermal support technology for in-transit ECMO provision.
- Test both devices under lab conditions.
- Test both devices under near clinical conditions.

Hypothesis: It is possible to produce miniaturised thermal control and maintenance technologies for in-hospital and in-transit ECMO that eliminate the need for mains water whilst offering adequate thermal exchange levels.

Chapter 4

Design

4.1 Introduction

Homeostasis is the term that refers to the body's ability to maintain its internal environment in response to changes externally. This term includes temperature regulation. It does that by mechanisms described in Chapter 1 in order to achieve normothermic levels of approximately 37 $^{\circ}C$. During ECMO procedures however, the body's ability to influence homeostasis is partially compromised due to the usage of anaesthetics and other drugs. For this reason, a number of additional steps are implemented in order to avoid unnecessary and uncontrolled heat loss, such as 1) Covering the patient with thermal blankets (Mylar blankets), 2) increased room temperature, 3) avoiding wet patient skin, and 4) the use of a heat exchanger. However, certain complications and challenges arise when trying to implement these four steps under normal clinical settings and during patient transport. During fixed ECMO procedures, the major influencing factor for temperature loss is variable ambient temperature and implementation of measures 1-3 do not impose challenges for well-equipped hospitals. However, complexity and convenience are challenged in relation to step 4

above. Conventional techniques for heat exchangers are water-based systems by which a secondary medium (mostly water) indirectly heats the circulating blood by means of conduction and convection (see Chapter 2.1 for more detail). The disadvantages of this design are augmentation of footprint, rather immobile handling, increased failure susceptibility and increased priming volumes used, ultimately posing additional risks to both patients and clinicians. In transport settings, the challenges are multifactorial and somewhat more pronounced. The lack of a mains power supply and space in transport vehicles such as helicopters and ambulances often prevent the use of conventional heat exchangers altogether. Additionally, a hyper-variable ambience in those vehicles poses an increased challenge for the patient, further contributing to temperature loss and an imbalance in relation to efforts to maintain normothermia, further complicating the treatment going forward.

Figure 4.1: Specialised ECMO transport from Kadena Air Base, Japan, to San Antonio, Texas, 26.05.2009 (www.aetc.af.mil)

There are, therefore, two scenarios that should be addressed with considering innovation in thermal control for ECMO, 1) conventional water-dependent heater-cooler

units in the ITU settings, and 2) 'in-transit ECMO' in small, restricted environments without power and variable ambient temperatures.

Ideally, a common solution to both problems would be developed but we recognise the difficulties in achieving that based on the issues described above. We therefore set out to develop two distinct technologies to address the challenges with ECMO above:

- Solution 1: Heat Exchanger for Conventional ECMO Settings
- Solution 2: Heat Exchanger for in-transit ECMO

The aim is to address both issues, 1) to add heat by means of alternative heat exchanger methods and 2) to focus on minimising heat loss during ECMO transport; two different approaches targeting one common objective of maintaining the core temperature at normothermic levels by controlling the temperature of the blood and the environment intimate to the patient.

4.2 Design Criteria

4.2.1 Solution 1 - Heat Exchanger for Conventional ECMO

For a potentially successful use of a new heat exchange technology in clinical settings, certain requirements and standards need to be considered and implemented during the design phase. Firstly, a brief overview and pre-selection of different possible technologies is given which rely on basic criteria considered as important for realising a solution. Having selected the most promising solution, design requirements are established which will assist in guiding the prototype development.

In light of our project aims, important criteria used as a common denominator for selecting an appropriate heat source technology are 1. size, 2. cost, 3. complexity, 4. temperature reversibility, and 5. controllability. By looking at current ECMO technologies with its bulky components, a clear trend for future developments suggest a more integrated and smaller device, especially for transportable ECMO units. Smaller parts ultimately reduce the complexity of handling and also positively influence power consumption which can result in significant cost reduction and the need for central services. Furthermore, there is a clear need for thermal control under certain clinical conditions (Doherty et al., 2009).

A number of different thermal technologies for possible implementation have been compared based on the four criteria mentioned above. A numerical rating system of 0-5 (0=worst, 5=best) has been applied to each criterion, validating their individual and overall potential use.

Comparison of possible heat source technologies include:

- Thermoelectric Technology

  Based on the Peltier effect, thermoelectric modules (TEMs) generate heat by supplying DC power to the input terminals. These very thin modules are based on solid-state elements that allow for thermal generation without any moving parts, thereby promising high reliability. Changing the polarity of the power source leads to reversing the direction of the heat transfer, enabling cooling- as well as heating operation. Geometric dimensions vary from as small as 2x2 mm to 62x62 mm, offering solutions for small-scale applications. A further characteristic is the precise controllability under steady-state operation, with achievable $\pm 0.01\ ^{\circ}C$ deviation (Laird-Technologies, 2010). Typical examples of

thermoelectric applications are:

Figure 4.2: Thermoelectric generator applied in automobiles; to capture waste heat and convert into electrical energy which can be used to power other appliances. (taken from www.caradvice.com)

Figure 4.3: Making use of temperature differences in gadgets; exploiting ice beverage and ambient temperatures in order to induce electrical energy to charge phone. (taken from www.tweaktown.com)

Figure 4.4: Thermoelectric element applied in wrist watches, making use of temperature differential between body heat and ambient temperature. (taken from www.ecofriend.com)

- Induction Heating

  Induction heating is based on the principle of coupled electromagnetism by which a high-frequency AC source applied to a coil induces eddy-currents in a separate conducting material effectively leading to Joule heating. This compact technology comprises of quick and locally applied heat on an area that can be precisely determined with a accuracy of approximately $3°C$ (db Prüftechnik, 2013). According to Callebaut (2007), installation of induction heating systems are considered to be more expensive in purchase compared to alternative systems. Another disadvantage of this technology would be the lack of temperature reversibility that does not cover the small dedicated call for cooling.

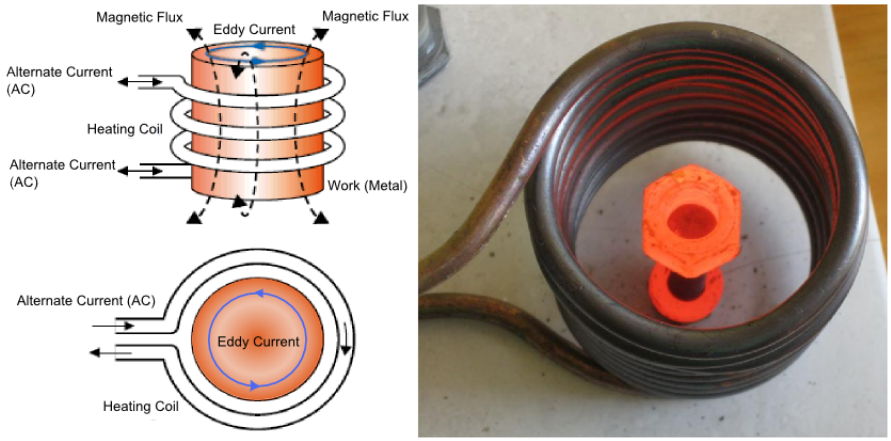

Figure 4.5: Induction Heating; Schematic (left) and example of heating a screw and bolt (right). Taken from www.avio.co.jp and uzzors2k.4hv.org, respectively.

- Electric Heating

  Electric heating, Joule heating, or resistive heating are synonymous for another form of electrically powered systems found in various application examples such as electric radiators or kettles. This very compact and cost efficient technology even allows integration and implementation onto microfluidic devices, achieving levels of control of $\pm 0.2\ ^{\circ}C$ (Mello et al., 2004). A usable example of such technology within our context could be adhesive heating-pads. They are available in various sizes and therefore can cover a great area. The complexity of the heating pads are minimal and are easily controllable via thermocouples. Unfortunately, this very promising technology does not provide the option for cooling.

Figure 4.6: Examples of electric heating technology (Taken from www.explainthatstuff.com, shaddack.twibright.com, www.thelightworks.net, www.tipmont.org)

A direct comparison of all five heating methods based on the criteria mentioned above lead to a summary of the Table 4.1.

	size	cost	complexity	temperature reversibility	controllability
Thermoelectric Technology	5	4	5	5	5
Induction Heating	4	3	5	1	4
Electric Heating	5	5	5	1	5

Table 4.1: Summary of potentially relevant heat technology options

Both inductive and electric heating are strong alternatives for powering our heat exchanger. The ratings on size, cost, complexity, and controllability are all in favour

for both technologies. However, our requirements for controlled cooling of the patient blood renders them redundant, hence the low rating.

The versatility of thermoelectric devices proved advantageous in contrast to all other alternative methods. Using the very compact design of currently available TEMs could prevent a potential bulking of the finalised heat exchanger, reducing its overall contribution to the system foot-print. A comparison of different commercial TEM-providers show that purchasing costs fall below GBP 100 for a variety of different sizes. Furthermore, taking into consideration the tendency for cheaper thermoelectric materials to appear in future allows us to potentially use them for disposable purposes. The implementation and usage of TEMs is straightforward; one component that includes two leads for power supply. No parts require modification or assembly. Polarity change at the terminals permitting temperature reversibility, effectively leading to heat being pumped in the opposite direction. Using well-designed circuits, a temperature window of $\pm 0.1\ ^{\circ}C$ can be achieved and maintained (Ma, 2003). For these reasons, we have chosen to work with thermoelectric devices for our novel heat exchange solution.

Further descriptions and detailed workings of the thermoelectric effect and their subsequent devices are discussed in Chapter 5.1 and 5.2.

Having selected a heating/cooling technology for our application from a number of considered methods, the heat exchanger itself can now be designed. In order to achieve best results, the following requirements and desired characteristics were considered and used as a crude design guide:

- size,
- flow resistance,

- cross-section area,
- thermal contact,
- material,
- manufacturing.

Size is one of the biggest motivational factor behind this project and the main drive for achieving a miniaturised and compact heat exchanger. The aim is to replace the existing water-based technologies by more advanced concepts. Miniaturising the heat exchanger serves multiple important purposes. The first aspect is the reduced need for large priming volume. Priming solutions can affect normal blood coagulation, haemostasis, and oxygen carrying potential (Ruttmann and James, 1998; De Jonge et al., 1998).There is a natural drive towards minimising the priming volume in neonatal ECMO circuits due to the possibility of an exaggerated level of patient haemodilution associated with it. Gourlay et al. (2003) demonstrated the consequences of haemodilution and the subsequent statistically significant increase in neutrophil activation. He also proved that the magnitude of inflammatory response is proportional to the surface area. Another motivational aspect behind miniaturisation is the possibility of reducing the complexity of conventional water-driven heat-exchange systems which incorporate components for both water and electrical circuitries, further impeding mobile usage and introducing greater potential for system errors. We therefore aim to reduce the overall size and footprint of the heat exchanger to a minimum.

Flow resistance of the heat exchanger should ideally be kept to a minimum in order to avoid unacceptable mechanical forces. From a hydrodynamical point of view, shear forces arise caused by the opposing effects of fluid propagation, thus higher shear forces result in higher resistance values. The degree of resistance typically depends on multiple factors, such as the cross-sectional area, surface finish, velocity and fluid

properties. All ECMO components will resist the motion of blood flow to some degree and it is the combined R-value (Resistance) that needs to be exceeded in order for the motion of fluid to occur. Only a pressure differential big enough to overcome the combined R-value will commence blood flow, evidently leading to higher pressure requirements for larger resistances. In order to minimise the haemolytic effects caused by high resistive and high pressured systems, we aim to keep the flow resistance of our heat exchanger to a minimum.

The **cross-sectional area** of the blood flow path through the heat exchanger should remain constant, for two main reasons. Firstly, a constant cross-section provides the opportunity for uniform flow velocities and therefore equal loading of the heating elements which may help to achieve the best heating/cooling results. The second reason behind a constant cross-sectional area is to avoid the development of turbulent flow patterns as this may lead to haemolysis (Kameneva et al., 2004).

Thermal contact is the connection between thermoelectric devices and the heat exchanger. Due to the flat nature of the TEM, it would be apparent to adopt similar geometries for the heat exchanger in order to provide the best impact on thermal performance through optimising the thermal source/heat exchanger coupling.

Material considerations should cover manufacturability, assembly and biocompatibility. For the purpose of a disposable heat exchanger whose costs should be minimised, manufacturing processes should be inexpensive, fast, and uncomplicated. Factors influencing this are materials and the overall complexity of a design. Biocompatible materials also require consideration to avoid any complications such as platelet activation and triggering the coagulation and inflammatory cascades.

4.2.2 Solution 2 - Heat Exchanger for in-transit ECMO

The objective of this aspect of the work is to develop a heat exchanger for use during the transport of ECMO patients with the aim of reducing thermal loss under exceptional ambient conditions.

It is recognised that the biggest surface area of the ECMO circuit is the membrane lung where the greatest temperature loss occurs during operation (Sinard and Bartlett, 1990). Other parts of the circuit which are prone to heat loss are non-insulated tubings and the pump. The conventional procedure to compensate for the combined thermal losses is by implementing a heat exchanger situated as the last part of the ECMO circuit before blood returns to the patient. However, problems arise in situations where power sources for 'energy hungry' heat exchangers are not available, such as in military- and ambulatory transport or technologically deprived areas. Taking the former as an example, not only are there no power sources available for heating the blood directly, nor are there any heated air vents (conventionally found in automobiles) that could potentially raise the cabin temperatures and provide indirect thermal support to a neonate. Environmental challenges like these impede the maintenance of normothermic core temperatures and require a solution. Dealing with these hyper-variable ambient conditions from an ECMO-perspective requires an exceptional strategy. Instead of focusing on traditional methods of heat compensation, i.e. by means of adding heat through a conventional heat exchanger, we focused on minimising heat loss during ECMO procedures. The result of this approach is that if one can insulate and potentially add heat to the oxygenator then heat loss will be reduced.

The following requirements were considered during the design stage for the heat exchanger in-transit solution:

- **Good Insulation and Potentially Adding Heat**

  The main design requirement for our novel heat exchanger is to minimise temperature loss with available methods. This implies a solution that is able to provide effective insulating properties across a broad range of temperatures, covering conductive- as well as convective heat transfer. With the option of adding heat to the insulated device, the inherent temperature loss may be even more slowed down possibly prolonging adverse physiological reactions.

- **No Interference with other ECMO-Related Operations**

  ECMO therapy requires constant surveillance of monitored values and access to all parts of the circuit at any time. The new heat exchanger must not obstruct of any procedures through visual or physical impairment. The overall goal of the design is to ensure a good enough insulation without impeding the functionality of any circuit components or access by clinical members of staff.

- **Easy Application**

  Time during ECMO transport is a very crucial factor for the survival of the patient, especially during power shortages and hyper-variable ambient conditions. Swift handling of all ECMO-related equipment contributes to positive patient impact. Therefore, we aim to design and develop a new heat exchanger that permits quick and easy installation as well as handling during perioperative periods.

- **Lightweight and Compact**

  It is also important for our new device to be lightweight and compact. These elements are crucial in locations with limited space, and a need for low complexity. A balance between size and efficiency may need to be found.

These self-imposed key requirements will ultimately help us guide the development of our new heat exchanger.

4.3 Design Process

4.3.1 Solution 1 - Heat Exchanger for Conventional ECMO

The established design criteria in Chapter 4.2.1 can now be used as a guide throughout the design process of the heat exchanger.

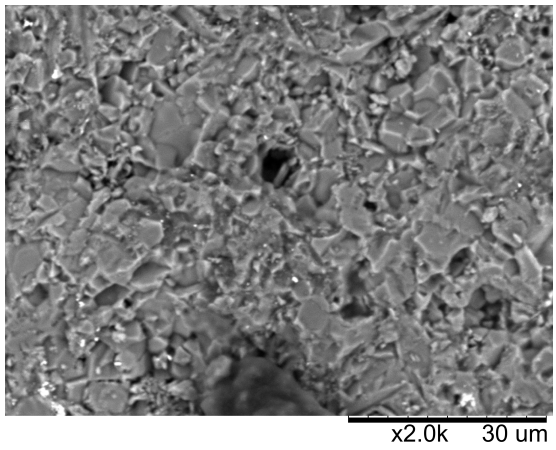

Figure 4.7: Scanning electron microscope (SEM) image showing imperfections in surface material of the thermoelectric device. (SEM model Hitachi TM-1000)

A tendency towards a flat design has emerged during initial idea generation processes, motivated by the planar nature of the thermoelectric elements used. Although TEM surfaces purport an exact flat surface, imperfections can be noticed on microscopic levels. These imperfections create air pockets that when interfaced - fixed by clamps for example - with the heat exchanger surface result in decreased thermal energy conduction due to the insulating properties of air (see Figure 4.7). One remedial action would be to use a thin layer of thermal compound, a liquid paste which when

applied fills those air gaps for improved heat conductance. Non-flat surfaces would require more thermal compound material in order to adhere to the flat structure of the TEM, lowering overall thermal efficiency but also produce non-uniform heat transfer into the blood (Lynn, 2012). Therefore, all TEMs used should be separated from the blood flow by a thin layer of conductive material, leading to the sequence of TEM - thermal compound - separation layer - blood (Figure 4.8).

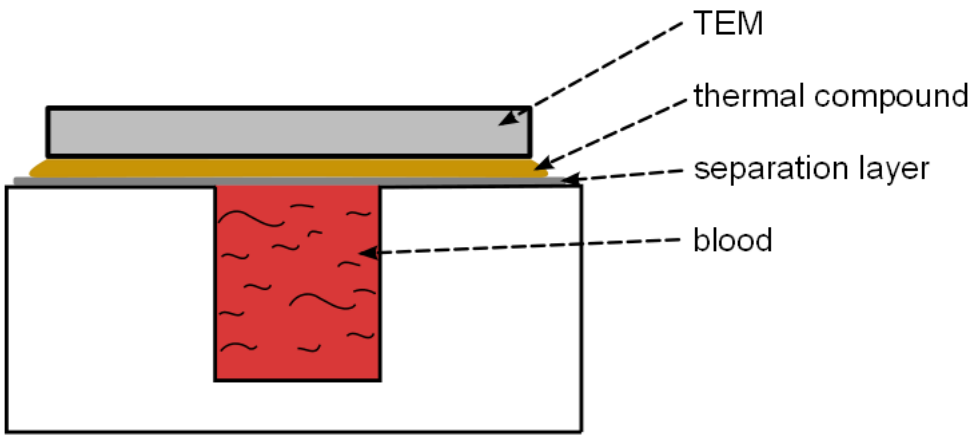

Figure 4.8: TEM - thermal compound - separation layer - blood

Attention should also be paid to the structure and volume of the device as these factors are related to the specific heat capacity and therefore influence the speed of heating/cooling processes. Since the thermal energy generated by the TEMs should primarily be absorbed by the blood, a minimal amount of material of high specific heat capacity is desirable to build the interface. Also, insulating materials should be employed at interfaces that are not in direct contact with the heat source, to minimise heat losses. On the contrary, conducting materials should be utilised on interfaces between the heat source and the blood to maximise the influence of the TEMs. Thermal paste will fulfil this function.

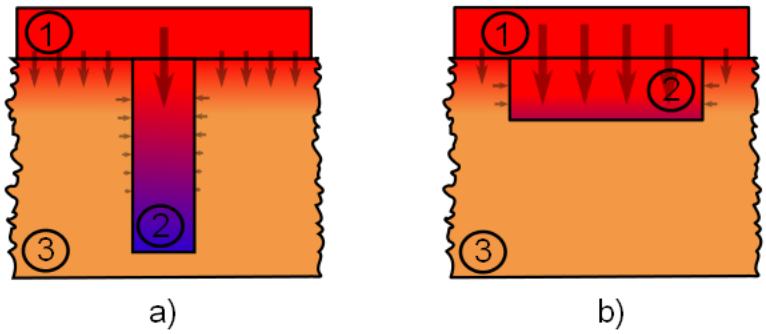

Figure 4.9: Channel Size Impact Comparison. This diagram represents two separate cross-sections through an element, *a*) and *b*), that contains *1*) Heat source, *2*) Fluid channel, and *3*) Heat exchanger material surrounding the fluid channel. The heat source with constant power $P = const$ conducts thermal energy parallel into *2* and *3*. The passing fluid absorbs the majority of heat directly from the top, *1*, and only little from the surroundings, *3*. Therefore, greater surface areas such as in *b*) allow to capture more of the provided heat compared to *a*).

The overall size of the overall heat exchanger is the main drive to achieve a more compact, transportable system. The cross-sectional area of the fluid path directly influences the overall size of the heat exchanger, i.e. bigger fluid channel dimensions directly correlate to larger overall heat exchanger dimensions. Also, the cross-sectional dimensions of the fluid path have proportional affects on the resistance to fluid flow and blood velocity. However, not only is the overall size of the heat exchanger affected by varying the fluid channel dimensions but also the rate at which the heat is transferred as it passes along the TEMs (Lynn, 2012). This notion can be shown by two (extreme) examples. Thermal energy is first transported from the TEMs into the heat exchanger via conduction before it branches out into parallel processes as shown in Figure 4.9. Heat is then taken up from all sides (mainly from the top where the TEM is mounted) by the flowing medium through forced convection. A fluid channel with reduced height (and increased width to preserve a sufficient cross-sectional area) such as a thin film would heat up the flowing blood more rapidly compared to a tall

and narrow channel. This can be explained by the simple fact that the majority of heating power is delivered from the top, and the larger the (top-)surface area the more energy can be transferred during a fixed time interval. Therefore, a higher ratio of fluid channel width/hight will be designed in order to exploit the majority of thermal energy provided by the TEM's.

So far, we have progressed in our theoretical design procedure to show that in order to reduce overall heat exchanger size, a flat structure made of conducting material through which a rectangular fluid channel is cut seems to be the most appropriate approach to meet the design requirements. Additionally, TEMs are attached to the heat exchanger's top surface via thermal compound for improved heat transfer through the elimination of "dead spaces". To further reduce the complexity of the heat exchanger, the number of TEMs employed will be limited to two. We chose a 55 x 55 mm thermoelectric heat pump (Module: 9500/241/085B; Ferrotec Corp. Santa Clara, CA, USA) for quality and customer service reasons. For the heat exchanger to perform sufficiently even during flow rates of 300 ml/min, multiple flow loops are required to increase the exposure time of the fluid during the passage. The answer to the question of *'How many flow loops are required?'* depends on two factors, the size of both TEMs and the width of the fluid channel. Ideally, the surface area of both TEMs should cover the majority of the fluid channel profile to allow for maximum thermal coupling. Since FerroTec's device dimensions are already known, the fluid channel width remains to be determined.

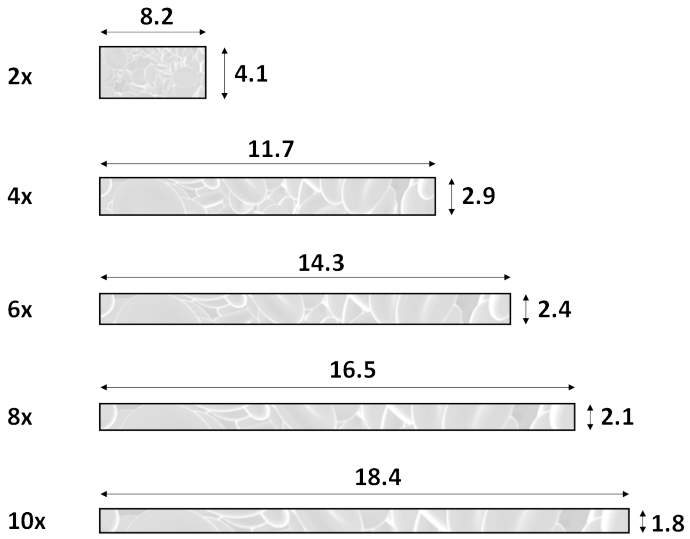

Figure 4.10: Iteration of fluid channel dimensions [mm]

As previously discussed, there is great merit in reducing flow resistance. For this reason, we aim to maintain a cross sectional area within the heat exchanger at the same level as the inlet and outlet connections, in this case 34 mm^2. Varying channel widths will ultimately affect channel height, under constant cross-sectional area. Greater channel widths will result in increased (top)-surface area, leading to improved heat transfer between TEM and blood. Figure 4.10 illustrates the relationship between channel width and height, an n-multiple of height from top to bottom. Upon consideration of appropriate channel dimensions, it was decided to continue the heat exchanger design process with a channel size of 17 x 2 mm. If at any later stage evidence should indicate insufficient channel width/height, re-dimensioning can be performed.

Having determined the size of the channel it is now necessary to calculate the number of flow loops within the heat exchanger. The TEM with its 55 mm provides enough space for three loops (55 mm / 17 mm = 3.23).

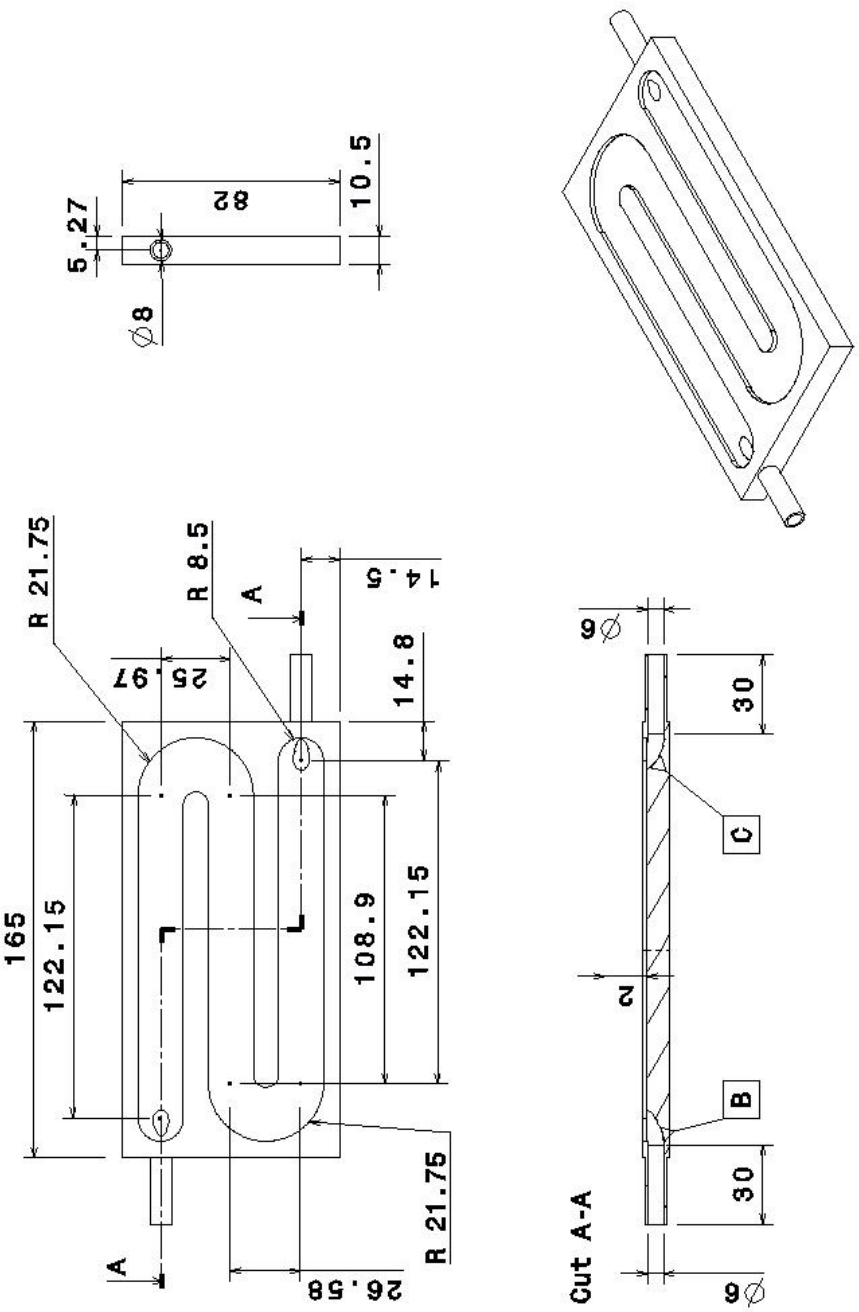

Figure 4.11: CAD Drawing of proposed Heat Exchanger. All dimensions in mm. Top plate intentionally left out for displaying purposes.

Taking into consideration all previously discussed design criteria in Section 4.2 as well as theoretical outcomes deduced from this section, we suggest the following technical drawing for the development of a prototype displayed in Figure 4.11.

4.3.2 Solution 2 - Heat Exchanger for in-transit ECMO

Overall, the following material properties should be considered in our approach:

- reduced thermal conductivity

  Materials with a high air content have a tendency of low thermal conductivity, i.e. act as a thermal insulator. This is due to the air pockets encapsulating stationary air molecules. These molecules are responsible for the majority of heat transfer and Restricting their movements will also restrict the carrying of heat energy. The lower the thermal conductivity, i.e. approaching that of stationary air, the better the insulating properties.

- ability to absorb moisture

  Moisture generally reduces insulation properties if absorbed by the material. Therefore, only materials which can resist the absorption of moisture (non-hygroscopic) should be used.

- adequate mechanical strength

  Good insulation materials tend to be weaker in structural properties due to the intrinsic high void content and may require additional support using secondary support structures or scaffolds.

In the first instance, we compared different materials used extensively in the civil engineering sector. Among them were:

- Vermiculite
- Gypsum
- Coconut fibres
- Cork
- Rock wool
- Cellulose
- Expanded foam-type cellular plastics
- Fibre glass
- Styrofoam

The above list of suggested materials can be categorised as pure mechanical means of insulation. However, further research into each material from above indicated good insulation properties demonstrated in long-term usage, none of them are actually able to induce heat of any degree. For this reason, a solution based solely on any of the above materials was rejected. Instead, a solution was proposed that actively induces heat without the common means of electrical power and water supply, but is based on a exothermic chemical reactions.

The proposed system is based on sodium acetate, a sodium salt of acetic acid that is used in commercially available consumer heating pads and hand warmers. These hand warmers enclose the liquid sodium acetate in a sealed plastic pouch together with a small metal disc. The small disc which normally has small slits in the thin metal activates the crystallisation process, transforming the solution into solid sodium acetate trihydrate. The process involves particles that are trapped between the slits of the disk and when manually operated, experience a higher melting point that act as seeds for the surrounding sodium acetate liquid (Barrett and Benson,

1988). The crystallisation process itself is of exothermic nature, releasing energy in form of heat of about 264 - 289 kJ/kg (Dincer and Rosen, 2002). The reversibility of the crystallisation is performed by placing the pouch in boiling water thereby allowing multiple reuse of the item, rendering it somewhat superior to disposable hand warmers. The duration of heat depends on three factors, 1) size, 2) form of usage, and 3) the insulation around the pouch, typically lasting from 20 min to 2 hours (HotSnapZ, 2013). Additionally, the purchase of the main part of this technology, sodium acetate, is relatively inexpensive, safe, and well understood and is therefore fit for our purpose.

The traditional passive form of insulation and the active exothermic chemical-based form offer two separate approaches, the former preventing heat loss from the system and the latter inducing heat into the system. The intention is to use the external surface of the oxygenator as a heat exchanger interface. It is here where the exothermic energy from the sodium-acetate reaction is induced into the body of the oxygenator in order to maintain the heat of the blood that passes through it. The passive form of insulation would be applied additionally around the oxygenator-sodium acetate combination to further minimise any heat loss and simultaneously maximise heat made available to the oxygenator.

Figure 4.12: Example of sodium acetate pocket warmer pouch (taken from Wikipedia)

The three influencing factors - size, form of usage, and additional insulation - play an important role in the performance of the Active Sodium Acetate Heat Exchanger Device (ASAHED).

Ideally the oxygenator bag should be suitable for a wide range of oxygenators. However, in the context of the present work, we determined to tailor our device to the most commonly used oxygenator type for neonatal applications, the Medos HILITE 800LT.

Figure 4.13: Medos HILITE 800LT Hollow Fibre Oxygenator

The second criterion - the form of usage - defines the environment in which the ASAHED is employed. The main application for this device is within realms that lack power sources crucial for the usage of conventional heat exchangers in order to compensate for temperature loss. The idea is to tightly wrap the ASAHED all around the oxygenator which when activated through the metal clip inside, provides an external temperature higher or at least equal to the blood temperature, thereby limiting potential losses. To avoid any losses from the ASAHED into the environment, additional insulation will be needed, which ultimately leads to the third point; a light, cheap, and yet structurally supportive material that can be used to encapsulate the pouch wrapped around the oxygenator, leaving only openings for the PVC tubings. This proposed design will be further addressed in later parts of this chapter.

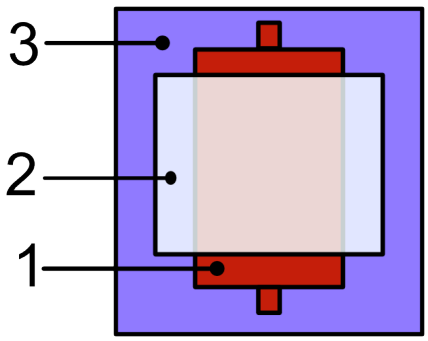

Figure 4.14: Schematic of the ASAHED (2 and 3) wrapped around an oxygenator (1)

The technical development of this device will follow a logical sequence of iterative steps which is part of a standard design cycle, also applied to other aspects of this thesis.

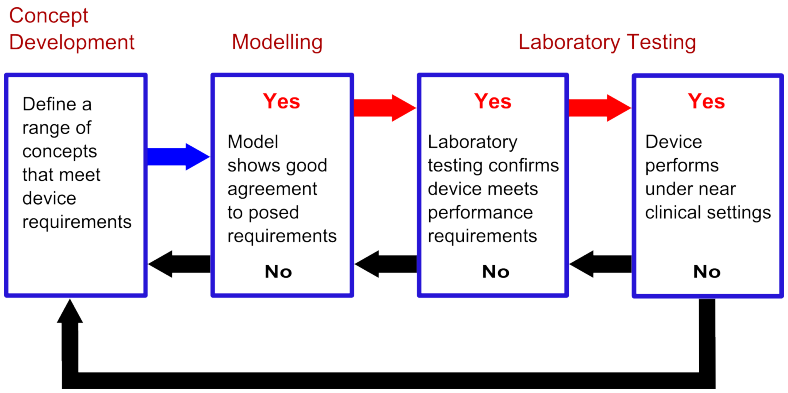

Figure 4.15: Flow chart showing a typical part within the life cycle of a technical device (Lynn, 2012)

The *'Concept Development'* segment, based on ideal requirements, has already been discussed in this chapter. The next logical stage would be *'Modelling'*. Although this concept of the ASAHED is part of a feasibility study, we believe that it lends itself to an uncomplicated design cycle. This view is supported by the fact that commercially available sodium acetate hand-warmers do work and are widely used in other applications.

Figure **??** illustrates our proposed CAD-design for an external heat exchanger concept for the Medos HILITE 800LT oxygenator.

Similar to commercial pouches, the thickness of the ASAHED when filled is 10 mm. Made of one piece but separated into adjacent sections, when folded and set-up properly, the pouch should envelop the entire oxygenator, covering most areas of the oxygenator and therefore offering good insulation. The pouch itself is made of medical grade PVC containing sodium acetate and a small metal button that activates the exothermic chemical reaction. Additionally, a thermal print on one of the pouch-sides expresses the temperature of the bag in colours, informing the user of the overall effectiveness and when it is no longer effective needs replacing. The ASAHED can be easily replaced during running operations when efficacy levels decrease. Figure 4.17 depicts the heat exchanger in its solid and liquid stages.

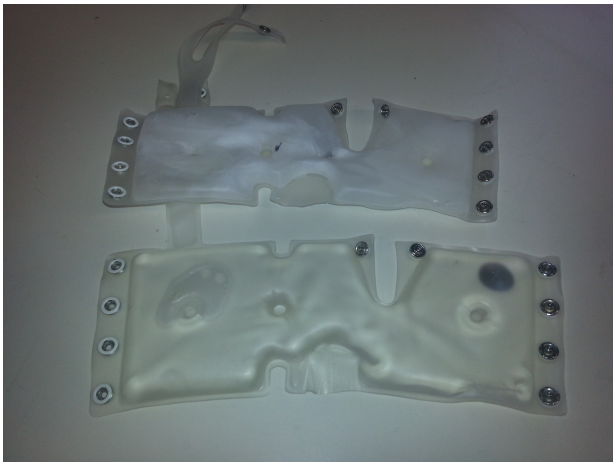

Figure 4.17: Sodium Acetate Filled Heat Exchanger; activated and solid sodium acetate condition (top), liquid sodium acetate condition (bottom)

After attaching and activating the ASAHED, one can recognise that at least 50 per cent of the PVC surface area is exposed to the external environment and is not in contact with the oxygenator itself; see Figure 4.18. The natural consequence of this would be substantial losses of thermal energy into the environment, potentially

reducing overall efficiency of the device. In order to reduce the effects of heat loss to the surrounding, one option would be to introduce additional insulation around the oxygenator bag, ideally in the form of a closed cavity in order to capture the majority of thermal energy.

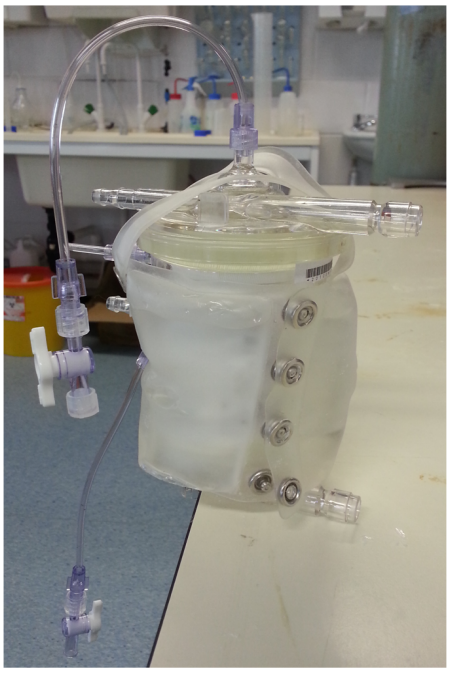

Figure 4.18: ASAHED Attached to Oxygenator

Similar to the design process of the heat exchanger, a set of requirements is necessary to successfully guide the prototype development of the additional insulation. Emphasise was put on the following criteria:

- **Insulation:** First and foremost, the major goal of the design is to provide good insulation in order to prevent heat loss from the oxygenator.
- **Flexibility:** A rigid and maybe even brittle insulation has the potential of cracking or even breaking, thereby potentially negatively influencing the insulation performance. Also, heavy and bulky materials or designs may compromise

the overall goal of a compact device. The main aim therefore is to find light material(s) that are also thin and flexible enough that when put together prevent permanent deformation and remain compact.

- **Ability to mount and dismount during operation:** It is vital for qualified staff to have access to the oxygenator and heat exchanger whenever required without the need to interrupt the ECMO procedure, i.e. disconnect and reconnect the tubing to the oxygenator. Therefore, the design of the insulation requires a feature that allows the possibility of disassembly, but enabling changeout.

- **Fully encasing the entire oxygenator plus heat exchanger:** In order to avoid any possible heat loss from the system (oxygenator plus heat exchanger), a design that features a full enclosure is required.

- **Minimal production costs:** It is vital to the project that costs for material and manufacturing remain as moderate as possible to encourage usage.

After researching several existing concepts for insulation in other applications such as double-glazing and two-component polymer castings, it was recognised that none of these technologies were suited to our application with the exception of the thermal insulation currently employed in camping cooling bags. It provides insulation based on three different layers of flexible materials which collectively are thick enough to even withstand light physical impact. The material can be cut, folded, and stitched to the desired shape, thus permitting full encapsulation and easy removal from the oxygenator when desired. Another great advantage is the ready accessible nature and low cost of the material.

Having decided on the concept and material of the oxygenator insulation, a design was considered. A suitable source of thermo-insulation in the form of a Thermos-4 Litre Radiance Cool Bag was tailored according to the combined dimensions of the oxygenator and the attached heat exchanger. The starting point was a blue-print on fleece that accommodated all tubing inlets and outlets to and from the oxygenator. The design resembles a cylindrical shape - inspired by the oxygenator itself - with a cap on top and bottom to fully enclose the system. Both lids will need to be designed in such a way that clinical staff are able to see into the system for safety reasons such as bubble formation. The insulation cover is held together by Velcro® stripes around the edges and holes which allow easy access to the system at all times.

Figure 4.19: Finished Heat Exchanger Insulation (inside silver lining)

Figure 4.21: Assembled heat exchanger bag with insulation

Figure 4.20: Finished Heat Exchanger Insulation (outside cover)

The completed and assembled heat exchanger bag with insulation can be seen in Figure 4.21.

The design proves to be a good fit for the proposed application, meeting all functional and design criteria, and produced an elegant solution to the encapsulation of the oxygenator and the ASAHED.

4.4 Summary

Conventional heat exchanger systems are mainly water-based devices that indirectly heat the circulating blood. It is recognised that these systems contribute to an augmented footprint, immobile handling, increased failure susceptibility and require larger priming volumes. Furthermore, when transporting patients, the lack of power supply in ambulatory vehicles prevent the use of these conventional power-intensive heat exchangers. For this reason, we aimed to address both scenarios individually, designing two separate technologies for ECMO.

Design approach No. 1 focussed on heat exchangers for conventional ECMO settings whereas design approach No. 2 focussed on heat exchangers for in-transit ECMO.

A comparison of different available technologies revealed the superiority of thermoelectric devices based on its robustness, reliable operation, temperature reversibility, and accuracy and was therefore used in our concept. Several design criteria such as size, flow resistance, cross-section, thermal contact, material, and manufacturing were also considered during the design stage, ultimately leading to a novel flat 3D CAD model of our proposed heat exchanger for conventional ECMO settings.

The design of the heat exchanger for in-transit use comprised of establishing device requirements that are specific to the transport environment. These included good insulation and potentially adding heat, no interference with other ECMO-related operations, easy applications, as well as a lightweight and compact form factor. A comparison of different materials revealed the advantages of an active solution instead of a passive insulator. Therefore, our design is based around the exothermic process of sodium acetate that is able to induce heat into the oxygenator. An additional

thermal insulator was also designed that encloses the device, offering extra insulation and minimising unnecessary heat loss.

Chapter 5

Modelling

The importance of maintaining adequate thermal levels in patients (discussed in chapter 1.7) are as crucial as maintaining adequate perfusion levels. Temperature loss on patient-ECMO system can have many origins. They can be induced by pharmacological interventions such as anaesthetics or invoked by as a result of ECMO therapy and the operational environment.

To compensate for temperature loss of any kind or origin and to enhance the performance, a novel and compact heat exchanger based on thermoelectric energy conversion has been designed in Chapter 4. This design is now to be implemented in form of a software model for easy and quick alterations as well as future controller tuning.

The motivation behind developing this new concept of heat exchange within ECMO therapy was to reduce the size, cost and logistics involved. The main parts of an ECMO circuit are pump, oxygenator, and heat exchanger, with a focus on the latter, aimed at developing a truly portable unit, that is independent of mains water and having a highly portable structure. The availability of space is very restricted for this new heat exchanger, a technology primarily based on thermal energy trans-

port which provides best results if conversely possessing a large surface area (Verma, 2004). All three major ECMO components are exposed to the patient's blood during therapy and the entire single unit is considered as disposable.

The proposed heat exchange technology is a highly improved design. Instead of long cylindrical two phase liquid heat exchangers which require a secondary medium (H2O) to allow temperature manipulation of the blood by means of forced convection, the proposed technology has a very flat profile through which blood flows in a serpentine manner through looped channels. The energy generation is implemented by means of two Peltier devices (also referred to as thermoelectric devices (TED); thermoelectric module (TEM); or Peltier module) which are connected to the upper surface of the aluminium body of the heat exchanger. The TEDs and the patient's blood are not in direct contact but are separated by a 0.5 mm thick aluminium sheet which forms the aluminium casing of the device. The two TEDs are attached by means of thermal adhesives and from this construct it is apparent that the heat produced by the Peltier modules conducts through the adhesive into the aluminium heat exchanger surface. Blood enters through one end and exits the opposite, as a single pass heat exchanger. During operation, the blood will absorb the thermal energy from the aluminium by means of forced convection and thereby progressively increase in temperature.

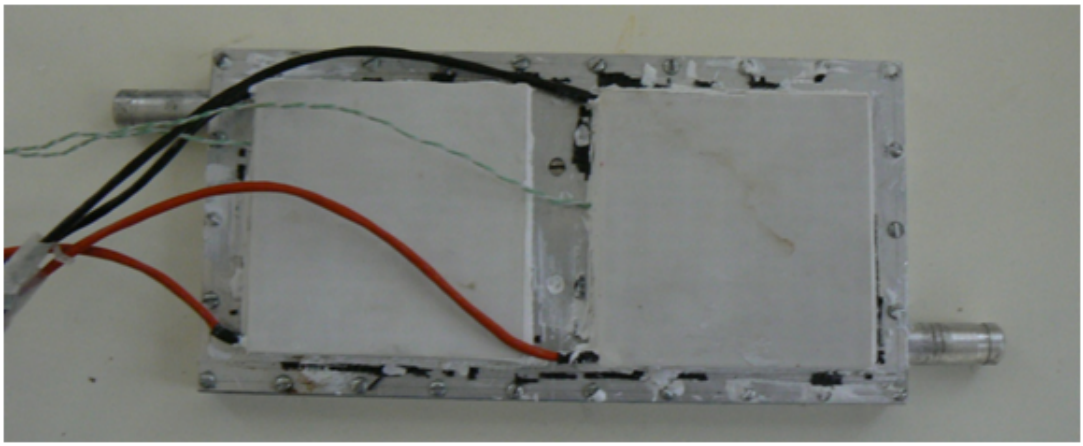

Figure 5.1: Heat exchanger with two TEMs attached to the top

This overall design of the heat exchanger meets our design criteria in Section 4. However, in light of modelling and controlling, a first critical assessment of the proposed heat exchanger design permits to point out weaknesses and highlight potential difficulties. For instance, one can notice the size of both TEDs which are - in comparison to the blood path width - much wider, covering almost all three heat exchanger loops. Since the temperature of the blood is different at each point within the heat exchanger, a resultant temperature gradient will occur across the surfaces of both TEDs. This can result in unexpected, suboptimal electrical behaviour. Therefore, some of the inherent implications for modelling and controlling based on the proposed design are:

- Varying thermal impedance across the surface of both TEDs

  The combined thermal impedance of blood and aluminium casing can have a direct affect on the electrical behaviour of the TED. Imposition of spatial temperature variation caused by the blood might lower the overall heating performance and can result in a suboptimal control regime.

- Location for temperature measurement

  Imposed requirements such as limiting the maximum input temperature to 42 degrees Celsius in order to prevent haemolysis might involve additional measurement strategies for successful implementation. This could be done in form of using several thermocouples to find an average heating temperature or an array of thermocouples to find the maximum temperature.

- Non-symmetry

  Analysing the geometry of the complete heat exchanger shows that no symmetry exists in any plane or axis; thereby reducing the options of simplifying the system. To demonstrate simplification due to symmetry, Fig 5.2 is a 3D stainless-steel MEMS heat exchanger model which can be analysed on just one unit cell, rather than the entire structure, in order to produce a realistic result (Comsol, 2011).

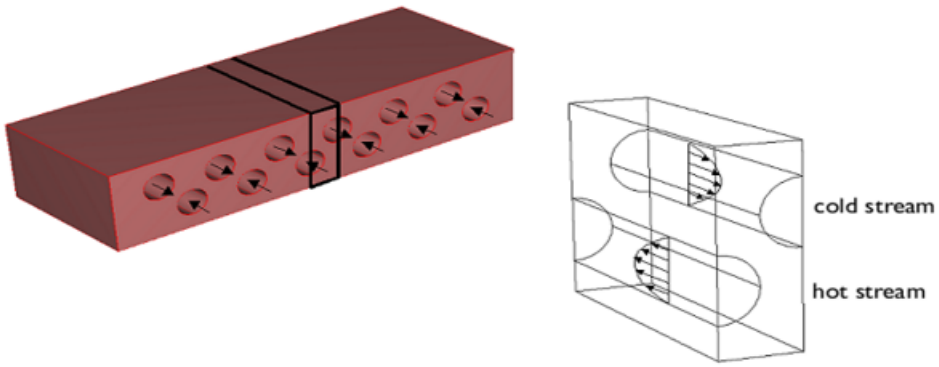

Figure 5.2: Example of simplification

In consideration of all above points including geometry and design of this multi-physical problem, finite element analysis (FEA) software is employed in this area of the work. This technique of modelling covers a wide range of engineering and physics

applications allowing the usage of complex materials, design of arbitrary shapes, and application of a multitude of different loads and boundary conditions (Antonova and Looman, 2005b). This ability to combine physical phenomena is very convenient, allowing modelling of more complex structures. The FEA program COMSOL Multiphysics® (COMSOL Ltd., Cambridge UK) supports an extensive variety of modules categorised as electrical, mechanical, fluid, and chemical which can all be combined to assess multifactorial effects depending on the physical structure of the model of interest. Modules of interest for the heat exchanger model are AC/DC, heat transfer, and CFD.

The modelling process has been divided into two parts, the thermoelectric element and heat exchanger casing, which are considered on an individual basis first and integrated at a later stage.

5.1 Thermoelectric Effects

In thermoelectric devices, three main effects manifest during the conversion of electrical energy to thermal energy or vice versa. They are termed Seebeck-, Peltier-, and Thomson effect with respect to their discoverer.

The Seebeck effect dates back to 1821 when Thomas Johann Seebeck discovered that when two dissimilar conducting materials are connected to each other, with each junction maintained at different temperatures, an electromotive force can be induced. A voltage differential across the two terminals arises which is proportional to the temperature difference applied to both junctions. The proportionality factor or Seebeck coefficient $\boldsymbol{\alpha(T)}$ therefore is:

$$\alpha(T) = \frac{dV}{dT} \tag{5.1}$$

Both magnitude and sign of the Seebeck coefficient depend upon the choice of material.

The Peltier effect was observed for the first time in 1834 by Jean Charles Peltier. He discovered heat being released or absorbed at junctions of two dissimilar materials connected to each other depending on the direction of the electrical current. The amount of heat P (in Watt) that can be absorbed or liberated at the junction depends proportionally upon the electrical current I (in Ampere); that is,

$$P = \pi(T)I \tag{5.2}$$

where $\boldsymbol{\pi(T)}$ is the proportionality factor or Peltier coefficient. Similarly to to the Seebeck effect, the Peltier effect cannot be attributed to one material alone but rather where two dissimilar materials meet.

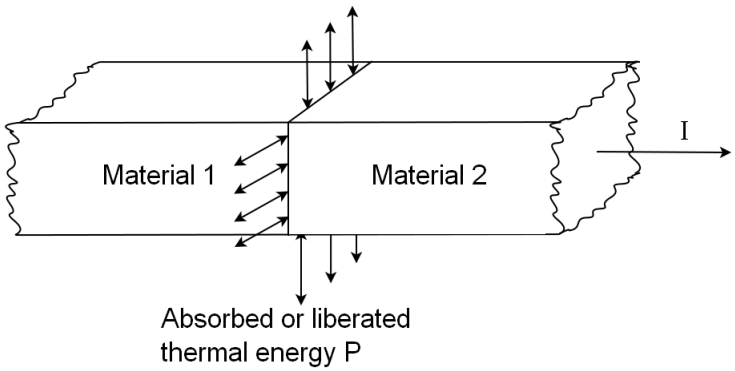

Figure 5.3: The Peltier Effect

The Thomson effect. In 1857, Thomson found that heat exchange with the surrounding takes place when a current is passed through a material that is exposed to a temperature gradient. It can be shown that the heat released or absorbed by

the conducting material is proportional to the spacial temperature difference and the electrical current, that is:

$$P = \tau(T) I \frac{dT}{dx} \tag{5.3}$$

where $\boldsymbol{\tau(T)}$ is the proportionality factor or Thomson coefficient. Contrary to the Seebeck- and Peltier effect, the Thomson effect is ascribed to individual materials and does not result at interfaces between two dissimilar materials. Due to the dependency of the product of current and temperature gradient, the Thomson effect can be considered as a second-order effect which can be neglected in the operation of thermoelectric devices (Soo, 1968).

5.2 Thermoelectric Device

The proposed ECMO heat exchanger module is provided by a set of a thermoelectric heat pumps in which electrical power is applied to, allowing "pumping" of heat against the temperature gradient. The nomenclature of thermoelectric devices varies in literature such as: Peltier or Seebeck device/element, TEC (Thermo-Electric Cooler), TEH (Thermo-Electric Heater), TEM (Thermo-Electric Module), or solid state heating element. The meaning of the device remains the same, irrespective of the nomenclature, merely the mode of operation changes. Thermoelectric devices are able to cool as well as heat an object, depending on the direction of the supplied electrical current.

Fig. 5.4 shows a schematic of one segment of a heat pump consisting of two pellets or one couple. Thermoelectric devices are arrays of N pairs, connected electrically in series and thermally in parallel. A typical material in commercially available devices is bismuth telluride (Bi_2Te_3) whose legs are alternately p-type and n-type doped.

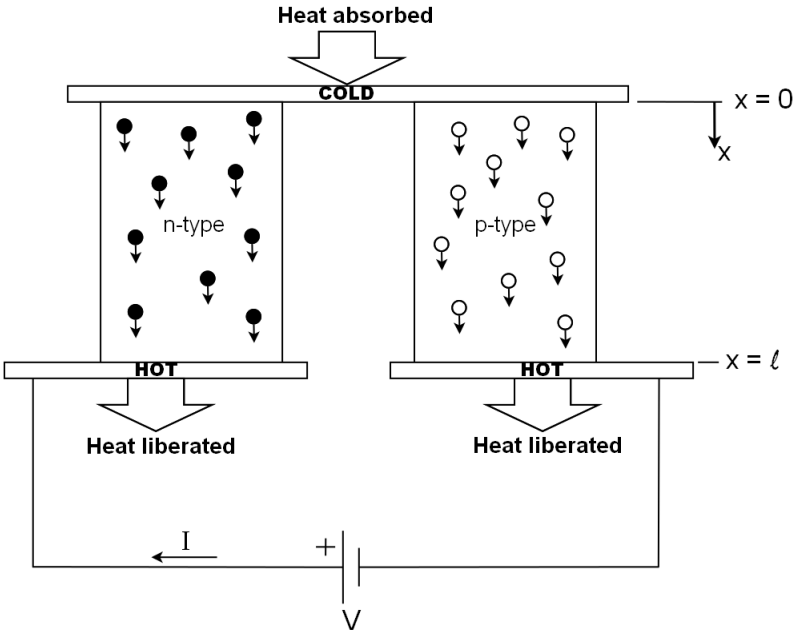

Figure 5.4: Schematic of Thermoelectric heat pump

P-type refers to a crystal when there are more free holes as majority carriers than electrons. In n-type semiconductors, there are more free electrons as majority carriers than holes. Both are the direct result of deliberately adding impurity atoms to the crystal. Current provided by the power supply results in downward movement of n-type electrons and p-type holes to the same side within the semiconductor material. The net affect is that thermal energy is absorbed at the upper side (cold) and pumped to the lower side (hot) from where it is liberated to the environment, thereby establishing a temperature difference between both sides.

To describe the performance of the thermoelectric device, an energy balance equation can be formulated according to the energy conservation techniques which are applied to the emitting and absorbing side of the TEM (Decher, 1997). The balance equation states that the net thermal power output must equal the electrical power

input if losses and the rate of stored energy are negligibly small.

$$P_e - P_a = P_{el} \tag{5.4}$$

The second Kelvin relation states a direct connection between the Seebeck coefficient and the Peltier coefficient; that is,

$$\pi = \alpha \cdot T. \tag{5.5}$$

Substituting (5.2), (5.4) and the Kelvin relation result in:

$$V = \alpha \left(T_e - T_a \right), \tag{5.6}$$

the electromotive force (EMF) of the TEC that allows thermal energy to be pumped up the temperature gradient.

The energy equilibrium with individual transport mechanisms at the emitting junction are:

- Internal thermal input P_π due to the Peltier effect
- Internal thermal input P_J due to resistive heating
- Internal thermal output P_F due to conduction down the temperature gradient (from hot to cold)
- Thermal energy output P_e as the result of the sum of P_π, P_J, and P_F

Equivalently, the energy contributions at the absorbing side are:

- Thermal energy input P_a from an external source (environment)

- Internal thermal output P_π due to the Peltier effect
- Internal thermal input P_J due to resistive heating
- Internal thermal input P_F due to conduction received from the emitting side

The four considered thermal effects on each side of the TEC give:

$$P_e = P_\pi + P_J - P_F \tag{5.7}$$

$$P_a = P_\pi - P_J - P_F \tag{5.8}$$

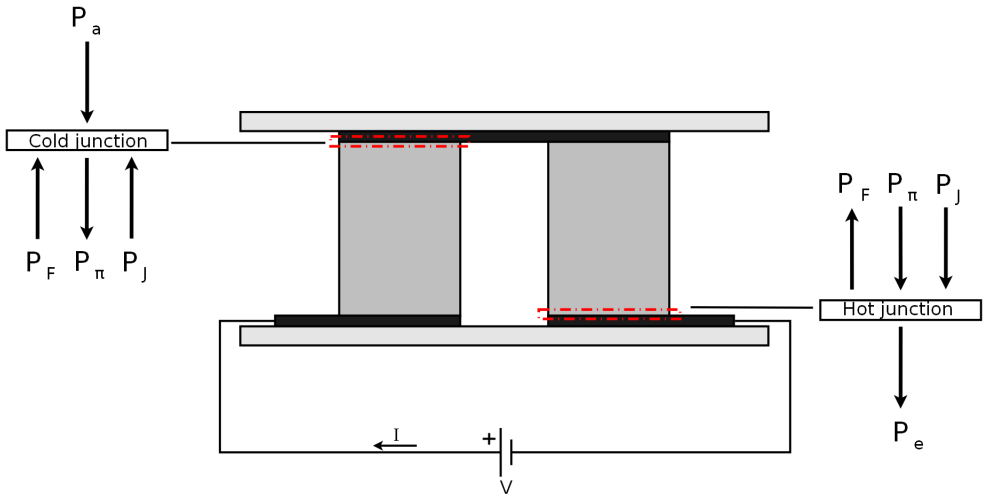

Figure 5.5: Schematic of energy balance in a thermoelectric couple

Figure 5.5 schematically represents the energy balance at the heat absorbing and emitting side. The magnitudes of various thermal components are:

$$P_J = I^2 R \tag{5.9}$$

where P_J is the product of the electrical current (in Ampere) squared and the ohmic resistance (in Ohm) of a couple of pellets; that is,

$$R = \rho \frac{2L}{A} \tag{5.10}$$

where ρ is the electrical resistivity (in Kelvin per Watt), L is the hight (in meter), and A is the cross-sectional area of the pellet (in meter squared).

Fourier heat or thermal conduction P_F (in Watt) also occurs in thermoelectric devices due to the temperature difference between hot and cold plate. The standard formula for 1-D heat transfer in a conducting material is (first part of (5.11):

$$P_F = -kA\frac{\partial T}{\partial x} \approx -kA\frac{\Delta T}{L} = -\frac{\Delta T}{2\Theta}, \tag{5.11}$$

with

$$\Delta T = T_e - T_a \tag{5.12}$$

where k is the mean thermal conductivity of the semiconductor material (in Watt per meter Kelvin) and $\partial T/\partial x$ is the heat propagation (in Kelvin per meter) through one couple along the height ∂x. Due to the small height of the pellets and small enough current, it is assumed that heat propagation occurs linearly and time independent, resulting in the middle term with ΔT. The thermal resistance Θ (in Kelvin per Watt) of one couple equates to:

$$\Theta = \frac{L}{2kA}. \tag{5.13}$$

The last thermal effect in each junction is the Peltier heat whose principle has been described in section 5.1. The liberated or absorbed energy is proportional to the

electrical current flowing through a junction of two dissimilar materials which mathematically is represented by (5.2) and a substitution of the second Kelvin relation:

$$P_{\pi_a} = \alpha T_a I \tag{5.14}$$

$$P_{\pi_e} = \alpha T_e I \tag{5.15}$$

where subscripts a and e define the particular heat-absorbing and heat-emitting junctions, respectively.

Considering a number of p- and n- doted leg pairs (as found in commercially available TEC's) one is encouraged to introduce slight changes to several equations. With N numbers of electrically-in-series leg pairs, one needs to calculate the overall TEC resistance; that is,

$$R_n = N \cdot R. \tag{5.16}$$

In terms of parallel heat distribution along the array of pn-pairs in the x-direction, the total thermal resistance is:

$$\Theta_n = \frac{\Theta}{N}. \tag{5.17}$$

For N couples in a TEM, the total Seebeck coefficient amounts to

$$\alpha_n = \alpha \cdot N. \tag{5.18}$$

The parameters representing a multiple of N couples (5.16) - (5.18) therefore affect previously discussed equations:

$$P_J = I^2 R_n, \tag{5.19}$$

$$P_F = -\frac{\Delta T}{\Theta_n}, \tag{5.20}$$

$$P_{\pi_a} = \alpha_n T_a I, \tag{5.21}$$

$$P_{\pi_e} = \alpha_n T_e I, \tag{5.22}$$

and

$$V = \alpha_n \left(T_e - T_a\right). \tag{5.23}$$

To combine equations (5.19) - (5.22) to form an energy equilibrium for the heat-emitting and absorbing side, one can write:

$$P_e = \alpha_n T_e I + \frac{1}{2} I^2 R_n - \frac{T_e - T_a}{\Theta_n} \tag{5.24}$$

$$P_a = \alpha_n T_a I - \frac{1}{2} I^2 R_n - \frac{T_e - T_a}{\Theta_n}, \tag{5.25}$$

in which half of the entire Joule heat contributes to each side. The complete electrical circuit of a TEM consists of the voltage V supplied that produces the EMF (5.23) as well as the current I running through the module's resistance R_n:

$$V = \alpha_n \left(T_e - T_a\right) + I R_n. \tag{5.26}$$

Several approaches for modelling thermoelectric devices exist in literature (Huang and Duang, 2000), (Chavez et al., 2000). The TED model by Huang and Duang is based on a first principle approach in which all physical quantities and processes involved are considered combined to partial deferential equations. A more original approach is presented by Chavez et al. (2000) who takes advantage of the analogy between thermal and electrical quantities. This allows the substitution of thermal elements such as heat or temperature with electrical current and voltage, respectively, to form and simulate an equivalent circuit of a TED in a low-cost simulation environment such as SPICE. Both of these approaches are considered as lumped parameter models by assuming the temperature to be uniform across the surfaces of the TED. As mentioned above, the geometry of both Peltier elements exceed the width of blood flow paths inside the heat exchanger resulting in temperature differences on the surface so that a lumped parameter approach is not feasible. Therefore, it was decided to use the available FEA analysis software COMSOL Multiphysics® for modelling the Peltier elements.

A quick and effective way of implementing the derived equations into COMSOL is by transferring them into the weak form. Appealing features of this weak form in COMSOL - compared to partial differential equations (PDE) or ordinary differential equations (ODE) form - are convenient input of energy derived equations ((5.19) - (5.25)) as well as the capability of solving a strong non-linear model (COMSOL, 2008). The coupled set of thermoelectric equations are heat flux $\mathbf{q}$ and electrical current density $\mathbf{J}$ (Landau and Lifshitz, 1984):

$$\boldsymbol{q} = -\mathrm{k} \cdot \nabla T + P \cdot \boldsymbol{J} \tag{5.27}$$

$$\boldsymbol{J} = -\sigma \cdot E - \sigma \cdot S \cdot \nabla T, \tag{5.28}$$

which are part of a global set of energy conservation equations for heat flow

$$\rho C \frac{\partial T}{\partial t} + \nabla \cdot \boldsymbol{q} = Q \tag{5.29}$$

and current continuity

$$\nabla \cdot \left(\boldsymbol{J} + \frac{\partial \boldsymbol{D}}{\partial t} \right) = 0; \tag{5.30}$$

with

$$\boldsymbol{D} = \epsilon \cdot \boldsymbol{E} \tag{5.31}$$

where

k = thermal conductivity, $W/m/K$

P = Peltier coefficient, V

$\boldsymbol{q}$ = heat flux, W/m^2

$\boldsymbol{J}$ = electric current density, A/m^2

σ = electric conductivity, S/m

S = Seebeck coefficient, V/K

ρ = density, kg/m^3

C = specific heat capacity, $J/kg/K$

Q = volumetric heat generation rate, W/m^3

$\boldsymbol{D}$ = electric flux density, C/m^2

T = absolute Temperature, K

V = electric potential, V

ϵ = dielectric permittivity, F/m

$\boldsymbol{E}$ = electric field intensity, V/m.

The irrotational electrical field $\boldsymbol{E}$ can be derived from a voltage differential

$$\boldsymbol{E} = -\nabla V \tag{5.32}$$

and the heat generation term Q combines Joule heating as well as Seebeck heating

$$Q = \boldsymbol{J} \cdot \boldsymbol{E} \tag{5.33}$$

according to (5.28). Equation (5.29) and (5.30) are converted into the weak form of partial differential equations for analysis in COMSOL. Therefore, each side of both equations are multiplied by a test function and integrated over the computational domain Ω. Additional mathematical manipulations such as vector identity and Gauss' theorem are applied leading to the weak expressions:

$$\begin{aligned} 0 = \int_{\Omega} \Bigg[& \underbrace{-\rho C_p \frac{\partial T}{\partial t} T_{test}}_{\text{weak derivative}} + \underbrace{(-k\nabla T) \cdot \nabla T_{test}}_{\text{weak thermal}} + \underbrace{(P\boldsymbol{J}) \cdot \nabla T_{test}}_{\text{weak Peltier}} + \underbrace{Q T_{test}}_{\text{weak source}} \Bigg] d\Omega - \\ & - \int_{\partial\Omega} \underbrace{(\boldsymbol{q} \cdot \boldsymbol{n})\, T_{test}}_{\text{Neumann BC}} \delta\Omega \end{aligned} \tag{5.34}$$

$$\begin{aligned} 0 = \int_{\Omega} \Bigg[& \underbrace{-\sigma \cdot E \cdot \nabla V_{test}}_{\text{weak Joule}} - \underbrace{\sigma \cdot S \cdot \nabla T \cdot \nabla V_{test}}_{\text{weak Seebeck}} + \underbrace{\frac{\partial \boldsymbol{D}}{\partial t} \cdot \nabla V_{test}}_{\text{weak derivative}} \Bigg] d\Omega - \\ & - \int_{\partial\Omega} \underbrace{\left[(\boldsymbol{J} \cdot \boldsymbol{n})\, V_{test} + \left(\frac{\partial \boldsymbol{D}}{\partial t} \cdot \boldsymbol{n} \right) V_{test} \right]}_{\text{Neumann BC}} \partial\Omega \end{aligned} \tag{5.35}$$

COMSOL's predefined modules already include most terms of equation (5.34) and (5.35) except the weak contribution due to Peltier and Seebeck which require to be implemented.

One of the main materials used in commercially available thermoelectric devices include a form of alloy, typically Bismuth-Telluride-Selenide for individual p- and n-doped legs, copper for bridging connections between individual legs, and ceramics (Al_3O_2) for top and bottom plates (Venkatasubramanian et al., 2001). Typical material properties for $(Bi_{0.5}Sb_{0.5})_2Te_3$ at 27° Celsius were taken from Seifert et al. (2002) and copper from Antonova and Looman (2005a).

		Thermoelectric Material	**Electrode (Copper)**
Seebeck coefficient	α, (V/K)	p: 200e-6 n: -200e-6	6.5e-6
Electric conductivity	σ, (S/m)	1.1e5	5.9e8
Thermal conductivity	λ, $(W/m/K)$	1.6	350
Density	ρ, (kg/m^3)	7740	8920
Heat capacity	C, $(J/kg/K)$	154.4	385

Table 5.1: Material properties (Seifert et al., 2002; Antonova and Looman, 2005a)

Constant material properties were assumed for a single thermoelectric leg during initial modelling processes. Upon comparison with the literature, one can conclude the validity of above relevant equations necessary for further modelling steps.

The constant material properties shown in Table 5.1 as well as (5.34) and (5.35) were only applied to a single leg with dimensions of $(1 \times 1 \times 6)mm$ capped by two $0.1mm$ layers of copper on top and bottom.

The different boundary conditions applied to the single leg model are:

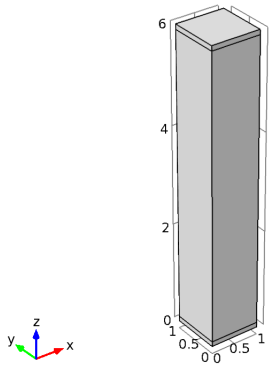

Figure 5.6: Single p-alloy leg with copper layers

- $T = 273°K$ @$z = 0mm$;
- $V = 0V$ @ $z = 0mm$;
- $V = 0.05V$ @ $z = 6mm$;
- all other boundaries are perfectly insulated (adiabatic boundary condition).

To begin, a 'slightly coarser' mesh of 1414 elements was applied. Under perfectly insulated conditions, results of steady-state analysis are shown in Fig. 5.7a.

The temperature distribution of approximately $61°C$ across the single leg correlates to solutions published by Jaegle (2008).

Meshing is a crucial step within the modelling process in order for the COMSOL solver (or any FEM software) to calculate meaningful results. It divides the geometry of the model into small elements for the purpose of applying relevant differential equations in order to obtain results between boundary conditions. The size and shape of the mesh directly influence the solution of the computation. Choosing fine elements for meshing (and thereby increasing the number of elements) allows for a potentially more accurate result at the cost of long computational running times. Vice versa,

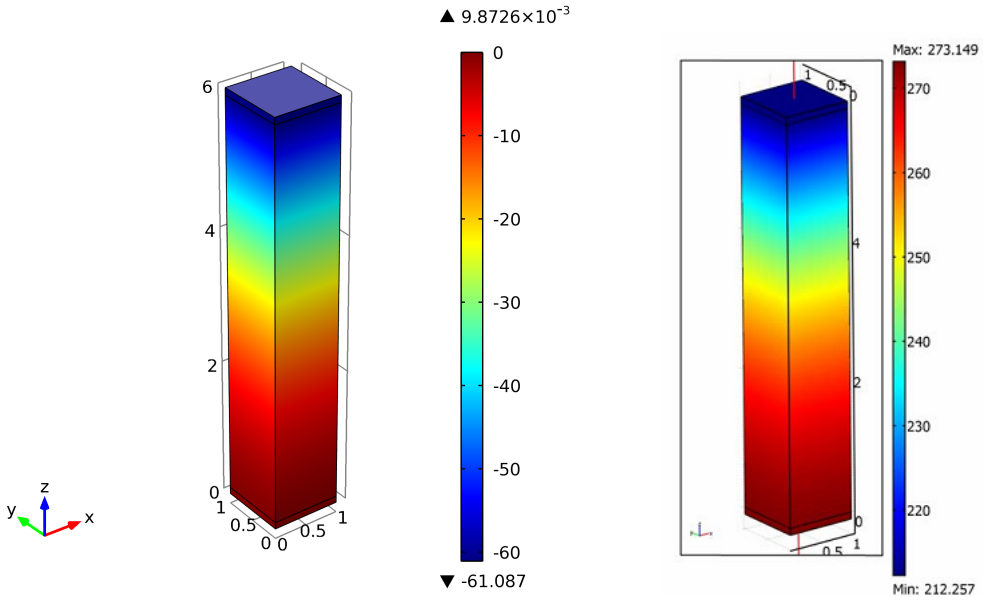

(a) Comsol simulation results of p-type thermoelectric leg (in degrees C)

(b) Temperature distribution according to Jaegle (2008) (in degrees Kelvin)

Figure 5.7: Temperature distribution comparison

coarser element sizes result in obtaining solutions faster at the cost of accuracy. To ensure that the result is independent of mesh size, time-dependent calculations were performed for all available options within Comsol, ranging from 'extremely fine' to 'extra coarse'. The same initial- and boundary conditions as above apply except for stationary solver. Mesh setting "extremely fine" was used as the base line for which all other sizes were measured against.

Fig. 5.8 shows the result of different mesh sizes and the amount of deviation during the process of time-dependent analysis. The 'coarser mesh' with 463 elements and 30 seconds computational time promises to give the most accurate results ($Variance = 0.06759$) following 'extremely fine'. Similar settings will be applied to further analysis.

Upon comparison with results found in the public domain, one can verify the accuracy of equation (5.34) and (5.34), mesh size, boundary- and initial conditions

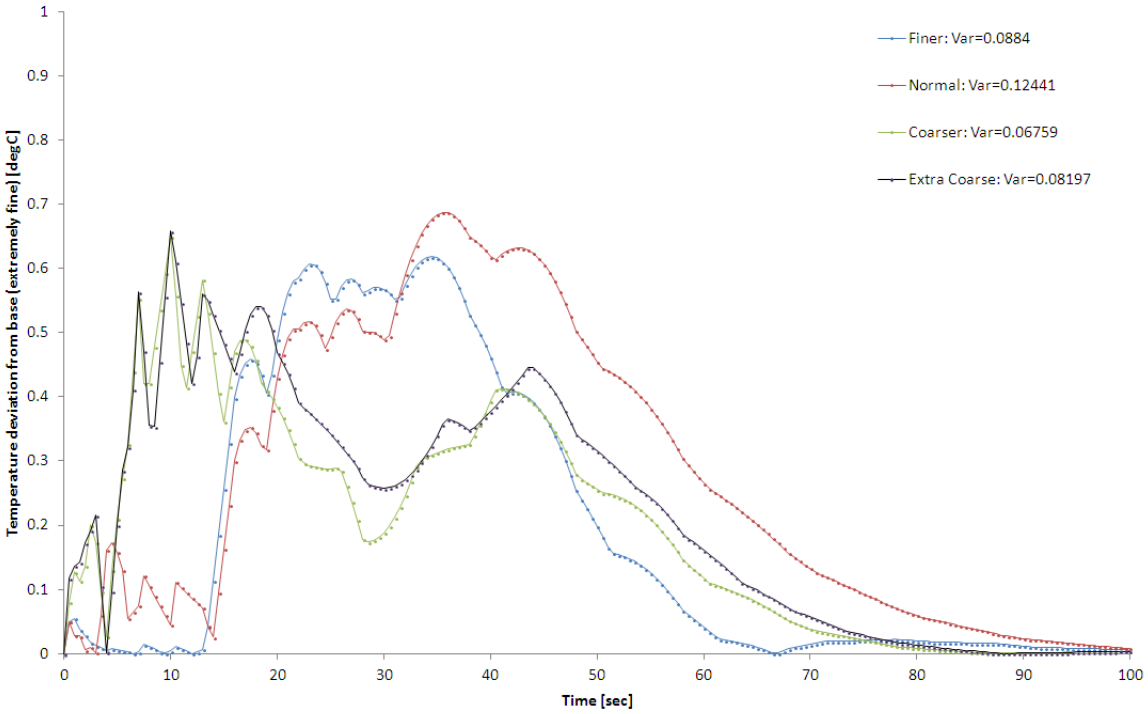

Figure 5.8: Time Dependent Temperature Deviation and Variance from "Extremely Fine" Mesh Size

to a single leg. The validated properties serve as a foundation for further modelling and can now be transferred and applied to a complete thermoelectric device model. However, in order to increase model accuracy, one is encouraged to substitute those constant values with real temperature dependent properties of Bismuth Telluride, as shown by Jaegle (2008).

However, the multitude of Bismuth Telluride-composite materials and design approaches found in literature (Poudel et al., 2008; Zhou, 2005; Panachaveettil, 2011; Angrist, 1982) require more details about the exact compounds or temperature dependent property data of $FerroTec's$ commercially available 482-leg thermoelectric cooler (9500/241/085BS). Contacting $FerroTec$ regarding either request resulted in

T, (K)	$\alpha(T)$, $(10^{-6}V/K)$	$\lambda(T)$, $(W/m/K)$	$\sigma(T)$, $(10^{3}A/V/m)$
100	75	2.5	185
150	125	2	142
200	170	1.55	100
250	200	1.35	72
300	218	1.28	60
350	225	1.35	55
400	218	1.75	70

Table 5.2: Temperature Dependent Material Properties of Bismuth Telluride (Seifert et al., 2002)

refusal. Alternatively, typical data of Bismuth Telluride such as in Table 5.2 were applied. However, it will be shown in Chapter 6 that results obtained by those standard properties prove to have poor correlation. A trial-and-error manipulation of temperature dependent values was chosen until the model's response was in agreement with the actual experimental results. The updated values are displayed in Table 5.3.

T, (K)	$\alpha(T)$, $(10^{-6}V/K)$	$\lambda(T)$, $(W/m/K)$	$\sigma(T)$, $(10^{3}A/V/m)$
298	212	1.2	55
323	224	1.14	43
348	228	1.1	31
373	230	1.13	20
393	228	1.15	13

Table 5.3: Updated Temperature Dependent Material Properties of Bismuth Telluride

The TEM-module offered by *FerroTec* has 482 semiconductor legs (241 p-legs and 241 n-legs) constructed in an array-type setting. Individual legs are connected electrically in series by thin copper metallisation, chain-linking all legs. The entire construct of serially concatenated leg-copper interfaces is mounted between two aluminium-ceramic (Al_3O_2) plates. Identified geometry and material attributions can easily be arranged within the Comsol environment.

Property	Bi_2Te_3	Copper	Al_3O_2
Length $[mm]$	1.2	3	55
Width $[mm]$	1.2	1.2	55
Hight $[mm]$	1.4	0.07	1.2
Density $[kg/m^3]$	7530	8960	3570
Thermal Conductivity $[W/m/K]$	Table 5.2	386	35.3
Specific Heat Capacity $[J/kg/K]$	544	385	837

Table 5.4: Geometry and Material Properties for TEM

Values in Tables 5.2 and 5.4 were applied to complete modelling $FerroTec's$ 482-leg thermoelectric device.

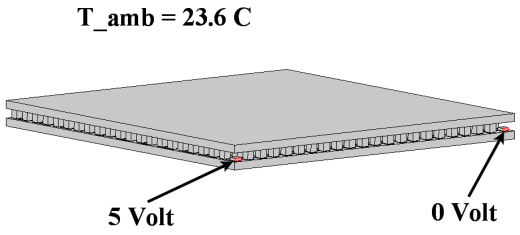

Figure 5.9: Complete model of FerroTec's (9500/241/085BS) module

Following geometry and material settings for the model, initial- as well as boundary conditions were applied next:

- $V = 5V$ at first copper interface,
- $V = 0V$ at last copper interface,
- $0V$ initial electrical potential across all pn-semiconductor legs,
- $\boldsymbol{n} \cdot \boldsymbol{J} = 0$ electrical insulation on all free leg boundaries,
- $T = 23.6°C$ ambient- and initial temperature of the entire TEM,
- $-\boldsymbol{n} \cdot (-k\nabla T) = 0$ thermal insulation.

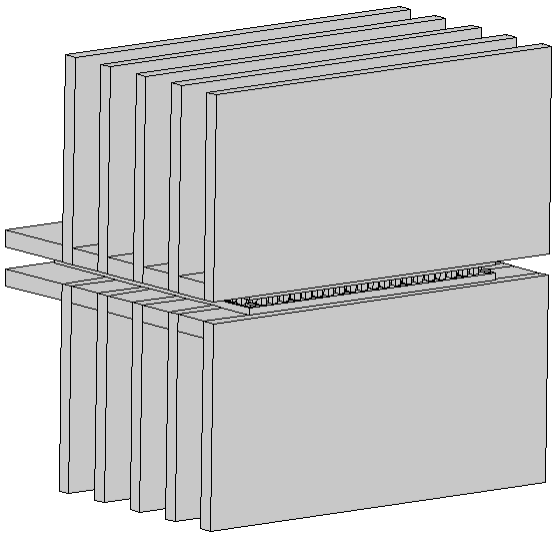

Figure 5.10: Model of TEM and heat sinks

A model of a 5-finned aluminium heat sink was attached to both sides of the TEM. The predicted processes occurring during simulation is that thermal energy is being absorbed by the surfaces of the lower heat sink (cold) and pumped up the temperature gradient to the opposite site of the TEM (hot) from where it is liberated. A thin thermally resistive layer of $300\mu m$ (with a thermal conductivity of 1.53 $W/m/K$) between TEM and heat sink represents the heat conducting paste used in experiments. External convective cooling (heat transfer coefficient $h = 2$

$W/m^2/K$) applies to all surfaces facing outwards. The complete TEM-heat sink model is displayed in Figure 5.10.

A free tetrahedral mesh was chosen for computation, comprising of 2,182,940 mesh elements for the entire geometry.

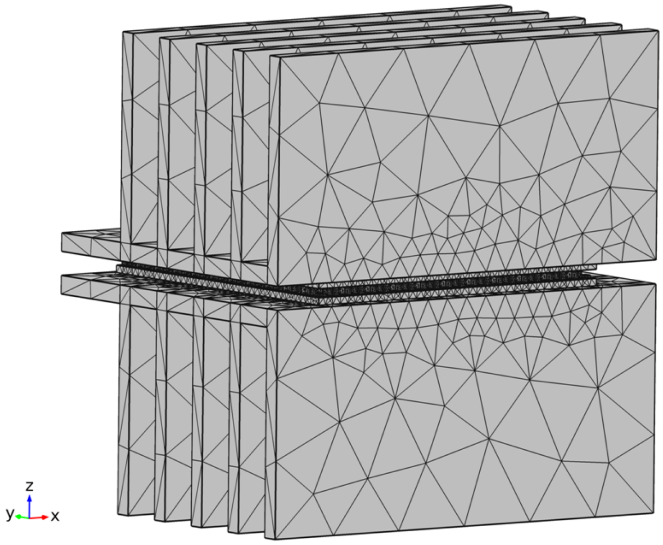

Figure 5.11: Physics Controlled Free Tetrahedral Mesh of TEM-Heat Sink Model

To investigate the performance of the TEM-model, a Comsol computation has been carried out with a time-dependent study, terminating at 780 seconds in 1 second time steps. The solvers used for the heat transfer calculation were a direct PARADISO with a segregated termination process. Nested dissection multithreaded methods were separately selected as a preordering algorithm analysis.

Computation results were saved and compared to experimental measurements recorded in the laboratory. The comparison to experimental results and model validation is presented in Chapter 6.

5.3 Heat-Exchanger Frame

The CAD drawing of the heat exchanger design from Section 4 was used as a template for modelling in a CFD environment. In order to establish a CFD model that produces meaningful results, one is required to observe, consider, and implement all relevant, physical characteristics that describe the functionality of the prototype.

Thermal energy exchange between blood and the thermoelectric device occurs within the heat exchanger frame by forced convective and conductive processes. Blood enters on one side of the heat exchanger and absorbs/releases heat during the passage before exiting at the opposite side.

Material properties of standard graded aluminium and water were applied to all domains (Table 5.5).

		Aluminium 6082 T6	**Water**
Thermal conductivity	λ, $(W/m/K)$	170	0.6
Density	ρ, (kg/m^3)	2700	1000
Heat capacity	C, $(J/kg/K)$	916.9	4200

Table 5.5: Material Properties for Heat Exchanger Frame

Two physics modules are required for computation analysis regarding our heat exchanger problem. One module deals with the heat transfer aspect and the other with laminar fluid flow. Boundary conditions within both modules need to be defined in order to achieve successful computation analysis.

The fluid path is separated from the solid aluminium frame by the wall boundary 'no slip' condition. Liquid enters with a laminar inflow profile and entrance length of 1 meter. Inlet velocity is averaged at constant 100 or 300 ml/min at 20.7 $^{\circ}C$ fluid temperature. Boundary conditions for the heat exchanger outlet valve are no viscous

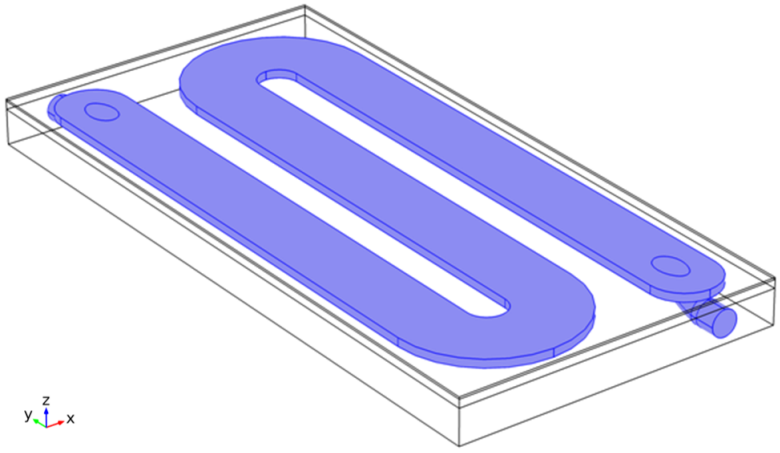

Figure 5.12: Fluid Path of the Heat Exchanger Model

stress and 0 Pa pressure. For practicality reasons in conducting lab experiments and comparing the results to the model, a fixed temperature heat source of 40 $°C$ was applied to the entire lower side of the heat exchanger frame instead of squares dedicated for future TED attachments. Ambient- and initial temperatures are 22 $°C$. All remaining exterior boundaries are subjected to convective cooling,

$$-\boldsymbol{n} \cdot (-k\nabla T) = h \cdot (T_{ext} - T) \tag{5.36}$$

with a temperature-dependent heat transfer coefficient according to Ashrae (1981) and Min (1956).

A free tetrahedral mesh was chosen, comprising of 8,647,884 mesh elements for the complete heat exchanger model.

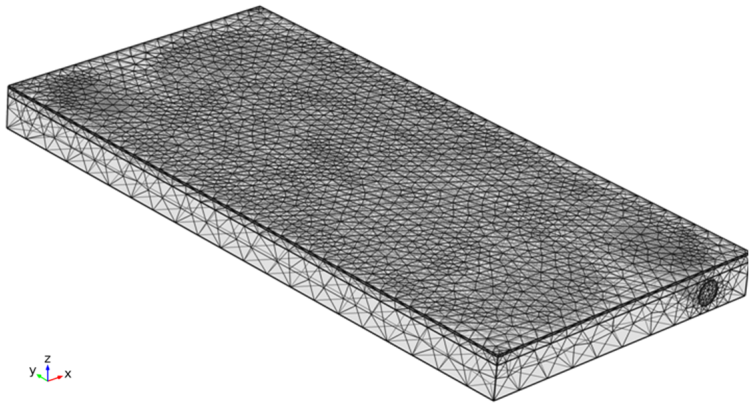

Figure 5.13: Physics Controlled Free Tetrahedral Mesh of Heat Exchanger Model

To investigate the performance of the heat exchanger model with imposed boundary conditions, a time-dependent study has been carried out with a run-time of 350 seconds in 1 second steps. The same solvers as with the TEM-model were employed to gain CFD results. Those results are compared to data obtained in experiments conducted in laboratory settings and published in Section 6.

5.4 TEM - Heat Exchanger Combination

In this section we cover the combined modelling of TEM and heat exchanger. The materials used for the thermoelectric device such as copper and bismuth telluride as well as aluminium for the heat exchanger were already assigned in previous sections and are transferable. The same applies to the underlying physics that were defined for each model such as *Laminar Flow*, *Heat Transfer*, and *Electric Current*.

Two TEMs were placed directly in contact with the top of the heat exchanger so that thermal energy can be exchanged by means of conduction between the two mod-

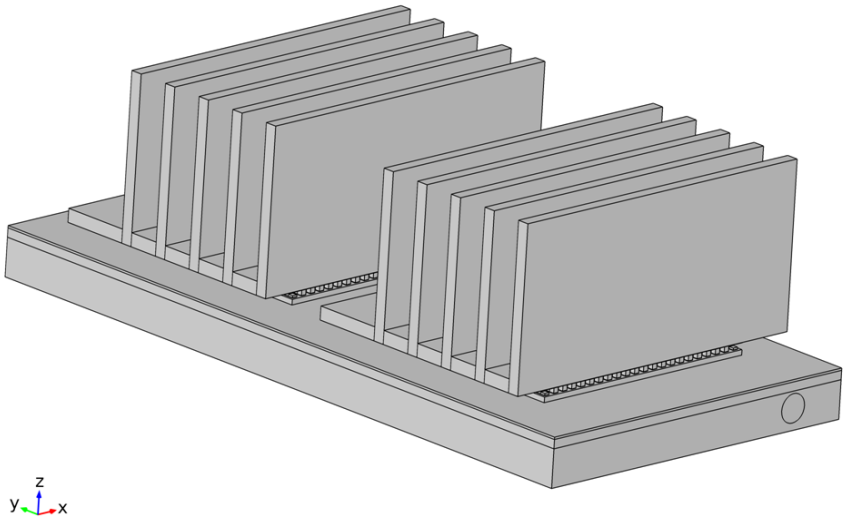

Figure 5.14: Model of Heat Exchanger and Two TEMs

els. The heat sinks are still placed on the top surface of each TEM from the previous section to improve heat transfer into the heat exchanger and increased performance.

A combination of previously discussed initial- and boundary conditions were applied. That entails voltage applied to TEM-terminals, initial electrical potential for PN semiconductor legs, electrical insulation and thermal insulation on PN legs, no-slip on fluid channel walls, laminar flow profile, no viscous stress and pressure at the heat exchanger outlet valve, convective cooling on exterior surfaces, fixed ambient temperature, and initial temperatures.

A free tetrahedral was chosen for the entire TEM-heat exchanger model with 11,574,623 elements, as shown in Figure 5.15.

To investigate the performance of the combined TEM-heat exchanger model with imposed boundary conditions, a time-dependent study has been carried out with a run-time of 500 seconds in 1 second intervals. The same solvers as in previous models were employed to gain computational results. The CFD results are then compared to

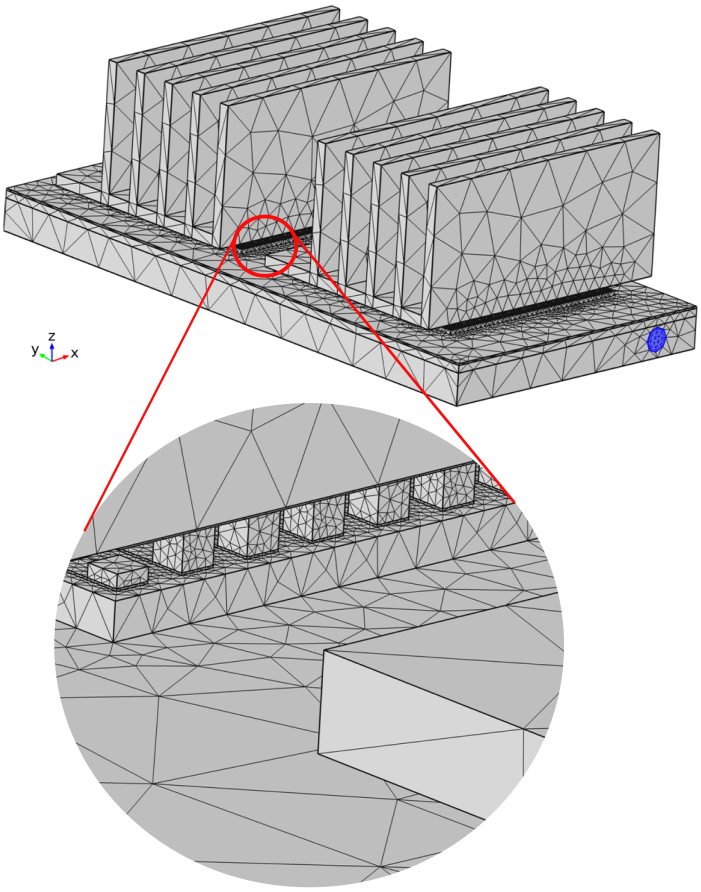

Figure 5.15: Mesh of TEM - Heat Exchanger Model

data obtained through experiments conducted in laboratory settings and presented in Section 6.

5.5 Summary

This chapter described the modelling aspect of the new conventional heat exchanger designed in Chapter 4. In order to provide a realistic model that allows a detailed analysis of heat transfer and fluid flow, it was decided that the modelling would be

undertaken in a FEA programme. Since the heat exchanger consists of two parts, 1) the static element through which blood flow is 'directed' and 2) the thermoelectric device for heating and cooling, both of them were individually modelled. The intrinsic physical effects of the TEM which were fully derived in a mathematical form were considered in order to implement them into the software. First, an individual leg of the TEM was analysed and validated with literature. A comparison revealed high correlation and this result confirmed the accuracy of the developed model. Based on this success, the entire TEM was modelled, implemented, and computed. The modelling of the heat exchanger was carried out separately with the same FEA software. The interaction between the laminar fluid flow and the surrounding aluminium were modelled. After meshing, a time-dependent study had been carried out which is compared to results obtained by physical testing in Chapter 6. Finally, both models were combined to fully represent the novel heat exchanger. The entire model was meshed and subsequently analysed by means of a time-dependent study whose results will be validated in the succeeding chapter.

Chapter 6

Simulation and Experimental Model Validation

This Chapter aims to outline the simulation- and validation processes of the models developed in Chapter 5. For measurement and control, a *cRio* (cRIO-9022, National Instruments Corporation, Austin, TX, USA) reconfigurable embedded control and acquisition system was used for control validation. The *cRIO* provides a compact host-to-target prototyping environment offering a wide range of hardware options for reconfigurable embedded control and monitoring applications. This platform serves as the core element which is connected to all hardware interfaces as well as hosting controller algorithms for real-time execution. Thermocouples of type K (TM Electronics Ltd., West Sussex, UK) were employed for temperature measurement and connected directly to the temperature module (NI 9214, National Instruments Corporation, Austin, TX, USA) of the *cRio*. A motor controller (MD03, Devantech Ltd., Norfolk, England) was used to translate power in a controlled manner from the power supply (CPX403A, TTi Inc., Fort Worth, Texas, USA) to the thermoelectric devices. The quantity and timing of power supplied is managed by the software on the *cRio*.

6.1 Experimental Setup and Methods

Our novel heat exchanger consists of mainly two parts; heat exchanger casing and the two TEMs. We therefore, considered a step-by-step individual approach for testing each part first and finalise with an integration of casing and TEMs.

For TEM-model validation, $FerroTec's$ thermoelectric module was sandwiched between two heat sinks whose thermal loads are known. For increased heat transfer between TEM and the heat sinks, thermally conductive adhesive (SE4486 CV, Dow Corning, Midland MI, USA) had been applied. Temperatures measurements were taken at the hot- and cold side of the TEM, using two thermocouples. Electrical power is directly provided to the motor controller and driven on demand according to the control signal given by the digital output (NI 9401, National Instruments Corporation, Austin, TX, USA). A software routine was developed within the LabVIEW (LabVIEW, National Instruments Corporation, Austin, TX, USA) environment for measuring, recording, and logging temperature values at a sample rate of $T_{sample} = 100$ ms. Also, a custom-made graphical user interface (GUI) allows the user to output pulse-width-modulated signals (PWM) on digital ports of the $cRIO$, thereby enabling the motor controller to drive the TEM. Variation in pulse-width translates directly in proportional changes of TEM-input voltages which in turn leads to temperature variations.

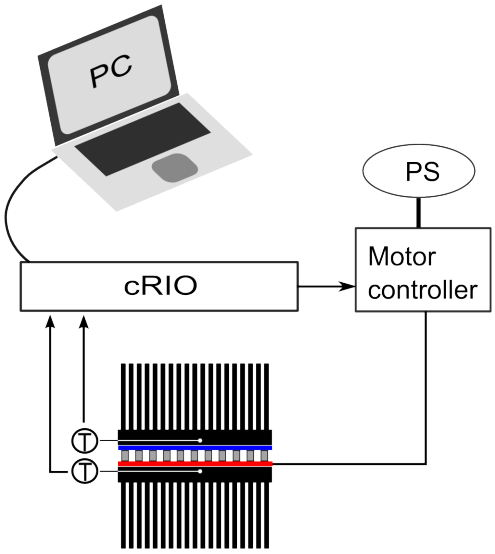

Figure 6.1: Schematic of test setup for TEM-model validation. The thermoelectric module is sandwiched between two heat sinks with thermocouples in between measuring the surface temperature.

A step-input command ($0\% \rightarrow 100\%$) was entered at the GUI which induced a jump in voltage from 0 Volt to 5 Volt at the terminals of the TEM. The step-input command was cancelled once steady state has been reached. This procedure was performed at different ambient temperatures 23.6, 30, 38 and 42 $^{\circ}C$ and repeated three times.

The second part of heat-exchanger model validation deals with the aluminium frame separately, without TEMs being attached. In order to see an externally applied heat source affecting the performance of the heat-exchanger, a steal block immersed in a temperature controlled water bath (Fisher Scientific, Leicestershire, UK) was used. Thermocouples were placed before and after inlet and outlet connectors, respectively, as well as top and bottom of the heat-exchanger frame. The same GUI and software routine as described above was used for measuring and logging temperature values. The circulation of liquid through the heat-exchanger was achieved by 1/4 inch Silicone

tubings connected to a rotary blood pump (Stökert, Munich, Germany). The liquid was drawn from a 2 litre reservoir at steady-state room temperature.

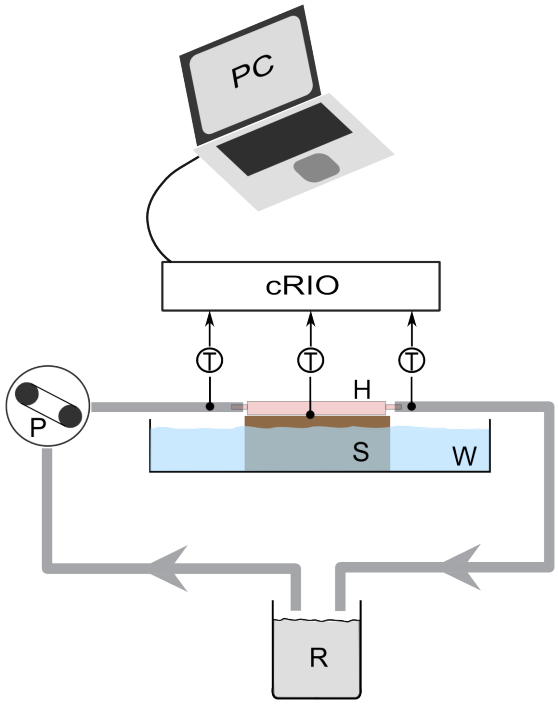

Figure 6.2: Schematic of test setup for heat exchanger frame validation; R) 2 litre reservoir, W) heated water bath, S) immersed steal block, H) heat exchanger frame

In order to perform a step-input response, the heat-exchanger was manually placed onto the hot surface of the steal block while liquid is passing through, thereby exhibiting a jump from room temperature to $T_{hotplate}$. Experiments were terminated once steady-state has been reached. This procedure was performed at different flow rates of 100 and 300 ml/min and repeated three times.

The last part of the heat-exchanger model validation process deals with the combination of TEM and casing together, as it would be used during clinical settings. Both TEMs are attached to the aluminium casing via thermal compound for improved heat transfer. The positive and negative wires of the TEMs were attached to the motor controller (MD03 24V 20A H-Bridge DC Motor Driver, Devantech Ltd, At-

tleborough, UK) and driven by a power supply (TTi CPX400A Dual 60V 20A PSU, Thurlby Thandar Instruments Ltd, Huntingdon, UK). Thermocouples were placed near inlet and outlet connectors, as well as under each TEM. A similar GUI and software routine as described above was used for commanding, measuring and logging temperature data. 1/4 inch Silicone tubings were connected to the rotary pump, heat-exchanger and water bath, as depicted in Figure 6.3.

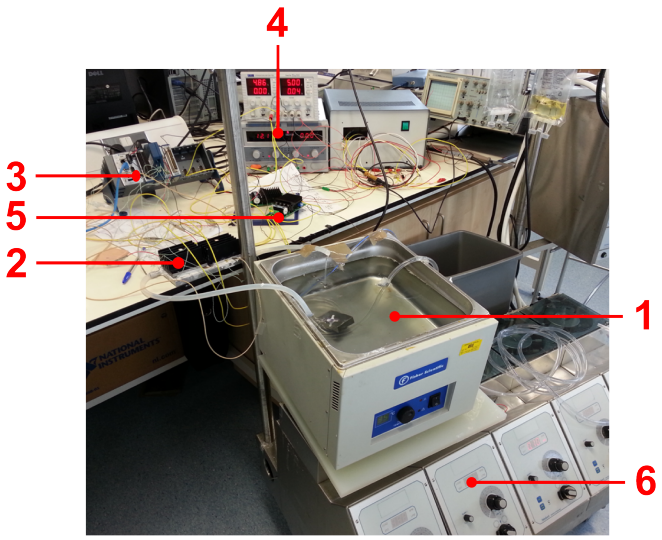

Figure 6.3: Experimental Setup of Heat Exchanger and TEMs; 1) Water Bath, 2) Heat Exchanger, 3) cRIO, 4) Power Supply, 5) Motor Controller, 6) Rotary Pump

While water is running through the heat-exchanger at a constant flow rate, a step-input is induced at both terminals of the TEMs. Temperatures of all deployed thermocouples were measured and the experiments were terminated once steady-state has been reached. This experiment was performed at different voltage levels of 3, 7, and 13 Volt at flow rates of 100 and 300 ml/min, and repeated three times.

6.2 Result Comparison and Discussion

Experimental- and simulation results of all modelled elements are discussed in detail in the following sections.

6.2.1 Thermoelectric Element

Temperature responses to step-input signals are compared for a thermoelectric device and the respective model developed in Chapter 5. The most suitable performance indicator for the accuracy of our model was determined to be the center-point surface temperature of the TEM. The results of the experiments and CFD simulations are represented as transient surface temperatures on the ordinate axis against time. Figure 6.4 and 6.5 display the transient surface temperatures (between ceramic plate and heat sink) at the cold- and hot sides of the TEM. The blue- and red plot in figure 6.4 show experimental results whereas the solid- and dashed lines represent model responses. At first, the model was simulated with standard temperature-dependent ma-

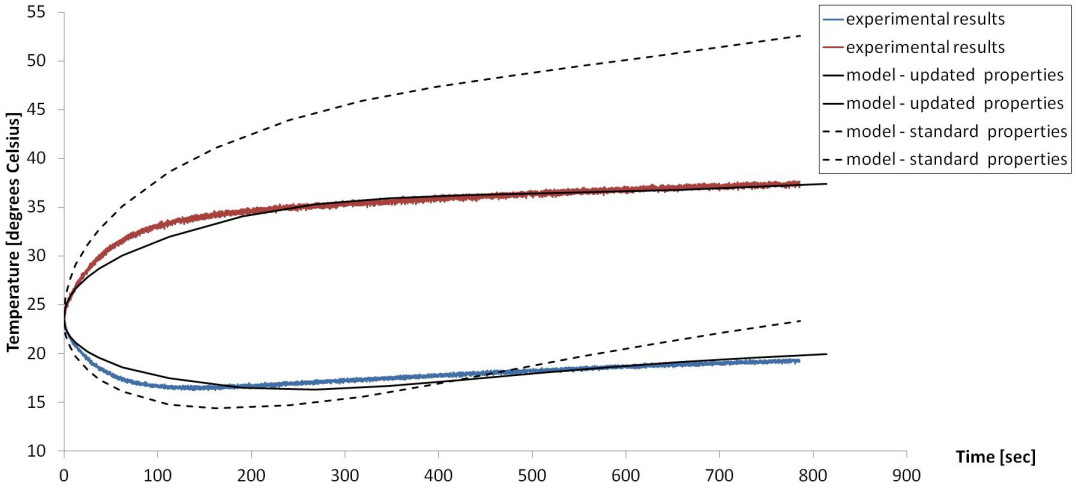

Figure 6.4: Experimental- and Simulation Results of a TEM with Heat Sinks Attached to Both Sides at 23.6 $°C$ Ambient Temperature

terial properties from Table 5.2 (dashed lines). However, deviations from experimental results were observed during transient- and steady state simulations indicating that noticeable differences in material composition and design existed between different thermoelectric devices, rendering Table 5.2 only as a guide. Therefore, temperature dependent material properties were adjusted in a trial-and-error approach in order to increase model accuracy. The closest fit was achieved with values from Table 5.3 after several iterations (solid lines). In the case of transient response ($t \lessapprox 200sec$), experimental data show a more underdamped result. The causes could originate from either deviations in dimensions of thermoelectric legs or material properties. However, despite not knowing the exact material composition of the commercial device, and therefore $\alpha(T)$, $\lambda(T)$, and $\sigma(T)$, the updated model created with Comsol matches the experimental data well.

The same procedure was carried out for ambient temperatures of 30, 38 and $42°C$ and compared to simulation results, as shown in Figure 6.5. Both, transient and steady-state model responses show good correlation to experimentally obtained values. Again, similar to Figure 6.4, model responses across all temperature ranges experience overdamped behaviour in the transient region and very minor steady-state deviations. The controller design however, can and will be tuned in order to incorporate uncertainties of this kind so that overall stable and predicted control behaviours can be established.

To help visualise the temperature distribution across the thermoelectric element and the attached heat sinks, a CFD thermal contour diagram is shown in Figure 6.6. The current-generated cold heat sink surface (bottom) absorbs thermal energy from the environment and pumps it through to the hot side of the TEM (top) via the 482

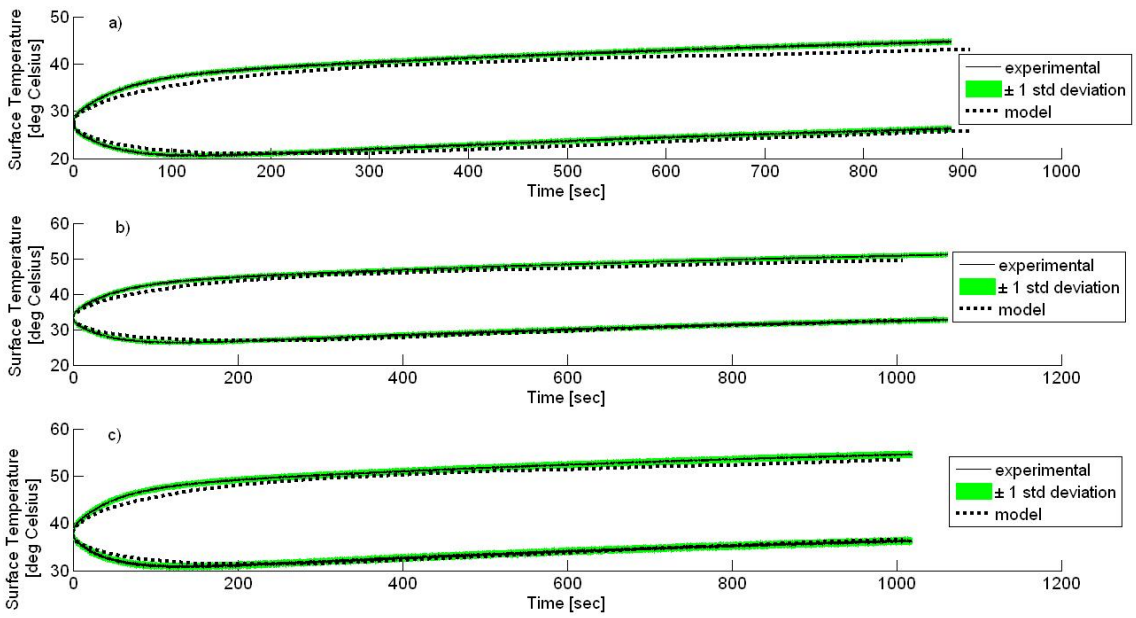

Figure 6.5: Experimental- and Simulation Response Comparison of TEM with Heat Sinks Attached to Both Sides. Excited by a Step Input of 5 Volt at Different Ambient Temperatures ±1 Standard Deviation; a) 30 degrees Celsius, b) 38 degrees Celsius, and c) 42 degrees Celsius.

semiconductor legs. This visible effect of the CFD analysis shows a rapid temperature gradient across the small legs.

The expected voltage progression across all 482 semiconductor legs in Figure 6.7 proves to be evenly distributed, helpful for fault detection during the modelling process. The example of a 5 V input and the resultant even distribution shows that the electrical resistance of all semiconductor legs has been successfully assigned during the modelling process.

6.2.2 Heat Exchanger Frame

In this section, we compare temperature responses to step-commands between the physical heat exchanger and the respective model developed in Chapter 5. Indicators

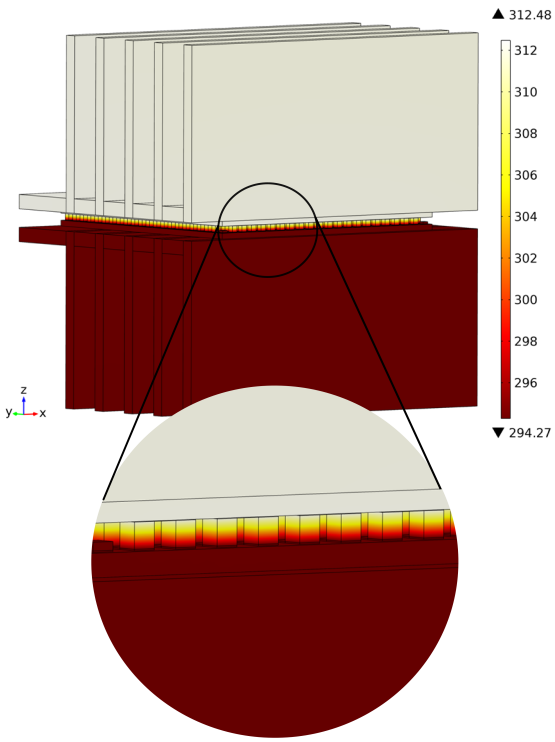

Figure 6.6: Thermal Contours of a CFD Thermoelectric Device with Heat Sinks in Kelvin

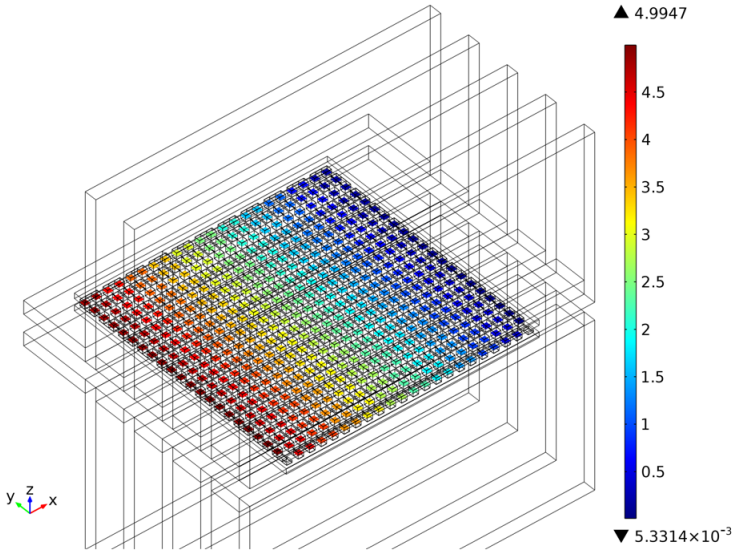

Figure 6.7: Voltage Distrubtion Across a Thermoelectric Device in Volt

used for suitable performance comparison are the area-weighted average temperatures of the heat exchanger outlet. The results of the lab experiment and CFD computation are represented as transient outlet temperatures with respect to time. Figure 6.8a and b display the trajectory at 100ml/min and 300ml/min, respectively.

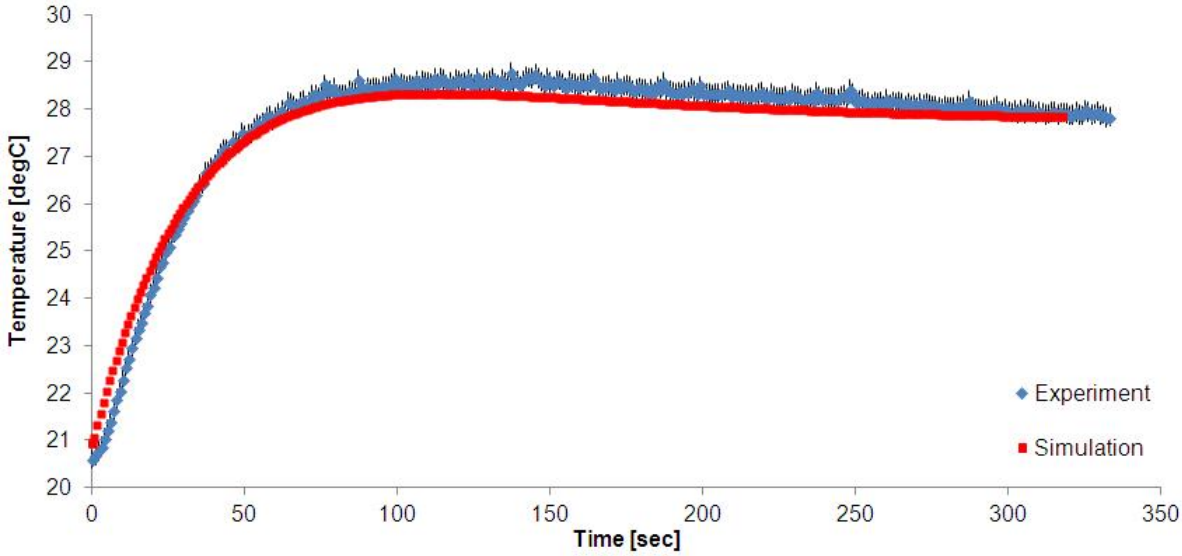

(a)

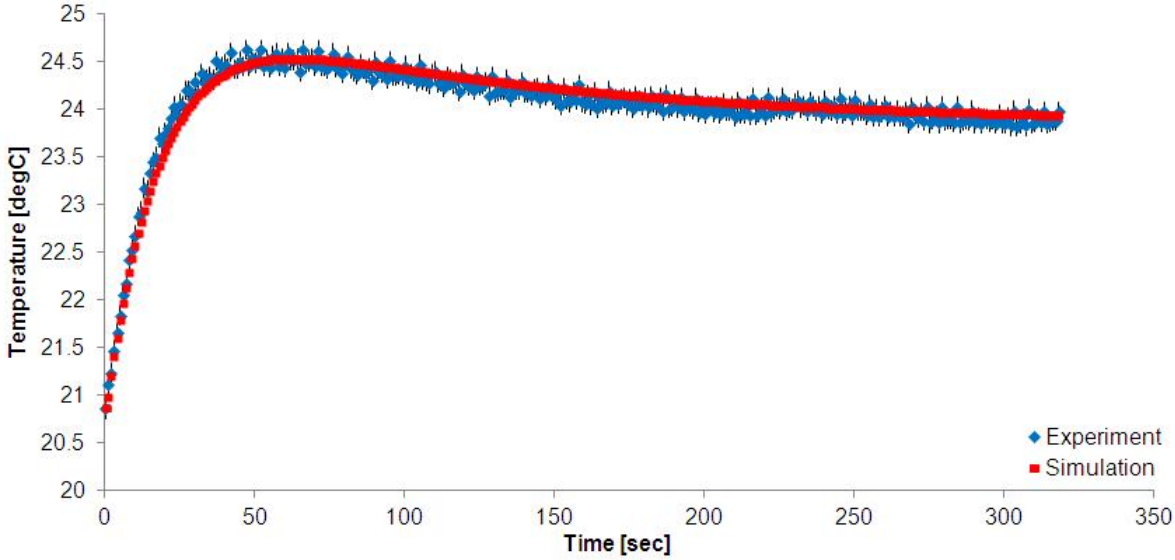

(b)

Figure 6.8: Experimental- (±1 Standard Deviation) and Simulation Results of Heat-Exchanger Casing Exposed to Step-Input Heat at Flow Rates of a) 100ml/min and b) 300ml/min.

Both, experiment (blue plot) and simulation (red plot) show good correlation not just in the transient part but also towards steady-state. In both cases, the maximum

outlet temperature decreases with increasing flow rates. This behaviour possibly arises from the exposure time to the inner heat exchanger wall surfaces that one unit volume of liquid experiences throughout the serpentine passage; i.e. longer exposure times correlating to increased thermal energy absorption. Figure 6.9 illustrates the relationship of different flow rates to increased temperature values.

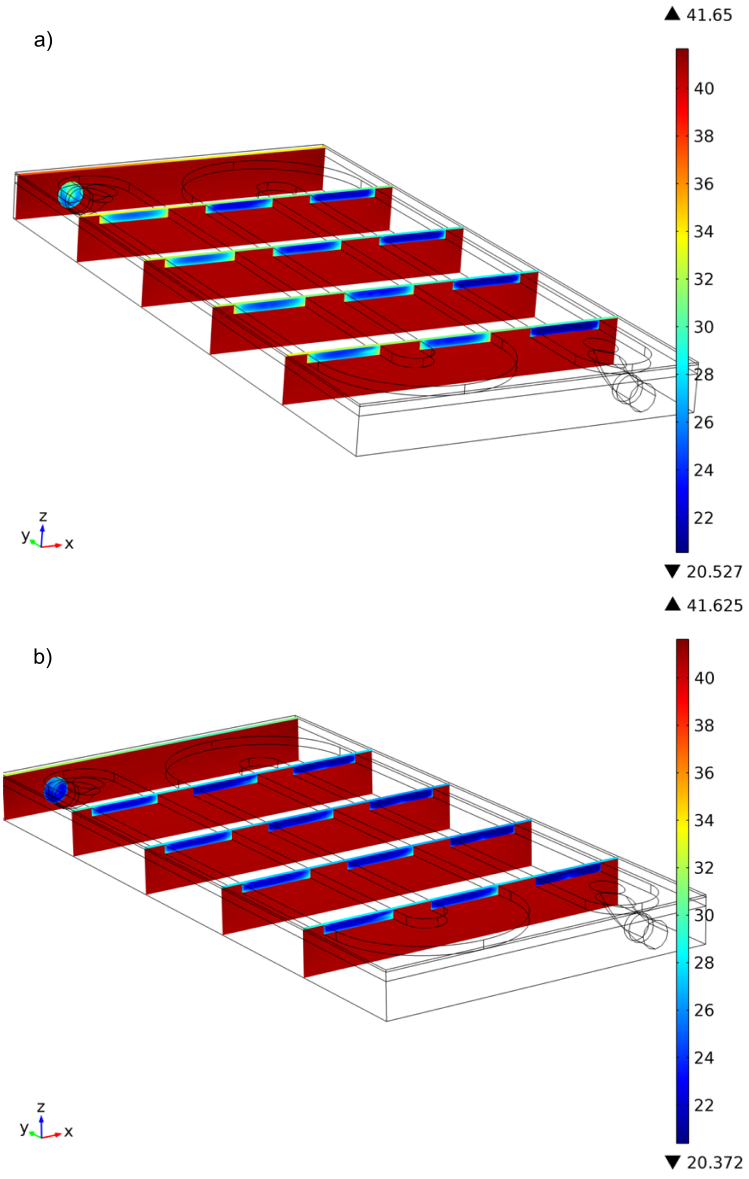

Figure 6.9: Fluid temperature at different flow rates, a) 100 ml/min, b) 300 ml/min

Shear stress related haemolysis plays a vital role in the field of artificial biotechnology (Pohl et al., 1998). Shear stresses contribute proportionally to blood destruction and in order to prevent excessive haemolysis within our heat exchanger, modelling is necessary. Figure 6.10 shows the result of shear stress modelling and areas of increased tendency.

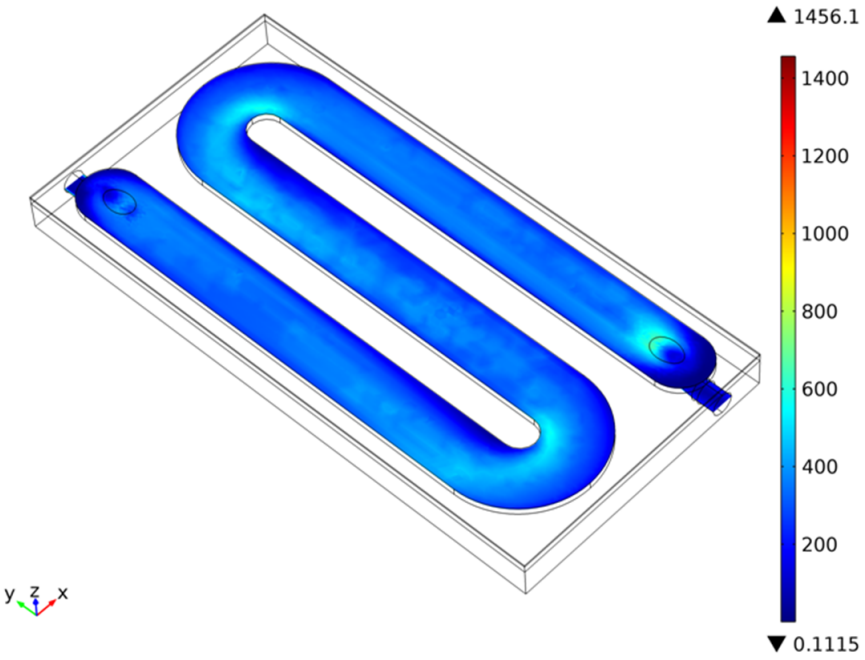

Figure 6.10: Shear Stress Analysis in Heat Exchanger Model [1/s]

To further highlight the flow distribution of fluid within the path, a velocity diagram is shown in Figure 6.11.

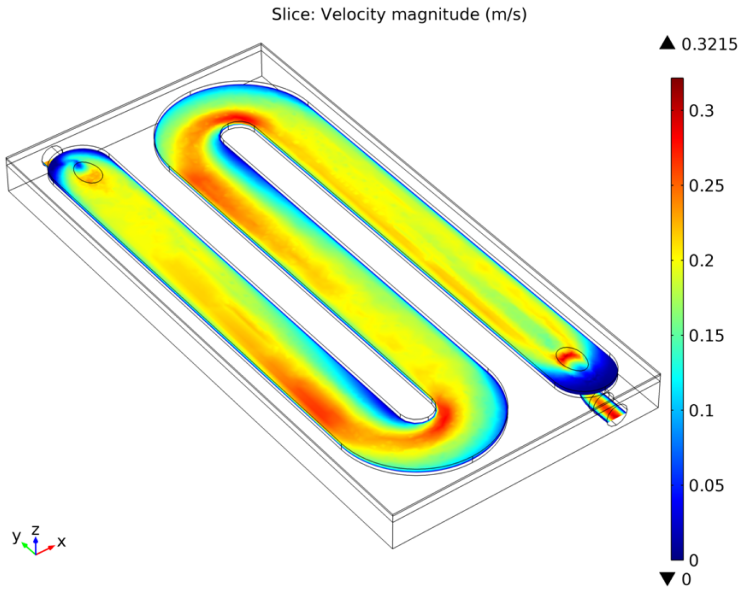

Figure 6.11: Velocity Field of Fluid within Heat Exchanger

It can be observed from Figure 6.10 and 6.11 that a correlation exist between shear forces and fluid velocity, especially at areas of rapid directional change. We tried to increase the turning radius of the fluid path in order to avoid shear stresses but unless the path exhibits a purely straight line throughout the heat exchanger, stress vectors are more likely to be present. Additionally, increased radii will contribute to overall size inflation, compromising the goal of a compact heat exchanger. The current design in Figure 6.11 displays the final stage of geometry modelling for the heat exchanger frame, reaching a compromise between fluid path dimension, curvature, and overall size.

6.2.3 TEM-Heat Exchanger Combination

The following section shows the results obtained from experiments and simulations of the entire heat exchanger plus TEM and compares them with each other, similar to the approach in Section 6.2.1 and 6.2.2.

Figure 6.12 shows the results of the step-response validation for the complete heat-exchanger and TEMs at 100 and 300ml/min. In the transient region, no major differences can be seen across the tested flow-rate region. However, slight steady-state discrepancies occur at the lower end of the voltage input, i.e. 3V which will be compensated for during controller tuning processes.

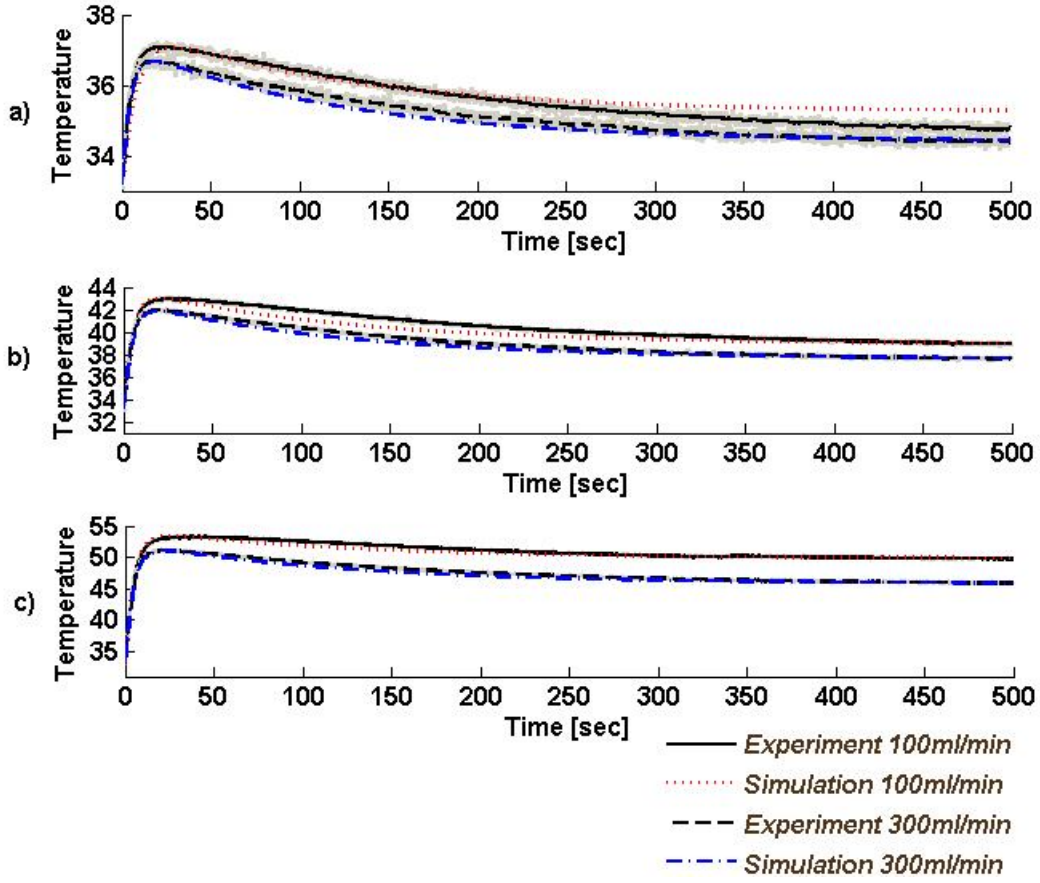

Figure 6.12: Experimental- ($\pm$1 Standard Deviation) and Simulation Results of the Entire Heat-Exchanger with TEM's at Constant Flow Rates of 100 and 300 ml/min; Exposed to Step-Inputs of of a) 3V b) 7V and c) 13V. Temperature in degrees Celsius

Model response behaviour across all elements of the heat exchanger overall show good correlation to physical recordings obtained during lab experiments (Figures 6.4

- 6.12). The developed model can now be implemented into a structure used for control design purposes.

6.3 Summary

In this chapter, we outlined the simulation and validation processes of the models with laboratory experiments. Similar to the proceedings of Chapter 5, each part of the heat exchanger was addressed and tested separately before comparing to model results. The first experiments dealt with the TEM alone, the second with the aluminium frame of the heat exchanger, and the third with the combination of both. At first, slight deviations were noticeable between model- and experimental results. However, after slight modification of the temperature dependent material properties of the model, these discrepancies were eliminated and correlation between both datasets could be found. The same applies to the remaining correlations where model and experimental data match well.

These experiments confirm the validity of our mathematical model which can now be used as a representation of the actual heat exchanger when designing a controller.

Chapter 7

Control Design

7.1 Introduction

In this chapter, we are describing the processes of a temperature control design based on the derived theoretical model established in the previous chapter. The aim is to choose an appropriate controller for our application and determine its parameters in order to achieve the desired overall system behaviour also defined in this chapter. The controlled process variable is the outlet blood temperature of the heat exchanger. A particular challenge to the controller design are variations of the environment, i.e. ambient- and blood inlet temperatures as well as flow rates.

Control systems are an integral part across many disciplines such as aviation, transportation, and also medical devices; especially where fail safe systems are employed. As described in Section 2.2, control systems have their integral place also in ECMO, allowing automated, iterative processes to measure and quantify the output performance of heat exchangers, oxygenators, and pumps. These can be used in feedback loops to make adjustments to input actuators in order for the system to

follow desired execution. The idea is for the device to perform without the interaction of a human being, in the case of the heat exchanger, the output temperature to stay at a certain level (preferably 37 degrees Celsius) and deviations should be constrained within narrow limits of acceptable temperature. This automation will ensure for normothermic blood- and hence body temperature in order to avoid any negative affects induced by hypo/hyperthermia. Similar types of controllers are employed in commercial heat exchangers, however the heat exchange technology is based on a different concept, see Section 2.1.5.

Due to simplicity of physical implementation and widespread use, classical control theory was applied for controller design. The heat exchanger can be represented as a single input single output (SISO) system whose analysis is carried out in the time domain. The input is in the form of electrical energy and the output is temperature at the outlet of the heat exchanger. The goal is to fulfil a set of requirements in the time-domain by analysing the step response of the heat exchanger model coupled with the control unit.

7.2 Temperature Control

In the previous Chapter 6.2, we were able to demonstrate the validity of our novel generated heat-exchanger model through experiments across a defined range.

The standard protocol for applying classical controller design techniques is to linearise a model at a number of operating points of interest in order to analyse system behaviours such as stability, disturbance rejection and reference tracking (Nelles, 2001). Our main operating point is the heat exchanger outlet temperature of around 37 degrees Celsius which the controller aims to achieve. The three major external

variables that influence the behaviour of the thermoelectric elements and hence the heat exchanger altogether, are:

- Ambient temperature,
- Blood temperature at heat exchanger inlet, and
- Blood flow rate.

All of these variables could change before or during the operation and the designed controller is required to keep the system stable. We therefore aim to simulate those changes in order to see the capabilities of our proposed controllers. The following self-proposed upper and lower limits for the heat exchanger system were examined in this context:

- Ambient temperature (max=35 $^{\circ}C$ and min=20 $^{\circ}C$),
- Blood temperature at heat exchanger inlet (max=40 $^{\circ}C$ and min=30 $^{\circ}C$), and
- Blood flow rate (max=300 ml/min and min=50 ml/min).

These three variables could go to either extreme resulting in a total of eight possible combinations; see Table 7.1.

Common controllers used among a wide range of industrial applications are of PI structure (proportional and integral) (Tipsuwan and Mo-Yuen, 2004). The main advantages of these PI controllers are the capability of eliminating any steady state errors originating from proportional (P) controller action (besides forced oscillations) as well as the handling of external disturbances and noise. Generally, a PI controller will slow down the speed of the system response slight but in many industry examples this is not a critical requirement for operations as demonstrated by the implementation of sensorless voltage regulation in PWM rectifiers (Bouafia, 2009), in DC/DC

	Ambient Temp.	Blood Inlet Temp.	Blood Flow Rate
1.	35 $^{\circ}C$	42 $^{\circ}C$	300 ml/min
2.	35 $^{\circ}C$	42 $^{\circ}C$	50 ml/min
3.	35 $^{\circ}C$	30 $^{\circ}C$	300 ml/min
4.	35 $^{\circ}C$	30 $^{\circ}C$	50 ml/min
5.	20 $^{\circ}C$	42 $^{\circ}C$	300 ml/min
6.	20 $^{\circ}C$	42 $^{\circ}C$	50 ml/min
7.	20 $^{\circ}C$	30 $^{\circ}C$	300 ml/min
8.	20 $^{\circ}C$	30 $^{\circ}C$	50 ml/min

Table 7.1: Matrix of Possible Extreme Disturbance Conditions

converters (Guo, 2003), DIY tools (Chen, 1991), and also the control of the liquid level in a spherical tank (Sakthivel, 2011). Besides the aforementioned properties of a PI controller, the process of controlling the blood temperature is not of rapid nature and elimination of steady state errors is crucial for the adequate and successful operations of a heat exchanger. Therefore, a controller of PI structure was employed for temperature control of the heat exchanger. The two main elements of the heat exchanger which require control are both TEMs (individually) and the outlet temperature. As described in Chapter 5, the performance of thermoelectric devices strongly depends on thermal impedance. This was verified during initial lab experiments by which TEM surface temperatures vary with ambient temperatures (at constant electrical power input). Therefore, independent controllers were used for the first and second TEM (graphically summarised by C1/C2 in Figure 7.1). This setup results in

a system with one controlled variables, T_{outlet} which is of crucial interest to the end user.

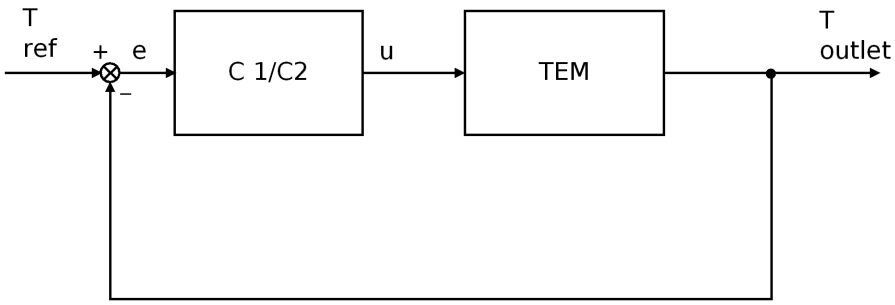

Figure 7.1: Principle Control Structure for Temperature Control

The outlet temperature of the heat exchanger is measured and compared to the reference temperature T_{ref} (provided by the user) to form the error signal e. The controllers calculate the control signal u based on the combination of error signal and controller constants and feed this signal to the TEM-driver unit for power supply. Additional integrator saturation (anti-windup) of the controllers ensures safe operation between 30 and 42 $°C$, to prevent the possibility of thermally induced haemolysis within the heat exchanger. This is realised by additional thermocouple probes attached to the surfaces of each TEM which feed into the algorithm as a safety feature.

$$f_{PI} = \begin{cases} 42°C & \forall \text{ T} \geq 42°C; \\ T & \forall \ 30°C \leq \text{T} \leq 42°C; \\ 30°C & \forall \text{ T} \leq 30°C. \end{cases}$$

Our strategy for tuning the controller was based on a 'trial-and-error' method which is an accepted procedure within the control community (Lee et al., 1998; Maeda and Murakami, 1992). Therefore, proportional (P) and integral (I) controller values were implemented and adjusted in Comsol Multiphysics until satisfactory results were achieved. Both PI-controllers were tuned in order to cope with the maximum and minimum conditions proposed in Table 7.1. Our two main requirements for controller tuning include minimised system overshoots ($\leq$ 5 %) and settling time of less than 500 seconds. Also, in order to avoid any formation of gaseous microemboli and thus the danger of potential brain oedema, incremental heating and cooling of the blood is crucial in ECMO patients (Geissler, 1997). Our trial-and-error method resulted in the following controller values which were used for further simulations: P_{C2}=0.1, and I_{C2}=0.05.

A series of simulations were carried out focusing on the behaviour of the heat exchanger outlet temperature in conjunction with the TEM performance Figure 7.1. For these simulations, boundary and initial conditions of Table 7.1 were employed as well as a maximum Voltage input of 13 V. The reference input temperature for the TEMs is 37 $^{\circ}C$. The reference temperature of the heat exchanger outlet is always 37 $^{\circ}C$ with requirements of zero overshoot and settling time below our set target of 500 seconds.

Throughout all experiments, the performance relationship of TEMs compared to the heat exchanger outlet temperature were apparent. The individual TEMs are required to achieve higher temperatures during the simulation runs (depicted in Figures 7.4, 7.5, 7.8, and 7.9) in order to produce a 37 $^{\circ}C$ outlet temperature. Similarly, the scenario for the cooling simulations (Figures 7.2, 7.3, 7.6, and 7.7) in which the

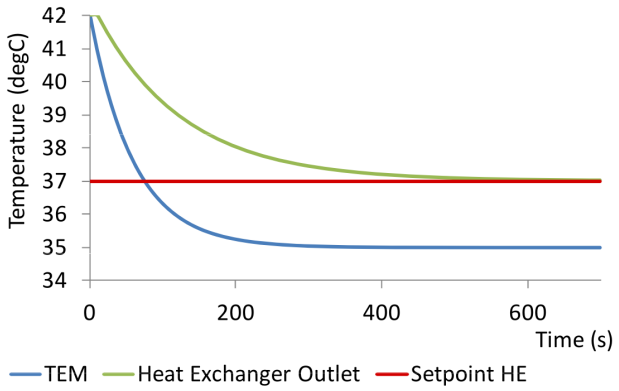

Figure 7.2: Case No 1; Heat exchanger outlet as well as TEM temperature response to 37 $^{\circ}C$ reference input

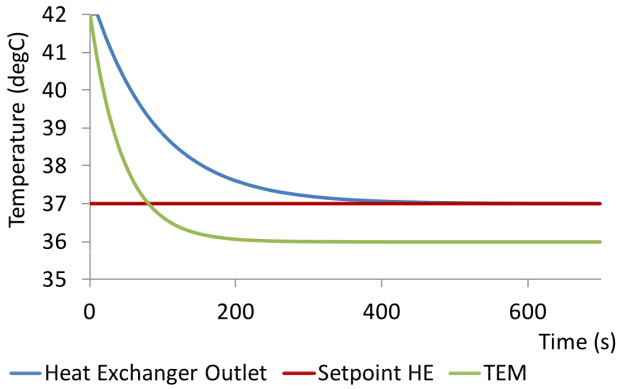

Figure 7.3: Case No 2; Heat exchanger outlet as well as TEM temperature response to 37 $^{\circ}C$ reference input

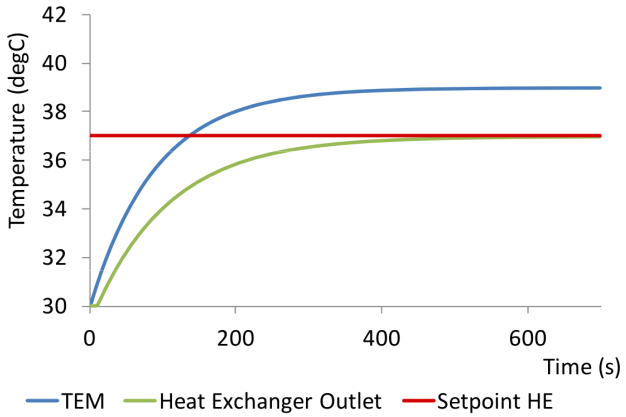

Figure 7.4: Case No 3; Heat exchanger outlet as well as TEM temperature response to 37 $^{\circ}C$ reference input

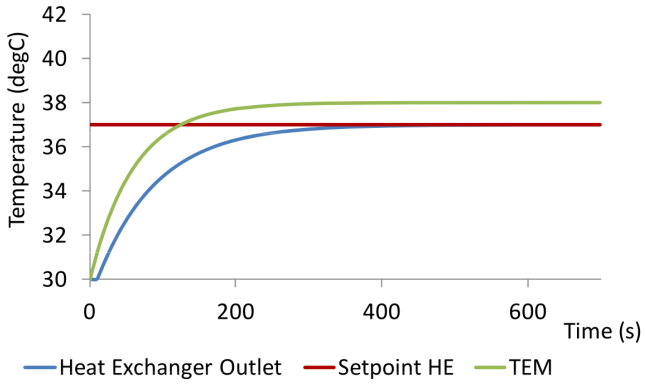

Figure 7.5: Case No 4; Heat exchanger outlet as well as TEM temperature response to 37 $^{\circ}C$ reference input

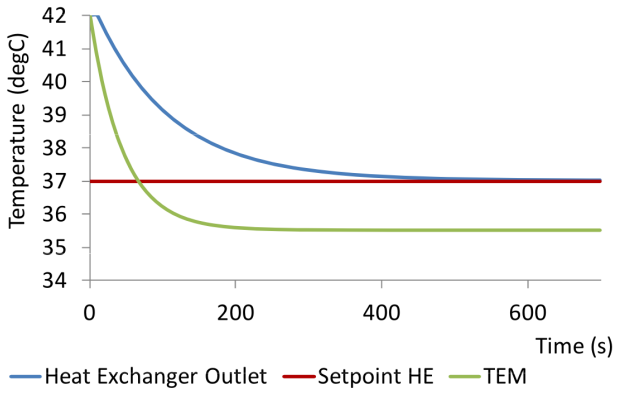

Figure 7.6: Case No 5; Heat exchanger outlet as well as TEM temperature response to 37 $^{\circ}C$ reference input

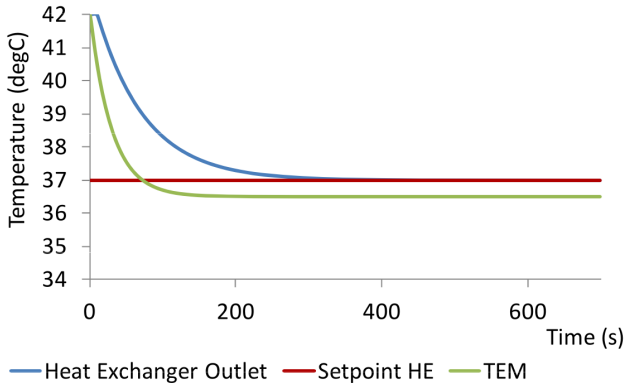

Figure 7.7: Case No 6; Heat exchanger outlet as well as TEM temperature response to 37 $^{\circ}C$ reference input

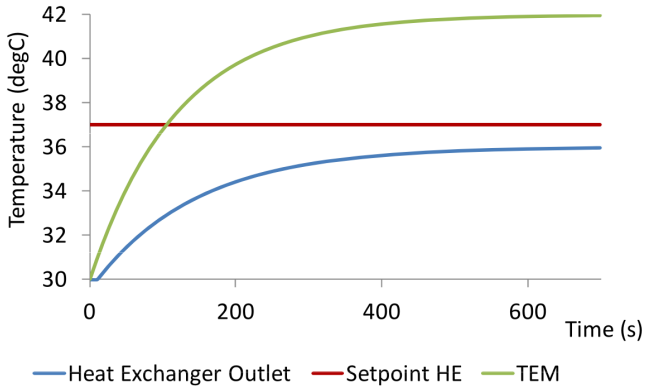

Figure 7.8: Case No 7; Heat exchanger outlet as well as TEM temperature response to 37 $°C$ reference input

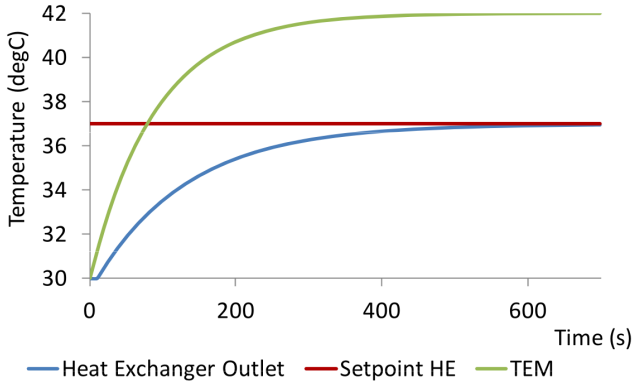

Figure 7.9: Case No 8; Heat exchanger outlet as well as TEM temperature response to 37 $°C$ reference input

TEMs are required to achieve lower temperatures in order to produce a 37 $°C$ outlet temperature are clear. This behaviour is understandable considering the pre-set initial conditions in Table 7.1. All cases performed according to our requirements, that is, achieved the desired outlet temperatures of the heat exchanger - except Case No 7. During this simulation, the temperature produced by the TEMs went from 30 to 42 $°C$ where it remained until the end. The implemented anti-windup saturation levels limited a further temperature increase beyond 42 $°C$ in order to avoid any blood destruction. Unfortunately, this protective mechanism was triggered before the desired

outlet temperature was reached, hence the simulation for this case underperformed as can be seen from Figure 7.8. After the TEM reached the maximum temperature, heat exchanger outlet temperature only read 35.9 $^{\circ}C$, 1.1 $^{\circ}C$ below the desired reference temperature. This case was simulated at a flow rate of 300 ml/min with ambient temperature of 20 $^{\circ}C$ as well as blood temperature of 30 $^{\circ}C$. The combined thermal impedance in Case No. 7 was too large for two TEMs in order to achieve results based on our requirements.

Despite the unsatisfactory results of Case No. 7, successful temperature response behaviours occurred across all simulations. The conservatively tuned PI gains allowed for a slightly overdamped system which resulted in no overshoots in any of the test cases. Also, desired temperature values in all successful runs were reached within the required 500 seconds.

Based on the successful accomplishment of all other simulations including controller behaviour, we decided to continue with experiments under the current design.

7.3 Summary

This chapter described the processes involved with designing control procedures for the heat exchanger for conventional ECMO settings.

A theoretical design approach lead to a computational model of the heat exchanger (in previous chapter) which was exposed to control simulations that allowed the adjustment of control parameters until desired results were achieved. Simulations with defined controller parameters displayed successful response behaviours of the heat exchanger model for all pre-defined operating conditions except for one case where underperformance was detected with respect to posed requirements. This coincidentally also happened to be the thermally most challenging case amongst all tests.

Chapter 8

Laboratory Experiments

8.1 Temperature Control for Heat Exchanger in Conventional ECMO

The PI-controller developed in Chapter 7 was to be implemented and tested in a real-time, lab-type environment using the heat exchanger designed in Chapter 4. The aims of the following experiments were to determine the performance, reliability, and repeatability of the proposed system. These experiments should provide clarity and reassurance for potential clinical deployment.

8.1.1 Materials and Methods

The PI-controller was implemented in a software routine (*LabView*) and executed through a cRIO 9122 real-time platform from National Instruments (Figure 8.1).

A rotary pump (Stökert, Munich, Germany) circulates a saline solution[1] from a two-litre water bath reservoir through the PVC tubings into the heat exchanger

[1]A typical blood substitute often used as a volume expander, consisting of sodium chloride, glycerine, and distilled water.

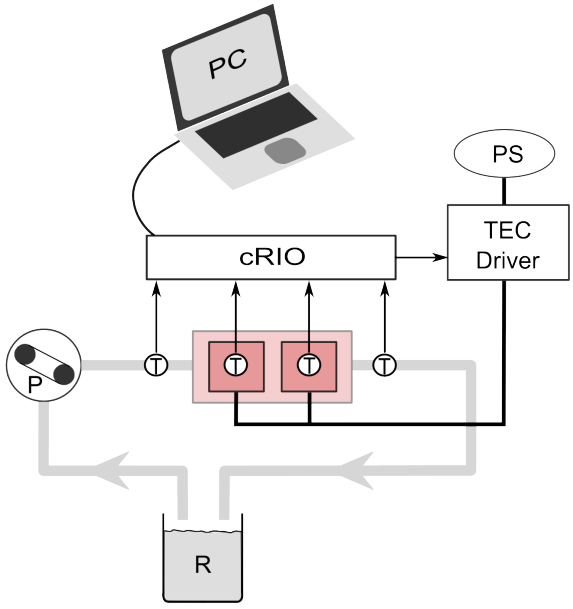

Figure 8.1: Experimental Setup; R: Reservoir, P: Pump, T: Thermocouples, PS: Power Supply

and back. T-type thermocouples (Physitemp Instruments Inc., Clifton, NJ, USA) for measuring temperature values were placed at the inlet- and outlet of the heat exchanger as well as below each TEM. The software algorithm, which runs and executes on the cRIO device, monitors and logs the temperature of all thermocouples and feeds the information directly into the PI-control algorithm. According to the calculated power requirements, a signal is forwarded to the motor controller adjusting the available power supply demands delivered to both TEMs. This control loop cycles continuously comparing the required temperature values set by the user through a PC and the actual values determined by the thermocouples.

As initial experiments are carried out with water, slight differences will be expected when performed with blood due to their unequal physical and chemical properties such as specific heat capacity and viscosity values. Blood has a lower value for specific heat capacity (3.49 kJ/kg) compared to water (4.18 kJ/kg), thus requiring

less energy in comparison to blood for the same temperature increase (Vanggaard, 2004). A faster temperature response is therefore expected when conducting initial experiments with water. For future experiments with blood, different response times as well as steady state values are to be expected under identical experimental conditions. Viscosity differences exist between blood and water due to various molecular interactions of plasma constituents and cells. Blood is a non-Newtonian fluid and its viscosity strongly depends on haematocrit levels and temperature (**?**)). A 2% increase in viscosity is attributed to a reduction of one degree Celsius whereas relative viscosity more than doubles with doubling haematocrit levels due to its non-linear nature. Overall, the physiological consequence of viscosity changes seem more relevant when considering pump designs due to the increased work load requirements or oxygenator design for improved gas exchange. But since viscosity changes do not impact the operations of a heat exchanger per se, less time was spent in considering this effect during our project.

The first set of experiments focused purely on the behaviour of the heat exchanger to changing reference temperature values whereas the second set of experiments focused more on the maintenance of patient temperature.

In order to test the capabilities of the heat exchanger, the first set of experiments focuses on maintaining temperature values between mild hypothermia (approximately 35°C) and normothermia (37°C) which are standard practice for ECMO patients in clinical settings (ELSO, 2014). The focus of these experiments is achieving these temperature values at the heat exchanger outlet for low flow rates (100 ml/min) and higher flow rates (300 ml/min), mimicking clinical scenarios of considerable ECMO support and weaning of the patient, respectively. By analysing the step changes at varying flow rates with respect to overshoots, rise time, and steady state

values, one can conclude the successful implementation of the proposed controller and potentially contribute to the validation of the heat exchanger design as well. At the start of the experiment, the flow rate was adjusted to constant values by means of a rotary pump (Stokert, Munich, Germany), and a water bath provided the circulating of water in a closed loop system. At first, a desired heat exchanger outlet temperature of 35 °C is requested. After approximately 1000 seconds when steady-state has been reached, a drop from 35 to 32 °C will be initiated in order to see the negative step-change responses. Again, after about a further 1000 seconds, a positive step-change of 32 to 37 °C will be commenced. These step changes were induced by means of a power supply (TTi CPX400A Dual 60V 20A PSU,Thurlby Thandar Instruments Ltd,Huntingdon, UK), PC (cRIO-9022, National Instruments Corporation, Austin, TX, USA), and thermoelectric driver (MD03 24V 20A H-Bridge DC Motor Driver, Devantech Ltd, Attleborough, UK), see Figure 8.2. Thermocouples were placed at the heat exchanger inlet and outlet, under the TECs, and in the water bath. The entire procedure is conducted at flow rates of 100, 200, and 300 ml/min and repeated 3 times. Heat exchanger inlet- and ambient temperatures were kept constant throughout all experimental runs in order to achieve reliable and repeatable results.

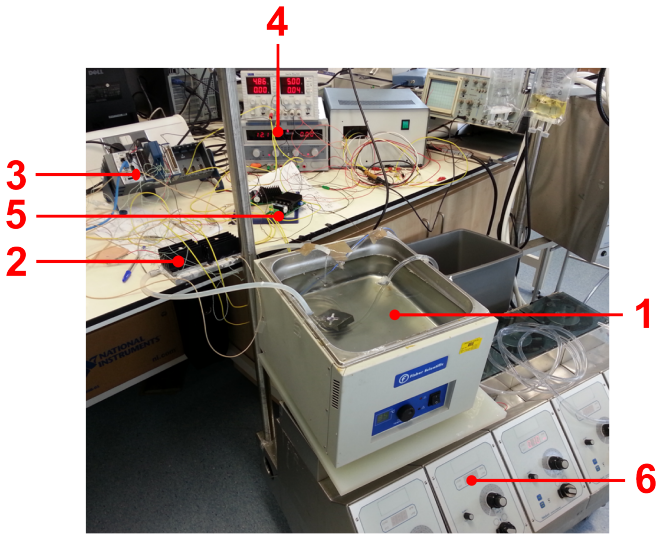

Figure 8.2: Experimental Setup of Heat Exchanger and TEMs; 1) Water Bath, 2) Heat Exchanger, 3) cRIO, 4) Power Supply, 5) Thermoelectric Driver, 6) Rotary Pump

A separate part of the experiments involved testing the cooling capability of the heat exchanger. The ability to cool the patient's blood during epidemics such as SIRS helps in preventing the patient of overheating and thus the inherent pathophysiological consequences associated with it. The possibility of reversing and controlling undesirable hyperthermia potentially avoids interferences with the clinical treatment going forward. In this regard, the water bath temperature was kept constant at 35 °C with the aim of reducing the heat exchanger outlet temperature with respect to the inlet temperature. Step tests were employed in order to see the transient and steady-state responses of the system, similar to the experimental procedure described above. The following four step tests were carried out: 34 to 36 °C, 36 to 35 °C, 35 to 33 °C, and 33 to 37 °C. The experiment was conducted three times at constant ambient temperature of 24 °C.

8.1.2 Results and Discussion

Figure 8.3 shows a typical response behaviour to input changes of 30 to 35 °C, 35 to 32 °C, and 32 to 37 °C at 100 ml/min from which both time-dependent and stationary control response behaviours can be extracted from. The first step-response demanded a jump from 30 to 35 °C at the outlet of the heat exchanger (Figure 8.3c). Both TEMs reacted to this request in form of heating (Figure 8.3a and b), initiated by separate temperature setpoints. It can be seen that in order for the heat exchanger to reach the requested outlet temperature of 35 °C, both TEMs overshot slightly and settled below maximum temperature of 42 °C for steady-state. The outlet temperature was reduced after 1000 seconds from 35 to 32 °C, reaching steady-state in approximately 250 seconds. Again, both TEMs bring about this outcome by the cascaded control structure explained in Section 7. After 2000 seconds, a step-input demand of 32 to 37 °C for the outlet temperature was induced. The time-dependent behaviour of both TEMs proceeded in a rapid manner, achieving a settling time in approximately 200 seconds. However, the software-limited maximum temperature of 42 °C does not allow any further increase, thereby limiting the overall outlet temperature to 35.9 °C for this case. Analogous results can be seen for higher flow rates with even further reduced outlet temperatures.

Results obtained through the aforementioned experiments require further consideration in connection to our model results. The requirements for model development of the heat exchanger incorporated stringent no-overshoot limits based on the potential for haemolysis generation. Model results obtained in Chapter 7 fulfil this requirement, however, discrepancies occurred during experimental procedures. The reason for this behaviour could result from either model inaccuracies or insufficient control tuning or even a combination of both. However, both aspects - heat exchanger

modelling and control tuning - were addressed and validated successfully in previous chapters. Based on our requirements, steady-state responses for heating and cooling of approximately 250 seconds each are good results, staying well below our 400 and 600 seconds proposed limits (Chapter 7). Even comparing model results to the actual experimental results show good correlation. The heat exchanger struggled with reaching 37 °C outlet temperature at lower flow rates of 100 ml/min and it was predicted through simulations in previous Chapters that only the worst-case scenario of much higher flow rates (300 ml/min) leads to poor performance, yet experiments suggested discrepancies much earlier.

The second set of experiments focused mainly on the behaviour and performance associated with the heating and cooling capabilities of the heat exchanger. Setup and procedure are identical to the previous experiments except for greater step-input size and different inlet temperature. The experiments were conducted with an inlet temperature of 34.8 °C but also took cooling into consideration (Figure 8.4). The first step was carried out from 34.8 to 36 °C with a good settling time of less than 200 seconds, similar to results presented in Figure 8.3.

After about 550 seconds, the reverse step was initiated and carried out with slight undershoot in both TEMs (Figure 8.4a and b). Cooling was induced at approximately 1000 seconds with a negative step-input of 34.8 to 33 °C, below inlet fluid temperature. The step-response of both TEMs and therefore the overall heat exchanger takes marginally longer (300 seconds) compared to heating mode. The reason for this behaviour originated from the entire heat exchanger frame being 'thermally charged' by the thermoelectric devices to 34.8 °C. The intentional and sudden switch from heating to cooling mode represents a challenge due to the greater

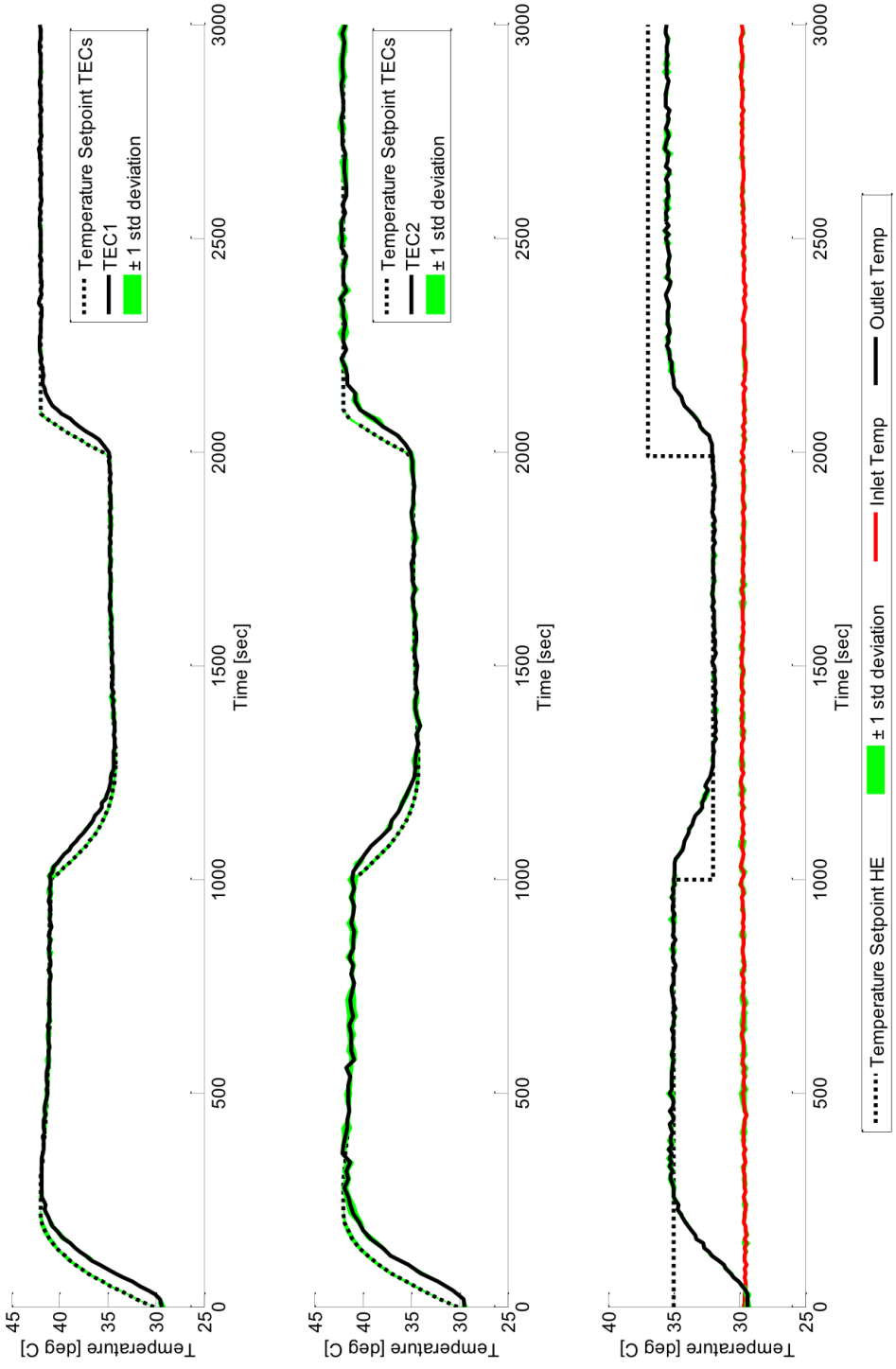

Figure 8.3: Example of experimental lab test subjected to various step-input signals. Typical response behaviour of controlled temperatures for both TEMs (a,b) and overall heat exchanger (c) at 100ml/min.

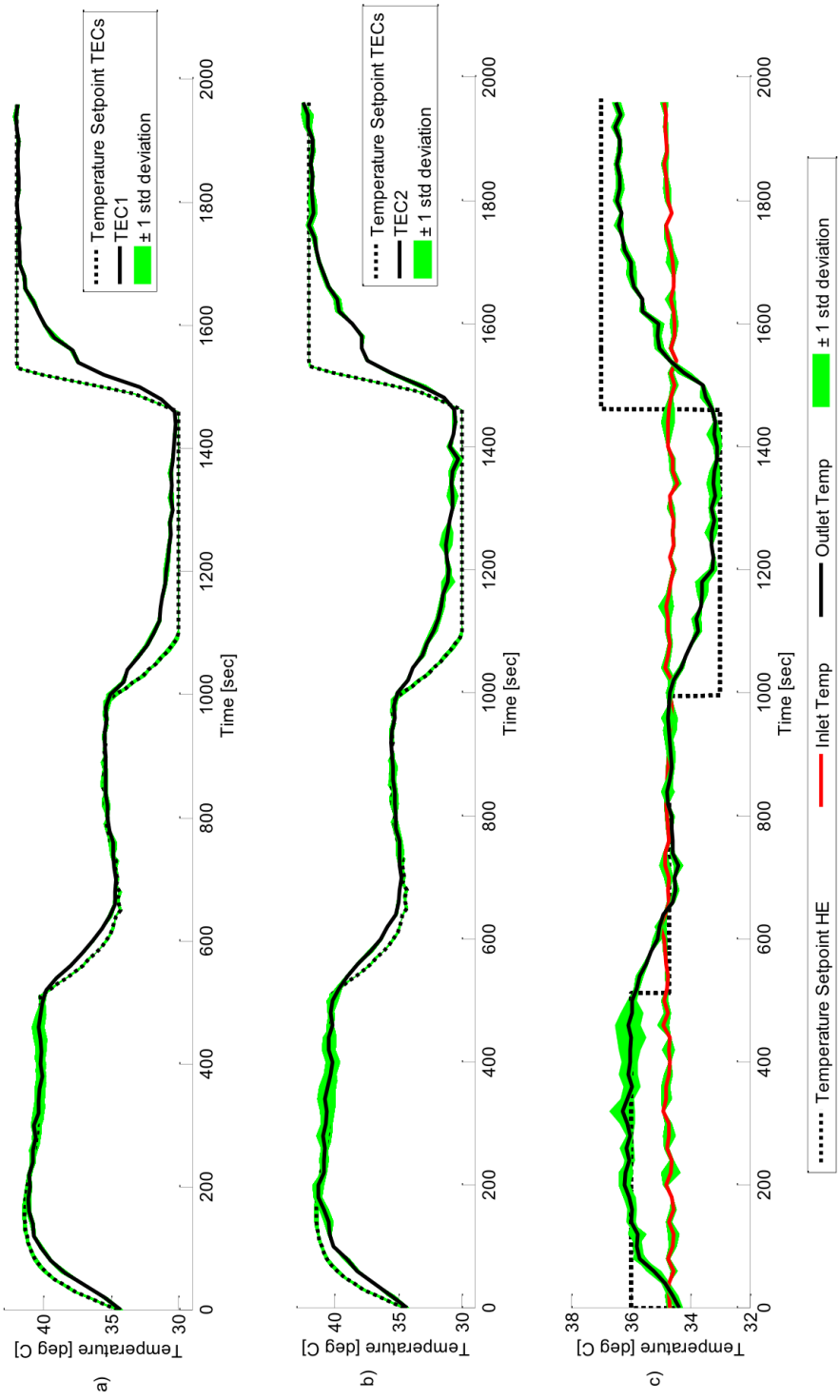

Figure 8.4: Example of experimental lab test results subjected to various step-input signals. Typical response behaviour for controlled temperatures in both TEMs (a,b) and overall heat exchanger (c) at 300ml/min.

thermal load that needs to be overcome. This is reflected in the settling time of 300 seconds. Having reached steady-state at about 1300 seconds, another step-input was triggered from 33 to 37 °C. This extensive step clearly represents a challenge for the current heat exchanger configuration, and only reaching 36.5 °C from a temperature of 34.8 °C. Both TEMs have reached the maximum allowed temperature of 42 °C and still an offset between desired- and actual temperature exist. However, the fact that both thermoelectric devices heat up somewhat symmetrically and reach the pre-set limit for surface temperature of 42 °C demonstrate the successful function of the control algorithm.

8.1.3 Conclusion

The experiments conducted have successfully confirmed control-related aspects of the heat exchanger. Maximum permissible temperature limits were reached throughout experiments. Additionally, settling times were below the maximum of 400 and 600 seconds. However, the current heat exchanger design struggles to reach and maintain outlet temperatures of 37 °C for a broad range of flow rates and inlet temperatures despite successful validation of models and controllers. Overall, the experimental results have helped to identify:

1. the discrepancies between model and physical device,
2. the limits of the current design, and
3. that with some re-design, the concept appears feasible.

Instead of entering into an iterative loop of further modelling, refinement and development, we decided to accept the inherent insufficiencies of our model and physical device and completely re-design our system.

The same stringent device requirements apply to our new system, including the following points:

- More TEMs are required to increase the effective heating area and thus the possibility of increased input of heating power. This will also contribute to a more even temperature distribution across the heat exchanger surface.
- Besides adding more TEMs, the active surface area of the blood-aluminium interface should also be increased in order to benefit (increased efficiency) from the increased heat supply by the TEMs.
- In order to maximise exposure time of the blood, the design should also focus on allowing a unit volume to remain within the heat exchanger as long as possible.
- Instead of employing miniaturised electronics in the feasibility phase of product development, industrial control elements for reasons of reliability and more robust operation should be used. Miniaturisation of a fully working and reliable system can be commenced at any future point if desired.

8.2 Second Iteration

The results discussed in the previous section clearly revealed sub-optimal performance levels with respect to our requirements and expectations. Yet, the outcome is indicative of real promise, but require alterations of the current design.

The re-designed heat exchanger must be carried out according to the goals defined at the start of this project as well as addressing the issues raised in our first pass experimentation.

This complies with the conventional iterative design process where each subsequent iteration is informed by the results of prior design and testing cycles, whilst maintaining a common set of objectives.

8.2.1 Design Criteria

The shortcomings highlighted in Chapter 8.1, which were derived from laboratory experiments, implied that further development and refinement is necessary in order to satisfy the critical criteria. The main drawback of the previous configuration was the failure to meet acceptable performance standards and it is for this reason that a revision of the heat exchanger is necessary.

Based on the life cycle of technical developments illustrated on page 102, a new concept needs to be developed first that takes into consideration and is influenced by the insufficiencies and results of the previous model while aiming to improve overall performance and maintaining set goals. This *'Concept Development'* stage is followed by *'Development'* and *'Laboratory Testing'* and test results will indicate whether performance criteria have been met. The shortcomings will result in further development cycles.

In the previous design, TEMs were only mounted on one side of the heat exchanger which leaves the opposite side exposed to the environment causing unnecessary heat loss and contributing to overall system inefficiency. Therefore, the new design should provide the opportunity to accommodate TEMs on both side of the heat exchanger with the appropriate internal construction supporting the structure.

In the previous design, one shallow channel was traversing through the heat exchanger in a serpentine manner, completing two loops along the length. With higher flow rates, the exposure time of the blood going through the channel might be insufficiently short and thereby not fully utilising potential heat exchange. Therefore, more loops will increase the exposure time and thus provide greater heat exchange. For this reason, the new design should focus on incorporating multiple loops for increased heat absorption (in heating mode) or release (in cooling mode).

Other specifications from the previous design also apply to the new model which included:

- The size of the overall heat exchanger is still one of the greatest motivational factors of this project. Within this category, the previous model has achieved a satisfying result which should be maintained and carried over to the new design.
- The cross-sectional area of the blood flow path should still remain constant. This provides uniform flow patterns within the heat exchanger aiding equal loading on the TEMs and simultaneously reducing haemolysis-causing turbulence.
- Due to the success of the previous model, a flat design should be chosen again that provides good fixation of the TEMs.
- Due to the success of the previous model, the same materials as in the previous model should be employed.
- Achieve and maintain a blood temperature of 37 °C at the heat exchanger outlet. This must be done in a controlled way at approximately 400 seconds at a blood flow rate of 300 ml/min. Inlet temperature should be kept at 30 °C

throughout the entire test procedure. Ambient temperature should be kept at at 20 °C.

- Achieve and maintain a blood temperature of 32 °C at the heat exchanger outlet. This must also be done in a controlled way at approximately 400 seconds at a blood flow rate of 300 ml/min. The inlet temperature should be kept at 42 °C throughout the entire test procedure. Ambient temperature should be kept at 35 °C.

- The control response for TEMs must limit overshoot/undershoot to 0.1 °C for all experiments.

- These two specifications (in the above points) represent the most challenging cases for the TEMs, i.e. with the greatest thermal load. This is not just to prove the controller response but also the feasibility of achieving large temperature jumps of the blood temperature. Variations of these cases represent a reduced thermal load but are still important in order to prove controller performance under diverse conditions. The following variations should be tested: flow rates of 100 and 300 ml/min, inlet temperatures of 30 and 42 °C, and ambient temperatures of 20 and 35 °C. These three variables will create a table of 8 possibilities which are shown below (Table 8.1). Each case is required to achieve the desired temperatures within 400 seconds with overshoots/undershoots limited to 0.1 °C.

8.2.2 Design Process

The revised criteria in Chapter 8.2.1 are implemented and used as a guide throughout the design process of the improved heat exchanger.

	Ambient Temp.	Blood Inlet Temp.	Blood Flow Rate
1.	35 $°C$	42 $°C$	300 ml/min
2.	35 $°C$	42 $°C$	50 ml/min
3.	35 $°C$	30 $°C$	300 ml/min
4.	35 $°C$	30 $°C$	50 ml/min
5.	20 $°C$	42 $°C$	300 ml/min
6.	20 $°C$	42 $°C$	50 ml/min
7.	20 $°C$	30 $°C$	300 ml/min
8.	20 $°C$	30 $°C$	50 ml/min

Table 8.1: Matrix of Possible Extreme Disturbance Conditions

As discussed in Chapter 8.1, we recognise the main shortcomings of the first heat exchanger model as:

- Surface area of blood-metal boundary is not sufficiently large for required heat transfer.
- Two large TEMs on one side of the heat exchanger seem to be inadequate for the task of heating the blood to desired levels.
- Thermal energy was only applied to one side of the heat exchanger leaving out potential other areas.

These shortcomings were eradicated by implementing the solutions described below. The redesign was based on the first concept with the following modifications.

The heat exchanger of the first iteration suffered from a limited blood-surface boundary - caused by only one narrow channel - which did not fully utilise maximum surface area and thus, contributing to the overall reduction of heat exchanger efficiency. In the revised design, two intertwined arrays of fins that are 4 mm apart enable a serpentine flow pattern with 43 loops ultimately offering a much greater exposure of surface area (Figure 8.5).

Instead of using two large TEMs which leave uncovered areas, several smaller ones should be mounted instead. This provides the opportunity for improved heat delivery and increased efficiency if placed close to each other. The size of the chosen TEMs are 30 x 30 mm and the new design allows to place four on both upper and lower sides of the heat exchanger, covering more surface area altogether (Figure 8.9 and Figure 8.10).

The amount of heat required to raise the temperature of an object can be established with the following formula:

$$Q = c_p \cdot m \cdot dT \tag{8.1}$$

where

Q = amount of heat (kJ), c_p = specific heat (kJ/kg/K), m = mass (kg), and dT = temperature difference between hot and cold state (K).

The above formula was used in estimating the energy required to heat up the heat exchanger as well as the circulating blood from 30 to 37 °C. For the aluminium heat exchanger and for the total blood volume, approximately 3.22 kJ and 14.28 kJ are necessary, respectively.

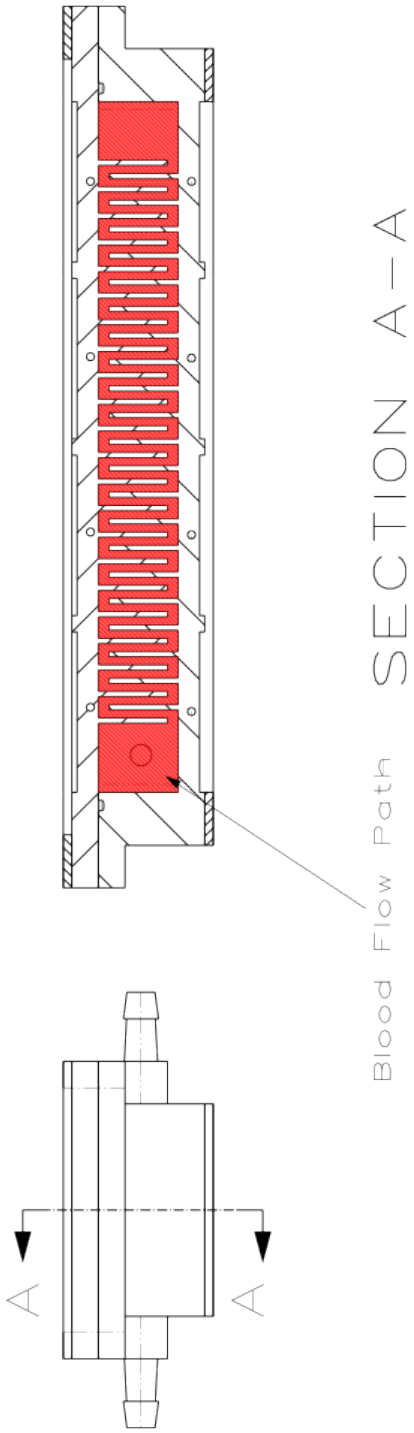

Figure 8.5: Front view and cross section of the new heat exchanger model. The blood path is clearly visible (in red) in the side view.

$$Q_{heatexchanger} = 0.92 \cdot 0.5 \cdot 7 = 3.22kJ \tag{8.2}$$

$$Q_{blood} = 1.02 \cdot 2 \cdot 7 = 14.28kJ \tag{8.3}$$

0.5 kg mass and 0.92 kJ/kg/K specific heat for the heat exchanger as well as 2 kg and 1.02 kJ/kg/K specific heat for the blood. Summed up, this will amount to approximately 17.5 kJ. Assuming that heat loss and coupling factor amount to 30 percent, in order to achieve 17.5 kJ, 22.75 kJ of thermal input energy is required.

One of the requirements was to achieve the target temperature within 400 seconds. This allows us to calculate the required power of:

$$P = 22.75kJ \div 400sec = 56.86W \tag{8.4}$$

or

$$56.86W \div 8TECs = 7.1W/TEC \tag{8.5}$$

With a power supply output of 10 A, 8 TECs would draw on average 1.25 A. This needs to be considered when choosing a thermoelectric device. A suitable thermoelectric device was chosen based on the ability to pump heat at the maximum current of 1.25 A.

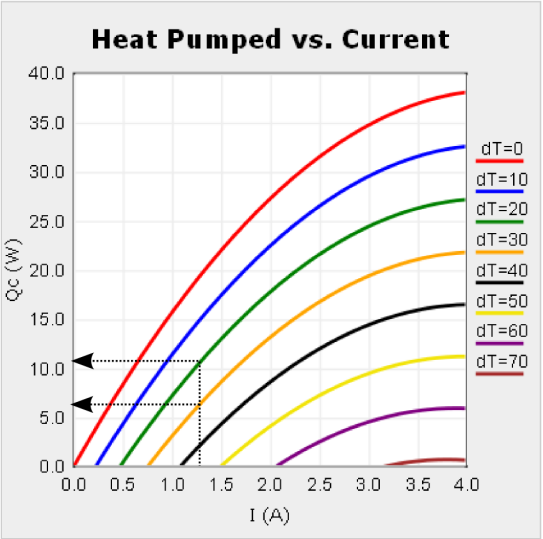

Figure 8.6: Heat Pumped vs. Current; Ferrotec Thermoelectric Module 9501/127/040B

As indicated in Figure 8.6, at a current of 1.25 A, one TEC is able to deliver heat at approximately 7 - 11 W if the temperature between hot and cold plate is within in the range of 30 - 20 °C, respectively. Under these conditions, 5.2 - 8.1 TECs would be required mathematically to maintain 56.86 W. To build in redundancy, 8 TECs of the type 9501/127/040B (Ferrotec, Santa Clara, California, USA) are chosen in order to maintain this power requirement.

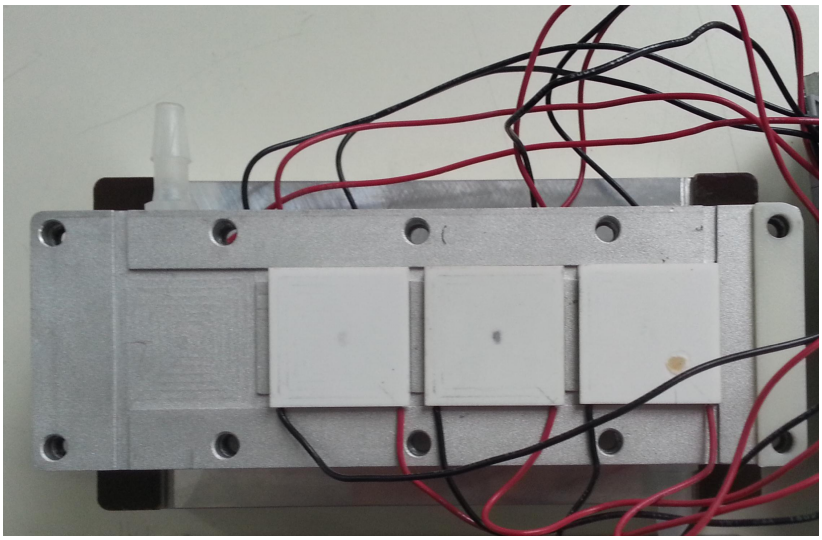

Figure 8.7: Prototype of heat exchanger and thermoelectric devices on top (upper side)

The new heat exchanger was milled by an in-house CNC machine (Figure 8.8).

Figure 8.8: CNC machine

Heat sinks are required to be designed and attached to the thermoelectric devices in order to maintain the temperature difference between both TEC sides below 30 °C, as discussed above.

A thermal analogy of electrical circuits can be applied when calculating the appropriate size of heat sinks. According to the analogy, Ohm's law V = R · I can be represented by T_{TEC} - T_{ambi} = $R_{thermal}$ · P_V, where

T_{TEC} = surface temperature of the thermoelectric device (K),

T_{ambi} = ambient temperature (K),

$R_{thermal}$ = thermal resistance (K/W),

P_V = the power dissipating at the top surface of the TEC (W).

During the design stage, we mainly considered the case of 'cooling' (to 30 °C) as this requires more energy compared to heating (to 37 °C). This is caused by the facts that when in heating mode, the upper TEC side which is attached to the heat sink will be colder and thus is warmed by ambient temperature. Additionally, the blood is naturally closer to 37 °C and requires less heat input compared to cooling down to 30 °C. Considering the case of cooling down to 30 °C, in order to maintain a temperature differential of maximum 30 °C as indicated by the orange graph in Figure 8.6, the maximum temperature of the TEC's upper side is 60 °C. With an ambient temperature of approximately 24 °C and a total combined heating power of 28 W (4 TECs x 7 W), the total thermal resistance is:

$$R_{thermal} = \frac{T_{TEC} - T_{ambient}}{P_V} = \frac{60 - 40}{28} = 1.29 K/W \tag{8.6}$$

This means the combined thermal resistance of heat paste and heat sink should be around 1.29 K/W in order to achieve the amount of heat dissipation to maintain

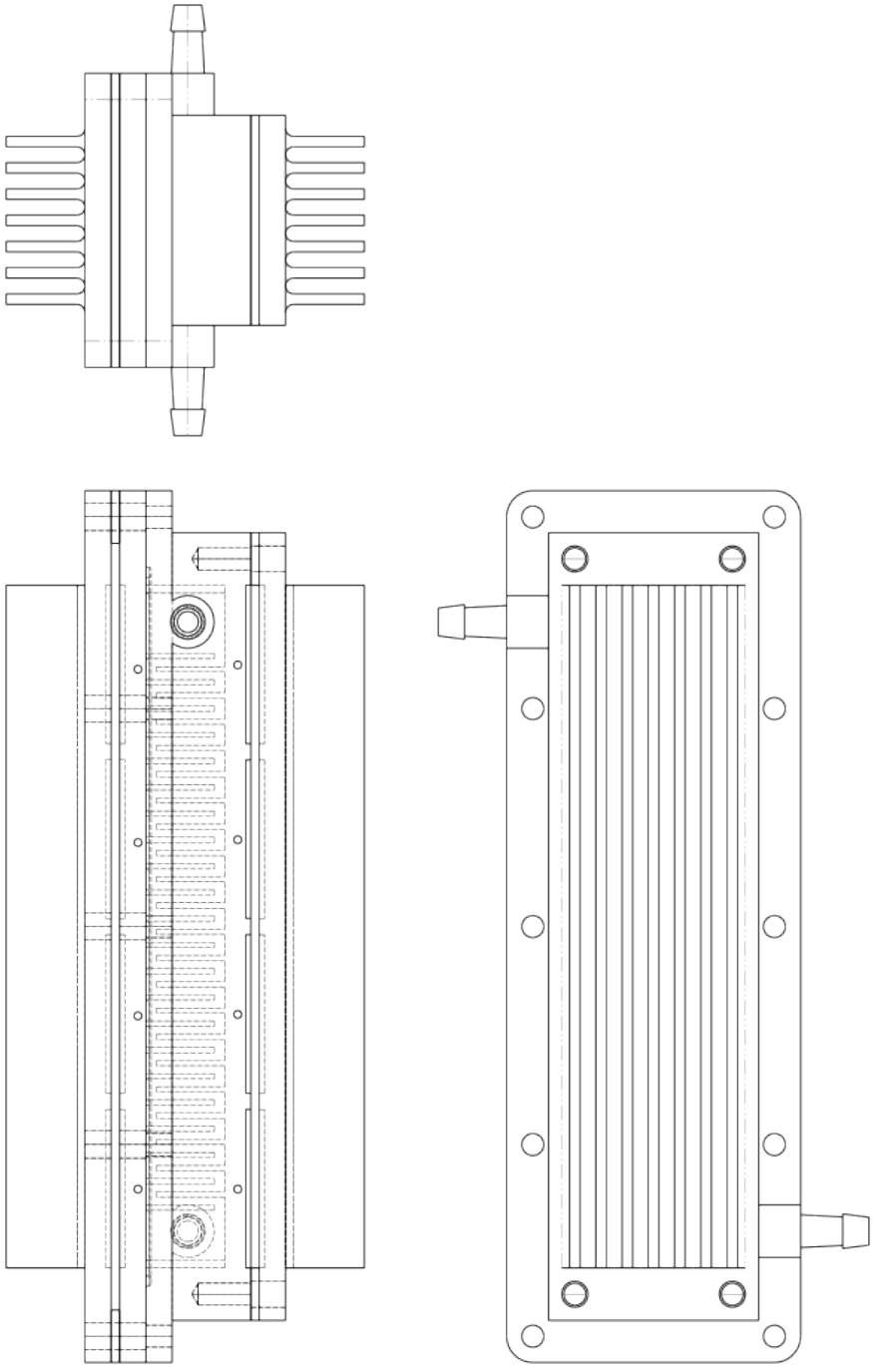

Figure 8.9: 3-sided view of proposed heat exchanger with heat sinks on top and bottom (measurements in mm)

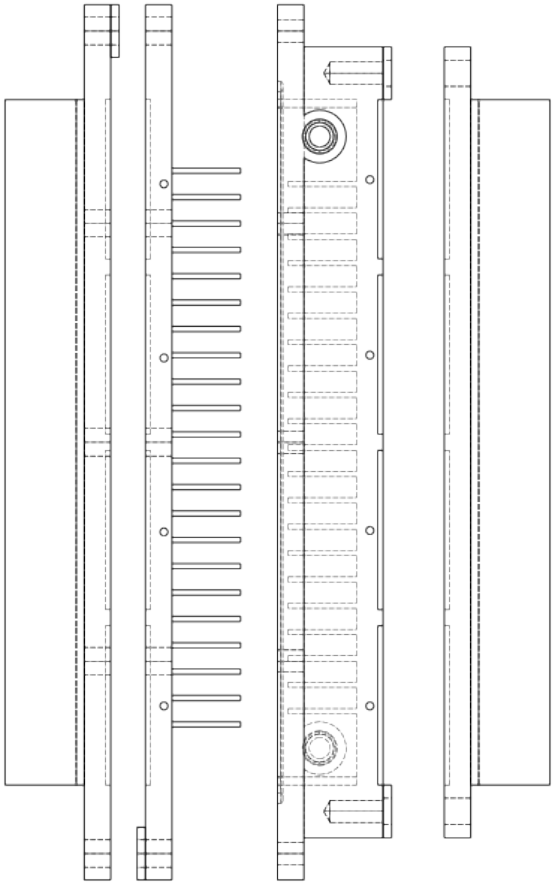

Figure 8.10: Individual components of the heat exchanger (measurements in mm)

a temperature differential of 30 °C between TEC sides. Thermal resistance of paste can be calculate as

$$R_{paste} = \frac{l}{k \cdot A} = \frac{0.05 \cdot 10^{-3}}{25.2 \cdot 0.9 \cdot 10^{-3}} = 2.2 \cdot 10^{-3} K/W \tag{8.7}$$

where

l = interface gap between TEC and heat sink (mm),

k = thermal conductivity of the zinc oxide paste (W/m/K),

A = cross sectional area of the TEC (m^2).

The thermal resistance value of the thermal paste applied to one TEC is negligibly small, and even smaller when considering the parallel nature of the setup. Therefore, we can assume $R_{thermal} = R_{heatsink}$.

The appropriate heat sinks were manufactured and mounted to the heat exchanger (Figure 8.11).

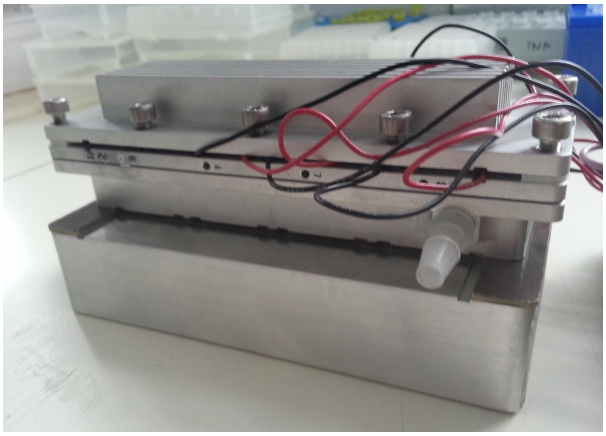

Figure 8.11: Final heat exchanger with heat sinks attached

8.2.3 Control Design

In the first iteration of our novel heat exchanger prototype, a successful temperature control process was demonstrated by experimental results, and thus a similar approach was chosen for the improved device. Instead of designing a mathematical model of the heat exchanger with a FEA software which was used for controller tuning, the manufactured heat exchanger instead was directly utilised for this task. For this approach, the analysis and observation of the temperature response behaviour was the primary focus, upon which controller parameters were tuned. Identical to previous proceedings, a PI controller was employed for temperature control. Initially, both P and I controller parameters were set to zero. Subsequently, changes to the proportional term were made and response behaviour of the outlet temperature was observed. Slowly increasing the proportional controller gain K_p results in more proportional action and faster control performance. K_p was iteratively increased to the point where the heat exchanger outlet temperature gradually approaches the desired temperature without any overshoots or oscillations. Very fast controller responses are not desired and in order to achieve smoother control behaviour, lower controller gains will suffice. However, with a proportional action only, the process variable will not reach the set temperature completely but an offset error will remain. This offset error will be eliminated by the integral gain K_i. Increasing K_i values will result in more integral action and ultimately faster control. Too much K_i gain and the system will overshoot, potentially reaching temperatures above acceptable limits. Therefore, the aim is to tune K_i in order to achieve zero overshoot and a smooth, asymptotical approach to the desired temperature. Derivative control action, or K_d, has been deliberately excluded due to potential noise in signal and missing of appropriate analogue filters.

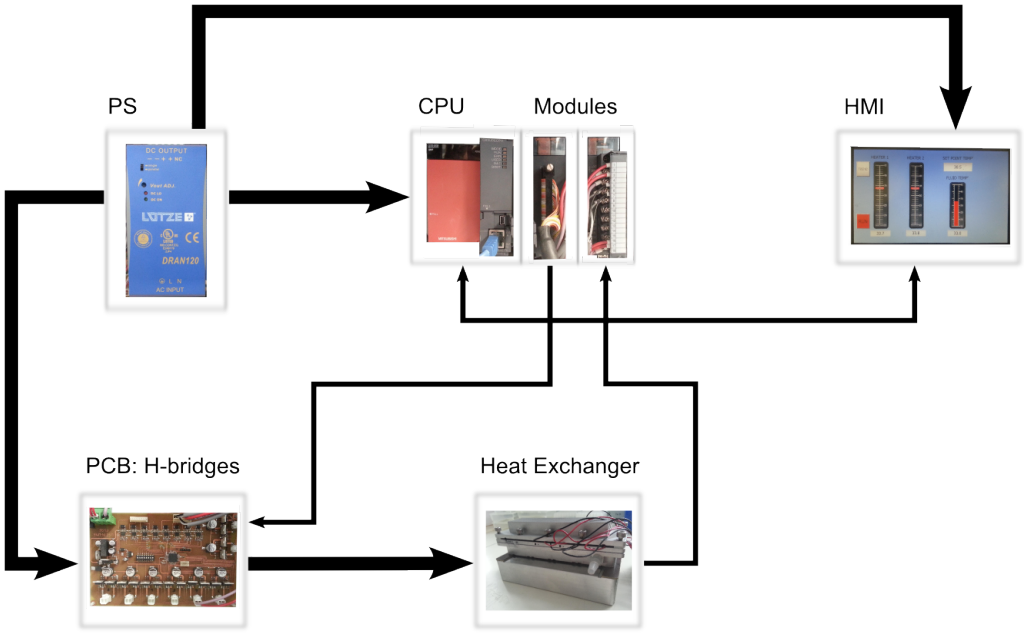

Figure 8.12: Diagram of interacting system components; bold lines = power connections, thin lines = signal communication

System hardware and configuration: The control algorithm - which is stored on the PLC microcontroller (Q61P, Mitsubishi Electric Corporation, Tokyo, Japan) - operates in a loop once activated by a user through the human machine interface (HMI) (iX Panel T7B, Beijer Electronics Products, Malmoe, Sweden); a touch screen user panel that allows to track, display, and record temperature progression. This interface requires the input of the desired temperature limits by the user which is subsequently stored within the CPU unit of the microcontroller. Once the control algorithm is initiated, it aims to reach the stored temperature limits on the heat exchanger outlet. It does this with the help of a printed circuit board (PCB) equipped with 8 H-bridges. Each H-bridge is responsible for implementing the direction of the electrical current and thereby influencing the mode of operation of each individual TEC, i.e. heating or cooling. A voltage is provided by the analogue output module (Q68DAVN, Mitsubishi Electric Corporation, Tokyo, Japan) which 'swings' from -10 V (cooling) to +10 V

(heating), regulating the direction of the current and also the magnitude of operation. The range of -10 V to +10 V merely dictates how much energy is allowed to be drawn from the power supply (Dran120, Friedrich Lütze GmbH, Weinstadt, Germany) and redirected to the TECs. A *dead zone* was introduced between +0.5 V to -0.5 V in order to prevent zero-switching problems (repeated activation-deactivation) on the output.

The efficiency of the thermoelectric module changes on how much energy is being provided. From Figure 8.13, efficiency (COP or coefficient of performance) increases very quickly to the maximum before it exponentially decays off. The performance depends on the temperature differential between both TEC sides. Having considered this during the design stage, based on the heat sinks, we aim to achieve a maximum difference (or dT) of 30 K. This coincidentally overlaps with the calculated current of 1.25 A per TEC.

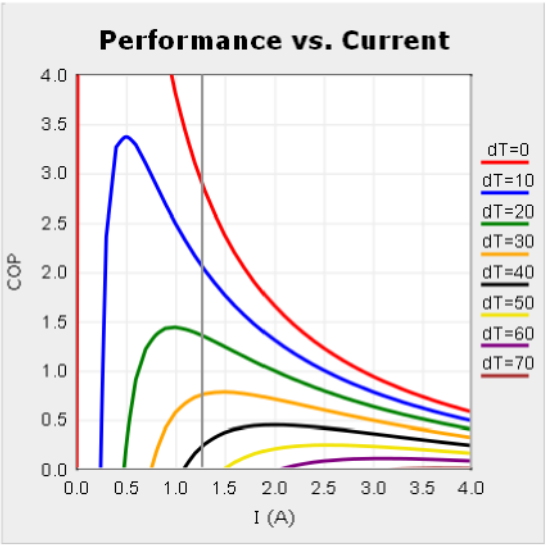

Figure 8.13: Performance vs. current of the implemented TEC 9501/127/040B. Maximum average current per TEC coincides with maximum COP (taken from www.ferrotec.com)

Therefore, in order to operate in an efficient manner, especially towards the initiation of the system, an electrical current of 1.25 A should be provided as the maximum. From the next graph (Figure 8.14), operating voltages of 6.6 V correspond to the said amount of current, providing a guide of operation.

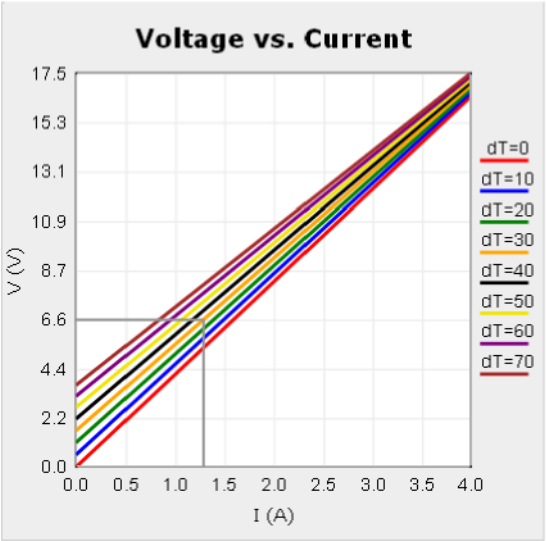

Figure 8.14: Voltage vs. current of the implemented TEC 9501/127/040B. Maximum average current per TEC corresponding to 6.6 V. (taken from www.ferrotec.com)

Thus, there is a need to constrain the energy input at the beginning of the control procedure by limiting the voltage to 6.6 V which was realised within the controlling software.

8.2.4 Materials and Methods

The redesigned heat exchanger and developed controller are to be tested in a laboratory environment mimicking clinical settings.

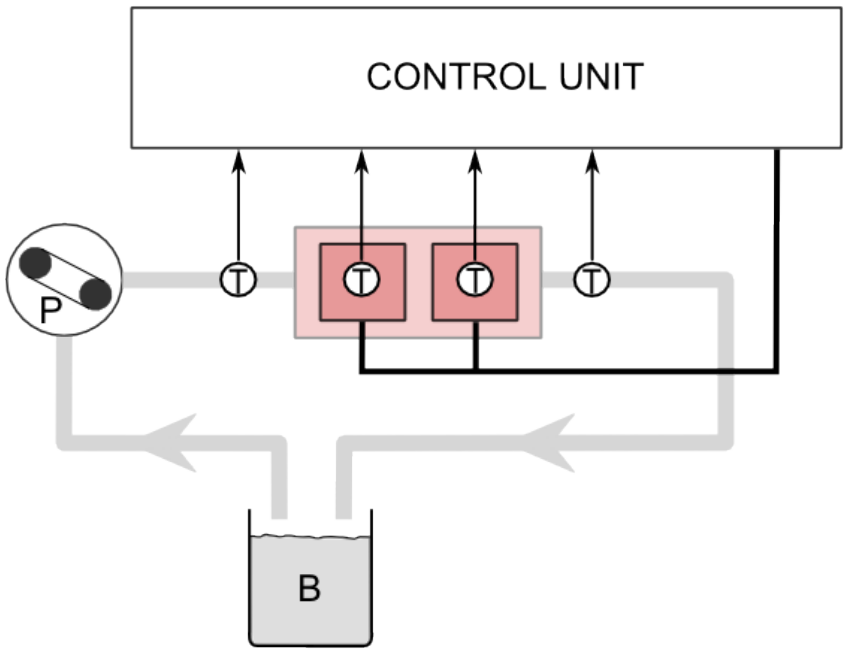

Figure 8.15: Experimental Setup; B: Blood Bag, P: Roller Pump, T: Thermocouples for upper and lower side, control unit: includes hardware and software such as power supply, CPU, data acquisition modules, human-machine interface, and control algorithm.

Both the developed controller and its accompanying hardware work in tandem with the heat exchanger in order to achieve the desired outlet temperature. The human-machine interface captures the desired heat exchanger outlet temperatures which are stored within the CPU. Upon initiation of the system, the control system in the CPU calculates the required power and forwards the respective (small)-signal to the PCB which in turn draws the required energy from the power supply and passes it on to the TEMs. The adjustable roller pump passes the blood from a 2-liter container, mimicking the patient, through the circuit in a closed-loop manner. Thermocouples for measuring the temperature are placed before and after heat exchanger inlet and outlet, respectively.

The first set of experiments continue where previous test results of the first-iteration device indicated insufficiencies. These tests ultimately represent a performance check by exposing the new device to the most thermally challenging conditions of our test routine, that is case 7 and 1 of Figure 7.1. Here, a step response from 30-37 °C was initiated at a flow rate of 300 ml/min. The same was carried out in the opposite direction for the cooling operation where the inflowing blood was reduced from 42 °C down to 32 °C at a flow rate of 300 ml/min. Water bath temperatures were kept constant during all experiments. Both experiments were repeated three times and terminated after approximately 1300 seconds.

	Ambient Temp.	Blood Inlet Temp.	Blood Flow Rate
1.	35 $°C$	42 $°C$	300 ml/min
2.	35 $°C$	42 $°C$	50 ml/min
3.	35 $°C$	30 $°C$	300 ml/min
4.	35 $°C$	30 $°C$	50 ml/min
5.	20 $°C$	42 $°C$	300 ml/min
6.	20 $°C$	42 $°C$	50 ml/min
7.	20 $°C$	30 $°C$	300 ml/min
8.	20 $°C$	30 $°C$	50 ml/min

Table 8.2: Original Table of Possible Extreme Cases

Other experiments - similar to previous test runs - were also executed according to conditions stated in Table 8.2. This means a step response from 30 to 42 °C or 42 to 32 °C at different flow rates and ambient temperatures. Again, all experiments were repeated three times and terminated after approximately 1300 seconds.

The last set of experiments focussed on the long-term stability of heat exchanger outlet temperatures. Here, cases 7 and 1 of Table 8.2 were repeated with a focus of maintaining the temperature for about 7000 seconds, or 11.5 minutes. Both experiments were again repeated three times.

8.2.5 Results and Discussion

Figures 8.16 to 8.25 display typical response behaviours to step input signals at a flow rate of 300 ml/min. The chosen approach to testing the system with the designed PI-controller was to select the most challenging environments first from Table 7.1, i.e. cases 7 and 1.

The first test was in the form of a step response from 30 to 37 °C at a flow rate of 300 ml/min and with an inlet temperature of approximately 30 °C (Figure 8.16). Both arrays of thermoelectric elements mounted to the upper and lower sides of the heat exchanger are reacting to the step input simultaneously, gradually heating up the casing and blood. Slight overshoots of the thermoelectric elements are noticeable, yet are acceptable due to their minimal nature being below 38 °C. However, no overshoots are recognised at the outlet and the target temperature of 37 °C was reached within the settling time of approximately 500 seconds, slightly over the self-proposed requirement of 400 seconds. After 1300 seconds, the experiment was terminated as it had reached a steady state condition.

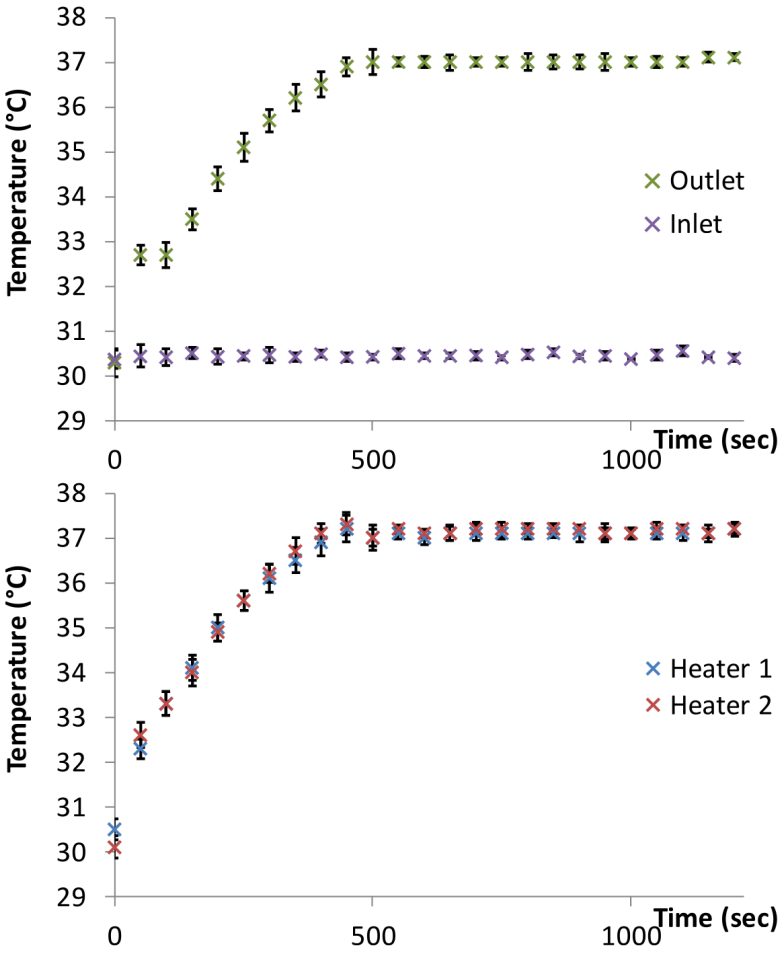

Figure 8.16: Step response curves of heat exchanger outlet temperature (top) and heater 1 and 2 (bottom) to positive input jump 30 - 37 °C. Measured at a flow rate of 300 ml/min, at ambient conditions of 20 °C, and constant inlet temperature of approximately 30 °C.

A similar experiment was carried out for cooling where a negative step input from 42 to 32 °C initiated a response behaviour of the system at a flow rate of 300 ml/min (Figure 8.17). Again, slight undershoots of the thermoelectric devices can be noticed, however, are considered to be negligible due to their minimal magnitude ($\leq$ 1 °C). No overshoots were recorded at the outlet of the heat exchanger and the desired temperature of 32 °C was reached within the settling time of approximately 500 seconds. This also is slightly above the self-proposed requirement of 400 seconds

and the overall experiment was terminated at around 1300 seconds when steady state was reached.

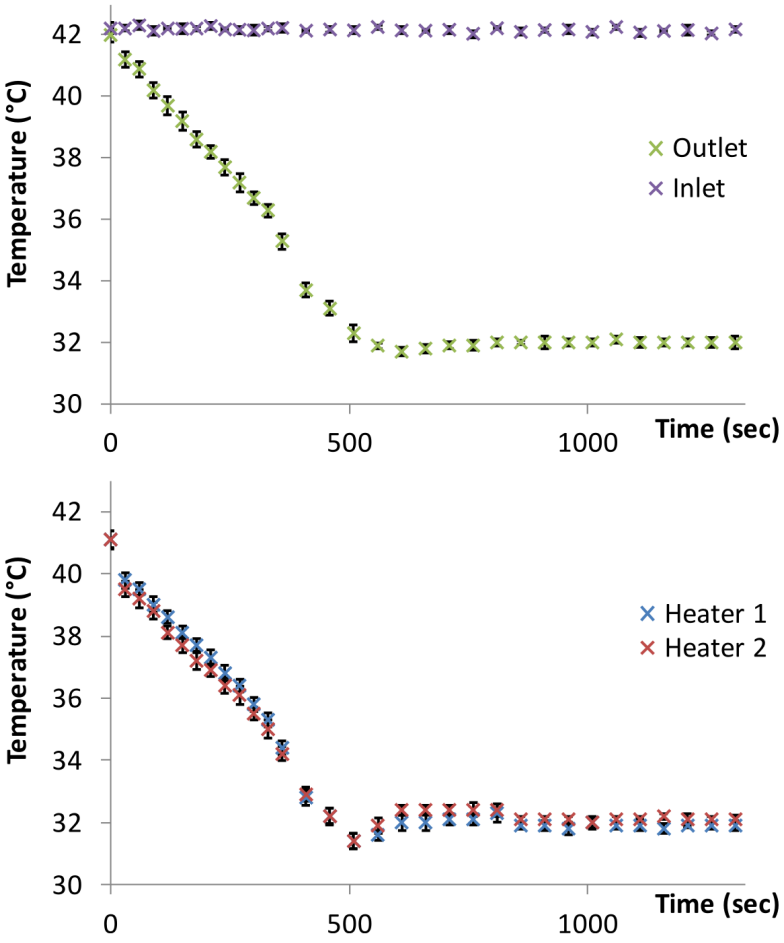

Figure 8.17: Step response curves of heat exchanger outlet temperature (top) and heater 1 and 2 (bottom) to negative input jump 42 - 32 °C. Measured at a flow rate of 300 ml/min, at ambient conditions of 35 °C, and constant inlet temperature of approximately 42 °C.

In terms of thermal loading, the previous two cases, 7 and 1, represented the most challenging test scenarios among all cases in Table 7.1 on page 159. As it was illustrated, most test requirements were achieved apart from reaching the desired temperature under 400 seconds.

Similar responses were expected for the remaining cases 2, 3, 4, 5, 6, and 8 in Table 7.1. These are illustrated in Figures 8.18, 8.19, 8.20, 8.21, 8.22, and 8.23, respectively. In all cases almost no overshoots/undershoots were experienced at the heat exchanger outlet (± 0.1 °C). Heater 1 and 2 were able to increase the outlet temperature to desired levels without exceeding the critical threshold of 42 °C. The desired outlet temperatures of 32 and 37 °C in cooling and heating mode, respectively were achieved in the settling time of approximately 500 seconds. A point of criticism is this slightly longer than originally proposed settling time. However, adjusting controller parameters in order to improve settling times resulted in undesirable overshoots/undershoots of heater 1 and 2 behaviour. The criteria to minimise any potential overshoots/undershoots due to possible blood damage takes precedence over settling time.

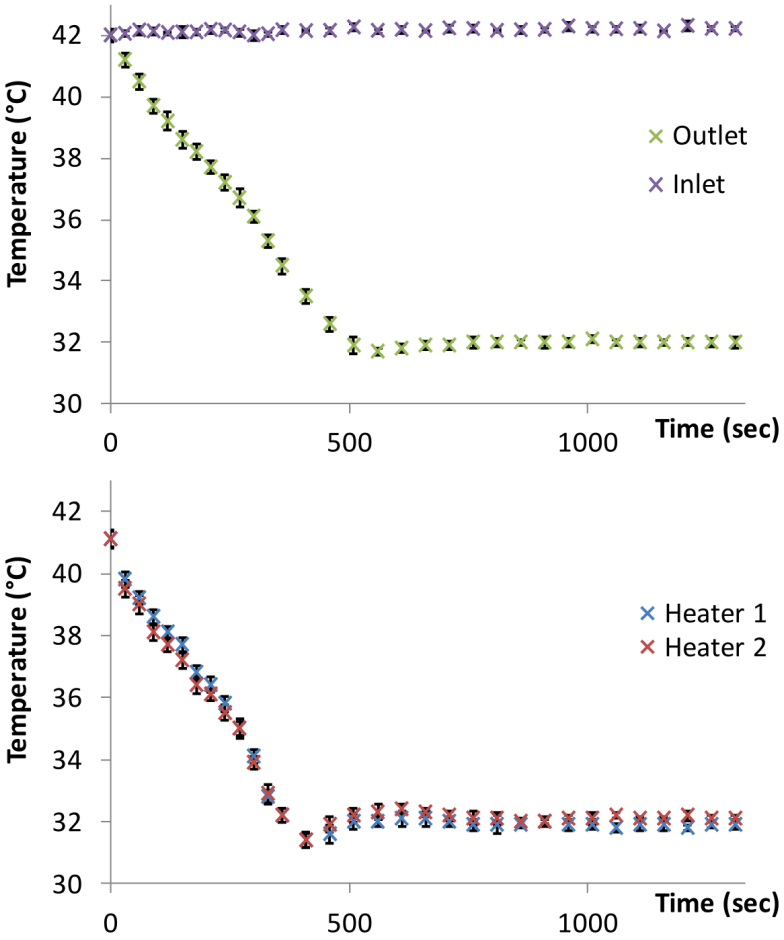

Figure 8.18: Step response curves of heat exchanger outlet temperature (top) and heater 1 and 2 (bottom) to negative input jump 42 - 32 °C. Measured at a flow rate of 50 ml/min, at ambient conditions of 35 °C, and constant inlet temperature of approximately 42 °C.

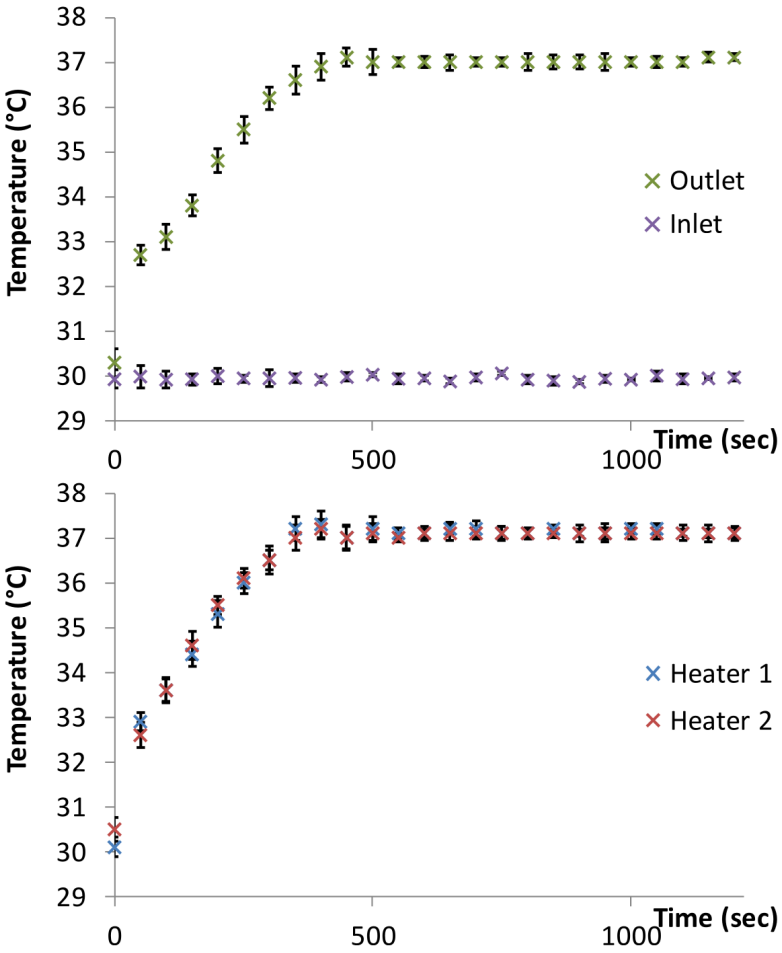

Figure 8.19: Step response curves of heat exchanger outlet temperature (top) and heater 1 and 2 (bottom) to positive input jump 30 - 37 °C. Measured at a flow rate of 300 ml/min, at ambient conditions of 35 °C, and constant inlet temperature of approximately 30 °C.

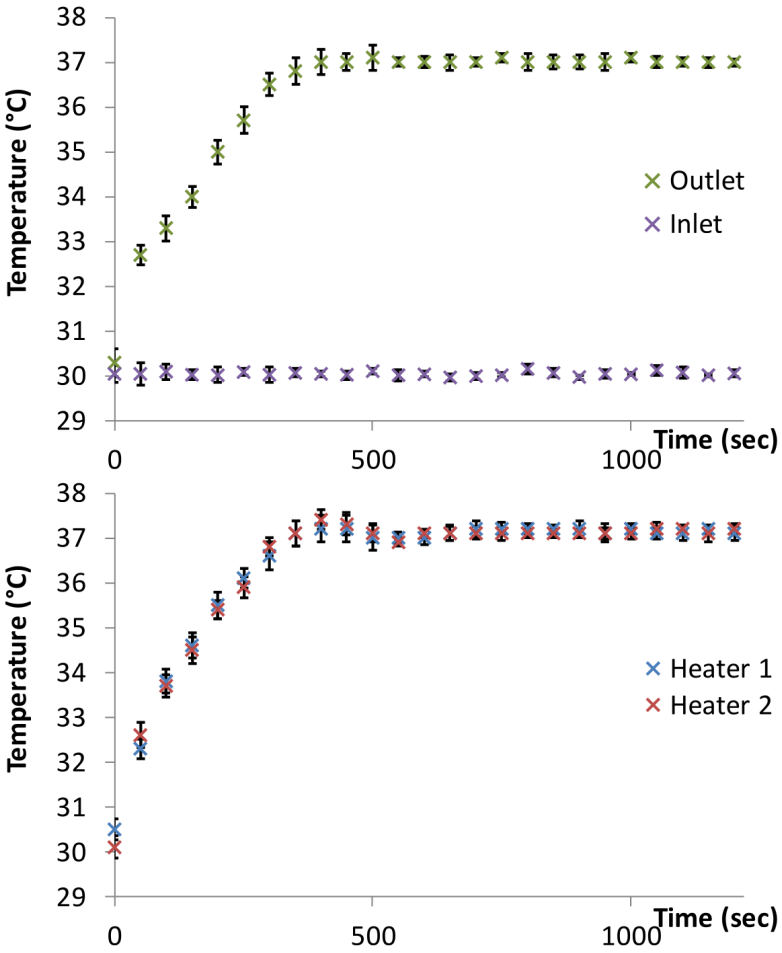

Figure 8.20: Step response curves of heat exchanger outlet temperature (top) and heater 1 and 2 (bottom) to positive input jump 30 - 37 °C. Measured at a flow rate of 50 ml/min, at ambient conditions of 35 °C, and constant inlet temperature of approximately 30 °C.

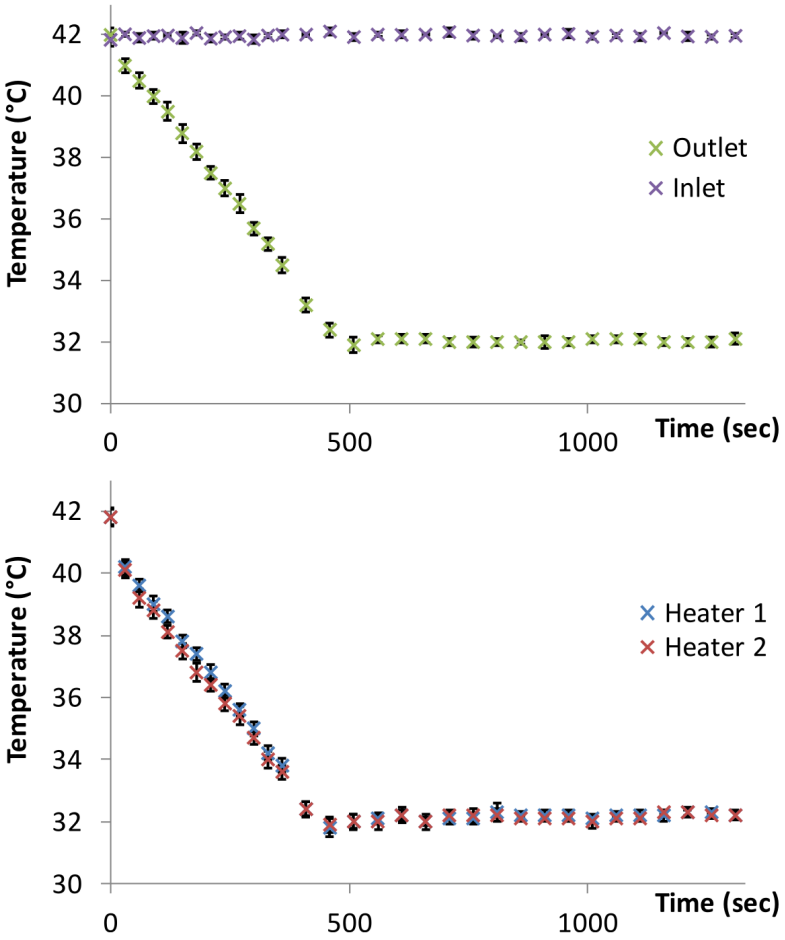

Figure 8.21: Step response curves of heat exchanger outlet temperature (top) and heater 1 and 2 (bottom) to negative input jump 42 - 32 °C. Measured at a flow rate of 300 ml/min, at ambient conditions of 20 °C, and constant inlet temperature of approximately 42 °C.

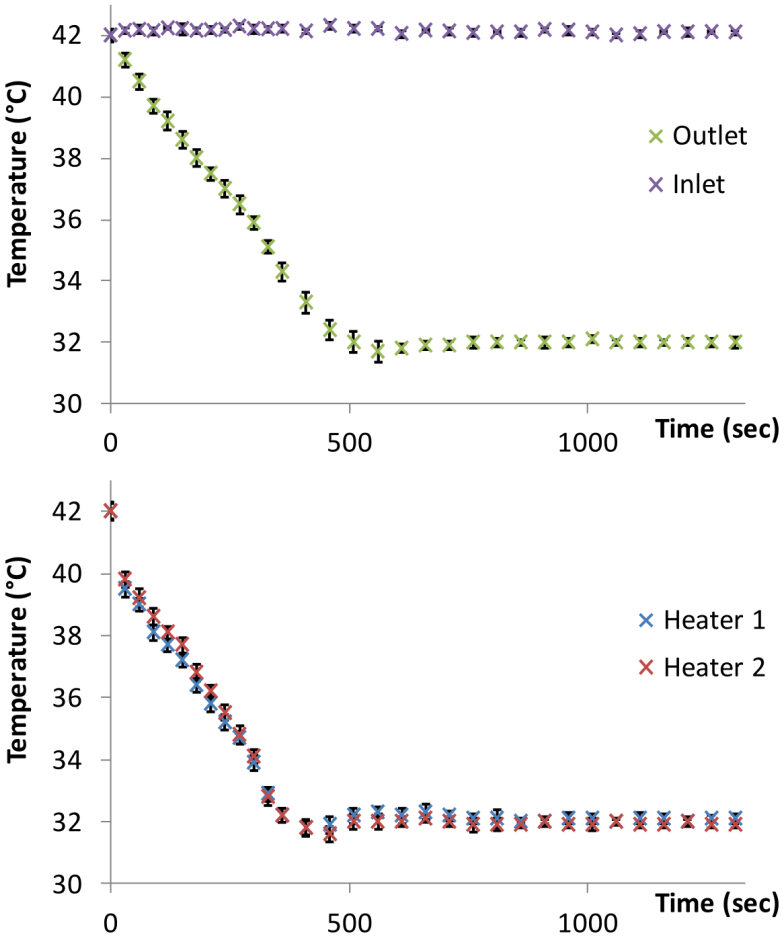

Figure 8.22: Step response curves of heat exchanger outlet temperature (top) and heater 1 and 2 (bottom) to negative input jump 42 - 32 °C. Measured at a flow rate of 50 ml/min, at ambient conditions of 20 °C, and constant inlet temperature of approximately 42 °C.

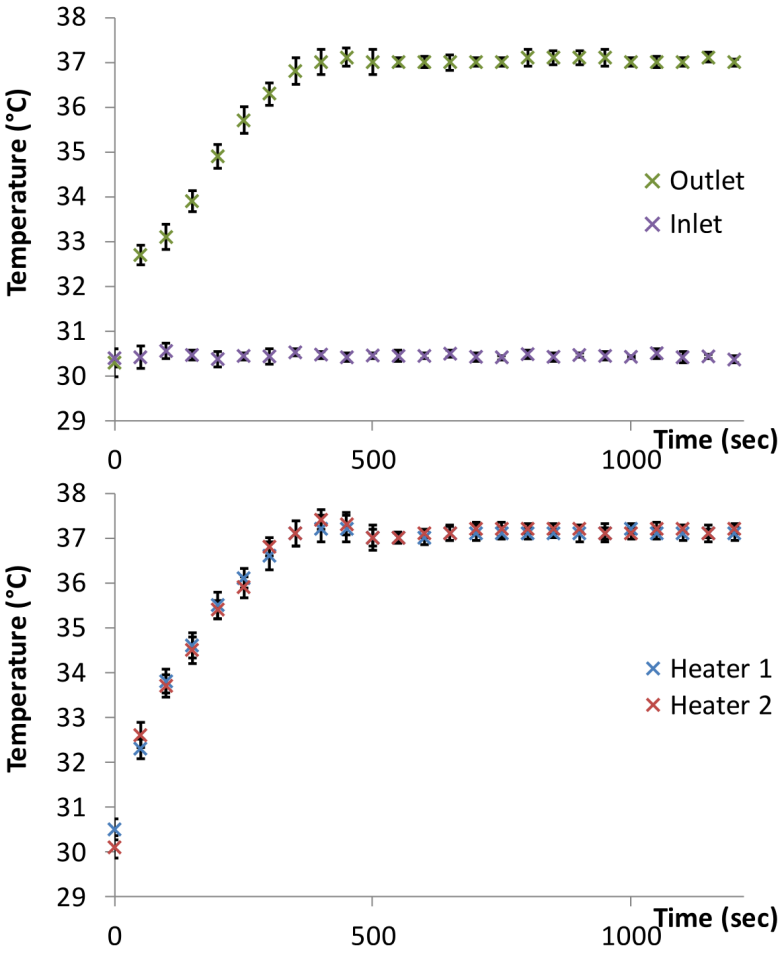

Figure 8.23: Step response curves of heat exchanger outlet temperature (top) and heater 1 and 2 (bottom) to positive input jump 30 - 37 °C. Measured at a flow rate of 50 ml/min, at ambient conditions of 20 °C, and constant inlet temperature of approximately 30 °C.

Preliminary long term tests were also carried out in both heating and cooling mode in order to investigate any potential deviations from the steady state situation. This type of experiment emphasises slightly more on the capabilities of the device with a secondary focus on the control response. Figures 8.25 and 8.25 display step input responses followed by continuous operation for approximately 7000 seconds or 11.5 minutes. All conditions remained the same throughout the entire experiments to demonstrate the capability of the device. It is evident from the graphs

that temperatures of TEMs and heat exchanger outlet remained constant throughout the experiment in both modes.

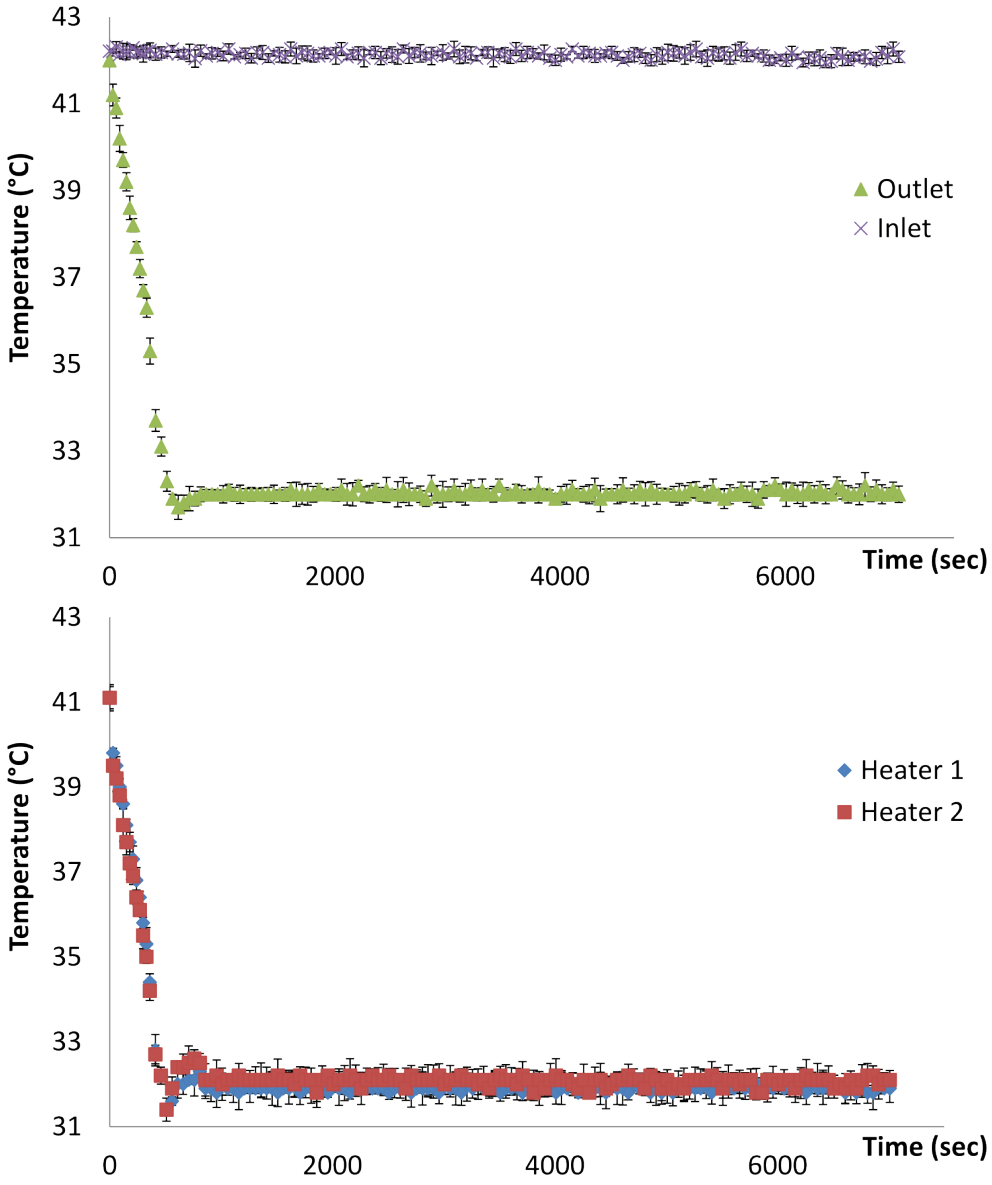

Figure 8.24: Step response curve followed by long term behaviour of upper and lower heaters, as well as heat exchanger outlet temperature measured at constant inlet temperature of approximately 42 °C.

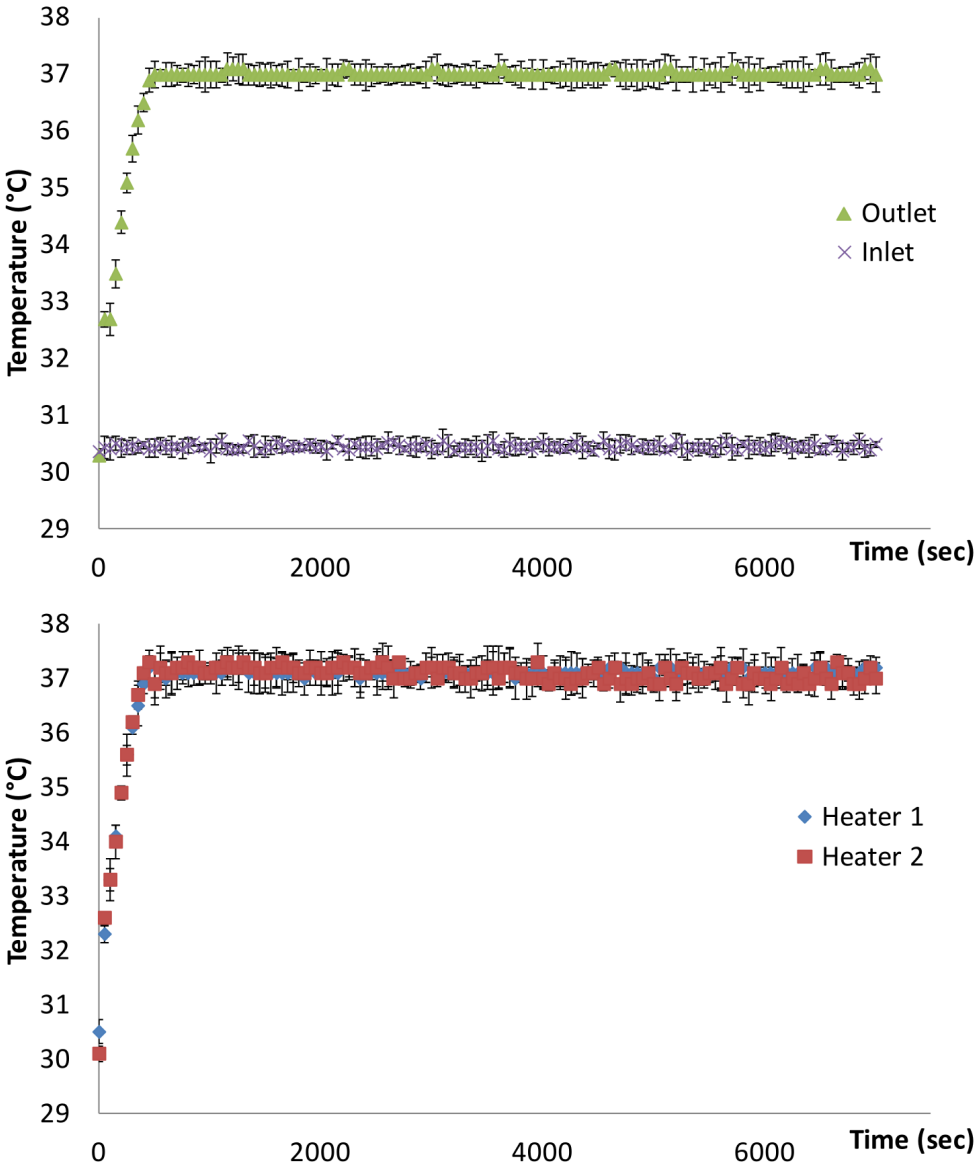

Figure 8.25: Step response curve followed by long term behaviour of upper and lower heaters, as well as heat exchanger outlet temperature measured at constant inlet temperature of approximately 30 °C.

8.2.6 Conclusion

The second iteration of the heat exchanger for conventional ECMO settings addressed the shortcomings of the first iteration such as TEM placement on only one side of

the heat exchanger as well as inefficient channel dimensions. The redesign considered these shortcomings and implemented 8 smaller TEM instead of 2 large ones. Also, a modified flow pattern was established that offers 43 loops instead of 2, ultimately leading to greater surface area for improved efficiency. Furthermore, heat sinks were also designed for optimal heat transfer between TEMs and the environment.

The control design of the second iteration heat exchanger was not based on a theoretical approach but instead focussed on physical tuning of controller parameters based on the plant behaviour. This required an iterative process of tuning and experimenting until satisfactory results were achieved. A similar controller (PI) was used - as in the previous iteration - and the heat exchanger responses proved the enhancements of the new prototype with overall expected functioning.

8.3 Temperature Control for Heat Exchanger for in-transit ECMO

The active chemical heat exchanger (ASAHED) developed in Section 4.2.2 was to be tested under laboratory and in-vivo conditions similar to near-clinical environments before this product can be deployed clinically. In this work, we report three sets of experiments, all with contrasting emphasis. The first set aims to establish and confirm the form of temperature decay of our developed device after activation under the influence of different ambient conditions. The second set of experiments focuses on the potential impact that our device may have on fluid temperatures under clinically mimetic operating conditions and in different environments. The third set of experiments focuses on maintaining a steady level of temperature within a closed

circuit under clinically mimetic operating conditions and the influence of different environments.

8.3.1 Materials and Methods

The first series of experiments examines the performance of the sodium-acetate bag on an individual basis, i.e. without any further insulation or cover. For these experiments, the ASAHED was tested in two different thermal environments, one at 23 °C and the other at approximately 7 °C, in order to measure the impact of extreme ambient conditions. A needle-probe (Physitemp Instruments Inc., Clifton, NJ, USA) was placed directly inside the oxygenator bag before the metal disc was activated which in turn initiated the exothermic reaction. It was anticipated that there would be a sharp rise in temperature values followed by a decay over a period of time. Colder ambient temperatures should increase the overall heat extraction at any given time due to greater temperature differentials between environment and the bag leading to faster cooling. Values were measured and recorded (TC-08, Pico Technology, Cambridgeshire, UK) every second over the course of the experiment. All experiments were repeated three times.

The second set of experiment focuses on the performance of the sodium-acetate bag in conjunction with the insulation developed in Section 4.3.2. The principle components used are represented in Figure 8.26.

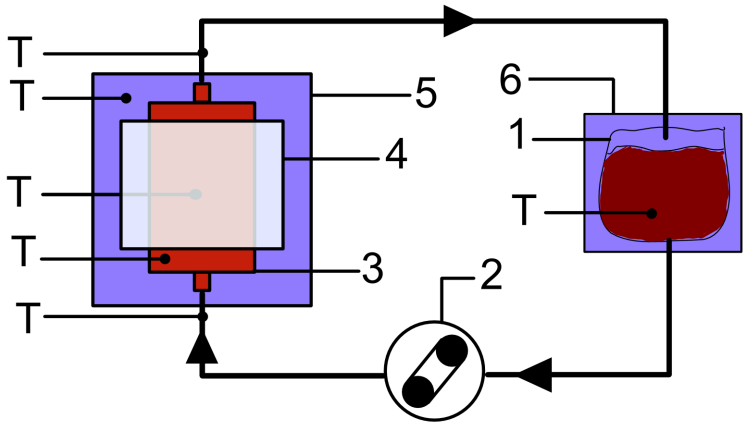

Figure 8.26: Diagram of the Physical Testing Configuration; T) Thermocouples, 1) Blood Bag, 2) Roller Pump, 3) Oxygenator, 4) Sodium-Acetate Bag, 5) Oxygenator Insulation, 6) Insulation (Survival Blanket)

A 2-liter bag filled with bovine blood was used to simulate the infant and brought to a temperature of approximately 37 °C using a water bath (Fisher Scientific, Leicestershire, UK). The blood bag was additionally covered by an emergency survival blanket in order to avoid heat loss into the environment, conditions that simulated clinical settings. The liquid is drawn out of the bag by a rotary pump (Stökert, Munich, Germany), circulated through the extracorporeal circuit and oxygenator, and injected back into the bag. To experience the affects of both increased and decreased flow rates, pump speeds were adjusted to 50 ml/min, 100 ml/min, and 300 ml/min. T-type thermocouples (Physitemp Instruments Inc., Clifton, NJ, USA) were placed in several locations to monitor the progression of temperatures. These were, 1) inside the blood bag, 2) inlet and outlet of oxygenator, 3) inside the oxygenator, 4) between oxygenator and heating bag, and 5) insulation cavity. Temperature measurements were recorded every second using a data logger (TC-08, Pico Technology, Cambridgeshire, UK). Temperature values were recorded with the activation of the ASAHED. At the beginning of the experiments, the blood bag has a core temperature

of 37 °C and a decay is expected to occur during the procedure due to thermal losses in different parts of the circuit. In order to see the impact of different environments on the performance of the oxygenator insulation, experiments were carried out on a broad range of varying ambient temperatures, one at room temperature of approximately 23 °C and the other at approximately 8 °C. The warmer ambient conditions (23 °C) were not controlled however, experiments were carried out when initial conditions were similar. Additional measures by means of a temperature controlled cold room were taken for the 8 °C experiments. To see the effects of the oxygenator insulation, two sets of experimental runs were conducted, with and without ASAHED and repeated three times each.

Figure 8.27 displays the laboratory setup with all relevant components highlighted.

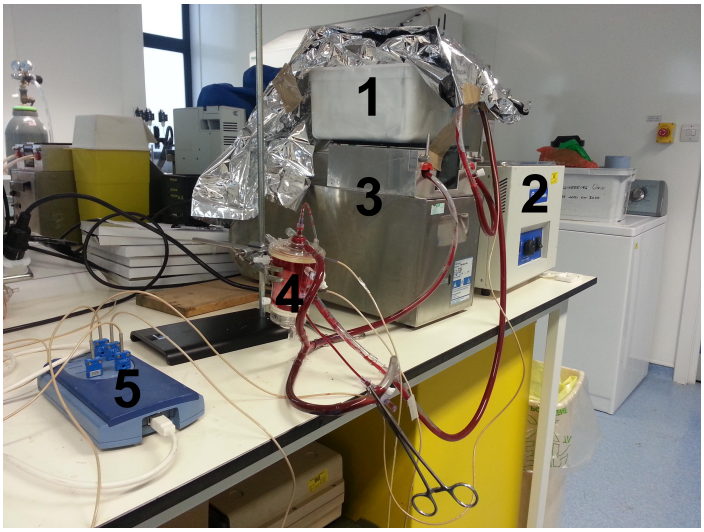

Figure 8.27: Example of laboratory setup for heat exchanger testing. 1) 2-liter blood bag wrapped in survival blanket, 2) Water bath, 3) Rotary pump, 4) Oxygenator to which our heat exchanger is attached, 5) Data logger

In the third set of experiments, we took a step towards aiming for greater maintenance of fluid temperature within the running circuit by eliminating sources of heat loss. For this experiment, the same setup applies as described in the previous ex-

periment regarding the placement of thermocouples, blood bag and survival blanket, oxygenator, heat exchanger, and insulation. Furthermore, additional insulation was used for PVC tubings (commercial polyethylene pipe insulation) between blood bag - pump - oxygenator - blood bag. At the beginning of the experiments, blood was pumped through the insulated circuit at 37 °C. Simultaneously, we activated the heat exchanger and measured the temperature decay at several sites (indicated in Figure 8.26). As the heat exchange ability reduces through the course of the experiments, approximately at the time when fluid temperature of oxygenator outlet reduces below to the inlet temperature (i.e. no heat exchange occurring), the heat exchanger would be removed and replaced with a new one, which will be subsequently activated. This process was repeated three times in total and performed under running operating conditions at a flow rate of 100 ml/min. For reasons of comparison, experiments were conducted with and without PVC insulation at ambient temperatures of approximately 24 and 6 °C. The entire process was repeated three times.

8.3.2 Results and Discussion

Temperature measurements of our sodium acetate heat exchanger bags occurred as expected during the experiments. After activation of the chemical reaction, the exothermic temperature rose to a maximum very quickly before exponentially decaying, slowly approaching ambient conditions; depicted in Figure 8.28. The decay rate within the first 2500 seconds is very similar in both environments before separation of the graphs occur. This result would suggest that lower temperature environments do not affect the rate of heat loss in the first phase but have a stronger impact thereafter. Differences in steady-state values are due to base level ambient temperatures of 24 and 7 °C. A greater temperature peak was achieved inside the bag as initially

expected, measuring above 50 °C. However, further testing revealed that the high temperature of the bag does not propagate through the polycarbonate casing of the oxygenator, thereby avoiding negative influence on blood components.

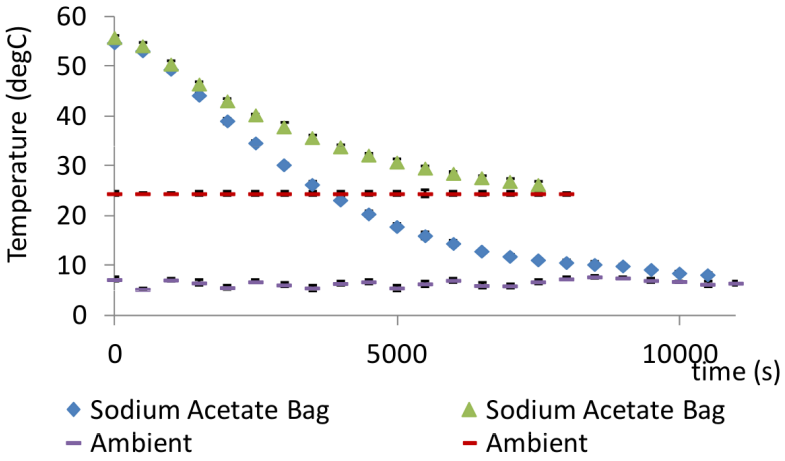

Figure 8.28: ASAHED activated and exposed to two different thermal environments, 24 and 7°C.

From this simple experiment, we can see that temperature values of the ASAHED stay well above ambient conditions for the majority of the time. Even for the first 2500 seconds (approx. 42 minutes), temperatures stayed over 40 °C, offering positive thermal input. Therefore, the prolonged duration of exothermic energy (of up to 5000 seconds at room temperatures of 23 °C) without insulation makes this technology a promising candidate for insulation purposes proposed in this project.

Results of the second set of experiments are shown in Figure 8.29 - 8.56. Figure 8.29 - 8.40 display typical temperature measurements on all locations of the circuit at all flow rates in both ambient conditions of 24 and 7 °C with and without heat exchanger and insulation. One can notice a collective temperature drop across all measured points in the circuit - similar to previous graphs. This is due to the

temperature loss through all parts of the circuit, tubings, blood bag, and oxygenator, all being exposed to ambient levels as well as reduced exothermic heat by the oxygenator bag over time.

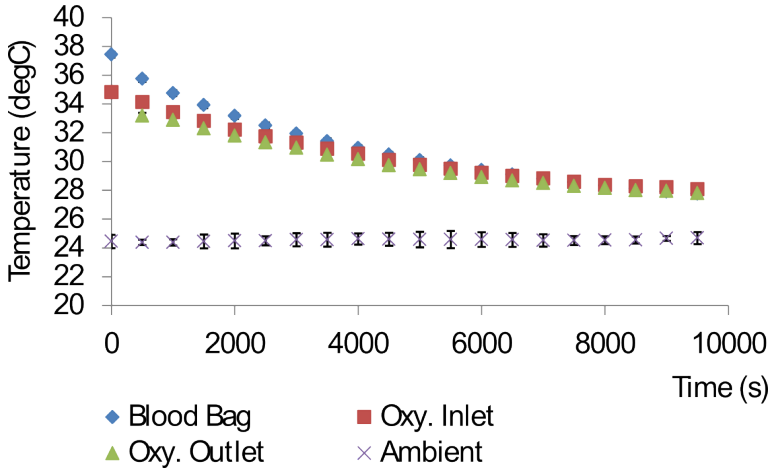

Figure 8.29: Temperature measurements of Blood Bag, Oxygenator Inlet, Oxygenator Outlet, and Ambient at flow rates of 50 ml/min without the ASAHED.

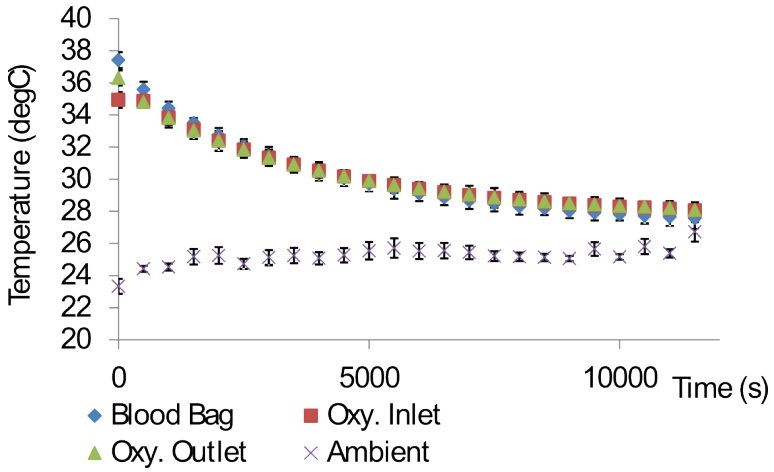

Figure 8.30: Temperature measurements of Blood Bag, Oxygenator Inlet, Oxygenator Outlet, and Ambient at flow rates of 100 ml/min without the ASAHED.

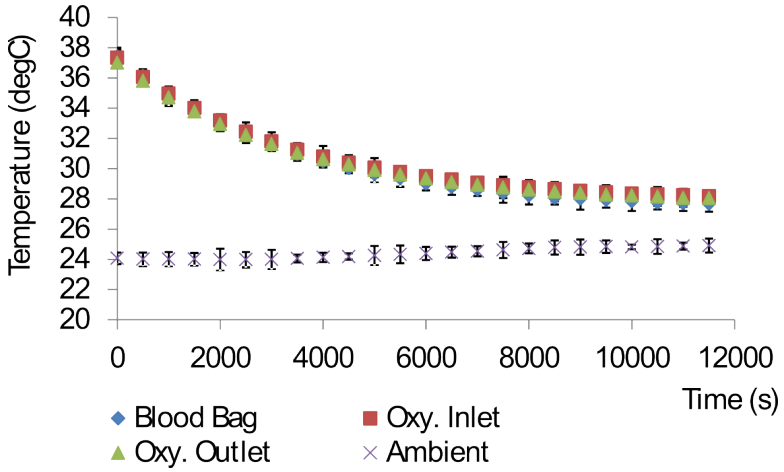

Figure 8.31: Temperature measurements of Blood Bag, Oxygenator Inlet, Oxygenator Outlet, and Ambient at flow rates of 300 ml/min without the ASAHED.

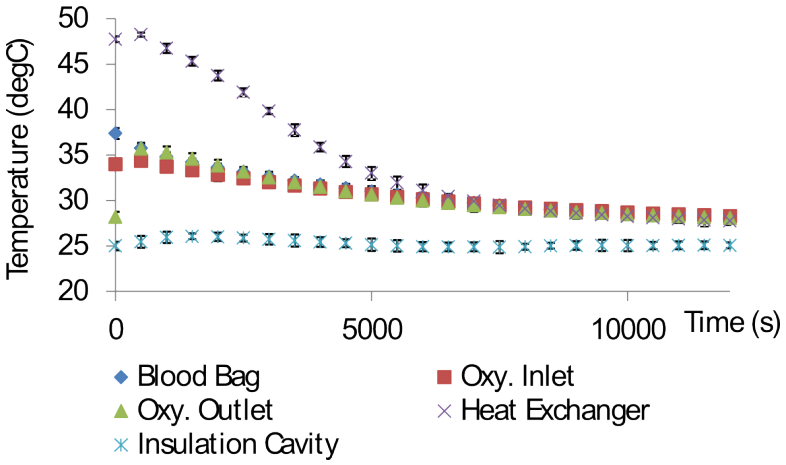

Figure 8.32: Temperature measurements of Blood Bag, Oxygenator Inlet, Oxygenator Outlet, Heat Exchanger, and Insulation Cavity at flow rates of 50 ml/min with the ASAHED.

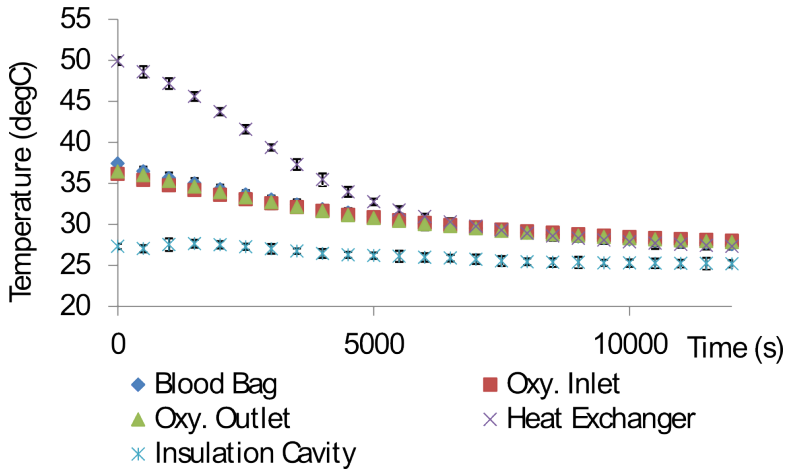

Figure 8.33: Temperature measurements of Blood Bag, Oxygenator Inlet, Oxygenator Outlet, Heat Exchanger, and Insulation Cavity at flow rates of 100 ml/min with the ASAHED.

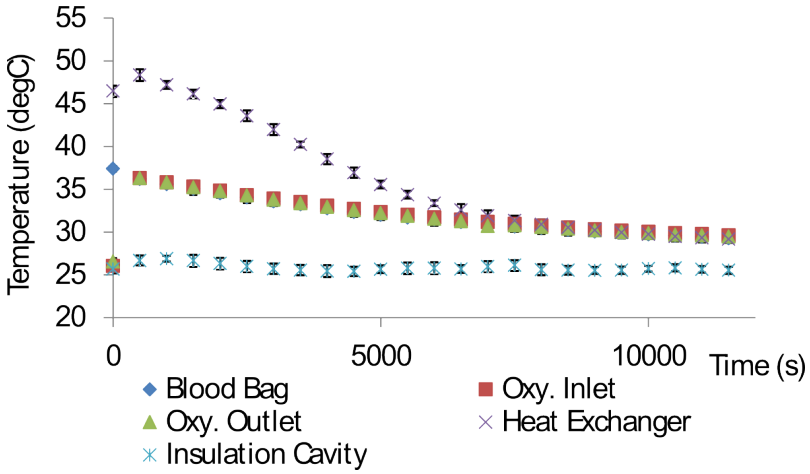

Figure 8.34: Temperature measurements of Blood Bag, Oxygenator Inlet, Oxygenator Outlet, Heat Exchanger, and Insulation Cavity at flow rates of 300 ml/min with the ASAHED.

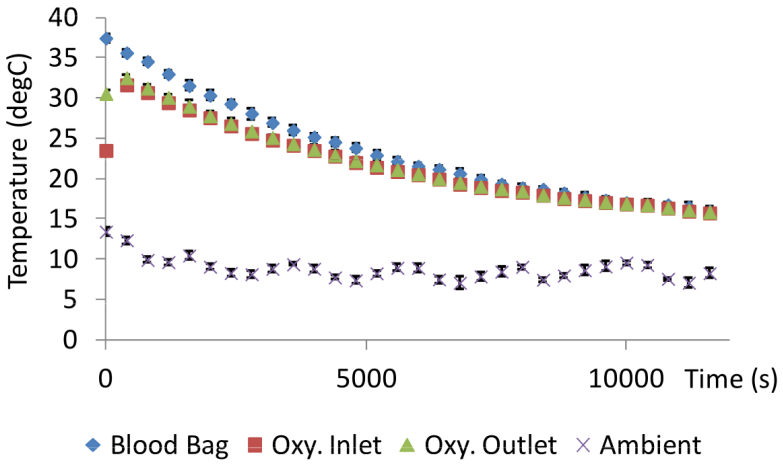

Figure 8.35: Temperature measurements of Blood Bag, Oxygenator Inlet, Oxygenator Outlet, and Ambient conducted in cold room at flow rates of 50 ml/min without the ASAHED.

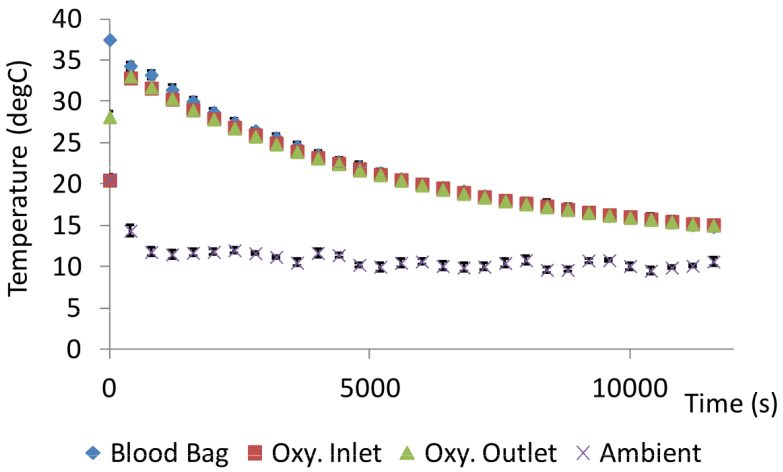

Figure 8.36: Temperature measurements of Blood Bag, Oxygenator Inlet, Oxygenator Outlet, and Ambient conducted in cold room at flow rates of 100 ml/min without the ASAHED.

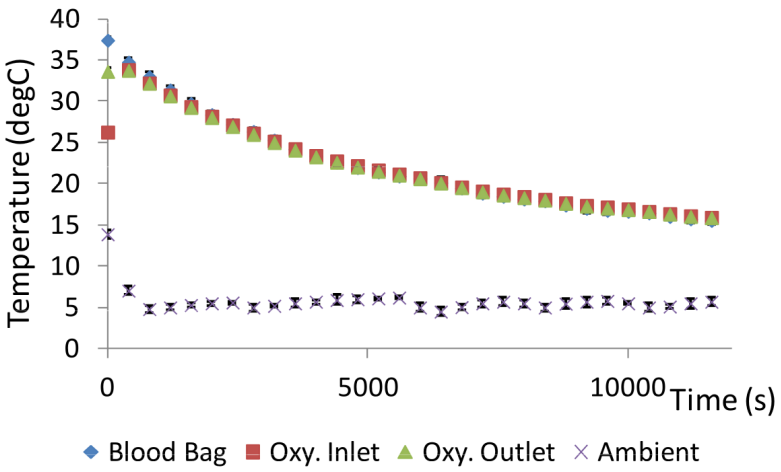

Figure 8.37: Temperature measurements of Blood Bag, Oxygenator Inlet, Oxygenator Outlet, and Ambient conducted in cold room at flow rates of 300 ml/min without the ASAHED.

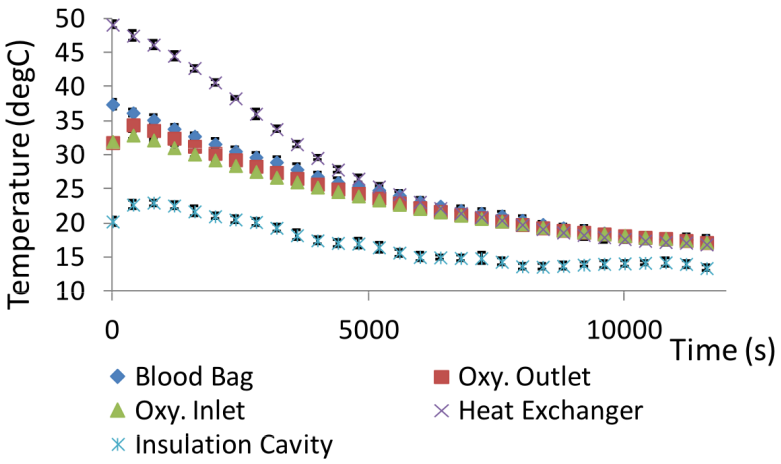

Figure 8.38: Temperature measurements of Blood Bag, Oxygenator Inlet, Oxygenator Outlet, Heat Exchanger and Insulation Cavity conducted in cold room at flow rates of 50 ml/min with the ASAHED.

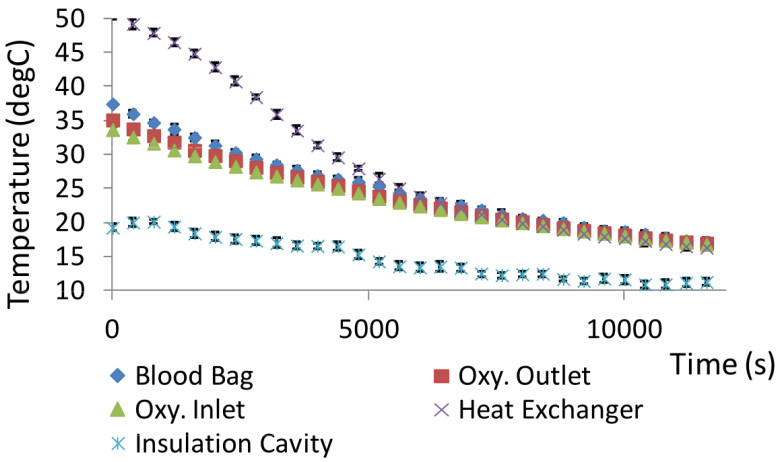

Figure 8.39: Temperature measurements of Blood Bag, Oxygenator Inlet, Oxygenator Outlet, Heat Exchanger and Insulation Cavity conducted in cold room at flow rates of 100 ml/min with the ASAHED.

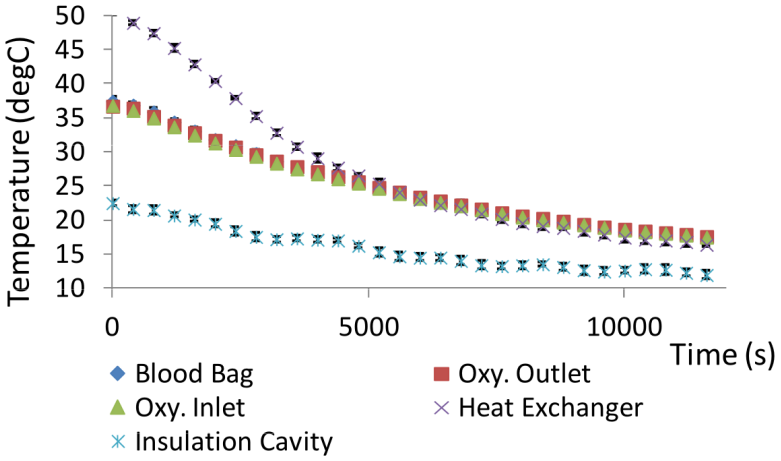

Figure 8.40: Temperature measurements of Blood Bag, Oxygenator Inlet, Oxygenator Outlet, Heat Exchanger and Insulation Cavity conducted in cold room at flow rates of 300 ml/min with the ASAHED.

Figure 8.41 - 8.44 compares the affects of different flow rates on the blood bag with and without heat exchanger in both ambient conditions. The average temperature decay inside the blood bag seems to occur at similar rates in both environments with and without insulation despite variations in blood flow rates. It would appear from

this comparison that the temperature decay inside the blood bag has an independent relationship to varying flow rates. In other words, ramping flow rates up or down has only minimal effects on heat conservation and usage of the heat exchanger.

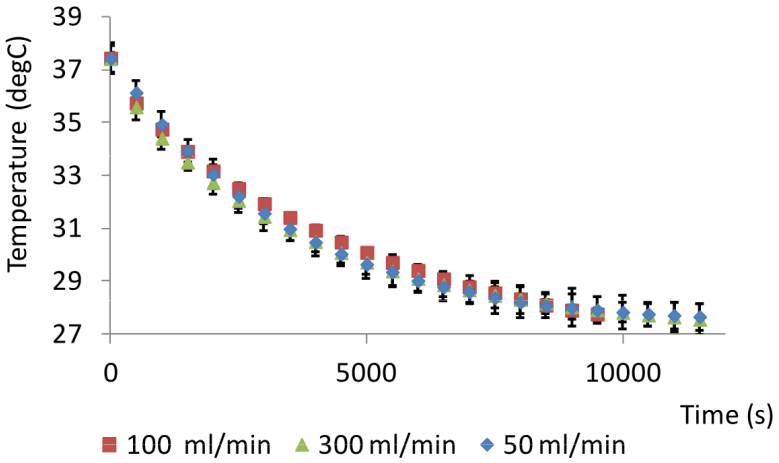

Figure 8.41: Blood Bag temperature comparison conducted at different flow rates without the ASAHED at 24 °C ambient temperature.

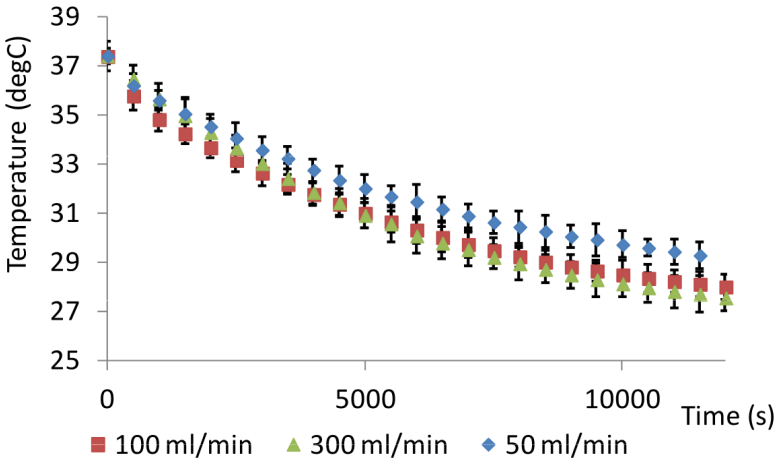

Figure 8.42: Blood Bag temperature comparison conducted at different flow rates with the ASAHED at 24 °C ambient temperature.

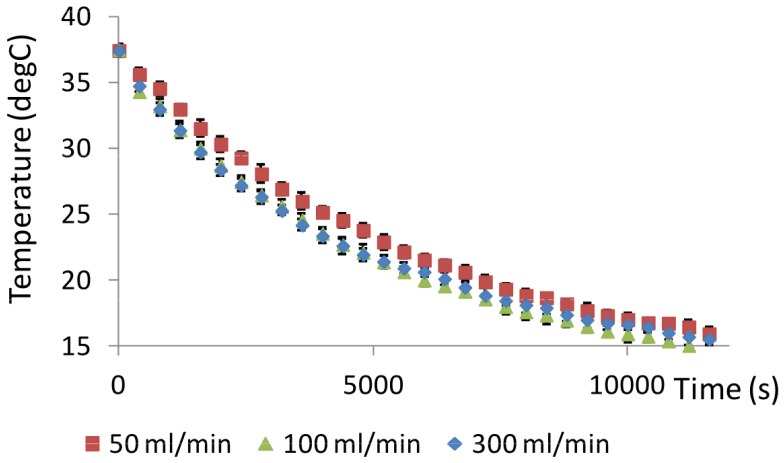

Figure 8.43: Blood Bag temperature comparison conducted at different flow rates without the ASAHED at 7 °C ambient temperature.

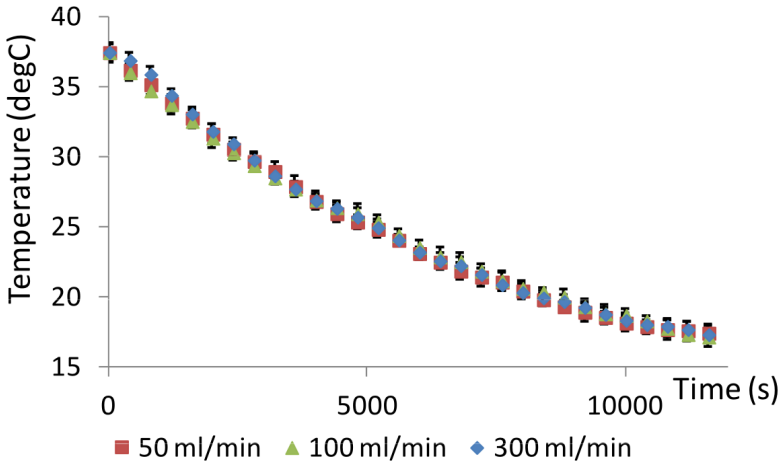

Figure 8.44: Blood Bag temperature comparison conducted at different flow rates with the ASAHED at 7 °C ambient temperature.

Figure 8.45 - 8.50 compares the results of blood bag temperatures with and without heat exchanger at equal flow rates and equal ambient conditions. It is apparent from these graphs that a shift to the left occurred for all cases with the heat exchanger, i.e. blood bag temperatures were preserved longer during the full range of flow rates and different ambient conditions. In all cases, median temperature values of

experiments conducted with heat exchangers were above the ones without, indicating heat preservation.

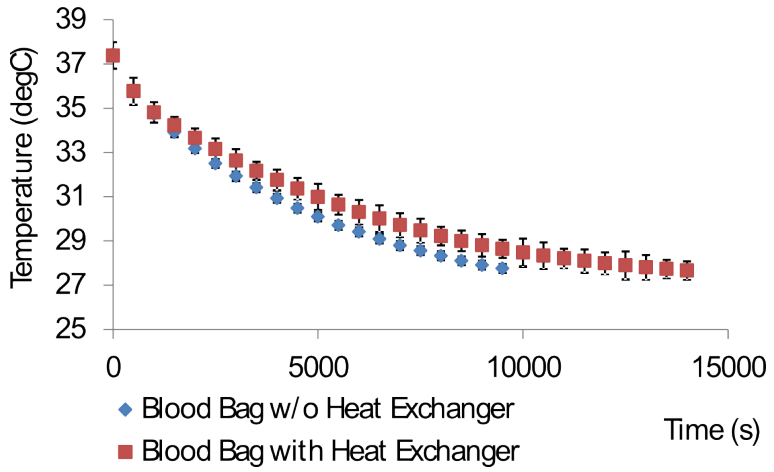

Figure 8.45: Blood Bag temperature comparison with and without the ASAHED at a flow rate of 50 ml/min and 24 °C ambient temperature.

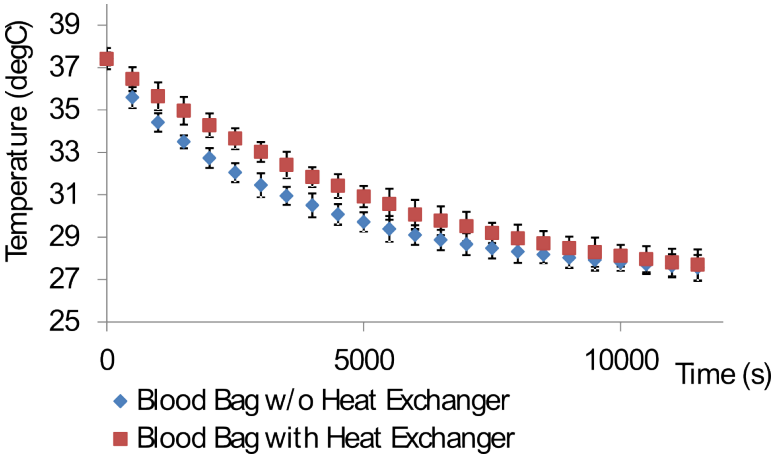

Figure 8.46: Blood Bag temperature comparison with and without the ASAHED at a flow rate of 100 ml/min and 24 °C ambient temperature.

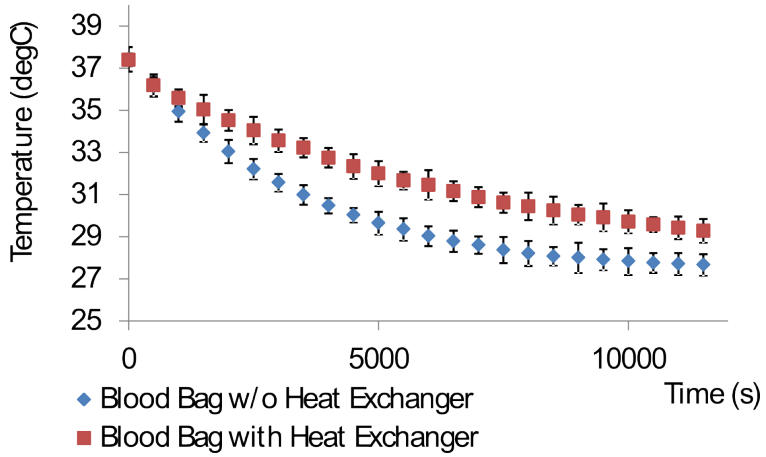

Figure 8.47: Blood Bag temperature comparison with and without the ASAHED at a flow rate of 300 ml/min and 24 °C ambient temperature.

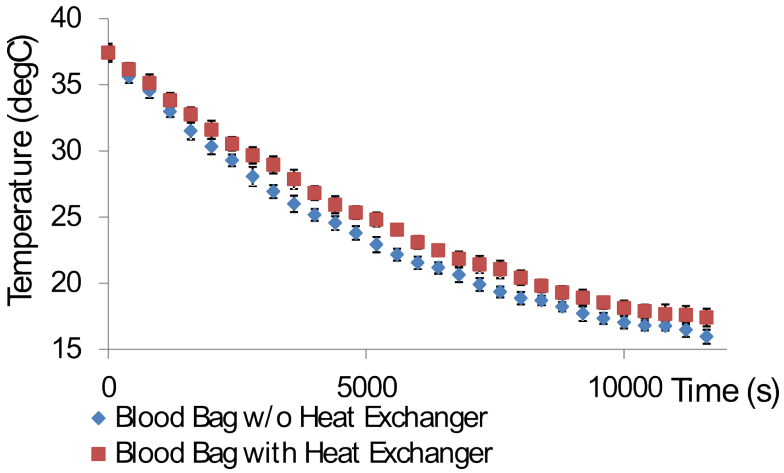

Figure 8.48: Blood Bag temperature comparison with and without the ASAHED at a flow rate of 50 ml/min and 7 °C ambient temperature.

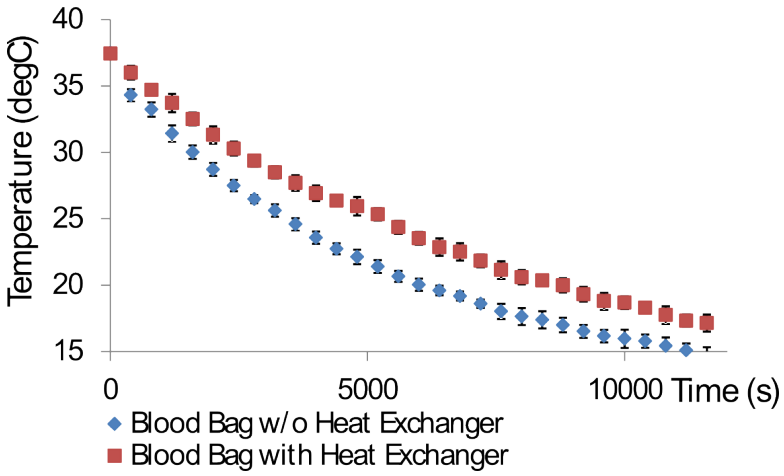

Figure 8.49: Blood Bag temperature comparison with and without the ASAHED at a flow rate of 100 ml/min and 7 °C ambient temperature.

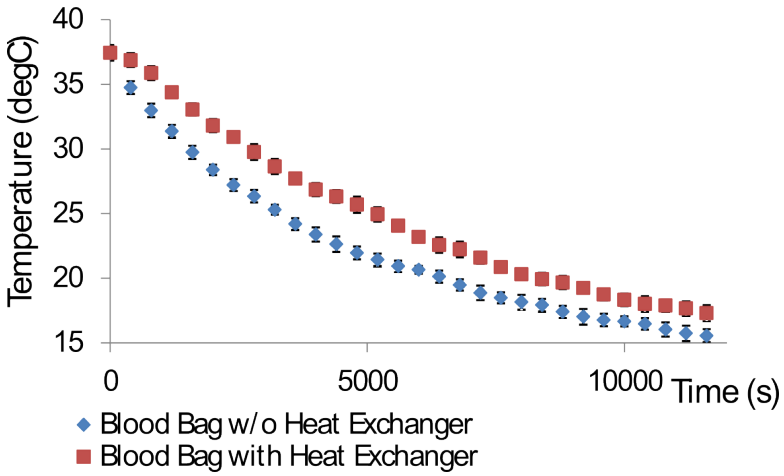

Figure 8.50: Blood Bag temperature comparison with and without the ASAHED at a flow rate of 300 ml/min and 7 °C ambient temperature.

Figure 8.51 - 8.56 shows the temperature differences between oxygenator input and output during flow. In order to visualise the effects of our heat exchanger, temperature differences of experiments with and without heat exchanger were compared. This was done for all flow rates and ambient conditions.

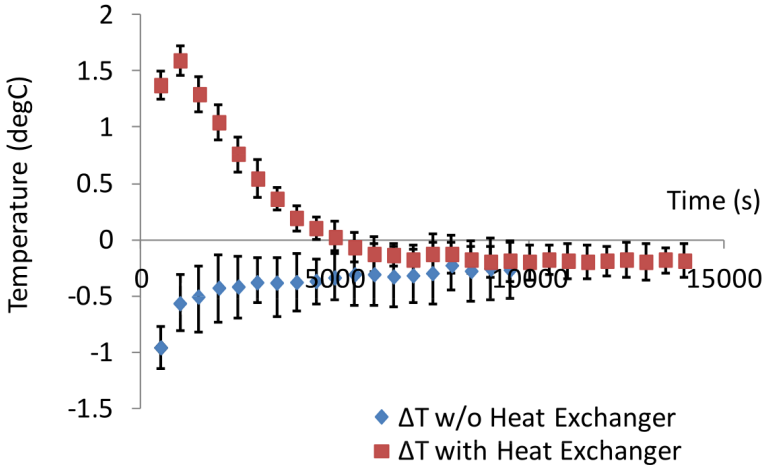

Figure 8.51: Temperature difference comparison (ΔT=T$_{outlet}$-T$_{inlet}$) with and without the ASAHED at a flow rate of 50 ml/min and 24 °C ambient temperature.

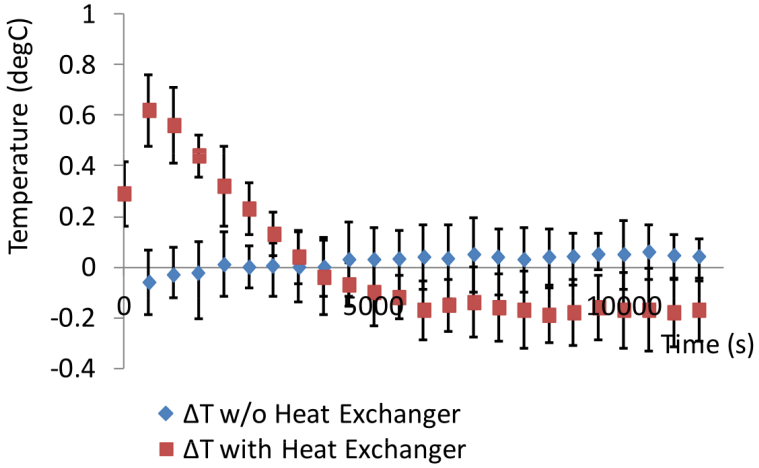

Figure 8.52: Temperature difference comparison (ΔT=T$_{outlet}$-T$_{inlet}$) with and without the ASAHED at a flow rate of 100 ml/min and 24 °C ambient temperature.

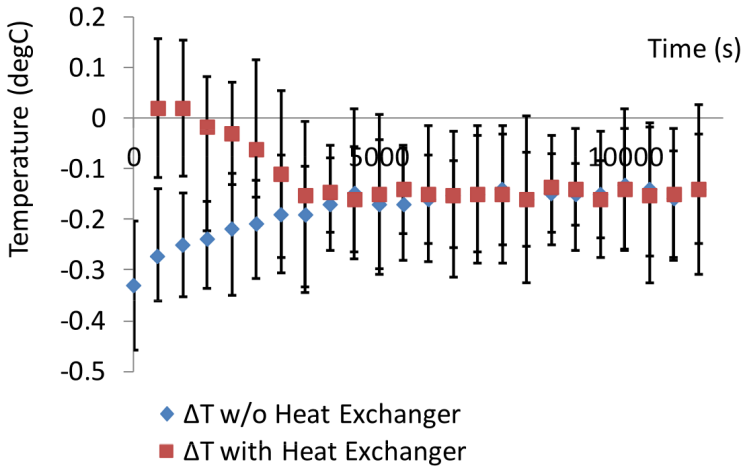

Figure 8.53: Temperature difference comparison (ΔT=T_{outlet}-T_{inlet}) with and without the ASAHED at a flow rate of 300 ml/min and 24 °C ambient temperature.

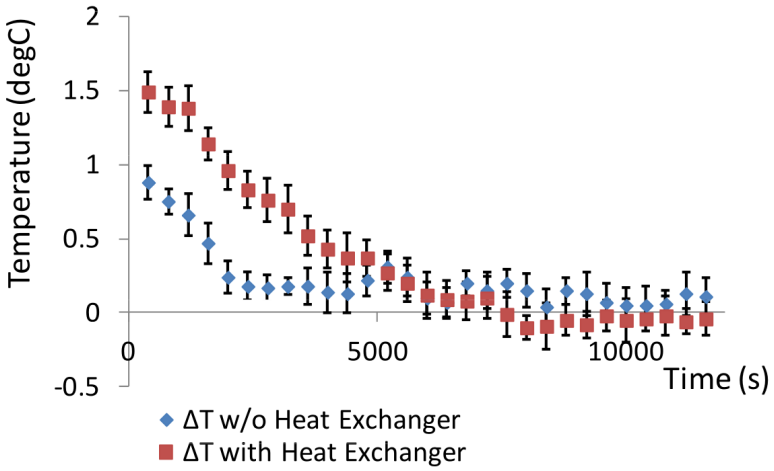

Figure 8.54: Temperature difference comparison (ΔT=T_{outlet}-T_{inlet}) with and without the ASAHED at a flow rate of 50 ml/min and 7 °C ambient temperature.

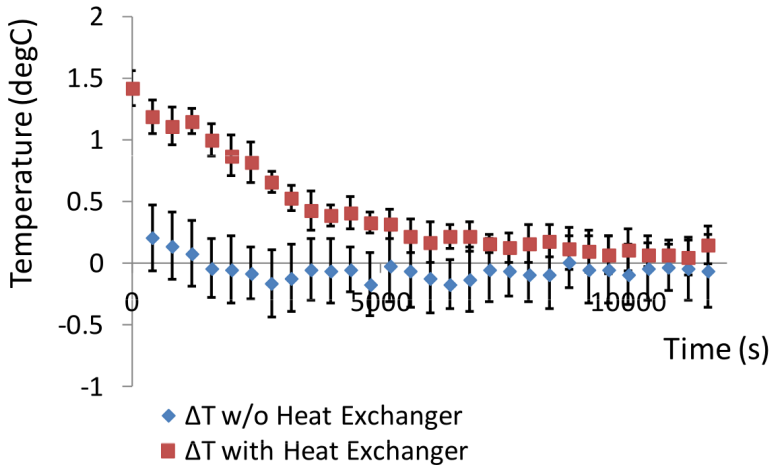

Figure 8.55: Temperature difference comparison (ΔT=T_{outlet}-T_{inlet}) with and without the ASAHED at a flow rate of 100 ml/min and 7 °C ambient temperature.

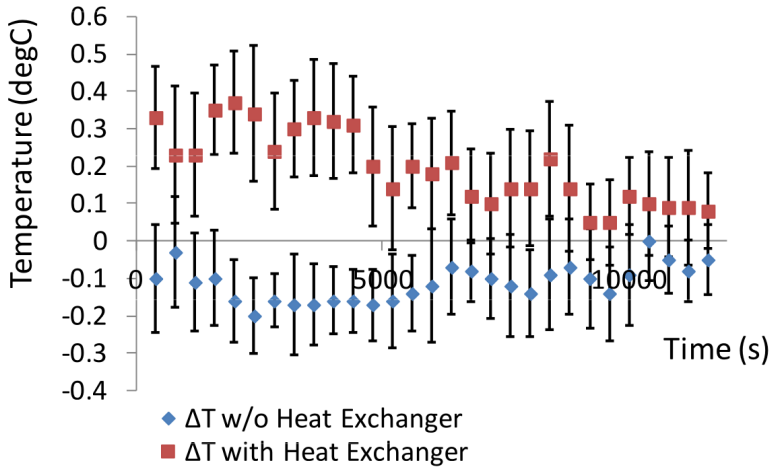

Figure 8.56: Temperature difference comparison (ΔT=T_{outlet}-T_{inlet}) with and without the ASAHED at a flow rate of 300 ml/min and 7 °C ambient temperature.

The blue plot can be interpreted as the baseline measurement, representing experiments without heat exchanger which the red plot can be compared to. Due to thermally contributing effects of our device, a temperature increase was expected from the experiments and therefore calculations are based on ΔT(t)= T_{Output}(t)-T_{Input}(t); reflecting positive values as temperature increases within the oxygenator.

It is noticeable that baseline values in all graphs are grouped much closer to the abscissa, indicating fewer gain/loss. Also noticeable is the increased gain/loss of the baseline graph at the start of the experiment, gradually decreasing/increasing over time. This effect could be due to the higher stored temperatures of the fluid at the beginning of the experiment, resulting in greater temperature loss. An alternative explanation could be the potential impact of the stored thermal energy within the oxygenator materials such as fibres and casing. These elements contain a thermal charge of ambient conditions and the possibility of energy exchange between them and the flowing liquid can occur. Even more pronounced are the higher values at the start of the experiments in the cases where the ASAHED is used which over time reduce to a minimum. This minimum coincides with the baseline values of no heat exchange. Higher flow rates seem to dampen the initially strong thermal peaks as well as faster baseline returns during ambient temperatures of 24 °C, as exhibited in Figure 8.51, 8.52, and 8.53. This suggests that the effective duration of the insulation at room temperature is inversely related to flow rates. However, observing efficiency levels between experiments conducted at two temperature environments, no significant differences were to be found. Magnitude levels as well as rate of decay seem to be very similar at room temperatures of 24 °C and 7 °C.

The results of the third set of experiments are shown in Figures 8.57 - 8.70. Figure 8.57 - 8.60 displays measurements over the entire experiment of all deployed thermocouples in the circuitry. One can clearly see the three rising peaks of the heat exchanger temperature followed by a natural decay. These represent the activation, usage, and substitution of the three sodium acetate bags. Also noticeable is the

resultant affect that this procedure has on oxygenator outlet, blood bag, and cavity temperature, represented by small surges during operation.

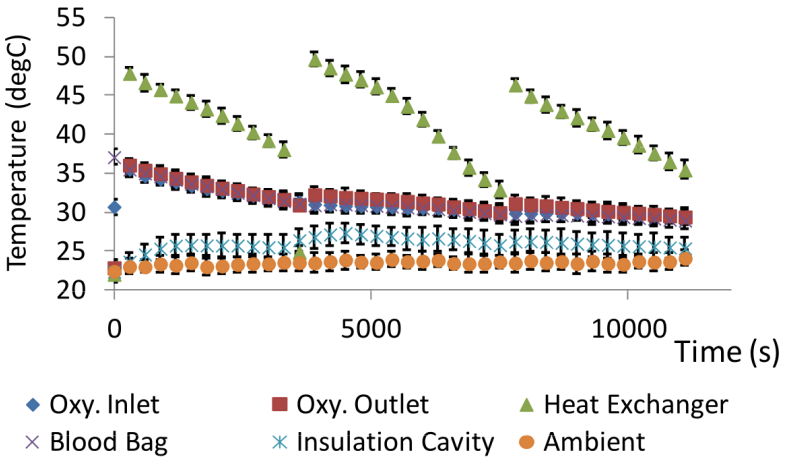

Figure 8.57: Temperature measurements of Oxygenator Inlet, Oxygenator Outlet, Heat Exchanger Bag, Blood Bag, Insulation Cavity, and Ambient at a flow rate of 100 ml/min, ambient temperatures of approx. 24 °C, without tubing insulation.

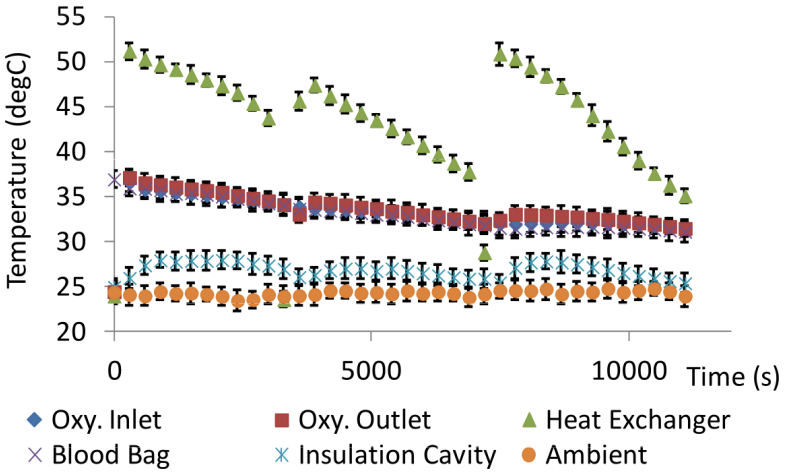

Figure 8.58: Temperature measurements of Oxygenator Inlet, Oxygenator Outlet, Heat Exchanger Bag, Blood Bag, Insulation Cavity, and Ambient at a flow rate of 100 ml/min, ambient temperatures of approx. 24 °C, with tubing insulation.

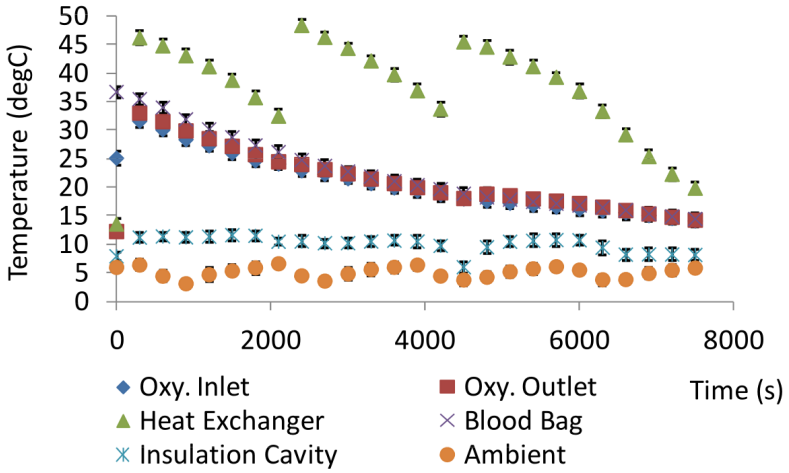

Figure 8.59: Temperature measurements of Oxygenator Inlet, Oxygenator Outlet, Heat Exchanger Bag, Blood Bag, Insulation Cavity, and Ambient at a flow rate of 100 ml/min, ambient temperatures of approx. 7 °C, without tubing insulation.

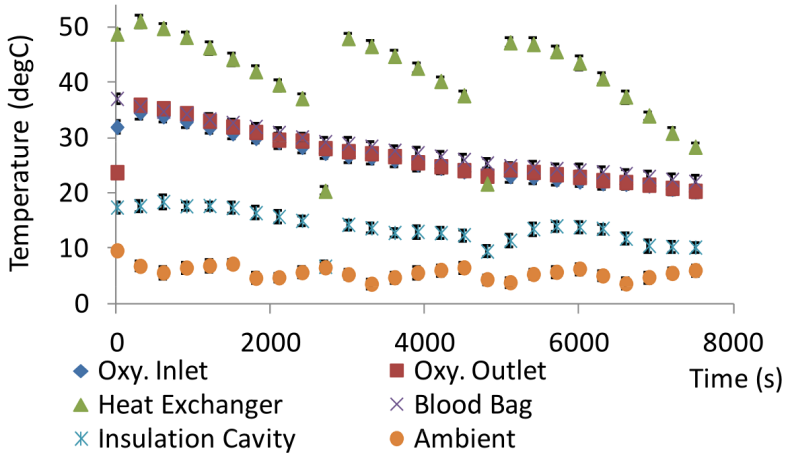

Figure 8.60: Temperature measurements of Oxygenator Inlet, Oxygenator Outlet, Heat Exchanger Bag, Blood Bag, Insulation Cavity, and Ambient at a flow rate of 100 ml/min, ambient temperatures of approx. 7 °C, with tubing insulation.

Figure 8.61 - 8.64 offer a closer look into the oxygenator inlet and outlet temperature behaviour of our experiment. The blue plot represents the uninterrupted exponential decay of inlet temperature whereas the red plot displays a similar pattern overlaid with temperature spikes, caused by the re-activation of our ASAHED.

From Figure 8.61 and 8.62, one can see that the temperature differences are more pronounced with the second and third substitution of an ASAHED compared to the first set. This can be explained by the fact of temperature differences between the fluid and the ASAHED. The greater the temperature differences the greater the heat exchange between the two entities. At the start of the activation of the sodium acetate, when the temperature surge is the greatest, this is the moment of maximum heat exchange leading to the maximum spike of temperature at the oxygenator outlet. This effect is more noticeable the more the fluid temperature approaches ambient levels where the rate of the asymptotical reduces. Therefore, Figure 8.63 and 8.64 show less added heat compared to Figure 8.61 and 8.62 due to increased temperature differences between blood and room temperature. However, in both ambient conditions, irrespective of added pipe insulation, our heat exchanger is able to add heat to the fluid as shown in these figures.

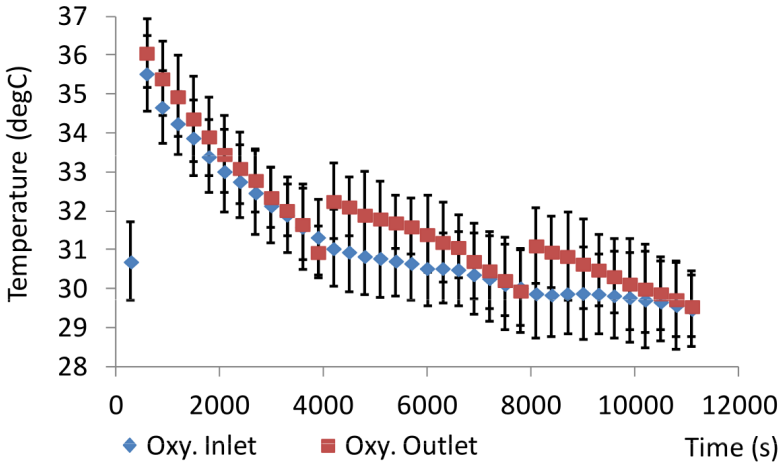

Figure 8.61: Oxygenator inlet and outlet temperature response to heat exchanger without tubing insulation at a flow rate of 100 ml/min at 24 °C ambient.

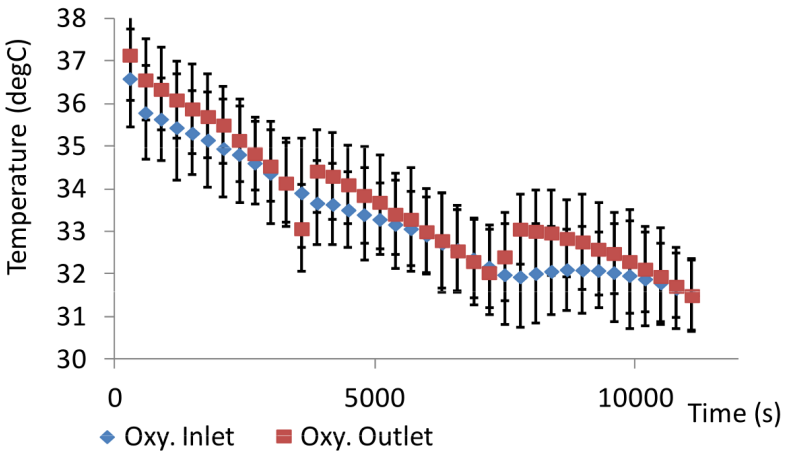

Figure 8.62: Oxygenator inlet and outlet temperature response to heat exchanger with additional tubing insulation at a flow rate of 100 ml/min at 24 °C ambient.

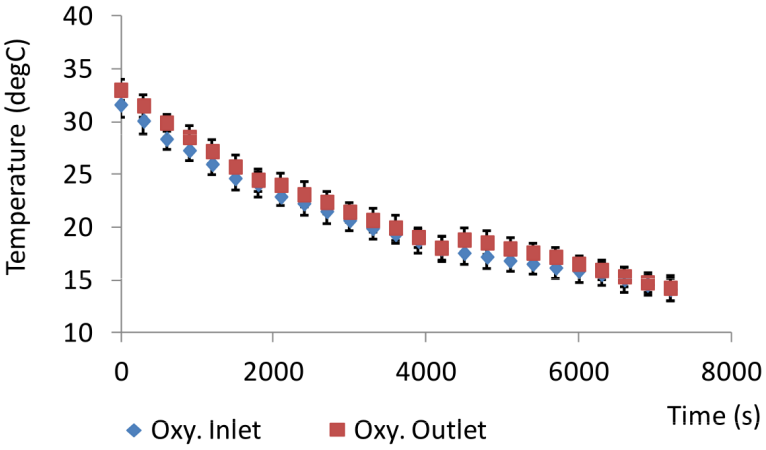

Figure 8.63: Oxygenator inlet and outlet temperature response to heat exchanger without tubing insulation at a flow rate of 100 ml/min at 7 °C ambient.

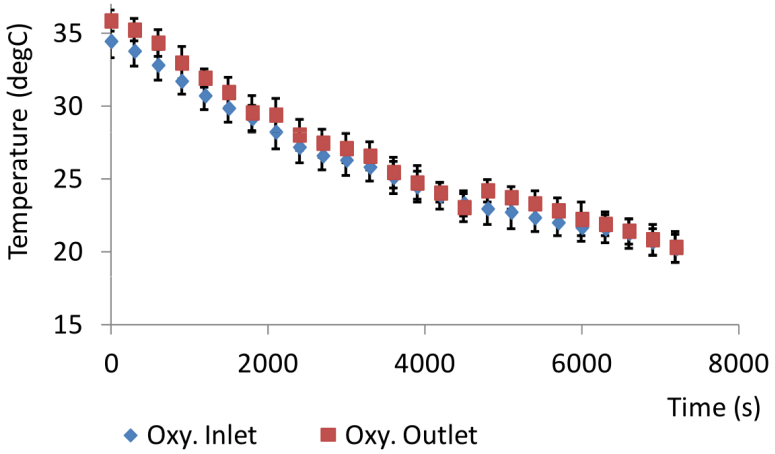

Figure 8.64: Oxygenator inlet and outlet temperature response to heat exchanger with additional tubing insulation at a flow rate of 100 ml/min at 7 °C ambient.

Figure 8.65 and 8.66 display a comparison of temperature differences between oxygenator outlet and inlet. The applied formula is: ΔT(t)=T$_{Output}$(t)-T$_{Input}$(t). Figure 8.65 compares temperature values of experiments conducted at ambient temperatures of approximately 24 °C and Figure 8.66 at 7 °C. One can see a similar pattern of employing and changing the heat exchangers during the experiments. The majority of the time, values were positive, indicating outlet temperatures being greater than inlet temperatures. Indicative for negative values are lowered thermal charges of our heat exchanger and the subsequent exchange with a new one. Both cases, insulation vs. non-insulation, show very similar patterns with almost identical magnitudes which suggests that heat added by the heat exchangers continues in the same fashion irrespective of additional pipe insulation.

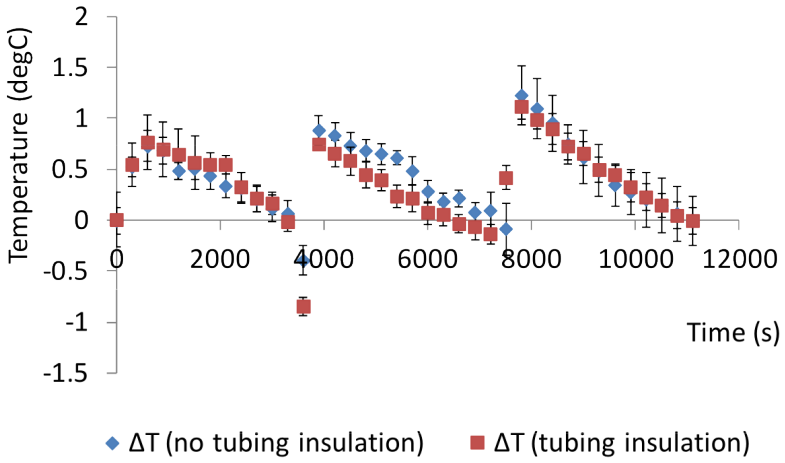

Figure 8.65: Outlet-inlet temperature difference comparison between experiments conducted with and without tubing insulation at ambient conditions of 24 °C at 100 ml/min.

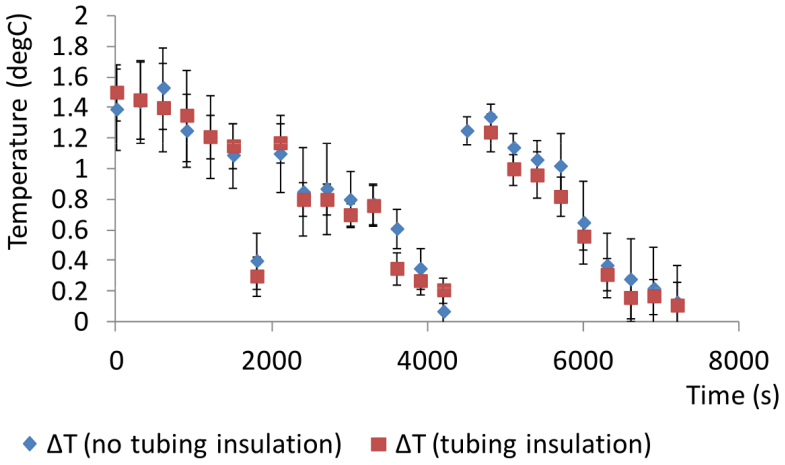

Figure 8.66: Outlet-inlet temperature difference comparison between experiments conducted with and without tubing insulation at ambient conditions of 7 °C at 100 ml/min.

To illustrate the impact of tubing insulation on the ability to preserve heat within the circuitry, Oxygenator Inlet temperatures of Figure 8.61 and 8.62 and Figure 8.63 and 8.64 were combined and adjusted to the same temperature-time frame in Figure 8.67 and 8.68. From these figures, one can clearly identify the impact of tubing

insulation on heat preservation. Additional tables were provided to quantify the impact in numerical terms (Table 8.3 and 8.4).

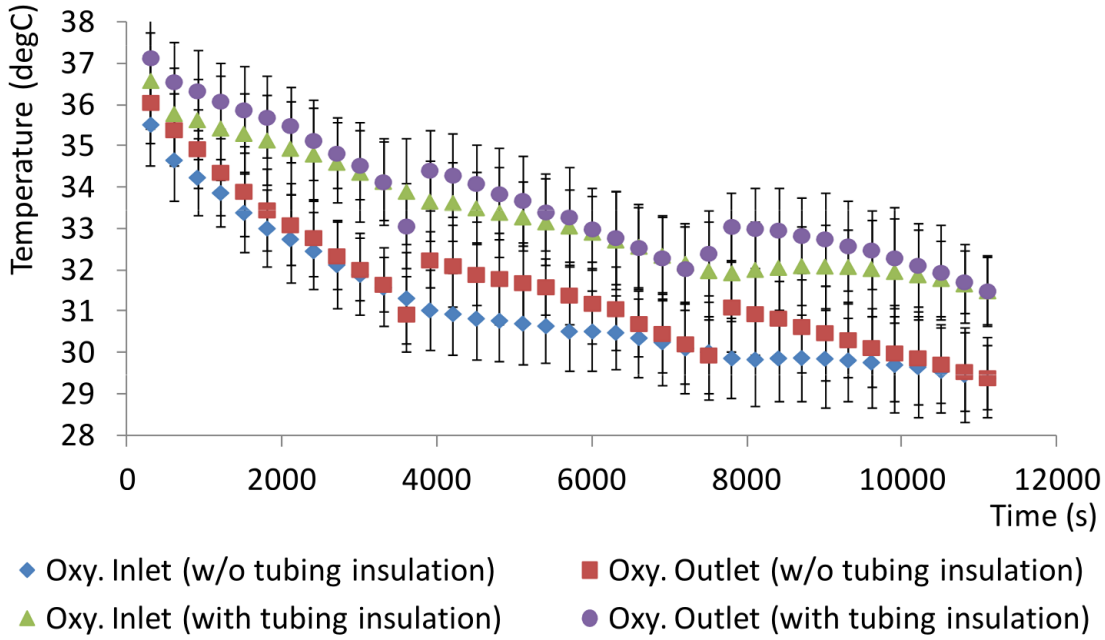

Figure 8.67: Oxygenator inlet and outlet temperatures comparison for experiments conducted with and without tubing insulation at ambient temperatures of 24 °C at 100 ml/min.

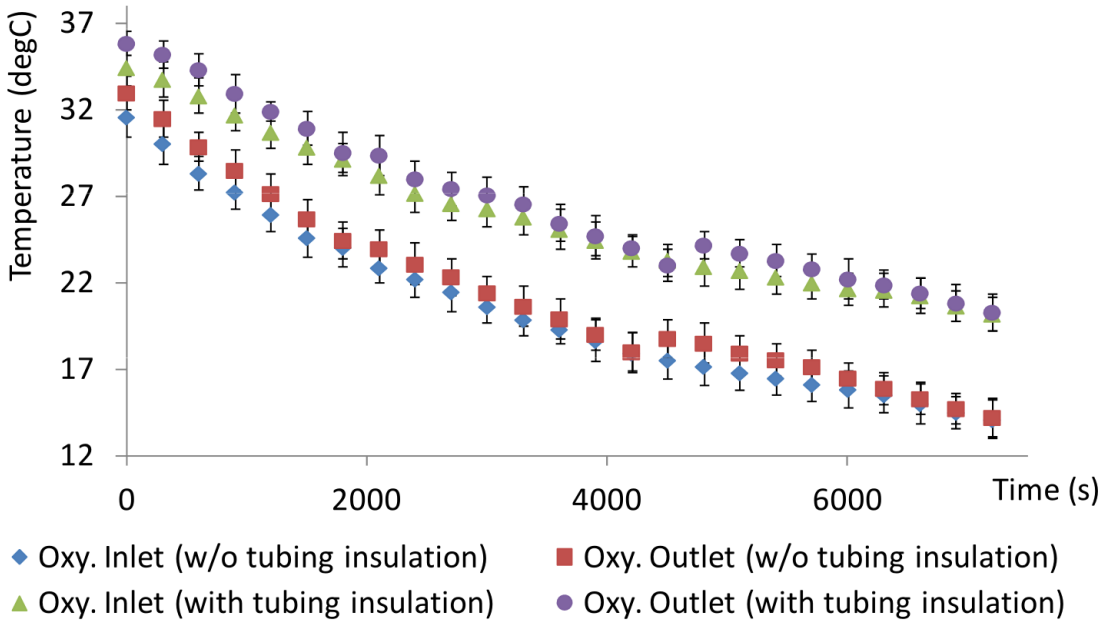

Figure 8.68: Oxygenator inlet and outlet temperatures comparison for experiments conducted with and without tubing insulation at ambient temperatures of 7 °C at 100 ml/min.

Temperature	With insulation	w/o insulation	Time difference
34 $^{\circ}C$	3450 sec	1050 sec	2400 sec
33 $^{\circ}C$	5850 sec	1800 sec	4050 sec
32 $^{\circ}C$	7500 sec	2900 sec	4600 sec

Table 8.3: Oxygenator inlet temperature differences for tubings with and without insulation at ambient conditions of 24 $^{\circ}C$. Starting temperature is 37 $^{\circ}C$.

When comparing both, insulated and non-insulated tubings under ambient temperatures of 24 $^{\circ}C$, for fluid temperature to drop from approximately 37 $^{\circ}C$

down to 34 $^{\circ}C$, a gap of 2400 seconds (40 minutes) can be achieved. This means that a temperature drop of 3 $^{\circ}C$ can be prolonged with means of tubing insulation by 40 minutes compared to conventional methods. As the procedure progresses, this time gap increases to 4050 seconds (67 minutes) and 4600 seconds (77 minutes) at 33 and 32 $^{\circ}C$, respectively. Similar results were obtained at ambient temperatures of 7 $^{\circ}C$, where temperature values collectively drop at a much faster rate. However, despite the rapid decrease in temperature, a buffer of time exists between insulated vs. non-insulated tubings. They are 1150, 1550, and 2250 seconds (19, 26, and 38 minutes) at inlet temperatures of 30, 28, and 25 $^{\circ}C$, respectively.

Temperature	With insulation	w/o insulation	Time difference
30 $^{\circ}C$	1750 sec	600 sec	1150 sec
28 $^{\circ}C$	2550 sec	1000 sec	1550 sec
25 $^{\circ}C$	3950 sec	1700 sec	2250 sec

Table 8.4: Oxygenator inlet temperature differences for tubings with and without insulation at ambient conditions of 7 $^{\circ}C$.

So far, our analysis has directly focused on heat exchanger performance in proximity of the oxygenator. The real aim of these experiments is to preserve heat in our blood bag, simulating the patient. Blood bag temperature decays in Figure 8.69 and 8.70 represent the differences between experiments conducted with and without tubing insulation.

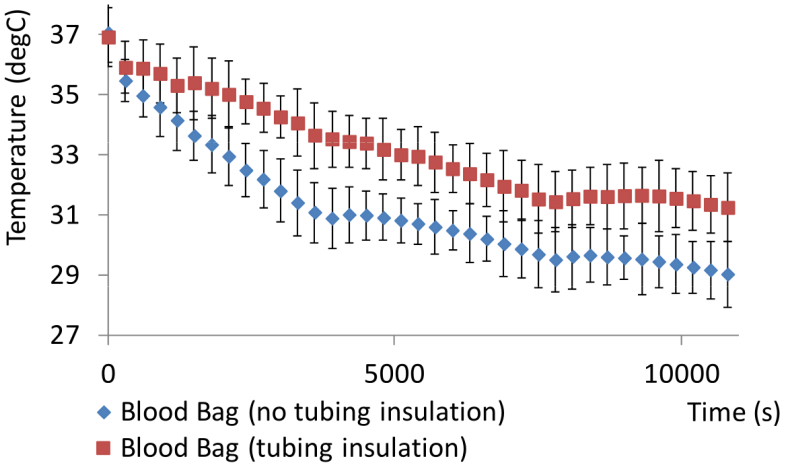

Figure 8.69: Comparison of blood bag temperature decays with and without tubing insulation at ambient conditions of 24 $^{\circ}C$.

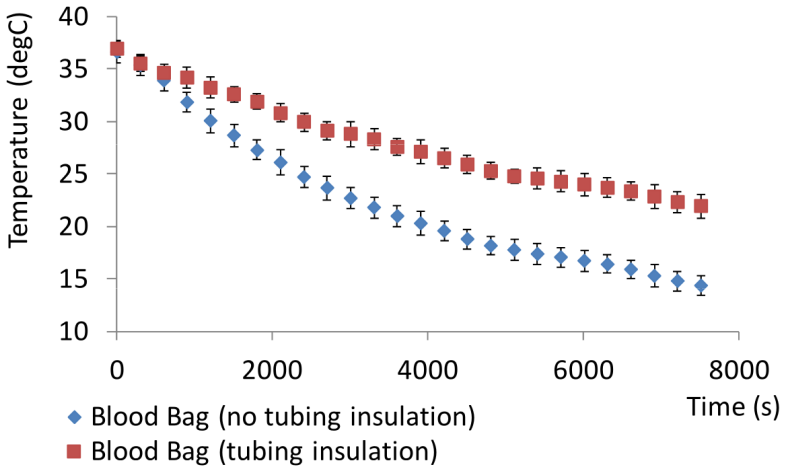

Figure 8.70: Comparison of blood bag temperature decays with and without tubing insulation at ambient conditions of 7 $^{\circ}C$.

The red plot represents the decay of the average fluid temperature inside the 2-liter bag during the experiment with insulation around tubings and the blue plot without insulation. Large temperature differences between experiments of insulation and non-insulation can be taken from both figures. The supplemental tables help to quantify the difference in time that insulation is able to achieve at various temper-

ature levels (Figure 8.5 and 8.6). A greater difference in decay time can be noticed between both plots with increasing duration of the experiments. Both experiments started at approximately 37 $°C$ and the blood bag without any circuit tubing insulation reached 35 $°C$ 1500 seconds (approx. 24 minutes) earlier than the circuit with insulation. This lag time is doubled for temperature levels of 33 $°C$. Similar behaviour can be observed for experiments conducted at ambient temperatures of 7 $°C$, only in a more accelerated manner, with delays of 600 and 950 seconds at 33 $°C$ and 31 $°C$, respectively (see Table 8.6). The results show that an overall prolongation of core bag temperature can be achieved even under more extreme ambient conditions.

Temperature	With insulation	w/o insulation	Time difference
35 $°C$	2100 sec	600 sec	1500 sec
33 $°C$	5100 sec	2100 sec	3000 sec
31 $°C$	11100 sec	3750 sec	7350 sec

Table 8.5: Blood bag temperature differences for tubings with and without insulation at ambient conditions of 24 $°C$.

Temperature	With insulation	w/o insulation	Time difference
35 $^{\circ}C$	400 sec	400 sec	0 sec
33 $^{\circ}C$	1350 sec	750 sec	600 sec
31 $^{\circ}C$	2000 sec	1050 sec	950 sec

Table 8.6: Blood bag temperature differences for tubings with and without insulation at ambient conditions of 7 $^{\circ}C$.

8.4 Summary

Our 1st iteration heat exchanger for conventional ECMO was able to provide fast responses to temperature demands but failed to reach the desired temperature levels despite good model accuracy in the previous chapter. Testing has revealed that those performance limitations are design- much more than control related and required a practical re-design of the heat exchanger unit. Refinement of the heat exchanger lead to a new device which was tested under the same conditions as the previous iteration. We replicated and applied the same testing conditions as in our previously sub-optimal heat exchanger-experiment to our refined model and used those as our benchmark in order to validate the new technology. The results showed that the new heat exchanger managed to eradicate all shortcomings of our previous model and supplied heat even under the most thermally challenging situations.

It is important to consider the effects of incremental heating and cooling in clinical settings. The rapid heating or cooling may release gases within the ECMO circuit

which can act as microemboli and potentially block blood flow to micro capillaries (Geissler, 1997). It is therefore important to follow guidelines such as Kurusz (1985) and Pollard (1961) in order to avoid negative effects, e.g. brain oedemas in patients during ECMO therapy. Since our control scheme in conjunction with the heat exchanger is able to limit upper and lower temperature boundaries, an additional high-level programme can be implemented to control the rate of heating and cooling more strictly, for example 2 $^{\circ}C$ per 10 minutes, or any other desirable rate, so to avoid unnecessary complications caused by gaseous microemboli.

Our in-transit heat exchanger solution based on sodium-acetate and additional insulation layer was rigorously tested under laboratory conditions. The rapid temperature increase followed by an exponential decay makes this technology a promising solution for thermal applications in situations with limited resources. Initial experiments with our sodium acetate bag illustrated the strong proportional influence that ambient temperature has on thermal exchange performance. The colder the ambient temperature, the faster the bag loses temperature, effectively reducing the time of operation before a recharge is required. The effect that the ASAHED had on fluid temperature with varying flow rates, and extreme ambient conditions was shown in clinically mimetic conditions. Our experiments concluded that flow rate variations seem not to affect heat exchanger performance across ambient temperatures. Ambient temperatures, however, have a negative affect on both heat exchanger and blood bag, severely reducing thermal charge. Despite different flow rates and ambient conditions, the ASAHED has a positive thermally additive affect on blood bag temperatures. This has been demonstrated by time-differences between experiments conducted with and without (baseline) our heat exchanger solution. A maximum delay of 2100 seconds for the cooling of the blood bag to 30.5 $^{\circ}C$ at flow rates of 100

ml/min was achieved. Further proof of thermal contribution of the ASAHED to the system were positive temperature differences of outlet-inlet relationships, indicating that outlet temperatures were higher than input temperatures, confirming thermal transfer.

The effects of multiple ASAHEDs on temperature maintenance within the system has also been demonstrated in this chapter. In particular, a second and third activated and deployed heat exchanger managed to raise the outlet temperature of the oxygenator compared to baseline levels. These positive effects were reinforced by additional insulation around exposed circuit tubings. Heat loss was significantly reduced with the additional insulation, saving several degrees and prolonging performance. Considering a temperature drop from 37 $^{\circ}C$ to 32 $^{\circ}C$, we were able to save up to 4600 seconds with our combination strategy consisting of heat exchanger plus tubing insulation, at ambient temperatures of 24 $^{\circ}C$. At ambient temperatures of 7 $^{\circ}C$ where a much more rapid temperature drop from 37 $^{\circ}C$ to 30 $^{\circ}C$ occurred, a time saving of over 1150 seconds were observed, confirming the significant influence of ambient temperature on the thermal transfer pathway.

In context of clinical impact, the results of our experiments support the idea of a potentially novel way of prolonging temperature loss and thereby avoid the negative consequences induced by hypothermia of the neonatal patient. If repeatedly and correctly attached to the oxygenator, a patient's core temperature can be maintained above 30 $^{\circ}C$ for approximately 30 minutes longer compared to no insulation at all. Not just limited to this, a further and more severe core temperature drop to 25 $^{\circ}C$ can be avoided by approximately 65 minutes. Failure to provide a thermally stable environment and/or avoid temperature losses from the patient-ECMO system could

result in a variety of pathophysiological consequences starting with vasoconstriction in extremities. Excessive vasoconstriction for prolonged periods of time and further reduction of core temperature can restrict adequate blood flow to tissues and cells, causing reversible- and irreversible shock and ultimately cell death in affected areas (Meyer, 1995). If left untreated for extended periods of time this could progress to multiple organ dysfunction, reperfusion syndrome, and death; even after restoration of adequate flow rates (Jones, 2009). Therefore, the ASAHED has the ability to prolong the onsets of the pathophysiological consequences described above and may be the decisive factor between life and death in neonates.

Derived from the experimental data there is indication that even without the ASAHED, temperature loss from the ECMO-patient system can be greatly reduced by providing simple insulation around the tubings. Perhaps in future work, emphasis should also be placed on further improvement on tubing insulation in order to achieve negligible heat loss from the system aiming for an essentially redundant heat exchanger. Whether the properties of sodium acetate are able to support the R&D work of a bespoke system is to be seen.

Chapter 9

Conclusion and Discussion

9.1 Discussion and Conclusion

Life support technology has been utilised clinically for over 50 years. Two very specific life support systems - ECMO and CPB - provide support for critically ill patients by alleviating the functions of the heart and the lungs or allow the surgeon to perform heart surgery in a blood free environment over a relatively short time frame. Despite the life-saving capabilities of ECMO, morbidity and mortality rates are still high. The vast majority of patients treated by ECMO are neonates and their survival rates range from 43 - 63 percent depending on the type of support (ELSO, 2011). Generally, morbidity rates depend on either complications associated with patients or technical failures.

One important aspect of successful ECMO therapy revolves around thermal management of the patient. Failure to maintain normothermic levels may give rise to a cascade of pathophysiological events detrimental to the success of the therapy, potentially contributing to increased morbidity originally associated with technical shortcomings. Patient complications are also fairly common with ECMO therapy but

are mainly induced by the prolonged invasive procedure. Some of the complications include the tendency to haemorrhaging due to insufficient levels of coagulation factors or the development of inflammatory symptoms in response to the large foreign surface typically associated with ECMO systems (McILwain et al., 2010), (McManus et al., 1995). The latter has great implications as the large surface area of ECMO requires greater amounts of priming volumes for deployment. This induces a dilution of the patient's blood which results in low haematocrit and clotting factors. Furthermore, haemodilution has a significant effect on the activation of inflammatory cascades as demonstrated by Gourlay et al. (2003) and Habib and A. Zacharias (2003). These effects are even more pronounced in smaller patients such as children and neonates where the ratio of surface area to body mass is much larger.

The heat exchanger is a major contributor to the overall footprint of the ECMO system and to this day it is common for heat exchangers to be represented by old-fashioned, bulky technology. These water-based systems still depend on mains water supply or carry a large water reservoir, thus making the system less useful for deployment in transit setting. Challenges for in-transit settings are even more pronounced, as the complexities and dimensions of those conventional heat exchangers still remain the same. These systems are not employed in a mobile setting for logistical reasons. Added challenges are the reduced access to water- and power supply in-transit which often prevent the use of conventional heat exchanger altogether. Furthermore, a hypervariable environment in these emergency transport vehicles is an added danger to these patients, potentially further contributing to temperature loss. Simple technologies such as covering the patient with thermal blankets or avoiding the build-up of moisture on skin may not suffice to maintain normothermia in patients under in-

transit conditions. Ultimately, interference to maintain normothermia in patients can lead to further complications with the treatment going forward.

The large footprint and reliance on water for heating render the heat exchanger a device difficult to deploy in mobile emergency settings. The wider use of these heat exchangers has therefore been limited despite evidence suggesting the importance of maintaining normothermia in critically-ill patients (Frank et al., 1997), (Kurz et al., 1996), (Schmied et al., 1996). Due to the above mentioned challenges related to heat exchangers, increasingly, this part of intervention is limited to specialist centres, which, during periods of greater demand such as swine influenza may struggle to accommodate the increased demand.

Reviewing the literature suggests that the major obstacles for an increased deployment of current heat exchanger systems are:

- Large footprint
- External dependencies of water and power supply
- Size of current heat exchangers
- No temperature reversibility

In this thesis, we presented two independent approaches to reduce some of these significant challenges. One solutions deals with the miniaturisation of the heat exchanger whereas the other solution specifically targets the in-transit challenges. One aspect of the miniaturisation considered the total independence from water supply leading to an overall smaller heat exchanger with a smaller footprint. The other proposition looked at alternative means of heat conservation with the possibility of adding heat. In general, the approach to this work was broad and included design,

modelling, simulation, evaluation, and ultimately in-vivo study. During all stages of the prototype development and miniaturisation, it was important to consider performance requirements and device safety from the clinical perspective.

The design requirements and project objectives have been described in the early chapters of this thesis. These objectives and design criteria were used as a guide and defined the boundaries for the design and ultimately development process in the subsequent chapters. The prototype development of a medical device such as a heat exchanger is an expensive endeavour, considering the fact that multiple iterations are necessary for validation and refinement. In this work we took the view that a prototype development process based on physical iterations - that is where successes and failures of the previous version inform the new iteration - is a rather inelegant, time consuming, and expensive form of progress. In recent years, with increased computerisation and faster processing power, more sophisticated models have evolved that simulate complicated real-life physical systems which can also assist in the development and implementation of novel ECMO components, such as the oxygenator (Gage et al., 2002) and the blood pump (Chimenti et al., 2004). It is recognised that these computational tools help accelerate the design and development stages by simulating and validating a model as opposed to a real device (Burgreen et al., 2001). In this thesis, the decision of increased emphasis on modelling with less physical re-development was well founded. In this way, more complex computational models were developed which, when compared to experimental data, revealed significant correlation, verifying the approach. Ultimately, we were able to develop a prototype whose model simulations successfully performed according to requirements before tested under laboratory conditions.

One of the biggest motivational factors and main drives in this thesis is the miniaturisation of the heat exchanger. Conventional heat exchanger which are part of the ECMO system severely restrict mobility based on a large footprint and reliance on water supply or tanks. A variety of alternative thermal exchange mechanisms were considered and compared in this work before the appropriate technology was selected. Investigation into several possible means of heat generation revealed the use of thermoelectric devices whose characteristics are very desirable for deployment in our prototype development. These devices have already proven to work in a wide variety of different applications and conditions. They are manufactured in different sizes and can easily be interfaced with a thermally conductive surface. They are operable over a wide temperature range and have an accuracy of a tenth of a degree. Additionally, switching the polarity of the power source enables a temperature reversibility, i.e. both heating and cooling can be achieved. The excellent availability and low-cost price of these devices enable the possibility for a disposable item. These arguments for thermoelectric devices indicated great suitability for deployment in our application and ultimately was interfaced with the aluminium body of the heat exchanger which was later used during laboratory experiments.

The heat exchanger aluminium body guides the flow of blood and influences the flow characteristics and indirectly the amount of heat exchange. A laminar flow pattern was desirable due to the possibility of haemolysis caused by turbulent flow. Also, dimensions of the blood path directly influenced the overall size of the heat exchanger and at the same time impacted the efficiency of absorbing heat directly from the thermoelectric devices. A compromise was made in order to keep the overall heat exchanger size within acceptable pre-defined limits and simultaneously avoid haemolysis-causing turbulences. The compromise resulted in a fluid path cross section

of 17 mm x 2 mm with 2 loops, providing a thin blood film for absorbing/releasing thermal energy from the TEMs. Both, the design of the heat exchanger aluminium body as well as the thermoelectric devices were modelled with a FEA (finite element analysis) software. This involved the consideration and modelling of all physical interactions taking place in and around every element of the device. In order to minimise mistakes in the process of modelling, individual parts were modelled first and compared with literature for validation before further work was conducted. TEMs experience various cooling/heating behaviours depending on the semiconductor composite materials used (Goldsmid, 2010). In this regard, the modelling of the thermoelectric device presented some challenges as the exact material composition could not be ascertained. At first, standard materials properties were assumed which during the phase of experimental model validation proved to have poor correlation. As this aspect seemed to be the only considerable point of uncertainty on the model, a trial-and-error manipulation of temperature dependent values was carried out until experimental results corresponded to model results. A variety of different laboratory experiments confirmed the chosen material property values by displaying very good correlation during transient- and steady state laboratory results with the corresponding simulations. This validation of the model indicates a good fit for the physical heat exchanger and therefore can be used as the development going forward.

Since a working model of the physical heat exchanger has been established and validated, it lends itself to the process of controller design. Instead of dealing with multiple physical test setups and experimental runs, the model can be used instead in a simulated and accelerated software environment for swift results. A variety of different extreme situation for the heat exchanger that could potentially influence the controller performance were identified and also simulated within the software envi-

ronment. These extreme conditions set the boundaries for the control performance to which the controller must still satisfy the self-proposed requirements. It is here where a conventional proportional (P) and integral (I) controller was tuned in an iterative trial-and-error fashion until simulation results satisfied the required conditions. The overall transient- and steady state controller behaviour proved to have satisfying results. However, in terms of performance, the overall heat exchanger did not meet the required conditions and struggled to produce an outlet temperature of 37 $^{\circ}C$ in the thermally most challenging scenario. This shortcoming was less attributed to the controller performance but rather as a result of insufficient heat exchanger performance as the maximum TEM temperatures have been reached. Laboratory experiments confirmed this deficiency not just in the thermally most challenging experiment but also in other less-demanding cases. Again, similar to software simulations, control-related aspects of the heat exchanger were successful, confirming chosen control parameters.

The experimental results indicated inherent insufficiencies and limits of the heat exchanger and a re-design was therefore considered. Since the underlying problem of the first iteration was mainly related to a lack of power, our main focus was therefore to increase the thermal input while simultaneously increase the blood's absorption of heat. The second iteration commenced with a critical analysis of the first system which revealed several shortcomings that were mitigated by implementing logical and thermodynamically-related solutions. It was recognised that in order to increase the thermal input, one option was to attach more thermoelectric devices to the heat exchanger body, ultimately delivering more energy. Instead of attaching large TEMs to the heat exchanger, a set of smaller ones was chosen instead. This was due to the fact that larger TEMs were more likely to experience mechanical breaks as a result of thermal expansion and thus were required to be replaced more often than the devices

with a smaller form factor. It was also recognised that TEMs were only mounted to one side of the heat exchanger ultimately limiting heat supply to this particular side, leaving potential surfaces exposed and unused. Also, in order for the blood to increase thermal absorption, a greater exposure time to the heat exchanger body as well as greater surface area during traverse was required. Instead of guiding the blood flow through the heat exchanger body in a serpentine manner with just 2 loops, the new concept focused on adding a multiple of loops. This would ultimately lead to increased turbulence in the blood flow, aiding the augmentation of thermal energy but also contradicting one of the requirements setup in the first iteration. However, this improvement presented a compromise that needed to be made in order to increase the level of efficiency of the prototype.

The shortcomings of the previous iteration provided a clear roadmap for the direction of improvements, and similar to the first iteration, design requirements and processes were described in detail. The established objectives and design criteria conduced as boundaries for the development process with the aim of eradicating the weaknesses of the previous design and enhance overall performance. Due to time limitations and a clear direction of the necessary modifications, generally less modelling was required. The major changes consisted of an increased number of smaller TEMs (eight in total) that were applied to both sides of the heat exchanger and a fluid path comprising of 43 loops for increased thermal absorption. Controller tuning was conducted on the physical heat exchanger device where response behaviours of the system were observed and analysed. The same type of controller employed managed to perform in transient and in steady state conditions as expected, even under thermally challenging conditions which the previous heat exchanger struggled. The increased performance of the improved device was already recognised during controller tuning

as higher fluid temperatures under higher flow rate conditions were achieved. Experimental results proved an increase in performance and thereby confirmed the positive impact that the enhancements elicited. In all experiments, the heat exchanger was able to reach and maintain desired temperatures under realistic, clinically-mimetic conditions. However, transient cooling and heating would take longer than expected with these devices. According to Ichiba et al. (2003) and Guenther et al. (2009), fast cooling/heating responses in ECMO procedures are far less importance than being able to maintain normothermic or moderate hypothermic conditions. The novel TEC approach to thermal control in neonatal ECMO therapy presents a viable alternative - based on its dimensions and performance - to traditional, water-dependent systems.

An alternative approach was chosen for the heat exchanger targeting in-transit ECMO. Here, patients and clinicians are dealing with a hyper-variable environment with sometimes extreme ambient temperatures and a lack of power. These influences impede the maintenance of normothermia during ECMO therapy and therefore require a tailored strategy. During the research process for a heat exchanger targeting in-transit settings, instead of focussing on thermal compensations methods in the traditional sense, we targeted a solution with the focus on minimising heat loss and potentially adding some heat as well. This approach would enable us to reduce heat loss from the ECMO circuit and ultimately the patient as well, thereby prolonging the critical window of normothermia to moderate hypothermia. Apart from this main function, it was also important to consider other crucial aspects from a ECMO-related perspective such as minimal visual or physical interference with other procedures, easy application, as well as being lightweight and compact. A number of different insulating materials were considered and studied in this work but were rejected on the grounds of providing only insulation and failed to induce heat of any

degree. Instead, a solution was proposed that relied on a chemical reaction in order to produce some exothermic heat. The means of heat generation is based on sodium acetate, a sodium salt of acetic acid which after activation can last up to 2 hours. This technology has already proven to work in commercially available consumer heating pads and hand warmers and can be manufactured in different sizes. The straightforward availability, low-cost, and well-understood technology make it also possible for a disposable item. These characteristics of a sodium acetate solution are desirable for the in-transit heat exchanger prototype which was ultimately implemented during laboratory experiments. The idea was to employ this chemical solution to the external surface of the oxygenator, effectively providing insulation and a heat source. During the design stage of the sodium-acetate solution (ASAHED), it was important to consider the multiple tube connections of the oxygenator as these needed to be a accessible at any time during the normal ECMO procedures. The design also needed to ensure a swift mounting and detachment of the ASAHED for smooth operation. A combination of traditional static insulation as well as the sodium-acetate solution is providing improved structural support and further limits potential heat loss.

Simple time-series tests were performed before the actual experimentation in order to validate the extend and duration of the exothermic reaction. The test results demonstrated the potential of the technology for the in-transit heat exchanger as temperatures of the sodium acetate still remained above 40 °C even 42 minutes after initiation at ambient temperatures of 7 °C. Even better results of longer exothermal energy production was demonstrated for warmer environments. Interesting to note was that experimentation revealed a flow-rate independent temperature decay of the simulated patient. A comparison of different flow rates at the same ambient condition illustrated this point well as only little divergence between them were noticeable.

This positive property of the circuit translates into a predictable, constant heat loss from the patient across different flow rates and can be taken into consideration by clinical personnel. Further testing revealed the insulating properties of the novel heat exchanger which translated into a delayed temperature loss from the ASAHED and ultimately simulated patient. This is especially the case for higher flow rates and lower ambient temperatures. Tests also revealed that under extreme conditions of an ambient temperature of 7 °C, an average delay of approximately 18 minutes can be achieved by exchanging the ASAHED several times after its thermal energy has been depleted. Even more heat preservation was achieved when additional tubing insulation was applied to the ECMO circuit, potentially prolonging thermal loss by up to 77 minutes in comparison to no insulation. Therefore, the data derived from these experiments have confirmed a usable technology for thermal applications in situations with limited resources. The prototype has proven to have a thermally additive effect on the oxygenator and also the blood bag, potentially prolonging temperature loss and delaying the onset of hypothermia.

The objective of this thesis was to design, develop, and test two individual heat exchanger prototypes for different ECMO-related scenarios. One heat exchanger focussed on miniaturising and controlling a conventional systems whereas the other targeted in-transit solutions for transporting ECMO patients. Novelty was required in both designs, with a formal protocol of procedures developed for the individual design processes. The design of the heat exchanger for conventional ECMO followed a traditional engineering approach, comprising of the design of a concept, the theoretical modelling of the concept within a specialised computer environment, investigation and testing of the computer model, the physical modelling of the proposed system, and at last the validation of the theoretical model based on laboratory test of the

physical device. This process provided the basis for controller design, tuning, and optimisation in a simulated environment in order to maintain the heat exchanger outlet temperature. Great emphasise was placed on the aspects of miniaturisation and independence of a water supply as it was believed that addressing both would greatly reduce the footprint. A viable approach was developed that involved the use of thermoelectric devices based on their suitable properties of being highly compact, easily controllable, and operate independently of water. This form of heat source enabled the design of a low footprint heat exchanger whose test results confirmed the control of desired temperatures under realistic, clinically mimetic conditions. We also designed and developed a heat exchanger for in-transit ECMO, in a hyper-variable environment where thermal control is not always possible due to the lack of power supply and space. Therefore, the aim was to propose a miniaturised, novel technology that provides thermal maintenance independently of energy and water sources. A similar design protocol as to the conventional system was established which translated into the physical development of the device. Computer modelling was avoided altogether as the novel idea of heat induction was based on the exothermic chemical reaction of sodium acetate which can be found in commercially available consumer heating pads and hand warmers. A clever designed device containing the sodium acetate uses the neonatal oxygenator as a heat exchange interface, thereby insulating and adding heat to the extra-corporeal circuit. Tests confirmed a thermally additive effect and overall delayed heat loss of the oxygenator and the simulated patient, potentially saving critical time and avoiding the exacerbating consequences of hypothermia. It was also found that further insulating the ECMO circuit tubing greatly reduced overall temperature loss of the patient-ECMO system. Further development on both heat exchangers is certainly required, however, is not scope of this research work.

9.1.1 Scope of Thesis Objectives

- Design of a novel heat exchanger model with the use of computational simulation software - 100%.
- Development of a novel and compact heat exchanger for conventional ECMO that does not rely on water supply - 100%.
- To develop a novel heat exchanger for mobile ECMO applications that is able to reduce heat loss independent of mains or water supply - 100%.
- Demonstrate high accuracy in model correlation between virtual and physical results - 100%.

Through this work we have managed to design and develop novel functional solutions to thermal management for conventional and in-transit ECMO. The solutions require some further development and refinement to reach a stage where they can be considered for clinical deployment. However, the technologies described in the present work show real promise and, with particular regard to the in-transit technology, a genuine life saving solution for the most challenging clinical setting. Further, and considerable investment will be required and sought to develop these devices to the next stage.

Although all the fundamental objectives of our hypothesis have been met, an honest assessment of the overall work suggests a scope of 50% reached in terms of delivering a clinical solution.

9.2 Future Work

This research work represented a proof-of-concept project that investigated the feasibility of two independent concepts; 1) the miniaturisation of a waterless thermal control system for conventional in-hospital ECMO support and 2) the development a power and water independent thermal support technology for in-transit ECMO provision. Having successfully demonstrated both concepts, the next logical step of the technological evolution would dictate the optimisation of the functionality to a degree that permits clinical trials and the potential for a commercial device.

- Heat Exchanger for Conventional ECMO

The control algorithm for maintaining heat exchanger outlet temperatures could be modified and extended to allow faster and more efficient responses. This could be augmented by additional thermal measurements that incorporate the patient's core and the ambient temperature for a more intelligent control approach.

In order to optimise the overall performance of the heat exchanger, further computational fluid analysis of the blood flow path is required that helps identify a potential increase in surface area necessary for improved thermal exchange. Also, since greater turbulence aids the process of heat exchange but at the same time introduces haemolysis, this aspect would ultimately need to be explored in further detail in order to reach a compromise between these two significant attributes. At the same time, optimisation in terms of position and sizes of the thermoelectric devices can also be further explored in order to maximise the available energy input.

Our novel design is by no means perfect and before implementing into clinical settings, tests have to be designed in order to scrutinise the device for potential faults and complications followed by subsequent improvement. The heat exchanger

for conventional ECMO comprises of three technical areas; hardware, electronics, and software whereas complications could arise at any of these areas. Software failure could potentially cause undesired heat exchanger behaviours such as unresponsiveness to environmental key triggers or sudden shut downs. Typical faults in electronics are individual component failures leading to possible short circuits within the system, potentially damaging other parts and endangering the patient if safety critical systems are not in place or damaged as well. Hardware components such as the thermoelectric devices or the heat exchanger itself are susceptible to mechanical strain and stresses due to demanded thermal exposure. Particularly susceptible are the thermoelectric devices whose individual legs can break from the soldering point, leaving a gap and thereby interrupt the flow of electrical current rendering the device unusable."

- Heat Exchanger for Varying Patient Sizes with Built in Oxygenator

The demand for oxygenation increases with patient size, which is commonly reflected by using larger oxygenators. In order to still achieve a compact form factor, a strong drive towards integrating of the oxygenator with the heat exchanger has been noticed in recent years (ELSO, 2016). A potential path for future development and further improvement could also focus on the integration of our concept with (existing) oxygenators. This, however, requires initial work on the development of a heat exchanger for different patient sizes such as for adult ECMO, before any concepts of integration can be carried out. The same process as described in this work lends itself well for the development of heat exchangers for different patient requirements. Also, as the developed heat exchanger for in-transit solutions focussed on heat preservation as a stand-alone device, potential integration has not been considered in the original concept phase. Further work is therefore required in modifying existing concepts for potential integration with oxygenators followed by a complete R&D cycle.

- Heat Exchanger for in-transit ECMO

Tests have revealed the positive impact that our concept of the new heat exchanger has on delaying temperature loss at the oxygenator and simulated patient. Even more temperature loss can be avoided if this technology was applied to other parts of the ECMO circuit such as the tubings which are also main contributors to heat loss. Initial tests of insulating the tubings have indicated this substantial potential of preserving heat in an environment lacking of power- and water supply and therefore should be explored further in future research work.

Bibliography

GC Abel, RB Joan, and A Pilar. Extracorporeal lung assist in severe respiratory failure and ards. current situation and clinical applications. *Arch Bronconeumol*, 46:531–7, 2010.

JG Allen. *Extracorporeal Circulation*. Springfield, Thomas, 1958.

J. Anbe, T. Tobi, H. Nakajima, T. Akasaka, and K. Okinaga. Microcomputer-based automatic regulation of extracorporeal circulation: A trial for the application of fuzzy inference. *Artificial Organs*, 16(5):532–538, 1992.

SW Angrist. *Direct Energy Conversion*. Allyn and Bacon Inc, 1982.

E.E. Antonova and D.C Looman. Finite elements for thermoelectric device analysis in ansys. In *Int. Conference on Thermoelectrics*, page 200, 2005a.

Elena E. Antonova and David C. Looman. Finite elements for thermoelectric device analysis in ansys. Technical report, ANSYS Inc., 2005b.

K. Araki, H. Anai, M. Oshikawa, K. Nakamura, and T. Onitsuka. In vitro performance of a centrifugal, a mixed flow, and an axial flow blood pump. *Artificial organs*, 22 (5):366–370, 1998.

GJ Arthurs and M. Sudhakar. Carbon dioxide transport. *Continuing Education in Anaesthesia, Critical Care & Pain*, 5(6):207–210, 2005.

Ashrae. *Handbook of Fundamentals*. Ashrae, 1981.

I. Baća, W. Bieger, U. Mittmann, W. Saggau, H. Schmidt-Gayk, and HH Storch. Comparative studies on pulsatile and continuous flow during extracorporeal circulation. effects on liver function and endocrine pancreas secretion]. In *Chirurgisches Forum für experimentelle und klinische Forschung*, page 49, 1979.

P. F. Barrett and D. K. Benson. A mechanism for nucleating supercooled liquids. *Mater. Chem. Phys*, 20:171179, 1988.

R. Barthelemy, N. Chauveau, and JP Morucci. Automation in extracorporeal circulation. In S. HA, editor, *Proceeding of the sympoeium Thirty years of extracorporeal circulation*, pages 567–571, Mnchen, 1984.

R.H. Bartlett. Invited letter concerning: nonpulsatile flow–a noncontroversy. *The Journal of thoracic and cardiovascular surgery*, 107(2):644, 1994.

RH Bartlett, AB Gazzaniga, MR Jefferies, RF Huxtable, NJ Haiduc, and SW et al. Fong. Extracorporeal membrane oxygenation (ecmo) cardiopulmonary support in infancy. *Transactions-American Society for Artificial Internal Organs*, 22:80, 1976.

M. Battezzati and C. Taddei. Descrizione di un apparechchio per la circolazione extracorporea e per la ossigenazione artificiale. *Minerva Chir.*, 9:333–341, 1954.

JR Bell and P. Grosberg. Diffusion through porous materials. *Nature*, 189:980–981, 1961.

F.O. Belzer, B.S. Ashby, J.S. Huang, and J.E. Dunphy. Etiology of rising perfusion pressure in isolated organ perfusion. *Annals of surgery*, 168(3):382, 1968.

T. Beppu, Y. Imai, and Y. Fukui. A computerized control system for cardiopulmonary bypass. *The Journal of Thoracic and Cardiovascular Surgery*, 109(3):428–438, 1995.

E. Berg and N. Knudsen. Automatic data collection for cardiopulmonary bypass. *Perfusion*, 3(4):263–270, 1988.

EF Bernstein, LC Cosentino, S. Reich, P. Stasz, ID Levine, DR Scott, FD Dorman, and PL Blackshear Jr. A compact, low hemolysis, non-thrombogenic system for non-thoracotomy prolonged left ventricular bypass. *ASAIO Journal*, 20(1):643, 1974.

V.O. Bjrk. An artificial heart or cardiopulmonary machine. performance in animals. *Lancet*, 1:491–493, 1948.

BR Bodell, JM Head, LR Head, AJ Formolo, and JR Head. A capillary membrane oxygenator. *The Journal of thoracic and cardiovascular surgery*, 46:639, 1963.

Fateh ; Gaubert Jean-Paul Bouafia, Abdelouahab; Krim. Design and implementation of high performance direct power control of three-phase pwm rectifier, via fuzzy and pi controller for output voltage regulation. *Energy Conversion and Management*, Volume 50(Issue 1):6–13, 2009.

JK Boucher, LW Rudy Jr, and LH Edmunds Jr. Organ blood flow during pulsatile cardiopulmonary bypass. *Journal of applied physiology*, 36(1):86–90, 1974.

ML Bramson, JJ Osborn, F.B. Main, MF O'brien, JS Wright, and F. Gerbode. A new disposable membrane oxygenator with integral heat exchange. *The Journal of thoracic and cardiovascular surgery*, 50:391, 1965.

H. Brandes, JM Albes, A. Conzelmann, M. Wehrmann, and G. Ziemer. Comparison of pulsatile and nonpulsatile perfusion of the lung in an extracorporeal large animal model. *European surgical research*, 34(4):321–329, 2002.

PR Braun, BD L'Hommedieu, and WJ Klinedinst. Aluminum contamination by heat exchangers during cardiopulmonary bypass. In *Proc. Am. Acad. Cardiovasc. Perfusion*, volume 9, pages 69–72, 1988.

E. Braunwald and RA Kloner. The stunned myocardium: prolonged, postischemic ventricular dysfunction. *Circulation*, 66(6):1146–1149, 1982.

J.C. Briceño and T.M. Runge. Monitoring of blood gases during prolonged experimental cardiopulmonary bypass and their relationship to brain ph, po2, and pco2. *ASAIO journal*, 40(3):M344, 1994.

G. W. Burgreen, J. F. Antaki, Z. J. Wu, and A. J. Holmes. Computaitonal fluid dynamics as a development tool for rotary blood pumps. *Artificial Organs*, 25(5), 2001.

Jean Callebaut. *Induction Heating*. Leonardo Energy, Feb 2007.

Christopher; Matthews Gareth Chambers, David; Huang. *Basic Physiology for Anaesthetists*. Camebridge University Press, 2015.

RR Chaturvedi, D. Macrae, KL Brown, M. Schindler, EC Smith, KB Davis, G. Cohen, V. Tsang, M. Elliott, and M. et al. De Leval. Cardiac ecmo for biventricular hearts after paediatric open heart surgery. *Heart*, 90(5):545–551, 2004.

N. Chauveau, W. Van Meurs, R. Barthelemy, and JP Morucci. Automatic modules for extracorporeal circulation control. *The International journal of artificial organs*, 13(10):692, 1990.

JA Chavez, JA Ortega, J Salazar, AATA Turo, and M JAGMJ Garcia. Spice model of thermoelectric elements including thermal effects. *Instrumentation and Measurement Technology Conference*, 2:1019–1023, 2000.

Yih-Fang Chen, Bor-Sen; Chang. Robust pi controller design for a constant turning force system. *nternational Journal of Machine Tools and Manufacture*, 31(3):257–272, 1991.

D.E. Chenoweth, S.W. Cooper, T.E. Hugli, R.W. Stewart, E.H. Blackstone, and J.W. Kirklin. Complement activation during cardiopulmonary bypass. *New England Journal of Medicine*, 34(9):497–503, 1981.

M. Chimenti, L. Varela, E. de Forteza, and R. Favaloro. Computational fluid dynamics analysis of a novel axial flow blood pump with two counter-rotating impellers. *Mecanica Computacional*, 23(7), 2004.

R.E. Cilley, J.B. Zwischenberger, A.F. Andrews, R.A. Bowerman, D.W. Roloff, and R.H. Bartlett. Intracranial hemorrhage during extracorporeal membrane oxygenation in neonates. *Pediatrics*, 78(4):699–704, 1986.

L.C. Clark, F. Hooven, and F. Gollan. A large capacity, all-glass dispersion oxygenator and pump. *Review of Scientific Instruments*, 23:748, 1952.

GHA Clowes and WE Neville. *The Membrane Oxygenator: Extracorporeal Circulation*. Thomas, Charles C, 1958.

G.H.A. et al. Clowes. Extracorporeal maintenance of circulation and respiration. *Physiological reviews*, 40(4):826–919, 1960.

GH Clowes Jr, AL Hopkins, and WE Neville. An artificial lung dependent upon diffusion of oxygen and carbon dioxide through plastic membranes. *The Journal of thoracic surgery*, 32(5):630, 1956.

COMSOL. *Multiphysics Modeling Guide*. Comsol AB, 3.5a edition, November 2008.

Comsol. Non-isothermal heat exchanger (manual). Technical report, Comsol Multiphysics, 2011.

D.A. Cooley. Development of the roller pump for use in the cardiopulmonary bypass circuit. *Texas Heart Institute Journal*, 14(2):112, 1987.

JD Cornish and RH Clark. Principles and practice of vv extracorporeal membrane oxygenation. In RH Bartlett JB Zwischenberger, editor, *ECMO Extracorporeal Cardiopulmonary Support in Critical Care.* Ann Arbor, 1995.

C. Crafoord, B. Norberg, and A. Senning. Clinical studies in extracorporeal circulation with a heart-lung machine. *Survey of Anesthesiology*, 2(4):343, 1958.

FS Cross and EB Kay. Direct vision repair of intracardiac defects utilizing a rotating disc reservoir-oxygenator. *Surgery, gynecology & obstetrics*, 104(6):711, 1957.

J.R. Custer and R.H. Bartlett. Recent research in extracorporeal life support for respiratory failure. *ASAIO journal*, 38(4):754, 1992.

db Prüftechnik. *Professional induction bearing heaters: Fast, easy and reliable*. Alignment Systems GmbH, 85737 Ismaning, Germany, 2013.

E De Jonge, M Levi, F Berends, AE van der Ende, JW ten Cate, and CP Stoutenbeek. Impaired haemostasis by intravenous administration of a gelatin-based plasma expender in human subjects. *Thromb Haemost*, 79:286290, 1998.

J. De Paepe, PMA Pomerantzeff, K. Nakiri, E. Armelin, G. Verginelli, and EJ Zerbini. Observation of the microcirculation of the cerebral cortex of dogs subjected to pulsatile and non-pulsatile flow during extracorporeal circulation. A propos du debit pulse. Core Laboratories, Inc., Belgium 1979.

ME DeBakey. A simple continuous flow blood transfusion instrument. *New Orleans Med Surg J*, 87:386–9, 1934.

R. Decher. *Direct Energy Conversion Fundamentals of electric power production*. Oxford University press, Inc., 1997.

R.A. DeWall. The evolution of the helical reservoir pump-oxygenator system at the university of minnesota. *The Annals of Thoracic Surgery*, 76(6):S2210–S2215, 2003a.

R.A. DeWall. Origin of the helical reservoir bubble oxygenator heart-lung machine. *Perfusion*, 18(3):163–169, 2003b.

R.A. DeWall, VL Gott, CW Lillehei, R.C. Read, R.L. Varco, and HE Warden. Total body perfusion for open cardiotomy utilizing the bubble oxygenator; physiologic responses in man. *The Journal of thoracic surgery*, 32(5):591, 1956.

I. Di Bella, F. Pagani, C. Banfi, E. Ardemagni, A. Capo, C. Klersy, and M. Viganņ. Results with the novacor assist system and evaluation of long-term assistance. *European journal of cardio-thoracic surgery*, 18(1):112–116, 2000.

M.E. Dickson, M.A. Hirthler, J. Simoni, C.A. Bradley, and J.F. Goldthorn. Stunned myocardium during extracorporeal membrane oxygenation. *The American journal of surgery*, 160(6):644–646, 1990.

I Dincer and MA Rosen. *Thermal Energy Storage: Systems and Applications*. Wiley, 2002.

DR Doherty, CS Parshuram, I Gaboury, A Hoskote, J Lacroix, M Tucci, A Joffe, K Choong, and R Farrell. Hypothermia therapy after pediatric cardiac arrest. *Circu*, 119:1492–1500, 2009.

JJ Driessen, H. Dhaese, G. Fransen, P. Verrolst, L. Rondelez, L. Gevaert, M. van Becelaere, and E. Scheistraete. Pulsatile compared with nonpulsatile perfusion using a centrifugal pump for cardiopulmonary bypass during coronary artery bypass grafting. effects on systemic haemodynamics, oxygenation, and inflammatory response parameters. *Perfusion*, 10(1):3–12, 1995.

M. Drummond, D.M. Braile, A.P.M. Lima-Oliveira, A.S. Camim, R.S.K. Oyama, and G.H. Sandoval. Technological evolution of membrane oxygenators. *Revista Brasileira de Cirurgia Cardiovascular*, 20(4):432–437, 2005.

CP Dubbelman. Attempts to construct an oxygenator for temporary replacement of the human lung. *Acta physiologica et pharmacologica Neerlandica*, 2(3):320, 1952.

GG Dudell, M. Evans, and JD Cornish. Partition of blood flow during venoarterial extracorporeal membrane oxygenation (ecmo). *Pediatr Res*, 29:212A, 1991.

J. Dunn, MM Kirsh, J. Harness, M. Carroll, J. Straker, and H. Sloan. Hemodynamic, metabolic, and hematologic effects of pulsatile cardiopulmonary bypass. *The Journal of thoracic and cardiovascular surgery*, 68(1):138, 1974.

H.J. Eash, H.M. Jones, B.G. Hattler, and W.J. Federspiel. Evaluation of plasma resistant hollow fiber membranes for artificial lungs. *ASAIO journal*, 50(5):491, 2004.

LH Edmunds Jr and W Williams. Microemboli and the use of filters during cardiopulmonary bypass. In JR Utley, editor, *Pathophysiology and Techniques of Cardiopulmonary Bypass*, volume Volume 2. Baltimore, Williams and Wilkins, 1983.

LH Edmunds Jr, N Ellison, RW Colman, and et al. Platelet function during open heart surgery: comparison of the membrane and bubble oxygenators. . *Thorac Cardiovasc Surg*, 83:805–812, 1982.

ELSO. Elso registry form membrane lung list. Online, 2016. URL `https://www.elso.org/Registry/SupportDocuments/MembraneLungEquipmentList.aspx`.

The Extracorporeal Life Support Organization ELSO. Ecls registry report. Online document, July 2011.

The Extracorporeal Life Support Organization ELSO. *ELSO Anticoagulation Guideline*. Lequier, Laurance; Annich, Gail; Al-Ibrahim, Omar; Bembea, Melania; et. al., Ann Arbor, MI, USA, 2014 edition, 2014.

W.O. Emmons and D.B. Sacca. The design and development of a blood heat exchanger for open heart surgery. *General Motors Engineering Journal*, July – September:H055, 1958.

DO Fauza, MH Hines, and JM Wilson. Ecmo: Hemodynamics, perfusion, and blood volume. In RH Bartlett. JB Zwischenberger, editor, *ECMO Extracorporeal Cardiopulmonary Support in Critical Care.* Ann Arbor, Michigan, 1995.

RG Fiddian-Green. Gut mucosal ischemia during cardiac surgery. In *Seminars in thoracic and cardiovascular surgery*, volume 2, page 389, 1990.

V.B. Fiedler. Effects of pulsatile and non-pulsatile perfusion on the isolated canine heart. *Research in Experimental Medicine*, 179:183–198, 1981.

SM Frank, LA Fleisher, MJ Breslow, and et al. Perioperative maintenance of normothermia reduces the incidence of morbid cardiac events: a randomized clinical trial. *JAMA*, 277:1127–1134, 1997.

B. Frenckner and P. Radell. Respiratory failure and extracorporeal membrane oxygenation. In *Seminars in pediatric surgery*, volume 17, pages 34–41. Elsevier, 2008.

K. L. Gage, G. W. Burgreen, and W. R Wagner. Predicting membrane oxygenator pressure drop using computational fluid dynamics. *Artificial Organs*, 27(7), 2002.

P.M. Galletti and G.A. Brecher. *Heart-lung bypass: principles and techniques of extracorporeal circulation*. Grune & Stratton New York, 1962.

W.F. Ganong. *Review of medical physiology*. Lange Medical Books/McGraw-Hill, New York, 21st edition edition, 2003.

C. Gao, A.H. Stammers, R.L. Ahlgren, T.A. ELLIS, H.B. HOLCOMB, B.T. NUTTER, R.G. SCHMER, and L. HOCK. The effects of preprimed oxygenators on gas transfer efficiency. *The Journal of extra-corporeal technology*, 35(2):121–126, 2003.

J. D. S. Gaylor and S. et al. Hickey. Membrane oxygenators: influence of design on performance. *Perfusion*, 9:173–180, 1994.

SJ; Mehlhorn U; Davis-KL; de Vivie ER; Kurusz M; Butler BD Geissler, HJ; Allen. Cooling gradients and formation of gaseous microemboli with cardiopulmonary bypass: an echocardiographic study. *Ann Thorac Surg.*, 64:100–4, 1997.

JH Gibbon Jr. An oxygenator with a large surface-volume ratio. *J Lab Clin Med*, 24: 1192, 1939.

JH Gibbon Jr. The development of the heart-lung apparatus. *23*, 27(231):231–44, 1970.

J.H. et al. Gibbon Jr. Application of a mechanical heart and lung apparatus to cardiac surgery. *Minnesota medicine*, 37(3):171, 1954.

C. Göbel, A. Arvand, R. Eilers, O. Marseille, C. Bals, B. Meyns, W. Flameng, G. Rau, and H. Reul. Development of the medos/hia deltastream extracorporeal rotary blood pump. *Artificial organs*, 25(5):358–365, 2001.

L.R. Golding, L.K. Groves, M. Peter, G. Jacobs, R. Sukalac, Y. Nosé, and F.D. Loop. Initial clinical experience with a new temporary left ventricular assist device. *The Annals of thoracic surgery*, 29(1):66–69, 1980.

H. J. Goldsmid. *The Improvement of a Specific Material Bismuth Telluride*. Springer, 2010.

HL Goldsmith and VT Turitto. Rheological aspects of thrombosis and haemostasis: basic principles and applications. icth-report-subcommittee on rheology of the international committee on thrombosis and haemostasis. *Thrombosis and haemostasis*, 55(3):415–435, 1986.

D.J. Goldstein. Worldwide experience with the micromed debakey ventricular assist device® as a bridge to transplantation. *Circulation*, 108(10 suppl 1):II–272, 2003.

F. Gollan, P. Blos, and H. Schuman. Studies on hypothermia by means of a pump-oxygenator. *American Journal of Physiology–Legacy Content*, 171(2):331–340, 1952.

V.I. Gott, R.D. Sellers, R.A. Dewall, R.L. Varco, and C.W. Lillehei. A disposable unitized plastic sheet oxygenator for open heart surgery. *Diseases of the Chest*, 32 (6):615–625, 1957.

L. Gott Vincent, A. Dewall Richard, Z.M.N. Paneth Matthias, V.R.L. Weirich William, and C.W. Lillehei. A self-contained, disposable oxygenator of plastic sheet for intracardiac surgery: Experimental development and clinical application. *Thorax*, 12(1):1–9, 1957.

T. Gourlay and D. et al. Stefanou. The effect of methanol washing of plasticized polyvinyl chloride on biomateral-contact-mediated cd11b (mac-1) expression in a rate recirculation model. *Artificial Organs*, 26:5–9, 2002.

T. Gourlay and KM. Taylor. *Cardiopulmonary Bypass: Principles and Practice, 2nd edition*, chapter Chapter 10: Pulsatile Cardiopulmonary Bypass. Lippincott, Williams, and Wilkins, 2002.

T. Gourlay, I. Samartzis, and et al. The effect of haemodilution on blood-biomaterial contact-mediated cd11b expression on neutrophils: ex vivo studies. *Perfusion*, 18: 87–93, 2003.

Terry Gourlay. *Controlled pulsatile architecture in cardiopulmonary bypass: in vitro and clinical studies*. PhD thesis, University of Strathclyde, 1997.

U. Guenther, D. Varelmann, and et al. Extended therapeutic hypothermia for several days ducting extracorporeal membrane-oxygenation after drowning and cardiac arrest: Two cases of survival with no neurological sequelae. *Resuscitation*, 80(3), 2009.

Y.; Ichinokura O Guo, HJ; Shiroishi. Digital pi controller for high frequency switching dc/dc converters based on fpga. In *Telecommunications Energy Conference. INTELEC '03. The 25th International*, pages 536–541, 2003.

R. H. Habib and et al. A. Zacharias. Adverse effects of low hematocrit during cardiopulmonary bypass in the adult: Should current practice be changed? *The Journal of Thoracic and Cardiovascular Surgery*, 125:12, 2003.

Y. Hamada, T. Kohtani, and et al. Blood transfusion under cardiopulmonary bypass is a possible inducer for inflammation? *Kyobu Geka*, 54:4, 2001.

SD Hansbro, D.A.C. Sharpe, R. Catchpole, KR Welsh, CM Munsch, JP McGoldrick, and PH Kay. Haemolysis during cardiopulmonary bypass: an in vivo comparison of standard roller pumps, nonocclusive roller pumps and centrifugal pumps. *Perfusion*, 14(1):3–10, 1999.

AH Harken. The influence of pulsatile perfusion on oxygen uptake by the isolated canine hind limb. *The Journal of thoracic and cardiovascular surgery*, 70(2):237–41, 1975.

TS Harrison and JF Seaton. An analysis of pulse frequency as an adrenergic excitant in pulsatile circulatory support. *Surgery*, 73(6):868–74, 1973.

H. et al. Hensel. Thermoreception and temperature regulation. *Monographs of the physiological society*, 38:1, 1981.

WJ Herdman. The surgeon's pump. *Journal of the American medical association*, 9: 59–60, July-December 1887.

EN Hey. Thermal regulation in the newborn. *Br J Hosp Med*, 8:51–64, 1972.

EN Hey and G. Katz. Evaporative water loss in the new-born baby. *The Journal of physiology*, 200(3):605–619, 1969.

JD Hill. Acute pulmonary failure: treatment with extracorporeal oxygenation. *Medical instrumentation*, 11(4):198, 1977.

RB Hirschl. Devices. In Bartlett RH Zwischenberger JB, Steinhorn RB, editor, *ECMO: Extracorporeal Cardiopulmonary Support in Critical Care, Extracorporeal Life Support Organization; 2nd Edition*, pages 199–236. Ann Arbor, MI, 2000.

RB Hirschl and RH Bartlett. *Extracorporeal Membrane oxygenation (ECMO) in Cardiorespiratory Failure*. Chicago: Yearbook Medical Publishers, 1987.

R.B. Hirschl, K.F. Heiss, and R.H. Bartlett. Severe myocardial dysfunction during extracorporeal membrane oxygenation. *Journal of pediatric surgery*, 27(1):48–53, 1992.

& Co. Hirtz. Hico-variotherm 680 manual. Online, October 2006. URL `http://www.hico.de/files/hico_hypotherm_680_1006_72dpi.pdf`.

& Co. Hirtz. Hico-variotherm 550 manual. Online, March 2007. URL `www.hico.de/files/hico_variotherm_550_0307_72dpi.pdf`.

& Co. Hirtz. Hico-aquatherm 660 manual. Online, April 2009. URL `www.wtec.pt/demo/hirtz/hico-aquatherm_660.pdf`.

DR Hooker. A study of the isolated kidney - the influence of pulse pressure upon renal function. *American Journal of Physiology–Legacy Content*, 27(1):24–44, 1910.

MA Hopf, DE Brinsfield, FJ Martinez, and PM Galletti. Laboratory experience with long-lasting perfusion. *ASAIO Journal*, 8(1):57, 1962.

JR Horowitz and KP Lally. Host defences and systemic inflammatory response to extracorporeal life support (ecls). In RH Bartlett. JB Zwischenberger, editor, *ECMO Extracorporeal Cardiopulmonary Support in Critical Care.* Ann Arbor, Michigan, 1995.

H. Hoshi, J. Asama, T. Shinshi, K. Ohuchi, M. Nakamura, T. Mizuno, H. Arai, A. Shimokohbe, and S. Takatani. Disposable magnetically levitated centrifugal blood pump: design and in vitro performance. *Artificial organs*, 29(7):520–526, 2005.

HotSnapZ. Faqs. Online Source, 2013.

BJ Huang and CL Duang. System dynamic model and temperature control of a thermoelectric cooler. *International journal of refrigeration*, 23(3):197–207, 2000.

KA Hultquist, T Kinaia, V Jayasuasti, and et al. 1992 equipment analysis of the elso registry centres. In *ELSO: ECMO Pump Talk*, volume 1, 1993.

S. Ichiba, H. M. Killer, and et al. Pilot investigation of hypothermia in neonates receiving extracorporeal membrane oxygenation. *Archives of Diseases in Childhood - Fetal and Neonatal Edition*, 88:128–133, 2003.

H. Iwahashi, K. Yuri, and et al. Development of the oxygenator: Past, present and future. *Journal of Artificial Organs*, 7:111–120, 2004a.

H. Iwahashi, K. Yuri, and Y. Nosé. Development of the oxygenator: past, present, and future. *Journal of Artificial Organs*, 7(3):111–120, 2004b.

Martin Jaegle. Multiphysics simulation of thermoelectric systems - modeling of peltier-cooling and thermoelectric generation. In *Proceedings of the COMSOL Conference*, 2008.

E Janssenswillem, R Vanhouse, M Steenmans, and et al. Computerized data acquisition and processing during ecc: a more accurate way of handling cpb patients. In S. HA, editor, *Proceeding of the sympoeium Thirty years of extracorporeal circulation*, pages 573–8, Mnchen, 1984.

E Janssenwillem, M Steenmans, M Rucquoi, B Cham, and W. Welch. In line ph and bloodgas monitoring vs intermittent sampling during cpb. *Elsevier, Paris, FRANCE*, 7(3):179–181, 1985.

S.A. Jones, J.G.; Smith. Shock in the critically ill neonate. *J Perinat Neonat Nurs*, 23:346354, 2009.

MV Kameneva, GW Burgreen, K Kono, B Repko, JF Antaki, and M Umezu. Effects of turbulent stresses upon mechanical hemolysis: experimental and computational analysis. *ASAIO*, 50(5):418–23, 2004.

A. Kantrowitz, S. Reiner, and D. Abelson. An automatically controlled, inexpensive pump-oxygenator. *The Journal of thoracic and cardiovascular surgery*, 38:586–93, 1959.

K.E. Karlson, C. Dennis, D. Sanderson, and C.U. Culmer. An oxygenator with increased capacity: Multiple vertical revolving cylinders. *Experimental Biology and Medicine*, 71(2):204, 1949.

K. Kawahito and Y. Nosé. Hemolysis in different centrifugal pumps. *Artificial organs*, 21(4):323–326, 1997.

E.B. Kay, J.E. Galajda, A. Lux, and FS Cross. The use of convoluted discs in the rotating disc oxygenator. *The Journal of thoracic surgery*, 36(2):268, 1958.

W.G. Kim and C.J. Yoon. Roller pump induced tubing wear of polyvinylchloride and silicone rubber tubing: Phase contrast and scanning electron microscopic studies. *Artificial organs*, 22(10):892–897, 1998.

J.W. Kirklin, R.T. Dushane, D.D. Patrick, P.S. Donald, H.G. Hetzel, H.G. Harshberger, and E.H. Wood. Intracardiac surgery with the aid of a mechanical pump-oxygenator system (gibbon-type). report of eight cases. *Proc. Mayo Clin*, 30:201–206, 1955.

J.W. Kirklin, D.E. Donald, H.G. Harshbarger, P.S. Hetzel, R.T. Patrick, HJC Swan, and E.H. Wood. Studies in extracorporeal circulation. i. applicability of gibbon-type pump-oxygenator to human intracardiac surgery: 40 cases. *Annals of surgery*, 144(1):2, 1956.

J.W. Kirklin, R.T. Patrick, and R.A. Theye. Theory and practice in the use of a pump-oxygenator for open intracardiac surgery. *Thorax*, 12(2):93–98, 1957.

RE Klabunde. *Cardiovascular physiology Concepts Second Edition*. Lippincott Williams and Wilkins, 2011.

KG Kohlstdt and I.H. Page. The liberation of renin by perfusion of kidneys following reduction of pulse pressure. *The Journal of Experimental Medicine*, 72(2):201, 1940.

T. Kolobow and R.L. Bowman. Construction and evaluation of an alveolar membrane artificial heart-lung. *ASAIO Journal*, 9:238, 1963.

M. Kono, H. Orita, T. Shimanuki, M. Fukasawa, K. Inui, and M. Wasio. A clinical study of cerebral perfusion during pulsatile and nonpulsatile cardiopulmonary bypass]. *Nippon Geka Gakkai Zasshi*, 91(8):1016, 1990.

M. Kurusz. Gaseous microemboli: sources, causes, and clinical considerations. *Med Instrum*, 19:73–76, 1985.

M. Kurusz. May 6, 1953: The untold story. *ASAIO Journal*, 58(1):2, 2012.

Andrea Kurz, Daniel I. Sessler, and Rainer Lenhardt. Perioperative normothermia to reduce the incidence of surgical-wound infection and shorten hospitalization. *N Engl J Med*, 334:1209–1216, 1996.

Laird-Technologies. *Thermoelectric Handbook*. Laird Technologies, London, 2010.

L. D. Landau and E. M. Lifshitz. *Electrodynamics of Continuous Media*. Butterworth-Heinemann, 2 nd edition edition, 1984.

A.J. Landé, B. Parker, V.S. Robert G Carlson, and C.W. Lillehei. Methods for increasing the efficiency of a new dialyzer-membrane oxygenator. *ASAIO Journal*, 14(1):227, 1968.

C.; Butler K.; McRobb-C.; Mejak B. Lawson, S.; Ellis. Neonatal extracorporeal membrane oxygenation devices, techniques and team roles: 2011 survey results of the united states extracorporeal life support organization centers. *The Journal of Extra-Corporeal Technology*, 43(4):236244, 2011.

D.S.. Lawson, R. Walczak, A.F. Lawson, I.R. Shearer, R. Ing, S. Schulman, F. Kern, and J. Jaggers. North american neonatal extracorporeal membrane oxygenation (ecmo) devices: 2002 survey results. *The Journal of extra-corporeal technology*, 36 (1):16–21, 2004.

D.S. Lawson, A.F. Lawson, R. Walczak, C. McRobb, P. McDermott, I.R. Shearer, A. Lodge, and J. Jaggers. North american neonatal extracorporeal membrane oxygenation (ecmo) devices and team roles: 2008 survey results of extracorporeal life support organization (elso) centers. *The Journal of extra-corporeal technology*, 40(3):166–174, 2008.

E.L. Lazar, S.J. Abramson, S. Weinstein, and C.J.H. Stolar. Neuroimaging of brain injury in neonates treated with extracorporeal membrane oxygenation: lessons learned from serial examinations. *Journal of pediatric surgery*, 29(2):186–191, 1994.

Jietae Lee, Wonhui Cho, and Thomas F. Edgar. Multiloop {PI} controller tuning for interacting multivariable processes. *Computers & Chemical Engineering*, 22(11):1711 – 1723, 1998. ISSN 0098-1354. doi: http://dx.doi.org/10.1016/S0098-1354(98)00230-0. URL `http://www.sciencedirect.com/science/article/pii/S0098135498002300`.

WH Lee Jr, D. Krumhaar, EW Fonkalsrud, OA Schjeide, and JV Maloney Jr. Denaturation of plasma proteins as a cause of morbidity and death after intracardiac operations. *Surgery*, 50:29, 1961.

BM Leshchinskii, GP Itkin, and NK Zimin. Centrifugal pumps for blood forcing: Technical aspects. *Biomedical Engineering*, 24(1):33–37, 1990.

LB Leverett, JD Hellums, CP Alfrey, and EC Lynch. Red blood cell damage by shear stress. *Biophysical journal*, 12(3):257–273, 1972.

FJ Lewis, SJ Horwitz, and JB Naines Jr. Semiautomatic control for an extracorporeal blood pump. *The Journal of thoracic and cardiovascular surgery*, 43:392–396, 1962.

C.W. Lillehei, R.A. Dewall, R.C. Read, H.E. Warden, and R.L. Varco. Direct vision intracardiac surgery in man using a simple, disposable artificial oxygenator. *Diseases of the Chest*, 29(1):1–8, 1956.

A. Litzi, S. Stringer, M. Farhangnia, M. Tyebjee, T. Afzal, and B. Brian. Extracorporeal blood handling system with automatic flow control and methods of use., 09 2004. URL `http://www.google.com/patents?id=vBqfAAAAEBAJ&printsec=frontcover&dq=US+2004+0184953A1&hl=en&sa=X&ei=dmr1T_K5MsrD0QXQxIWpBw&ved=0CDMQ6AEwAA`.

E.L. Lloyd. *Hypothermia and cold stress*. Croom Helm London, 1986.

MF Lynch, D. Peterson, and V. et al. Baker. Centrifugal blood pumping for open heart surgery. *Minnesota medicine*, 61(9):536, 1978.

Christopher Lynn. *The development of a novel and integrated ECMO unit*. PhD thesis, University of Strathclyde, 2012.

Xiaoli Ma. Thermoelectrics: a review of present and potential applications. *Applied Thermal Engineering*, 23:913935, 2003.

Mikio Maeda and Shuta Murakami. A self-tuning fuzzy controller. *Fuzzy Sets and Systems*, 51(1):29 – 40, 1992. ISSN 0165-0114. doi: http://dx.doi.org/10.1016/0165-0114(92)90073-D. URL `http://www.sciencedirect.com/science/article/pii/016501149290073D`.

M. Many, HS Soroff, WC Birtwell, F. Giron, H. Wise, and R.A. Deterling Jr. The physiologic role of pulsatile and nonpulsatile blood flow: Ii. effects on renal function. *Archives of Surgery*, 95(5):762, 1967.

G.R. Martin, L. Chauvin, and B.L. Short. Effects of hydralazine on cardiac performance in infants receiving extracorporeal membrane oxygenation. *The Journal of pediatrics*, 118(6):944–948, 1991.

F. Martini. *Anatomy and Physiology' 2011 Ed.* Pearson Higher Education, 2011.

B. McILwain, J. Timpa, A. R. Kurundkar, D. W. Holt, D. R. Kelly, and Y. Hartman. Maheshwari, a. (2010). plasma concentrations of inflammatory cytokines rise rapidly during ecmo-related sirs due to the release of pre-formed stores in the intestine. laboratory investigation. *Journal of Technical Methods and Pathology*, 90 (1):128139, 2010.

M.L. McManus, S.V. Kevy, L.K. Bower, and P.R. Hickey. Coagulation factor deficiencies during initiation of extracorporeal membrane oxygenation. *The Journal of Pediatrics*, 26:900–4, 1995.

Medgadget. Axial flow pump. Online Archive, 2003. URL `http://www.medgadget.com/archives/img/8765ap1.jpg`.

de AJ. Mello, M Habgood, NL Lancaster, T Welton, and RCR Wootton. Precise temperature control in microfluidic devices using joule heating of ionic liquids. *MINIATURIS ATION FOR CHEMISTRY, BIOLOG Y & BIOENGINEERING*, 4:417419, 2004.

DG Melrose. A heart-lung machine for use in man. *The Journal of physiology*, 127 (3):51, 1955.

DG Melrose and I. Aird. Mechanical heartlung for use in man. *British medical journal*, 2(4827):57–62, 1953.

DM Meyer and ME Jessen. *Extracorporeal Life Support (Vademecum).* Landes Bioscience, spi edition edition, 2000.

M. E. Meyer, D. M.; Jessen. Results of extracorporeal membrane oxygenation in neonates with sepsis. the extracorporeal life support organization experience. *J Thorac Cardiovasc Surg*, 109:419–427, 1995.

B.J. Miller. Laboratory work preceding the first clinical application of cardiopulmonary bypass. *Perfusion*, 18(3):145–154, 2003.

BJ Miller, JH Gibbon Jr., and MH Gibbon. Recent advances in the development of a mechanical heart and lung apparatus. *Ann Surg*, 134:694708., 1951.

BJ Miller, JH Gibbon Jr, VF Greco, BA Smith, CH Cohn, and FF Allbritten Jr. The production and repair of interatrial septal defects under direct vision with the assistance of an extracorporeal pump-oxygenator circuit. *The Journal of thoracic surgery*, 26(6):598, 1953.

T.C. et al Min. Natural convection and radiation in a panel heated room. *ASHRAE Transactions*, 62:337–358, 1956.

AE Mirsky. Sulfhydryl groups in films of egg albumin. *The Journal of General Physiology*, 24(6):725–733, 1941.

B. J. E. Misgeld, Werner J., and Hexamer M. Robust and self-tuning blood flow control during extracorporeal circulation in the presence of system parameter uncertainties. *Medical and Biological Engineering and Computing*, 43:589–598, 2005.

Berno Johannes Engelbert Misgeld. *Automatic Control of the Heart-Lung Machine*. PhD thesis, Ruhr-Universit at Bochum, 2006.

F.D. Moore and J.G. Allen. *Extracorporeal circulation*. Thomas, 1958.

K. Mori, A. Watanabe, M. Onoe, S. Watarida, Y. Nakamura, T. Magara, R. Tabata, and Y. Okada. Regional blood flow in the liver, pancreas and kidney during pulsatile and nonpulsatile perfusion under profound hypothermia. *Jpn. Circ.*, 52(3):21927, 1988.

G. Moss. A device to maintain automatically and continuously an absolute or relative constant weight of a subject or container during perfusion. *Surgery*, 49:743, 1961.

Ltd. MTRE Advanced Technologies. Allon. `http://mtre.com/var/173/557689-allon%20brochure.pdf`.

ND Mukherjee, AV Beran, J. Hirai, A. Wakabayashi, DR Sperling, WF Taylor, and JE Connolly. In vivo determination of renal tissue oxygenation during pulsatile and nonpulsatile left heart bypass. *The Annals of Thoracic Surgery*, 15(4):354–363, 1973.

NA Murray, F Ulrich, and CV Mouritzen. An automatic flow control system for extracorporeal circulation. *Journal of thoracic and Cardiovascular Surgery*, 50: 260–264, 1965.

WR Murray, S. Mittra, D. Mittra, LB Roberts, and KM Taylor. The amylase-creatinine clearance ratio following cardiopulmonary bypass. *The Journal of thoracic and cardiovascular surgery*, 82(2):248, 1981.

K. Nakayama, T. Tamiya, K. Yamamoto, T. Izumi, S. Akimoto, S. Hashizume, T. Iimori, M. Odaka, and C. Yazawa. High-amplitude pulsatile pump in extracorporeal circulation with particular reference to hemodynamics. *Surgery*, 54:798, 1963.

O Nelles. *Nonlinear System Identification: from classical approaches to neural networks and fuzzy models*. Springer Verlag Berlin, 2001.

H. Nishida, T. Beppu, M. Nakajima, T. Nishinaka, H. Nakatani, K. Ihashi, T. Katsumata, M. Kitamura, S. Aomi, and M. et al. Endo. Development of an autoflow cruise control system for a centrifugal pump. *Artificial Organs*, 19(7):713–718, 1995.

A. Nonoyama. Hemodynamic studies on extracorporeal circulation with pulsatile and non-pulsatile blood flows. *Arch. Japan. Chir*, 29:1381–1406, 1960.

G.P. Noon, L.E. Kane, L. Feldman, J.A. Peterson, and M.E. DeBakey. Reduction of blood trauma in roller pumps for long-term perfusion. *World Journal of Surgery*, 9(1):65–71, 1985.

W.H. Northway Jr, R.C. Rosan, and D.Y. Porter. Pulmonary disease following respirator therapy of hyaline-membrane disease. *New England Journal of Medicine*, 276(7):357–368, 1967.

Yukihiko Nose. *Manual on artificial organs. Volume 2: The oxygenator*. C.V. Mosby Company, 1974.

T. Ogata, Y. Ida, and J. Takeda. Experimental studies on the extracorporeal circulation by use of our pulsatile arterial pump. *Lung*, 6:381–90, 1959.

F. Olmsted, W.j. Kolff, and D.b. Effler. Three safety devices for the heart-lung machine. *Cleveland Clinic quarterly*, 25(3):169, 1958.

D. B. Olsen. The history of continuous-flow blood pumps. *Artificial Organs,*, 6: 401–404, 2000.

J.M. Orenstein, N. Sato, B. Aaron, B. Buchholz, and S. Bloom. Microemboli observed in deaths following cardiopulmonary bypass surgery:: Silicone antifoam agents and polyvinyl chloridetubing as sources of emboli. *Human pathology*, 13(12):1082–1090, 1982.

G. Owens, J.E. Adams, and HW et al. Scott. Embolic fat as a measure of adequacy of various oxygenators. *Journal of Applied Physiology*, 15(6):999–1000, 1960.

OJ Panachaveettil. Development of thermoelectric devices for structural composites. Master's thesis, Oklahoma State University, 2011.

G. Pappas, SD Winter, CJ Kopriva, and PP Steele. Improvement of myocardial and other vital organ functions and metabolism with a simple method of pulsatile flow (iabp) during clinical cardiopulmonary bypass. *Surgery*, 77(1):34, 1975.

O.B. Paulson, G. Waldemar, J.F. Schmidt, and S. Strandgaard. Cerebral circulation under normal and pathologic conditions. *The American Journal of Cardiology*, 63 (6):C2–C5, 1989.

G.J. Peek, K. Wong, C. Morrison, H.M. Killer, and R.K. Firmin. Tubing failure during prolonged roller pump use: a laboratory study. *Perfusion*, 14(6):443–452, 1999.

D.G. Pennington, JP Merjavy, MT Swartz, and VL Willman. Clinical experience with a centrifugal pump ventricular assist device. *ASAIO Journal*, 28:93–hyhen, 1982.

M Pohl, O Samba, MO Wendt, and G Vlastos. Shear stress related hemolysis and its modelling by mechanical degradation of polymer solutions. *Int J Artif Organs.*, 21:107–13, 1998.

RJ; Timmes JJ et al. Pollard, HS; Fleischaker. Blood-brain barrier studies in extracorporeal cooling and warming. *J Thorac Cardiovasc Surg*, 42:772–77, 1961.

Bed Poudel, Qing Hao, Ma Yi, and Yucheng Lan. High-thermoelectric performance of nanostructured bismuth antimony telluride bulk alloys. *Science*, 320:634–638, 2008.

DJ Rawn, HK Harris, JB Riley, DN Yoda, and MM Blackwell. An under-occluded roller pump is less hemolytic than a centrifugal pump. *The Journal of extracorporeal technology*, 29(1):15–18, 1997.

H.M. Reul and M. et al. Akdis. Blood pumps for circulatory support. *PERFUSION-SEVENOAKS-*, 15(4):295–312, 2000.

JB Riley. A technique for computer assisted monitoring in the management of total heart-lung bypass. *J Extracorp Tech*, 13:171–6, 1981.

JJ Roche, I. Ungar, and HS Coleman. An electric apparatus for rapid and precise regulation of the venous blood-reservoir height on heart-lung machines. *Surgery*, 56:561, 1964.

A Romaine-Davis. John gibbon and his heart-lung machine. *Tex Heart Inst J*, 18: 245, 1991.

EM Rosenberg and JH Seguin. Selection criteria for use of ecls in neonates. In RH Bartlett JB Zwischenberger, editor, *ECMO: Extracorporeal Cardiopulmonary Support in Critical Care*. Ann Arbor, 1995.

D. Rottenberg, E. Sondak, JB Borman, E. Dviri, and G. Uretzky. Early experience with a true pulsatile pump for heart surgery. *Perfusion*, 10(3):171–175, 1995.

TG Ruttmann and I James, MFand Aronson. In vivo investigation into the effects of haemodilution with hydroxyethyl starch (200/0.5) and normal saline on coagulation. *Br J Anaesth*, 80:612616, 1998.

IH Rygg and E. Kyvsgaard. Further development of the heart-lung machine with the rygg-kyvsgaard plastic bag oxygenator. *Minerva chirurgica*, 13(23):1402, 1958.

W. Saggau, I. Baca, E. Ros, HH Storch, and W. Schmitz. Clinical and experimental studies on pulsatile and continuous flow during extracorporeal circulation (author's transl)]. *Herz*, 5(1):42, 1980.

T. S.; Natarajan S. P. Sakthivel, G; Anandhi. Modelling and real time implementation of digital pi controller for a non linear process. *Journal of Innovative Research in Engineering and Sciences*, 2(5):274–290, 2011.

JM Sanderson, G. Wright, and FW Sims. Brain damage in dogs immediately following pulsatile and non-pulsatile blood flows in extracorporeal circulation. *Thorax*, 27(3): 275, 1972.

JM Sanderson, PG Morton, TS Tolloczko, T. Vennart, and G. Wright. The morton-keele pumpa hydraulically activated pulsatile pump for use in extracorporeal circulation. *Medical and Biological Engineering and Computing*, 11(2):182–190, 1973.

RF Schmidt, G Thews, and F Lang. *Physiologie des Menschen*. Springer Verlag. Berlin, 2000.

H Schmied, A Kurz, DI Sessler, S Kozek, and A. Reiter. Mild hypothermia increases blood loss and transfusion requirements during total hip arthroplasty. *Lancet*, 347 (289-92), 1996.

W. Schröder. Über die bildungsstätte des harnstoffs. *Naunyn-Schmiedeberg's Archives of Pharmacology*, 15(5):364–402, 1882.

A. Schwarzhaupt, B. Qaqunda, and U. Kiencke. Entwurf eines prädiktiven mimo-reglers für herz-lungen-maschinen auf der grundlage eines modells der extrakorporalen zirkulation. *Biomedizinische Technik/Biomedical Engineering*, 43(s1):336–337, 1998.

JS Seeker-Walker, JF Edmonds, EH Spratt, and AW Conn. The source of coronary perfusion during partial bypass for extracorporeal membrane oxygenation (ecmo). *The Annals of Thoracic Surgery*, 21(2):138–143, 1976.

W. Seifert, M. Ueltzen, and E. Muller. One dimensional modelling of thermoelectric cooling. *phys.stat.sol*, 194(1):277 290, 2002.

L.L. Sell, M.L. Cullen, G.C. Whittlesey, S.T. Yedlin, A.I. Philippart, M.P. Bedard, and M.D. Klein. Hemorrhagic complications during extracorporeal membrane oxygenation: prevention and treatment. *Journal of pediatric surgery*, 21:1087–1091, 1986.

HB Shumacker. *A dream of the heart: the life of John H. Gibbon, Jr., father of the heart-lung machine*. Fithian Press, 1999.

JM Sinard and RH Bartlett. Extracorporeal membrane oxygenation (ecmo): prolonged bedside cardiopulmonary bypass. *Perfusion*, 5:239–249, 1990.

MG Sirotkina, OA Osipov, BS Bobrov, NA Super, and GI Gaev. Review and analysis of membrane oxygenators. *Biomedical Engineering*, 4(3):156–163, 1970.

L.T. Skeggs Jr. Persistence and prayer: from the artificial kidney to the autoanalyzer. *Clinical Chemistry*, 46(9):1425–1436, 2000.

J.P. Slater, E.A. Rose, H.R. Levin, OH Frazier, J.K. Roberts, A.D. Weinberg, and M.C. Oz. Low thromboembolic risk without anticoagulation using advanced-design left ventricular assist devices. *The Annals of thoracic surgery*, 62(5):1321–1328, 1996.

J. H. Smith. *Procedures of the Paediatric Intensive Care Unit*, chapter ECMO, VAD and Circulatory Support., pages 1–105. 2007.

Z. Song, C. Wang, and AH Stammers. Clinical comparison of pulsatile and non-pulsatile perfusion during cardiopulmonary bypass. *The Journal of extra-corporeal technology*, 29(4):170–175, 1997.

SL Soo. *Direct Energy Conversion*. London, U.K., 1968.

FH Splittgerber, GC Whittlesey, and MD Klein. New surface treatments to prevent thrombosis during extracorporeal circulation. *ASAIO Journal*, 31(1):474–478, 1985.

A.H. Stammers, B.L. Mejak, E.D. Rauch, S.N. Vang, and T.W. Viessman. Factors affecting perfusionists' decisions on equipment utilization: results of a united states survey. *JOURNAL OF EXTRACORPOREAL TECHNOLOGY*, 32(1):4–10, 2000.

E. Sulyok, E. Jequier, and LS Prod'Hom. Thermal balance of the newborn infant in a heat-gaining environment. *Pediatric Research*, 7(11):888–900, 1973.

G.A. Taylor, B.L. Short, and C.R. Fitz. Imaging of cerebrovascular injury in infants treated with extracorporeal membrane oxygenation. *The Journal of pediatrics*, 114 (4):635–639, 1989.

KM Taylor, WH Bain, M. Russell, JJ Brannan, and IJ Morton. Peripheral vascular resistance and angiotensin ii levels during pulsatile and no-pulsatile cardiopulmonary bypass. *Thorax*, 34(5):594–598, 1979.

K.M. Taylor, B.J. Devlin, S.M. Mittra, J.G. Gillan, J.J. Brannan, and J.M. McKenna. Assessment of cerebral damage during open-heart surgery a new experimental model. *Scandinavian Cardiovascular Journal*, 14(2):197–203, 1980.

GmbH The Surgical Company. Criticool; cooling with care manual. Online, 2006. URL `www.tsc-deutschland.de/uploads/file/criticool-broschure-de.pdf`.

JR Utely. Renal function and fluid balance with cardiopulmonary bypass. In JR Utley GP Gravlee, RF Davis, editor, *Cardiopulmonary Bypass*. Baltimore, Williams and Wilkins, 1993.

JR Utley, C. Wachtel, R.B. Cain, EA Spaw, J.C. Collins, and D.B. Stephens. Effects of hypothermia, hemodilution, and pump oxygenation on organ water content, blood flow and oxygen delivery, and renal function. *The Annals of thoracic surgery*, 31 (2):121–133, 1981.

Poul-Erik Vanggaard, Leif ; Paulev. *Thermoregulation, temperature and disorders*, chapter Chapter 21. Online, 2004.

Rama Venkatasubramanian, Edward Siivola, Thomas Colpitts, and Brooks O'Quinn. Thin-film thermoelectric devices with high room-temperature figures of merit. *Nature*, 413:597–602, October 2001.

P Verma. *Cooling Water Treatment Hand Book - Books on Water Treatment*. Albatros Fine Chem Ltd., 2004. ISBN 9788190188579. URL `http://books.google.co.uk/books?id=Ov0BvdrQMPYC`.

C. Vogler, C. Sotelo-Avila, D. Lagunoff, P. Braun, J.A. Schreifels, and T. Weber. Aluminum-containing emboli in infants treated with extracorporeal membrane oxygenation. *New England Journal of Medicine*, 319(2):75–79, 1988.

R. Waack, NH Alex, HL Frisch, V. Stannett, and M. Szwarc. Permeability of polymer films to gases and vapors. *Industrial & Engineering Chemistry*, 47(12):2524–2527, 1955.

R.K. Wampler, J.C. Moise, O.H. Frazier, and D.B. et al. Olsen. In vivo evaluation of a peripheral vascular access axial flow blood pump. *ASAIO transactions/American Society for Artificial Internal Organs*, 34(3):450, 1988.

G.M. Wieselthaler, H. Schima, M. Hiesmayr, R. Pacher, G. Laufer, G.P. Noon, M. DeBakey, and E. Wolner. First clinical experience with the debakey vad continuous-axial-flow pump for bridge to transplantation. *Circulation*, 101(4):356–359, 2000.

G. Wright. The hydraulic power outputs of pulsatile and nonpulsatile cardiopulmonary bypass pumps. *Perfusion*, 3(4):251–262, 1988.

G Wright, JST Sum Ping, CS Campbell, and Tobias MA. Computation of haemodynamic power and input impedance in the ascending aorta of human patients undergoing open-heart surgery. *Cardiovasc Res*, 22:179–84, 1988.

Y. Yamasaki and et al. T. Hayashi. Early experience with low-prime (99ml) extracorporeal membrane oxygenation support in children. *American Society of Artificial Internal Organs*, 52:5, 2006.

W.M. Zapol, M.T. Snider, J.D. Hill, R.J. Fallat, R.H. Bartlett, L.H. Edmunds, A.H. Morris, E.C. Peirce II, A.N. Thomas, H.J. Proctor, and et al. Extracorporeal membrane oxygenation in severe acute respiratory failure. *JAMA: the journal of the American Medical Association*, 242(20):2193–2196, 1979.

Jianhua et al Zhou. Measurement of thermoelectric properties of individual bismuth telluride nanowires. In *24th International Conference on IEEE*, volume Zhou, Jianhua, et al. "Measurement of thermoelectric properties of individual bismuth telluride nanowires." Thermoelectrics, 2005. ICT 2005. 24th International Conference on. IEEE, 2005., 2005.